Geology, geochemistry and Cr-Ni-Cu-PGE mineralization of the Bird River sill: Evidence for a multiple intrusion model

by

Caroline A. Mealin

A thesis
presented to the University of Waterloo
in fulfillment of the
thesis requirement for the degree of
Master of Science
in
Earth Sciences

Waterloo, Ontario, Canada, 2008

I hereby declare that I am the sole author of this thesis. This is a true copy of the thesis, including any required final revisions, as accepted by my examiners.

I understand that my thesis may be made electronically available to the public.

Abstract

The Bird River sill (BRS) is composed of several layered mafic-ultramafic intrusive bodies located in the northern portion of the Bird River greenstone belt in southeastern Manitoba. Layered intrusions, such as those that collectively make-up the BRS, are important hosts to base and precious metal deposits. This study was initiated to examine and develop a petrogenetic model for the emplacement of the western half of the BRS and to establish the controls on Cr-Ni-Cu-PGE mineralization.

The mafic-ultramafic bodies of the BRS complex were emplaced as separate intrusions through multiple-magmatic injections into different stratigraphic levels of the Lamprey Falls Formation. The intrusions share a common magma source which is geochemically akin to modern back-arc basin basalts but is also similar to mid-ocean ridge basalts. It is interpreted that the central BRS intrusions are connected and represent a part of a single conduit system. The BRS complex and the Lamprey Falls Formation are overlain by the metasedimentary rocks of the Peterson Creek Formation and were tilted southward from their original horizontal positions. Metagabbroic intrusions present in the Lamprey Falls Formation to the north of the BRS complex represent coarse-grained flows genetically related to the mafic volcanics of the Lamprey Falls Formation and do not appear to be related to the BRS.

The stratigraphy of the BRS complex is divided into four basic magmatic series which are from the base upwards: 1) marginal mafic series, 2) ultramafic series, 3) transition series, and 4) mafic series. All significant concentrations of Ni-Cu-PGE and Cr in the study area are contained in the ultramafic series of the BRS. Mineralization is magmatic in origin with significant Ni-Cu and PGE remobilization associated with late felsic magmatism. Ni-Cu remobilization is also associated with mineralized shear zones that cross-cut the BRS and extend into the Lamprey Falls Formation. The sulphur source could not be determined unambiguously based on sulphur isotopes alone but the $\delta^{34}S$ values of the separate BRS bodies suggests that the sulphur in the BRS is magmatic in origin and that two of the BRS bodies may have assimilated external sulphur from iron formations present within the Lamprey Falls Formation.

The findings of this investigation have considerable economic implications. The model that each BRS body is an individual intrusion implies each body may contain its own style of mineralization. The Page body is the most northern BRS intrusion and is interpreted to represent a turbulent magmatic environment and to be the first intrusion to form at the lowest stratigraphic level. The magmas that formed the stratigraphically higher BRS intrusions are believed to have passed through the Page intrusion. Therefore, the Page body is an excellent PGE exploration target as it represents a turbulent environment in which significant amounts of primitive magma have passed through which are two key factors in the formation of Ni-Cu-PGE deposits.

Acknowledgements

This study is part of a joint industry - government - university research program on the Bird River greenstone belt initiated by the University of Waterloo and Manitoba Geological Survey with financial support from Gossan Resources Limited, Mustang Minerals Corporation, Tantalum Mining Corporation of Canada Limited and a grant from the Natural Science and Engineering Research Council to Dr. S. Lin and Dr. R. Linnen. Financial and logistical support of this study is gratefully acknowledged.

I would like to thank my supervisors Dr. R. Linnen and Dr. S. Lin for their technical guidance, advice and support during this study. I would also like to thank M.T. Corkery, P. Gilbert, Dr. P. Theyer, Dr. M. Duguet and P. Kremer for sharing their ideas, encouragement and for making my summers in Manitoba so memorable. Special thanks are extended to R. Cooke and D. Reeson from Gossan Resources Limited for their constant enthusiasm and support and P. Lenton, B. Lenton, D. Savage and D. Camara for their assistance in digitizing maps, logistical support and preparation of samples for geochemical analysis.

To my friends and family, I could not have completed this project without your love and support over the last few years. I deeply appreciate everything you have all done for me. Last but not least, to Charlie, thank you for all of your patience and support and especially for keeping me sane during the writing of this thesis.

Table of Contents

List of Figures

List of Tables

Chapter 1: Introduction

1.1 General Introduction

The Bird River sill (BRS) is composed of several mafic-ultramafic intrusive bodies which intrude the northern portion of the Bird River greenstone belt. The Bird River greenstone belt is located in the western Superior Province of the Canadian Shield (Figure 1) approximately 150 km northeast of Winnipeg in southeastern Manitoba. The Bird River belt is composed of east-west trending metavolcanic and metasedimentary sequences and is approximately 50 km long and 10 km wide. It is situated between the metasedimentary rocks of the English River Subprovince to the north and the intermediate-felsic plutonic rocks of the Winnipeg River Subprovince to the south.

The Bird River belt is a significant district for ore deposits hosting the Tantalum Mining Corporation of Canada Limited (TANCO) rare-element (lithium, cesium and tantalum) pegmatite deposit, the Maskwa West Ni-Cu-Co-Platinum-Group Element (PGE) deposit, the Dumbarton Ni-Cu deposit and stratiform Cr-Ni-Cu-PGE mineralization (Figure 2). Of these deposits, the BRS is host to the Maskwa West mine, a massive sulphide Ni-Cu-Co-PGE deposit, and stratiform Cr-Ni-Cu-PGE mineralization. The Dumbarton mine, a stratabound massive sulphide Ni-Cu deposit, is present within the northern mafic volcanic sequence of the Bird River greenstone belt and borders the northern contact of the BRS Maskwa-Dumbarton intrusion (Figure 2). The Ni-Cu in the Dumbarton deposit is interpreted to have originated from the BRS (Juhas, 1973).

Numerous studies have produced conflicting models over the years on the emplacement of the BRS and its associated Ni-Cu-PGE and Cr mineralization. The purpose of this project is to investigate and develop a petrogenetic model for the emplacement of the western half of the BRS and establish the controls on mineralization.

1.2 Previous Work

1.2.1 Bird River greenstone belt

Geological investigations in the Bird River area began in 1898 (Tyrell, 1900). Upon the discovery of base metal sulphide mineralization, various studies on regional geology,

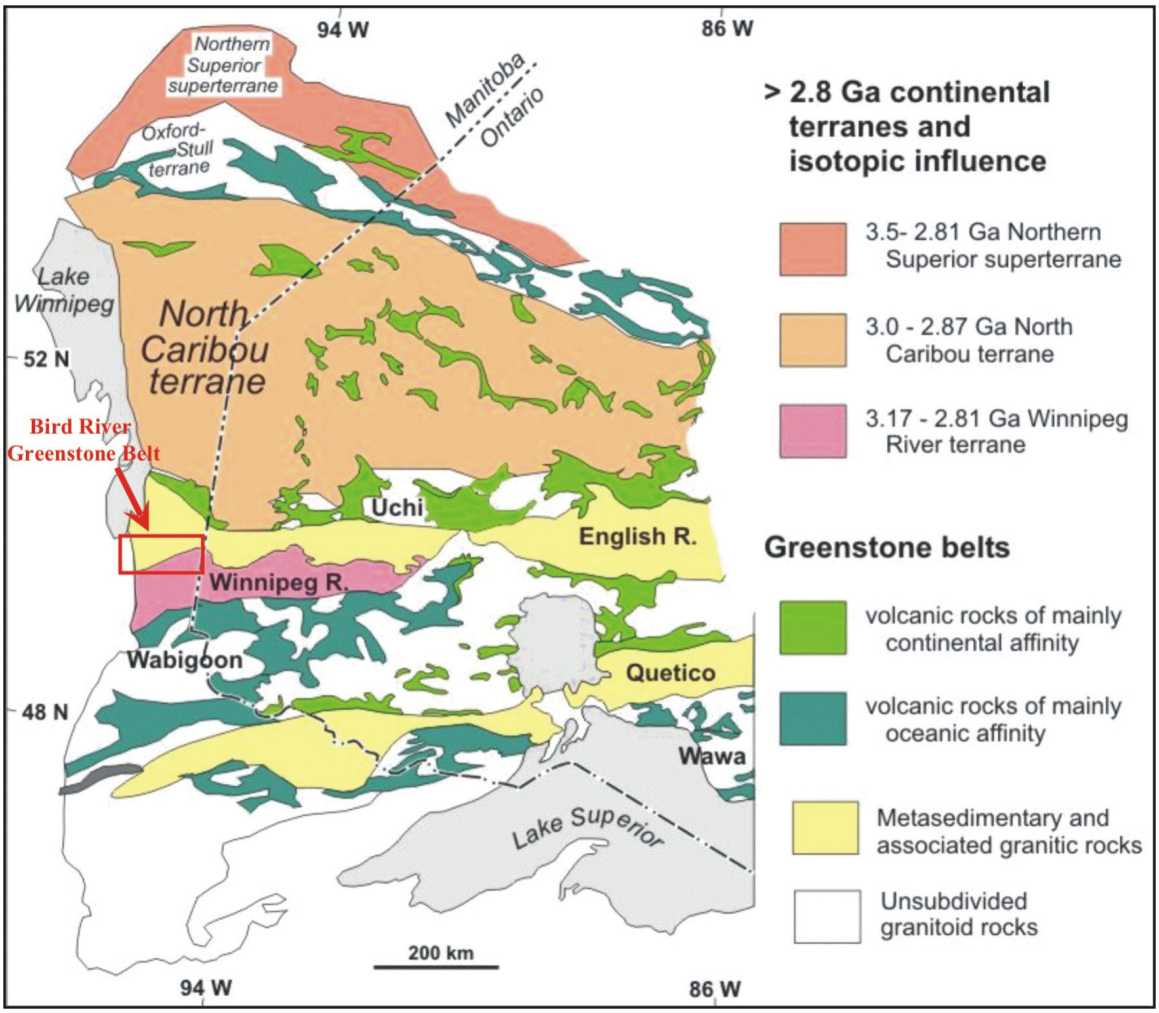

Figure 1: Geological map of the Western Superior Province (Natural Resources Canada, 2008). The location of the Bird River greenstone belt is outlined.

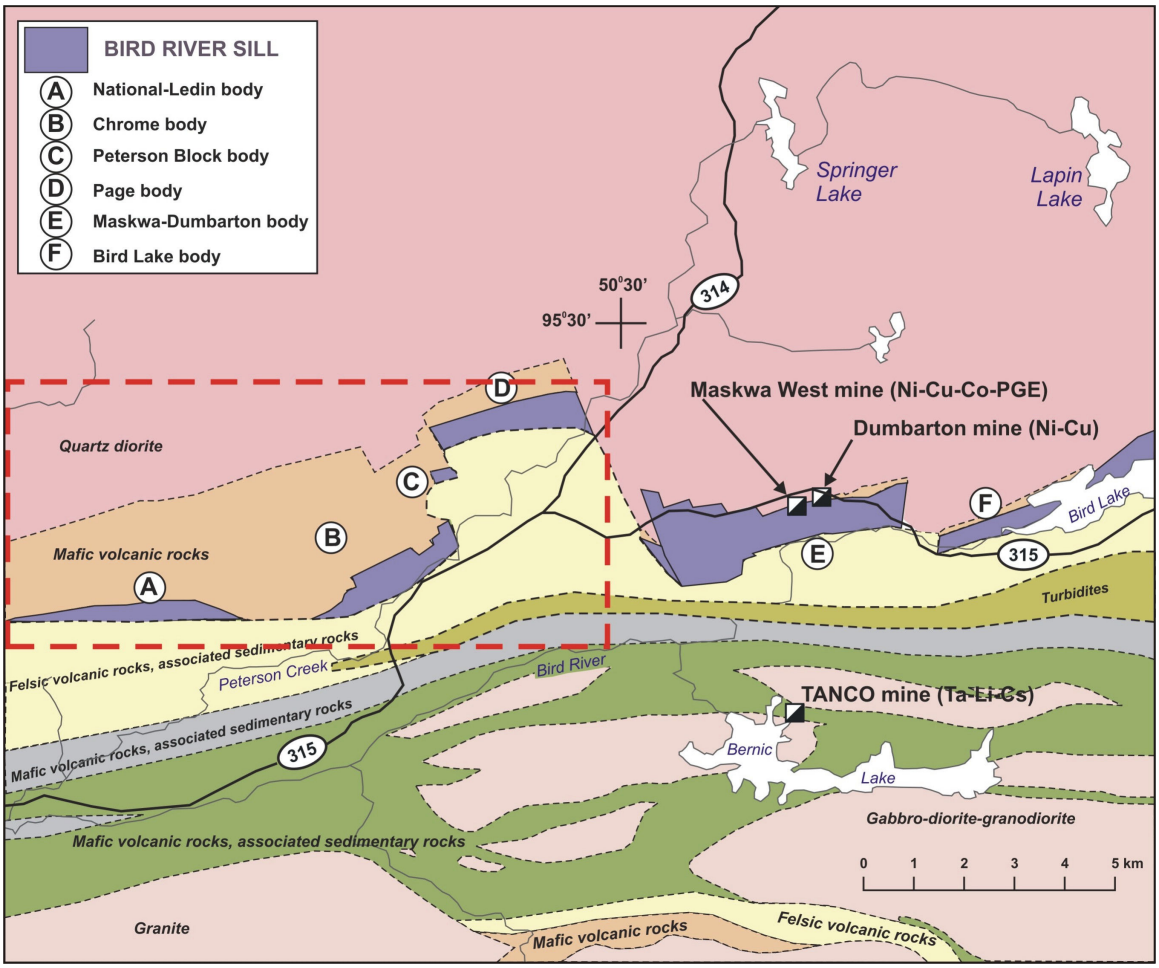

Figure 2: Simplified geological map of the central portion of the Bird River greenstone belt. The separate intrusive bodies of the Bird River sill and the locations of the Maskwa West mine, Dumbarton mine and TANCO mine are shown. A portion of the study area for the current investigation is outlined (study area extends further west). Map modified from Theyer et al. (2001) and based on mapping from this study and that of Duguet et al. (2007).

base metal mineralization and pegmatite deposits were completed. For details on earlier exploration and investigations in the Bird River area readers are referred to the works of Moore (1913), Colony (1920), McCann (1921), Cooke (1922), Wright (1926 and 1932), Childerhouse (1928), Springer (1948, 1949 and 1950), Davies (1952 and 1955), Trueman (1980), Timmins (1985) and Wang (1993).

The most recent investigations of the tectonic setting and stratigraphy of the Bird River area are Duguet et al. (2005, 2006 and 2007) and Gilbert (2005, 2006 and 2007). The most recent investigations of the rare-element-bearing pegmatite deposits in the Bird River greenstone belt are Kremer (2005) and Kremer and Lin (2006). These studies were the outcome of a joint industry - government - university project of which this thesis was also a part.

1.2.2 Bird River sill and associated mineralization

Chromite layers in the BRS were first discovered in 1941. Early investigations of the occurrences were completed by Brownell (1942 and 1943) who described the mineralogy of the chromite deposits and Bateman (1942, 1943 and 1945) who examined the extent and composition of the chromite deposits. Although there has been considerable interest in these deposits, particularly in the 1940's during WWII, the chromite deposits have never been exploited.

The BRS has supported two Ni-Cu mines, the Dumbarton mine and the Maskwa West mine. The Dumbarton mine was in production from 1969 to 1974 and the Maskwa West mine from 1974 to 1976. The work of Karup-Moller and Brummer (1971) discusses the geology of the Dumbarton mine and Coats et al. (1979) presents the geology of the Maskwa West nickel mine. Juhas (1973) completed a study on the origin of Ni-Cu mineralization in the Bird River area and paid particular attention to the Dumbarton Ni-Cu mine.

In the early 1980's an investigation of the BRS Chrome intrusion identified two enriched PGE horizons in the ultramafic series of the intrusion. Results are summarized in Theyer (1985). It was concluded that the ultramafic portion of the BRS may not be a simple intrusive body, but a multi-layered igneous complex which contains significant Pt and Pd (Theyer, 1985). The PGE-enriched intervals are interpreted to represent "reef-

type" mineralization (Peck and Theyer, 1998). An investigation on the BRS Chrome intrusion by the Geological Survey of Canada identified a third PGE enriched horizon and concluded that the disseminated sulphides and anomalous PGE values are consistent with a magmatic genesis (Scoates et al., 1989). Further investigations on the occurrence and potential of PGE in the ultramafic series of the BRS can be found in Theyer (1991, 2000 and 2002), Theyer et al. (2001), Murphy and Theyer (2005) and Stansell and Theyer (2005).

Platinum-Group Minerals (PGM) were first identified as inclusions in chromite in 1983 (Talkington et al., 1983). It has since been concluded that there is a strong association between PGE and Cr from the BRS Chrome intrusion which indicates that PGM were trapped during chromite crystallization (Ohnensetter et al., 1986). Additional investigations into the mineralogy and concentration mechanisms of PGE from the Chrome intrusion can be found in the works of Talkington and Watkinson (1986) and Scoates et al. (1988).

Since the economic potential of the BRS was identified there have been a variety of investigations on the stratigraphy, petrology and structure of the BRS. Osborne (1949) was the first to describe the magmatic lithologies of the sill in detail. Trueman (1971) completed an investigation on the petrological, structural and magnetic aspects of the BRS and authored three preliminary Mines Branch maps (1970 and 1975). In his studies, Trueman (1971) identified 45 layers within the BRS Chrome and Page bodies and proposed that crystallization occurred from the roof of the intrusion as well as accumulation on the floor of the magma chamber. Scoates (1983) established a preliminary stratigraphy for the BRS Chrome body and the works of Williamson (1990) produced detailed 1:100 scale geological maps of the BRS Chrome body. Peck and Theyer (1998) investigated the relationship between the mafic and ultramafic series of the BRS and concluded that the upper mafic series crystallized from plagioclase-rich residual liquids that were formed by fractional crystallization of the stratigraphically lower ultramafic series. Nageri (1990) investigated the relationship between the subsill ultramafic intrusions north of the BRS Maskwa-Dumbarton body and concluded that the subsill ultramafic intrusions are separate from the BRS and do not represent a feeder to the BRS.

In regards to the origin of the BRS, several different emplacement models have been proposed. The sill was considered by Bateman (1943) to be the result of two different magma pulses: the first being of ultramafic composition and the second of mafic composition. Osborne (1949) proposed a complex multi-injection model. Trueman (1971), Juhas (1973) and Scoates (1983) all supported a single magmatic injection model where the layering was formed by subsequent crystal fractionation and gravitational differentiation. Theyer (1985) interpreted unusual cooling conditions that require several magma pulses and cast doubt on a single magmatic intrusion model. The one similarity between these models is that all of them propose the BRS was originally emplaced as a single continuous intrusion that was subsequently block faulted producing the separate BRS bodies.

1.3 Objectives of this study

This project was initiated as part of a joint industry – government – university research program on the Bird River greenstone belt. The purpose of this project is to investigate and develop a petrogenetic model for the emplacement of the western half of the BRS and establish the controls on Cr-Ni-Cu-PGE mineralization. To accomplish this, several objectives were outlined:

1) map and compare the internal stratigraphy of the separate bodies of the BRS,
2) examine the contact relationships of the BRS to the surrounding Bird River greenstone belt formations,
3) determine the extent of block faulting and subsequent offsets within the BRS intrusive bodies,
4) test the single magmatic injection model against the multi-magmatic injection model,
5) characterize the Cr-Ni-Cu-PGE mineralization and examine the lateral continuity of mineralization across the separate bodies of the BRS, and
6) determine the nature of the sulphur source.

1.4 Method

To achieve the above objectives, both field and laboratory techniques were utilized. Field work was conducted during the summers of 2005 and 2006. The western bodies of the BRS and adjacent Bird River greenstone belt formations were mapped at a scale of 1:5000 (Mealin, 2005 and 2006) and diamond drill cores which were made available by Gossan Resources Ltd. were examined. Samples from outcrops and drill cores were collected for assay and whole rock lithogeochemical analyses. Of these, four samples were analyzed for full PGE suites and sulphur isotope analyses were completed on thirteen samples from various locations.

In addition to the outcrop grab samples and drill core, samples were submitted for whole rock lithogeochemical analyses from the western and central channel cuts collected by P. Theyer with the Manitoba Geological Survey between 1982 and 1984 (Theyer, 1985). The western channel samples crosscut the ultramafic portion of the BRS Chrome body and the central channel samples crosscut the gabbroic portion. These provide a nearly continuous cross-section of one of the BRS central bodies.

Whole rock lithogeochemical analyses, assays and full PGE suite geochemical analyses were performed by Activation Laboratories Ltd. located in Ancaster, Ontario. The samples were crushed and pulverized with mild steel which minimized contamination of the samples; the only possible contaminant added is Fe (up to 0.2%). The samples for whole-rock lithogeochemistry were digested in a weak nitric acid after lithium metaborate/tetraborate fusion. This digestion method ensured total metals, particularly for elements like rare-earth elements (REE) in resistant phases, were put into solution. The samples were then analyzed by Induced Coupled Plasma-Mass Spectrometry (ICP-MS). Samples for precious (Pt, Pd, Au) and base metal (Ni, Cu, Co) analysis were fire assayed using the lead fire assay method, digested in concentrated HCl and analyzed by ICP-MS. Of these samples, four were selected for full PGE suite (Os, Ir, Ru, Rh, Pt and Pd), Au and Re analysis. The samples were fire assayed using the nickel sulphide fire assay method and analyzed by Instrumental Neutron Activation Analysis (INAA).

Sulphur isotope analyses were performed by the University of Waterloo-Environmental Isotope Laboratory located in Waterloo, Ontario. Sulphide minerals were

manually separated from the rock samples using a dremel tool and weighed in tin capsules (approximately 0.1 mg). Vanadium pentoxide was added to each sample. The samples were analyzed using the Isochron Continuous Flow Stable Isotope Mass Spectrometer coupled to a Carlo Erba Elemental Analyzer. In most of the samples the sulphide minerals could not be separated therefore a mixture of sulphide minerals were used.

During the course of this study, forty-three thin sections and seventy-seven polished thin sections were prepared by the Manitoba Geological Survey and Vancouver Petrographics Ltd., respectively. Petrographic analysis was completed on each of the sections. Fine textural characteristics and mineral identification of various sulphide, oxide, and Platinum-Group Mineral (PGM) phases were aided by a scanning electron microscope (SEM) and semi-quantitative chemical analyses performed by the author using the ultrahigh resolution LEO 1530 FE-SEM with EDAX Pegasus 1200 integrated EDX (energy-dispersive X-ray spectroscopy) at the University of Waterloo Advanced Technology Lab.

Chapter 2: Geology of the Bird River greenstone belt

The supracrustal rocks of Bird River greenstone belt are subdivided into six formations (Trueman, 1980) which are from oldest to youngest; Eaglenest Lake Formation, Lamprey Falls Formation, Peterson Creek Formation, Bernic Lake Formation, Booster Lake Formation and Flanders Lake Formation. Numerous intrusive rocks, of which the mafic-ultramafic bodies of the BRS are included, intruded the Bird River greenstone belt at various stages in its formation. The most recent temporal sequence of emplacement of the Bird River greenstone belt formations and intrusive rocks is shown in Table 1. Recent investigations of the geology, deformation and metamorphic history of the Bird River greenstone belt are available in Duguet et al. (2005, 2006 and 2007), Gilbert (2005, 2006 and 2007), Kremer (2005) and Kremer and Lin (2006).

2.1 Supracrustal Formations

2.1.1 Eaglenest Lake Formation

The Eaglenest Lake Formation is exposed on the shores and islands of the Winnipeg River in the vicinity of Eaglenest Lake (Figure 3). To the south, the formation is in fault contact with the Winnipeg River Subprovince and to the north the formation lies in fault contact with the Lamprey Falls Formation.

The Eaglenest Lake Formation consists of metamorphosed volcanic and pebbly wackes, volcanic sandstones, biotite schists and amphibolites. Banded iron formations, composed of pyrrhotite, magnetite, pyrite and interlayered chert are reported near the northern fault contact with the Lamprey Falls Formation (Trueman, 1980). The original stratigraphic position of the Eaglenest Lake Formation is uncertain as it is in fault contact with the Lamprey Falls Formation (Duguet et al., 2007).

2.1.2 Lamprey Falls Formation

The Lamprey Falls Formation is considered to be one of the oldest units in the Bird River area (Gilbert, 2006) and is present in the northern and southern portions of the Bird River greenstone belt. The northern exposure of the Lamprey Falls Formation is host to

Table 1: Geological formations of the Bird River greenstone belt and intrusive rocks in the Bird River area. From Gilbert (2007) and references therein.

Late intrusive rocks
Granite, pegmatite, granodiorite, tonalite, quartz diorite
(Marijane Lake pluton, **2645.6 ±1.3 Ma** ; Lac du Bonnet batholith, **2660 ±3 Ma** ; Birse Lake pluton, **2723.2 ±0.7 Ma**)
Sedimentary rocks
FLANDERS LAKE FORMATION (**2697 ±18 Ma**)
Lithic arenite, polymictic conglomerate
========== ***Fault, inferred*** ==========
BOOSTER LAKE FORMATION (**2712 ±17 Ma**)
Greywacke-siltstone turbidite, conglomerate
~~ ***Unconformity, inferred*** ~~~~~~~~~~
Intrusive rocks
MISCELLANEOUS INTRUSIONS
Gabbro, diorite, quartz-feldspar porphyry; granodiorite
(Maskwa Lake batholith II, **2725 ±6 Ma** ; Pointe du Bois batholith, **2729 ±8.7 Ma**)
Metavolcanic and metasedimentary rocks
BERNIC LAKE FORMATION (**2724.6 ±1.1 Ma**)
Basalt, andesite, dacite and rhyolite (massive to fragmental); related intrusive rocks and heterolithic volcanic fragmental rocks
PETERSON CREEK FORMATION (**2731.1 ±1 Ma**)
Dacite, rhyolite (massive to fragmental); felsic tuff and heterolithic felsic volcanic fragmental rocks
DIVERSE ARC ASSEMBLAGE
Basalt, andesite, rhyolite, related fragmental and intrusive rocks; heterolithic volcanic fragmental rocks; greywacke-siltstone turbidite, chert, iron-formation; polymictic conglomerate (contains clasts derived from Bird River Sill)
~~ ***Unconformity, inferred*** ~~~~~~~~~~
Intrusive rocks
BIRD RIVER SILL (**2744.7 ±5.2 Ma**)
Dunite, peridotite, picrite, anorthosite and gabbro
========== ***Fault, inferred*** ==========
Metavolcanic and metasedimentary rocks
LAMPREY FALLS FORMATION
Basalt (aphyric to plagioclase-phyric; locally pillowed, amygdaloidal or megacrystic); related volcanic breccia; oxide-facies iron formation
========== ***Fault, inferred*** ==========
EAGLENEST LAKE FORMATION
Greywacke-siltstone turbidite
Older intrusive rocks
Granodiorite, diorite (Maskwa Lake batholith I, **2782 ±11 Ma**, **2844 ±12 Ma**)

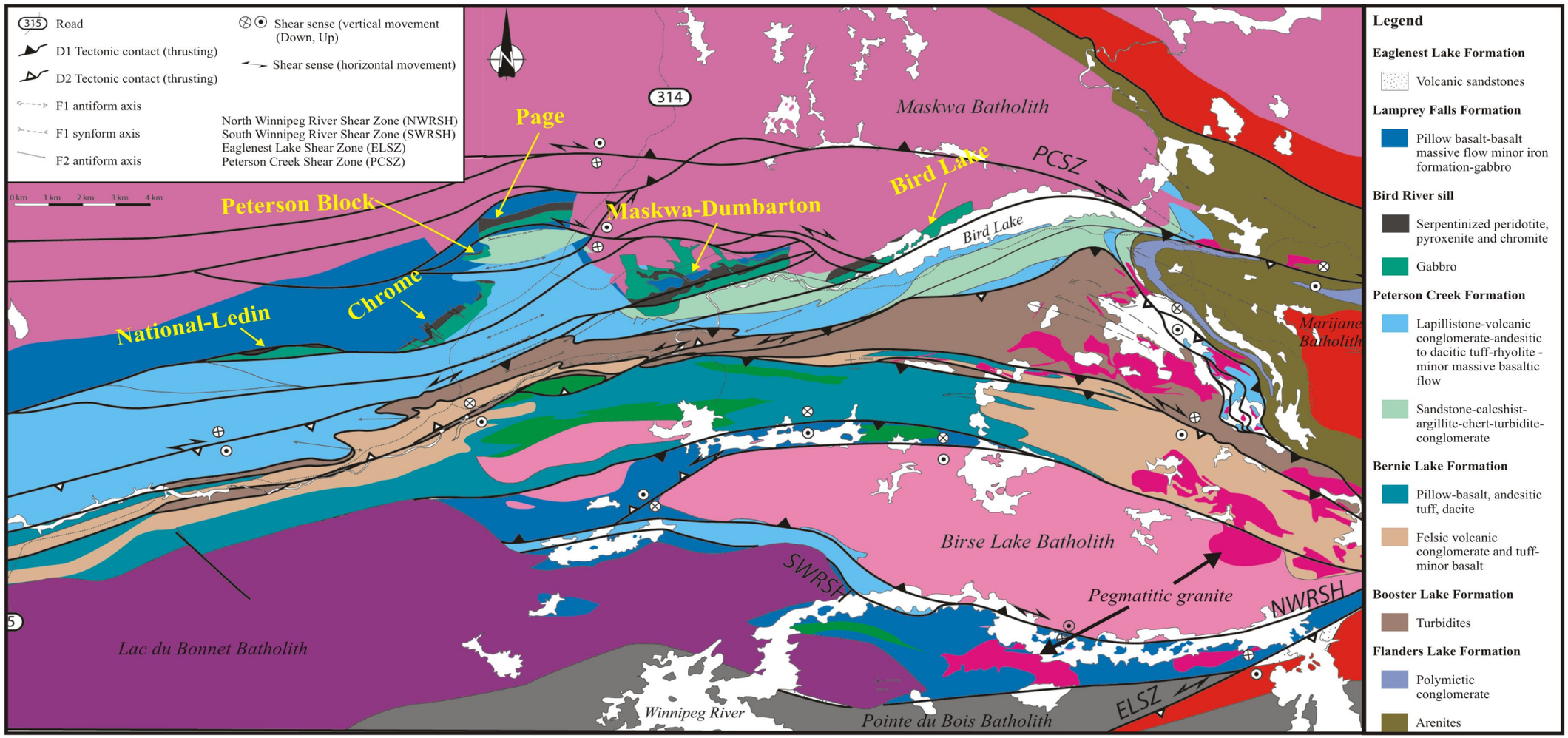

Figure 3: Geological map of the Bird River greenstone belt (Duguet et al., 2007).

the BRS (Figure 3) and numerous metagabbros believed by Trueman (1971) to represent hypabyssal metagabbro sills but the relationship to the BRS is unknown. The Lamprey Falls Formation intrudes the Maskwa Lake batholith and is unconformably overlain to the south by the Peterson Creek Formation. The Peterson Creek Formation in this location was originally classified as the Bernic Lake Formation by Trueman (1980) but has been reassigned by Duguet et al. (2006). In this study, the rocks in this area will be referred to as Peterson Creek Formation.

In the study area, the Lamprey Falls Formation is composed of massive to pillowed flows that range from aphyric to megacrystic. The pillowed basalts are metamorphosed to greenschist facies and are generally weak to moderately deformed and locally brecciated (Figure 4A and B). Alteration is minor and restricted to epidote and quartz veinlets introduced during deformation (Peck et al., 1999). Numerous chlorite veinlets were also observed in this study. Pillow tops indicate a south to southeast younging direction. Gilbert (2005) demonstrated that the basalt flows are geochemically akin to modern back-arc-basin basalt but are also similar to that of mid-ocean-ridge basalts (MORB).

Petrographic examination of the metabasalts in this study indicates the metabasalts are composed of tremolite-actinolite, chlorite, clinozoisite, plagioclase, quartz and trace amounts of unidentified Fe-oxide/hydroxide minerals. Tremolite-actinolite is the dominant metamorphic mineral, which formed at the expense of pyroxene. Clinozoisite and chlorite are present in subordinate amounts. Plagioclase exhibits extensive saussuritization with clinozoisite as the dominant product. Chlorite, present throughout many of the thin sections, is strongly concentrated within and along dominantly quartz-filled fractures and veinlets. The unidentified Fe-oxide/hydroxide minerals, together with rutile and/or anatase, formed at the expense of ilmenite.

Historically, the formation immediately south of the BRS Page body has been treated as part of the overlying sedimentary and mafic volcanic sequences of the Peterson Creek Formation (Figure 2). However, during the mapping in this study southward from the BRS Page body, southward facing pillowed metabasalts and massive metabasalts with similar appearance to the Lamprey Falls Formation were observed. It is interpreted that these metabasalts belong to the Lamprey Falls Formation. To test this interpretation,

samples were collected for lithogeochemical analysis to be compared with volcanic samples from the Lamprey Falls Formation and the Peterson Creek Formation. It is concluded that the metabasalts south of the BRS Page body are part of the Lamprey Falls Formation and thus the BRS is not in direct contact with the Peterson Creek Formation in the vicinity of the Page body. These results are presented and discussed in section 4.1 Geochemistry of the Lamprey Falls Formation and Peterson Creek Formation.

There are several east-west and north-west trending shear zones which cross-cut the Lamprey Falls Formation (Figure 3 and Figure 5). The position and extent of the shear zones are based on mapping from this study and that of Duguet (2006 and 2007). The east-west trending shear zone south of the BRS Page body and several of the minor northwest trending shear zones north of the BRS Chrome and Peterson Block bodies are mineralized with minor to trace amounts of chalcopyrite, pyrite and pyrrhotite. Galena was identified in quartz-veins north of the BRS Peterson Block body. Mineralization is addressed further in Chapter 5: Bird River Sill Cr-Ni-Cu-PGE Mineralization.

Lamprey Falls Formation Metagabbros

Davies (1952) mapped numerous east-trending gabbroic intrusions north of the BRS which are in this study referred to as the Lamprey Falls Formation metagabbros. The location and extent of the metagabbros in the study area (Figure 5) were interpreted from the total field magnetic survey made available by Gossan Resources Ltd. The Lamprey Falls Formation metagabbros are massive, weakly deformed and composed of saussuritized plagioclase in a matrix of tremolite-actinolite with lesser magnetite, unidentified Fe-oxide/hydroxide minerals, and secondary quartz and quartz-carbonate veining (Trueman, 1980). Contacts with host Lamprey Falls Formation metabasalts were not exposed in the study area but are reported to be sharp, exhibit a finer grain size relative to the rest of the metagabbro and are slightly sheared (Trueman, 1980).

The Lamprey Falls Formation metagabbros were interpreted by Juhas (1973) as part of the BRS, but they have since been treated as separate intrusions. Trueman (1980) interpreted them as Lamprey Falls Formation hypabyssal gabbroic intrusions. In summary, the nature of the metagabbros, their age and relationship to the BRS is unknown. To address this problem, two samples were collected for lithogeochemical analysis for a comparison study with samples from the Lamprey Falls Formation and

BRS. The results show the Lamprey Falls Formation metagabbros represent coarse-grained flows genetically related to the Lamprey Falls mafic volcanics. Results and discussion are presented in section 4.2 Geochemistry of the mafic series of the Bird River sill and metagabbroic intrusions from the Lamprey Falls Formation.

2.1.3 Peterson Creek Formation

The Peterson Creek Formation outcrops in the northern half of the Bird River greenstone belt. In the study area, the Peterson Creek Formation is in fault contact with but interpreted to overlie the southern exposure of the BRS and Lamprey Falls Formation. The Peterson Creek Formation also outcrops in the southern half of the Bird River greenstone belt and is in fault contact with the Winnipeg River Area Lamprey Falls Formation, Maskwa Lake batholith and the Booster Lake Formation (Figure 3).

The Peterson Creek Formation consists of rhyolite, andesite and minor basaltic flows, lapillistone tuff, pyroclastic breccia and volcanogenic sandstone (Duguet et al., 2007). Pyroclastic breccia and lapillistone predominate in the western and central map area and grade eastwards into lapillistone and tuff (Trueman, 1980). Cross-bedding structures were observed in this study in the western portion of the Bird River belt. A rhyolite from the Peterson Creek Formation has been dated and provided an age of 2731 +/- 1 Ma (Duguet et al., 2007). The chemistry indicates that the volcanic rocks of the Peterson Creek Formation were emplaced in an arc setting (Duguet et al., 2007) and have calcalkaline affinities (Gilbert, 2006 and Duguet et al, 2006).

South of the BRS there is a new, recently defined subzone of the Peterson Creek Formation (Figure 3). This subzone includes turbidites, chert, felsic to mafic tuff, mafic conglomerate, polymictic conglomerate and felsic and mafic volcanic flows (Duguet et al., 2006 and 2007, Gilbert 2006 and 2007) (Figure 4C, D, E and F). The unit is weakly deformed and folded by northeast to east trending upright folds (Duguet et al., 2007). The base of the unit is composed dominantly of mafic and polymictic conglomerate comprised of unsorted basalt, gabbro, rhyolite, wacke-siltstone and chert clasts locally interbedded with massive basalt (Gilbert, 2007). The basal subunit is overlain by a wacke-siltstone-conglomerate member and the upper subunit is comprised of white laminated chert (Duguet et al., 2006).

There are two models regarding the relationship between the BRS and Peterson Creek Formation. Prior to the study of Trueman (1980) the BRS was believed to have intruded along the Lamprey Falls Formation (metavolcanic) - Peterson Creek Formation (metasedimentary) contact. Trueman (1980) proposed that the Peterson Creek Formation overlies the BRS and the contact, everywhere delimited by a fault, represents an unconformity. This hypothesis was based on the identification of detritus from the sill (anorthosite, anorthositic gabbro and chromite) in the polymictic conglomerates, located south of the BRS Chrome body. A study by Peck et al. (1999) noted that the pebbles and cobbles in the conglomerates are subrounded indicating that the BRS was unroofed in order to produce the heterolithologic debris flow deposit which likely occurred in a subaerial or shallow marine environment. The presence of BRS detritus within polymictic conglomerates was confirmed in this study. Anorthosite and anorthositic gabbro were identified south of Chrome, Peterson block and National-Ledin bodies. Also, in an earlier study, a rhyolite from the Peterson Creek Formation was dated and has a U-Pb zircon age of 2741 Ma which indicates the Peterson Creek Formation is younger than the BRS (Peck et al, 1999).

2.1.4 Bernic Lake Formation

The Bernic Lake Formation outcrops in the central portion of the belt and is in fault contact with the Booster Lake and Peterson Creek Formations. The contact between the Bernic Lake and Booster Lake Formations is an unconformable contact (Trueman, 1980 and Gilbert, 2007). The Bernic Lake Formation displays geochemistry akin to arc-tholeiite (Gilbert, 2006).

The Bernic Lake Formation is composed of basalt with subordinate andesite, dacite, rhyolite, iron formation and minor volcanic sandstone (Duguet et al., 2007). The dominant rock type is conglomerate. Iron formations are interlayerd throughout as thin laterally persistent bands (Trueman, 1980). All these rock types have been metamorphosed up to the middle-amphibolite facies (Duguet et al., 2007). The formation is widely intruded by granodiorite, diorite and gabbro plutons (Duguet et al., 2007).

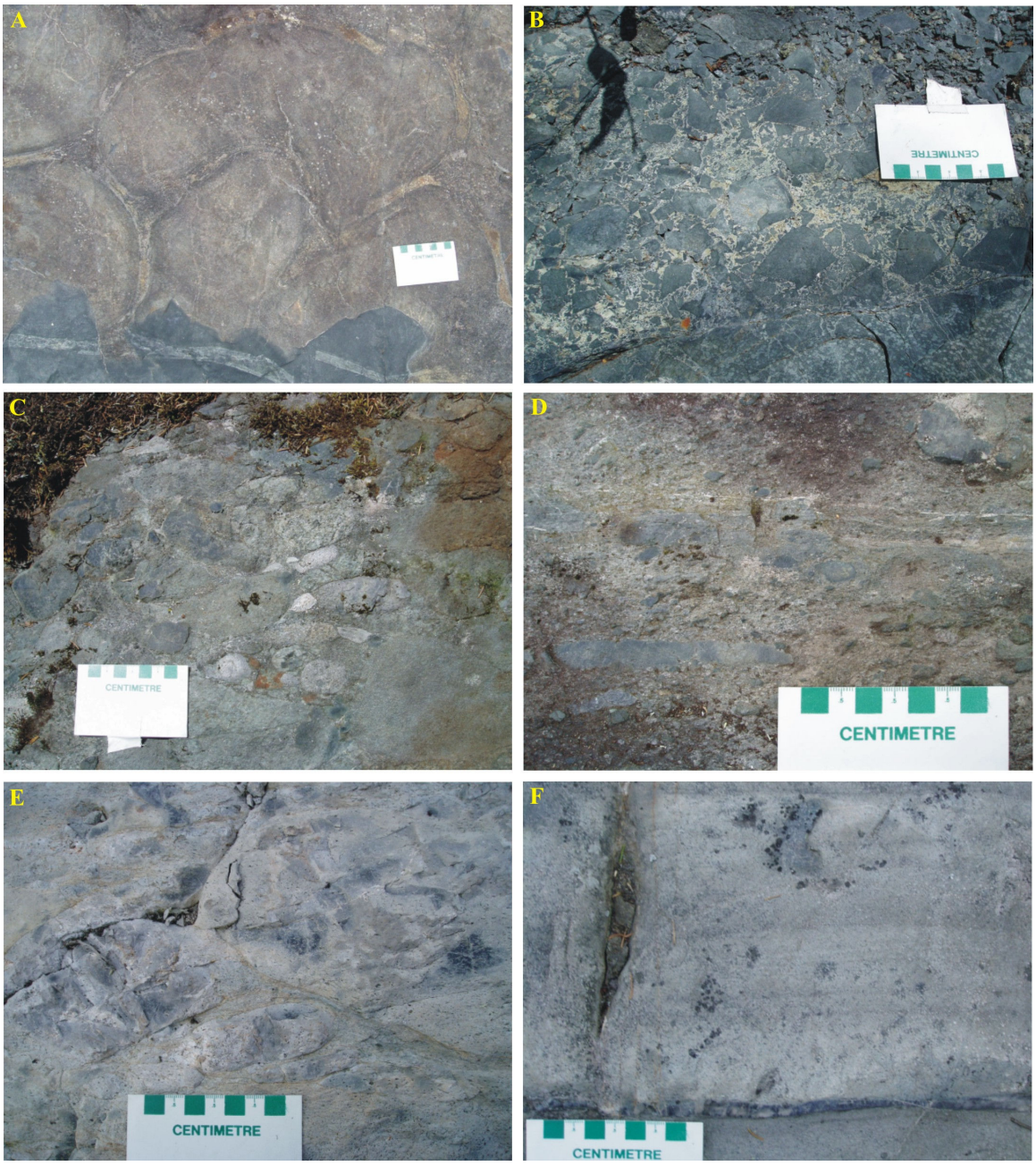

Figure 4: Photographs of the Lamprey Falls Formation metavolcanic and Peterson Creek Formation metasedimentary sequences. A) Weakly deformed pillowed basalts from the Lamprey Falls Formation. B) Brecciated pillowed basalt selvages in an epidote matrix from the Lamprey Falls Formation. C), D) and E) Polymictic conglomerate, from the Peterson Creek Formation south of the Bird River sill Page body. F) Turbidite, from the Peterson Creek Formation east of the Bird River sill Peterson Block body.

2.1.5 Booster Lake Formation

The Booster Lake Formation is present along the north contact of the Bernic Lake Formation. To the east, the Booster Lake Formation is in fault contact with the Flanders Lake Formation and to the north in fault contact with the Peterson Creek Formation.

Rock types of the Booster Lake Formation include wacke-mudstone turbidites and minor iron formations. Primary structures are abundant in the turbidites and include the classical Bouma sequence of graded bedding, laminated bedding, and ripple cross-bedding (Trueman, 1980). The formation exhibits regional amphibolite facies metamorphism (Gilbert, 2005).

2.1.6 Flanders Lake Formation

The Flanders Lake Formation is considered to be the youngest unit of the Bird River greenstone belt. The formation outcrops in the eastern portion of the Bird River belt in the areas of Flanders Lake - Ryerson Lake - Starr Lake - Reynar Lake. The formation is in fault contact with the Peterson Creek, Booster Lake and Bernic Lake Formations and is intruded by the Marijane Lake pluton (Duguet et al., 2007).

Rock types of the Flanders Lake Formation include polymictic conglomerate and related metamorphosed lithic arenite. The arenite is the dominant rock type in the formation and it exhibits graded bedding and cross-bedding (Trueman, 1980). The conglomerate contains pebble to cobble sized clasts of tonalite, basalt, gabbro, rhyolite, quartzite and iron formation. Primary sedimentary features including graded and inverse graded beds, cross-bedding, scour and fill structures, and laminations, are well preserved throughout the formation (Trueman, 1980).

2.2 Intrusive Rocks

The oldest intrusive rocks in the Bird River area are the granodiorite and diorite rocks of the Maskwa Lake batholith. The Maskwa Lake batholith is a large polyphase pluton, composed of several generations of melt (Duguet et al., 2007) and has been dated at 2725 +/- 6 Ma (U-Pb on zircon; Wang, 1993) and 2832 +/- 3 Ma (U-Pb on zircon; Duguet et al., 2007). It is composed of massive, coarse-grained granite, diorite and quartz-diorite. The dominant rock type is quartz-diorite with a moderately developed

gneissic fabric. The batholith is cross-cut by the Peterson Creek Shear Zone (Figure 3) and underwent heterogeneous deformation (Duguet et al., 2007).

The Lamprey Falls Formation overlies the Maskwa Lake batholith and numerous mafic dykes with REE profiles identical to those of the Lamprey Falls Formation cross-cut the Maskwa Lake batholith (Duguet et al., 2007). One interpretation of these dykes is that they are synvolcanic feeders to the Lamprey Falls Formation (Peck et al., 1999). The Maskwa Lake batholith is in contact with the northern margin of the BRS on the Bird Lake and Maskwa-Dumbarton bodies and the eastern boundary of the Page body. Contacts between the batholith and the BRS are not exposed in the study area but are reported to be faulted (Trueman, 1971).

Other intrusive rocks of the Bird River area include the BRS, numerous gabbro and quartz-feldspar porphyry dykes, granitic plutons and related pegmatites. The mafic series of the Chrome body of the BRS has an age of 2744.7 +/- 5.2 Ma (U-Pb on zircon; Wang, 1993). Granitic plutons in the Bird River area include the Pointe du Bois batholith (2729 +/- 8.7 Ma; Wang, 1993), Birse Lake pluton (2723.2 +/-0.7 Ma), Lac du Bonnet batholith (2660 +/-3 Ma; Wang, 1993), Marijane Lake pluton (2645.6 +/-1.3 Ma; Wang, 1993) and related dykes, stocks, sills of pegmatitic granite and pegmatite. Included in these are the rare-metal bearing pegmatite deposits (e.g. the TANCO mine) which intrude the Bernic Lake Formation of the Bird River greenstone belt.

Chapter 3: Geology of the Bird River sill

The purpose of this section is to compile the previous geological and structural data and augment these with new observations from this study to produce an accurate overall description of the BRS. The synthesis will address the first three objectives outlined in Chapter 1:

1. Examine and compare the internal stratigraphy of the separate bodies of the BRS.
2. Examine the contact relationships between the BRS and surrounding Bird River greenstone belt formations.
3. Determine the extent of block faulting and subsequent offsets within the BRS intrusive bodies.

3.1 General Geology

Mapping of the western half of the BRS and immediate surrounding formations of the Bird River greenstone belt was completed over the 2005 and 2006 summer field seasons. The final map (Map A in back pocket) is a compilation of the preliminary BRS map of Mealin (2005 and 2006) together with data from Davies (1952), Duguet et al. (2006) and interpretations from a total field magnetic survey (made available by Gossan Resources Ltd.).

The BRS is composed of differentiated, layered, mafic-ultramafic intrusions located within the Lamprey Falls Formation at/near the Peterson Creek Formation contact. The sill trends easterly, has a southward younging direction and has a U-Pb zircon age of 2744.7 ±5.2 Ma (Wang, 1993). The BRS is made-up of several separate mafic-ultramafic bodies known from west to east as: National-Ledin, Chrome, Peterson Block, Page, Maskwa-Dumbarton and Bird Lake (commonly referred to as the Petra-bar body) (Figure 3). This study focussed on the western half of the BRS (Page body to the National-Ledin body) (Figure 5). Therefore the following discussion is based on and relates to the western half of the BRS.

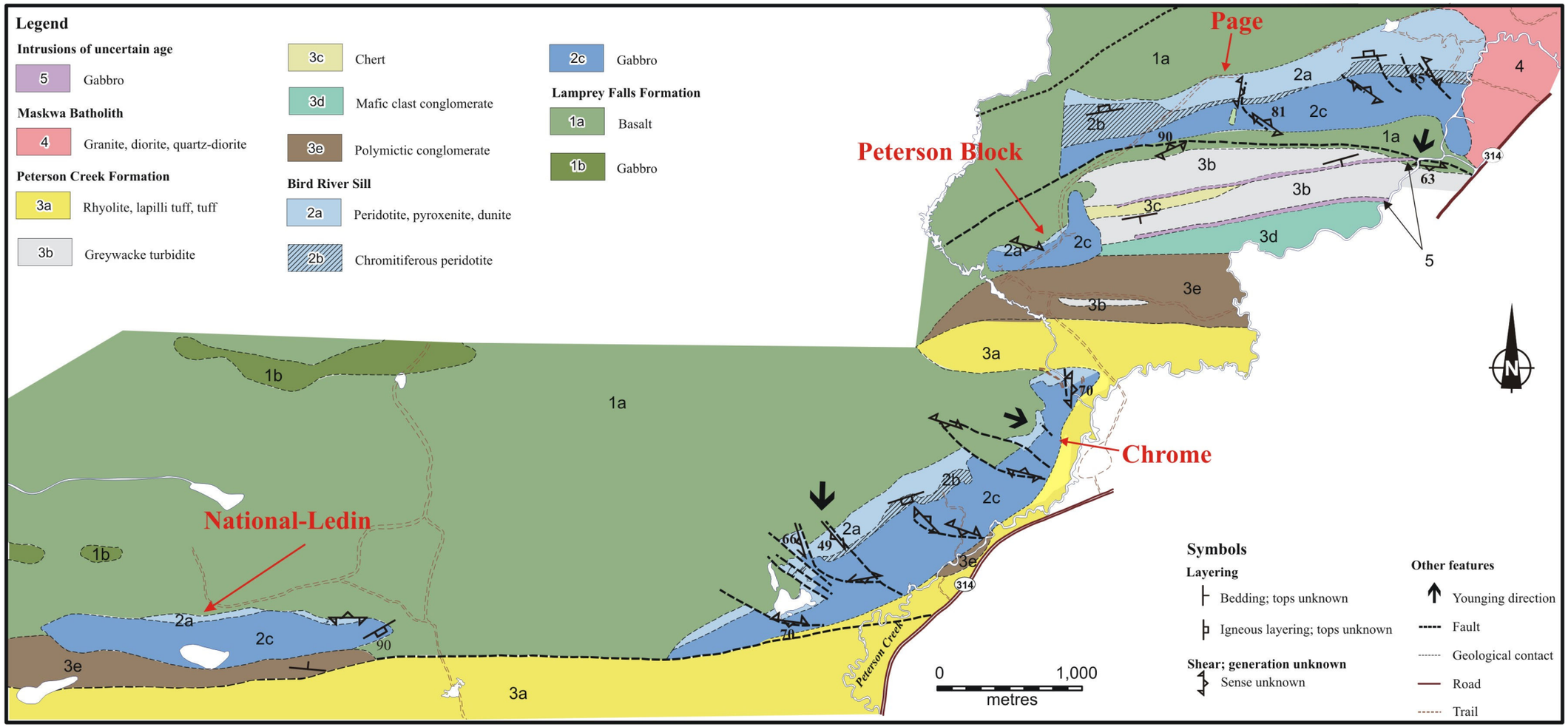

Figure 5: Simplified geological map of the National-Ledin, Chrome, Peterson Block and Page bodies of the Bird River sill. Map modified from Mealin (2006).

The Wards intrusion (commonly referred to as the Coppermine Bay intrusion) is a gabbroic body located in the west end of the study area (Map A in back pocket). The intrusion is unique in comparison to the BRS in that it is comprised of mineralized metagabbro and has no known ultramafic component. The intrusion differs from the nearby Lamprey Falls Formation metagabbros in that it is host to chromite and sulphide mineralization. Chromite mineralization occurs approximately 10 m above the base of the intrusion within a varitextured metagabbro and consists of massive seams, up to 1 m wide (Peck and Theyer, 1998). Disseminated pyrrhotite and chalcopyrite occur within an overlying disrupted anorthositic layer (Peck and Theyer, 1998). The Wards intrusion was not mapped in this study but the position and extent of the intrusion is inferred from the total field magnetics survey.

A magnetic anomaly of similar magnitude, stratigraphic position and orientation as the other BRS intrusions was identified west of the BRS National-Ledin body. The approximate location of the magnetic anomaly is outlined on Map A (back pocket). It is inferred that this magnetic anomaly may represent an extension of the BRS but due to lack of outcrop exposure in this area this interpretation could not be confirmed.

3.2 Stratigraphy and Metamorphism

Osborne (1949) originally subdivided the BRS into four basic magmatic series and starting from the base these are a marginal mafic series, an ultramafic series, a transition series, and a mafic series. Trueman (1971) divided the BRS into forty-five layers grouped into seven rock units: marginal gabbro, serpentinized peridotite, chromitiferous peridotite, pyroxenite, anorthositic gabbro, hornblende gabbro and porphyritic gabbro. The Trueman (1971) subdivision has since been expanded upon by Scoates (1983) and Williamson (1990). The stratigraphy is based on extensive detailed mapping of the exposed central portion of the BRS Chrome body. Observations from the current study confirmed the previously defined stratigraphy with some modifications (Figure 6). Descriptions of each stratigraphic unit from studies of Osborne (1949), Trueman (1971) and Scoates (1983), with new observations from the current study, are summarized in the following sections.

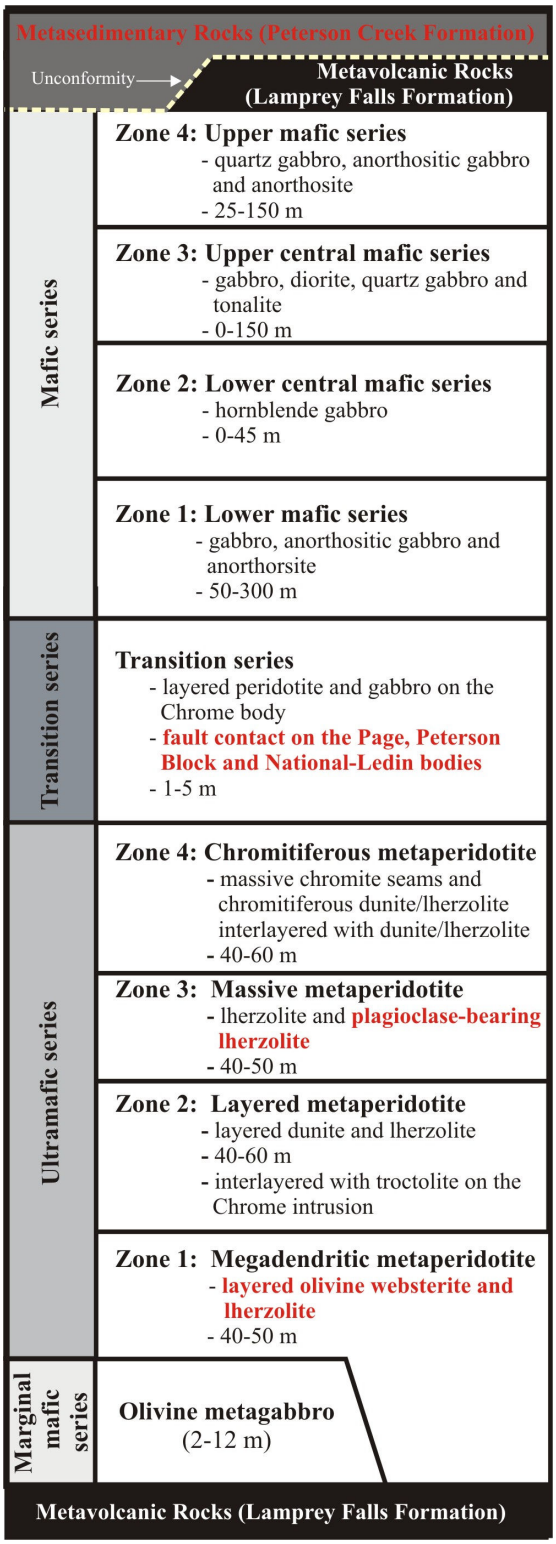

Figure 6: Generalized stratigraphic column of the Bird River sill modified after Trueman (1971) and Scoates (1983) with new observations from this study (highlighted in red). Zones within the ultramafic series and mafic series are based predominantly on the stratigraphy of the Bird River sill Chrome intrusion.

An alternative stratigraphy for the ultramafic series of the BRS is proposed by Theyer (1991), who divided the ultramafic series into a "lower ultramafic series" and an "upper ultramafic series", separated by a gabbroic zone. The lower ultramafic series is characterized by textural layering (each sequence referred to as a periodic unit) defined by systematically recurring variations of olivine crystal habits, size, and ratio of crystals versus matrix. The igneous cycles defined by Theyer (1991) are based on the morphology of serpentine pseudomorphs after olivine. The base of a periodic unit is characterized by a layer in which small (1.2 mm average long axis), tightly packed, equant, granular olivine crystals occur as an adcumulate (Theyer, 1991). Stratigraphically upwards, there is a gradational increase in average olivine crystal size and decrease in crystal packing density with rare interspersed large olivine crystals (2-3 mm average in length). The top portion of each periodic unit is characterized by a subunit marked by the appearance of increasing numbers of tabular olivine crystals which exhibit increasing curvature of their long axis (producing "hopper" olivines) stratigraphically upwards (Theyer, 1991). The rocks of the upper ultramafic series are comparable to those of the lower ultramafic series, comprising dunites, olivine bearing rocks with varying amounts of pyroxene and chromite but periodic units are absent (Theyer, 1991).

Metamorphic history of the BRS has been studied and is discussed by Juhas (1973), Coats and Buchan (1979) and Trueman (1980). In general, the sill has been metamorphosed to greenschist facies, and locally by contact metamorphism to lower amphibolite facies adjacent to granitic intrusions within the Maskwa-Dumbarton body. Primary minerals are extensively replaced but primary textures are preserved with some loss of primary textures due to metamorphism. The metamorphic assemblages are further discussed below.

3.2.1 Marginal Mafic Series

The marginal mafic series was initially reported by Osborne (1949) and included in the subdivision of Trueman (1971) but was omitted from subsequent work. In this study, a gabbroic unit was observed at the base of the BRS in contact with the underlying Lamprey Falls Formation on the Chrome and Page bodies of the BRS. An intrusive

contact between the ultramafic series of the Page body and the metabasalts of the Lamprey Falls Formation was also observed indicating that the marginal mafic series is not laterally continuous across the base of the Page body.

The petrography of the marginal gabbroic unit corresponds with the general description of the marginal gabbroic series defined by Osborne (1949). Osborne (1949) reported that this unit has a thickness in excess of 9 m (approximately 30 feet) and is comprised of a medium grained olivine pyroxene gabbro. The gabbro observed on the Page body of the BRS ranges from 2 to 12m thick, appears to be homogenous, is grey to grey-green in colour, non-magnetic and fine- to medium-grained. Abundant dark to black crystals comprised of pyroxene which appear to be altered to chlorite and fine-grained amphibole are present throughout. The marginal gabbro from the Chrome body is fine- to medium-grained, dark grey in colour and non-magnetic. Weathered surfaces have a rough patchy texture, pink-orange to pink-grey colour and are rusty along shear zones. Modal mineralogy based on whole-rock normative (CIPW) compositions of the mafic series from the Chrome and Page bodies indicates it is an olivine gabbro. The marginal gabbro from the Page body is enriched in plagioclase and depleted in olivine compared to that of the Chrome body (Table 1).

Table 2: Modal mineralogy of the marginal mafic series of the Chrome and Page bodies, Bird River sill

CIPW Norm Weight %: Marginal Mafic Series				
Mineral Name:	Chrome body:			Page body:
Plagioclase	20.7	19.6	11.2	49.7
Orthoclase	0.12	0.18	0.12	2.36
Corundum	9.16	9.38	16.02	0.00
Diopside	0.00	0.00	0.00	20.2
Orthopyroxene	21.1	21.3	19.0	10.6
Olivine	44.1	44.5	48.0	11.1
Ilmenite	2.07	2.32	2.47	3.21
Magnetite	2.65	2.78	3.15	2.28
Apatite	0.19	0.05	0.16	0.32
Zircon	0.00	0.00	0.00	0.01
Chromite	0.06	0.06	0.07	0.03
Pyrite	0.00	0.00	0.00	0.21
Total	100	100	100	100

Petrographic analysis in this study confirms the observation of Osborne (1949) that the only primary mineral preserved is plagioclase, but it is extensively replaced by clinozoisite. Parts of the unit consist of clinozoisite and plagioclase patches in a matrix of fine tremolite needles and mesh-like chlorite. Tremolite is also present as large platy crystals commonly enclosing clinozoisite and plagioclase patches.

The marginal olivine gabbro on the Chrome body is cut by several cm-wide chlorite-filled fractures which are sulphide-free (Figure 7A, B and C). A chill margin is visible at the contact with the metabasalts of the Lamprey Falls Formation (Figure 7D). Sulphide mineralization was observed in the marginal olivine gabbro from both the Chrome and Page bodies of the BRS and consists of trace fracture-bound chalcopyrite and trace to 2% disseminated pyrrhotite. The fractures are commonly quartz and chlorite filled.

Unique to the Chrome body is the presence of pyroxenite clasts near the Lamprey Falls Formation intrusive contact. The clasts are comprised of small (1-5 cm), black, rounded to elongate pebbles and large (up to 40 cm) angular blocks (Figure 8A and B). The clasts are more resistant to weathering than the surrounding marginal olivine gabbro and thus have a higher relief on outcrop. The clasts consist almost entirely of coarse, anhedral pyroxene crystals. Pyroxene has undergone moderate replacement by tremolite, serpentine and chlorite (Figure 8C). Trace amounts of sulphides were identified and consist of fine disseminated chalcopyrite and pyrite. Chalcopyrite is replaced by covellite along grain boundaries and pyrite exhibits replacement by an unidentified mineral (white-grey mineral under plane-polarized reflected light) (Figure 8D).

3.2.2 Ultramafic Series

The ultramafic series is host to all significant concentrations of Cr-Ni-Cu-PGE mineralization in the BRS. Mineralization is not addressed here but is discussed in Chapter 5: Bird River Sill Cr-Ni-Cu-PGE Mineralization. The ultramafic series varies from a few metres to 200 m in thickness within the Chrome and Page bodies of the BRS. In the Peterson Block and National-Ledin bodies the series is thinner and at most 2-3 metres in width. The ultramafic series is divided into four zones (Figure 6): 1) mega-dendritic metaperidotite zone, 2) layered metaperidotite zone, 3) massive metaperidotite

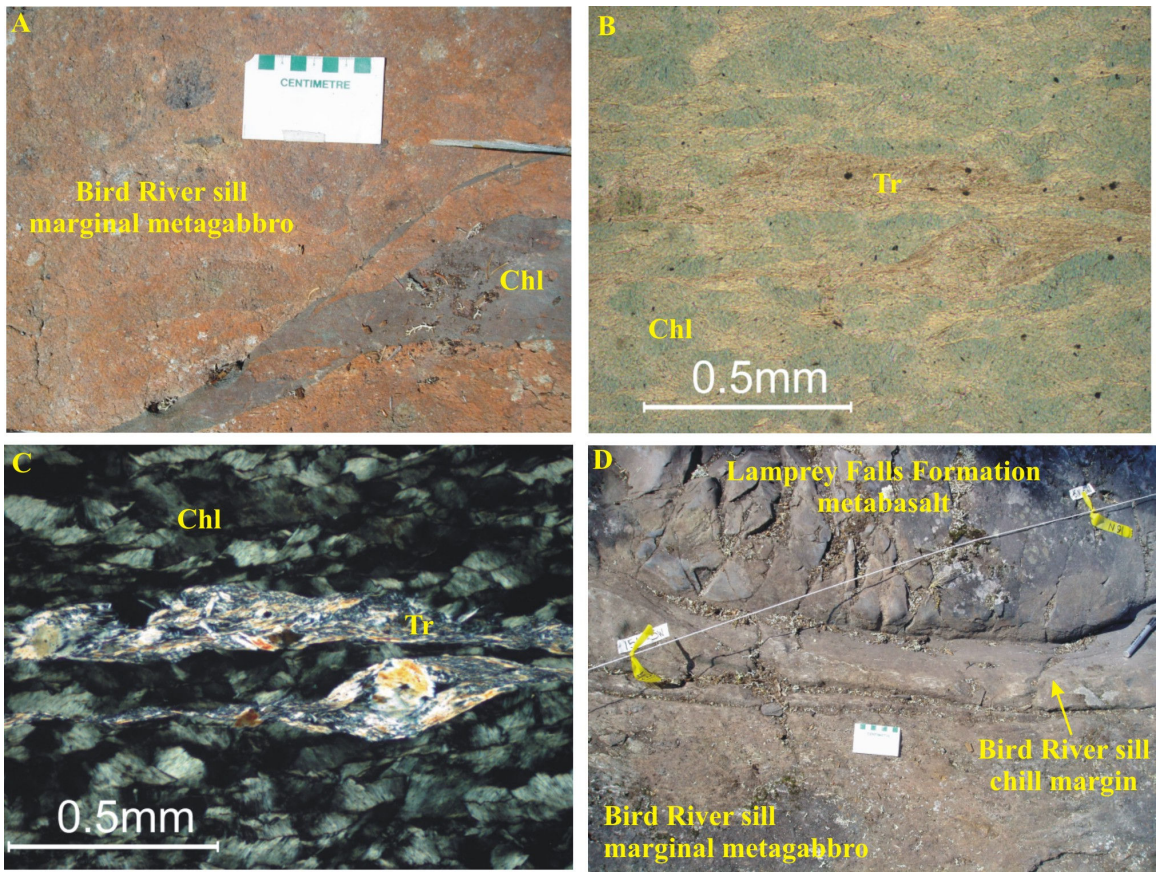

Figure 7: Photographs and photomicrographs of the marginal metagabbro and chill margin from the Chrome intrusion of the Bird River sill. A) Photograph of the chlorite filled fractures that cross-cut the marginal metagabbro of the Chrome intrusion. B) and C) Photomicrographs of the chlorite (Chl) filled fractures with tremolite (Tr) in the marginal metagabbro of the Chrome intrusion; plane-polarized (ppl) (top right) and cross-polarized (bottom left) transmitted light. D) Photograph of the intrusive contact between the Bird River sill marginal metagabbro and the Lamprey Falls Formation metabasalts.

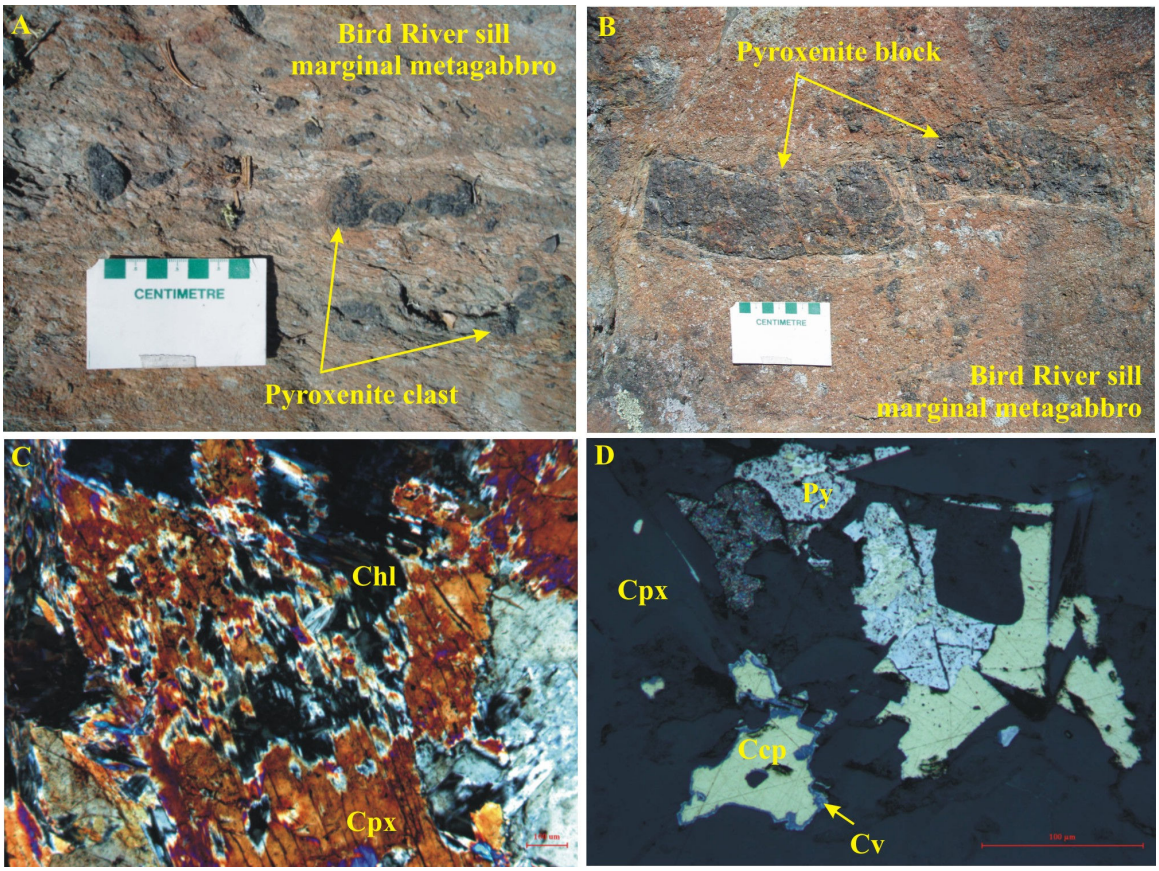

Figure 8: Photographs and photomicrographs of the pyroxenite clasts near the intrusive contact between the Bird River sill Chrome intrusion and the Lamprey Falls Formation. A) Photograph of the pyroxenite clasts in the marginal metagabbro of the Chrome intrusion. B) Photograph of the pyroxenite blocks in the marginal metagabbro of the Chrome intrusion. C) Photomicrograph of a pyroxenite clast showing clinopyroxene (Cpx) with moderate replacement by chlorite; cpl transmitted light. D) Photomicrograph of sulphide minerals present in the marginal metagabbro of the Chrome intrusion. Covellite (Cv) is present as a replacement along grain boundaries of chalcopyrite (Ccp). Pyrite (Py) exhibits replacement by unidentified white-grey mineral; ppl reflected light.

zone, and 4) chromitiferous metaperidotite zone. The following sections incorporate descriptions from Trueman (1971) and Scoates (1983) confirmed by the author in addition to new observations from this study. Due to the poor exposure of the ultramafic series on the Peterson Block and National-Ledin bodies, new observations from this study are dominantly based on the Chrome body but similar sequences are present on the Page body.

Zone 1 of the Ultramafic Series: Megadendritic Metaperidotite

The base of the ultramafic series consists of the megadendritic peridotite suite, as defined by Scoates (1983). The peridotite has a distinct knobby appearance that results from amphibole replacement of pyroxene and large portions of the suite contain long curving and branching amphibole crystals up to 15 cm long (Scoates, 1983). Serpentine pseudomorphs after olivine preserve the primary cumulate textures. The serpentine group minerals consist of antigorite and chrysotile. Antigorite has completely replaced the olivine and is in turn cut by vein and mesh chrysotile (Trueman, 1971). Poikilotic pyroxene (dominantly augite) encloses the serpentine pseudomorph (replaced olivine) grains and is extensively replaced by tremolite, serpentine and chlorite. Pyroxene commonly contains fine dusty magnetite mineralization along partings. Magnetite is also present along fractures within the serpentine pseudomorphs and along grain boundaries.

The mega-dendritic peridotite suites contain greater than 60% pyroxene enclosing fine, equant serpentine pseudomorphs and are interpreted in this study to represent olivine websterite. Pyroxene is extensively replaced by amphibole but relict clinopyroxene grains were observed. The olivine websterite suites are interlayered with lherzolite (where olivine, now serpentine, constitutes approximately 50-70% of the rock). On outcrop, the lherzolite layers exhibit relatively smooth, buff-weathering surfaces and the olivine websterite layers exhibit the distinctive knobby appearance discussed above (Figure 9).

Zone 2 of the Ultramafic Series: Layered Metaperidotite

Stratigraphically above the megadendritic metaperidotite zone is the layered metamorphosed dunite - lherzolite suite, as defined by Scoates (1983). The lherzolite has a rougher weathered surface compared to the very smooth weathered surface of dunite.

Unique to the Chrome body is the presence of troctolite interlayered with the dunite-lherzolite suites (Figure 10A). The troctolite layers were first identified by Theyer (1985) in his western channel cut of the Chrome body. The layers represent the gabbroic zone used to separate the ultramafic series into a "lower ultramafic series" and an "upper ultramafic series" in the alternative stratigraphy proposed by Theyer (1991). The troctolite layers were not observed on the Page body or within the limited exposures of the Peterson Block and National-Ledin bodies of the BRS.

Zone 3 of the Ultramafic Series: Massive Metaperidotite

Stratigraphically above the dunite-lherzolite layered suite is the massive peridotite zone. This zone separates the lower ultramafic series from the upper chromitiferous zone and consists entirely of lherzolite and plagioclase-bearing lherzolite. This peridotite suite ranges upward from a rough textured peridotite to densely packed serpentine-rich rocks that have very smooth weathered surfaces (Figure 10B) (Scoates, 1983). The zone was termed "quiescent peridotite" by Theyer (1985).

Zone 4 of the Ultramafic Series: Chromitiferous Metaperidotite

Chromite is present throughout the ultramafic series as euhedral crystals interstial to serpentine pseudomorphs after olivine ranging from 1 to 5% in abundance but is concentrated in the chromitiferous zone. The chromitiferous zone is located within the stratigraphically upper portions of the ultramafic series near the mafic-ultramafic transition series (Figure 6). The chromitiferous zone is absent on the Peterson Block body but was observed on the Chrome and Page bodies of the BRS and has been reported on the National-Ledin body.

The chromitiferous zone of the Chrome body is comprised of numerous, continuous, massive chromitite (>85% chromite) seams in planar contact with lherzolite and dunite suites, chromitiferous lherzolite (<85% chromite), chromitiferous dunite and 'disrupted' chromitite layers (Figure 10C, D and E). The disrupted chromitite layers commonly exhibit white halos which are interpreted by this study to be the result of extensive talc alteration of olivine surrounding the chromitite (Figure 10F). Chromite layers generally range from millimetres to metres in thickness. Scoates (1983) defined six distinctive chromitite layer suites; lower chromitites, disrupted layer suite, lower main suite, banded-

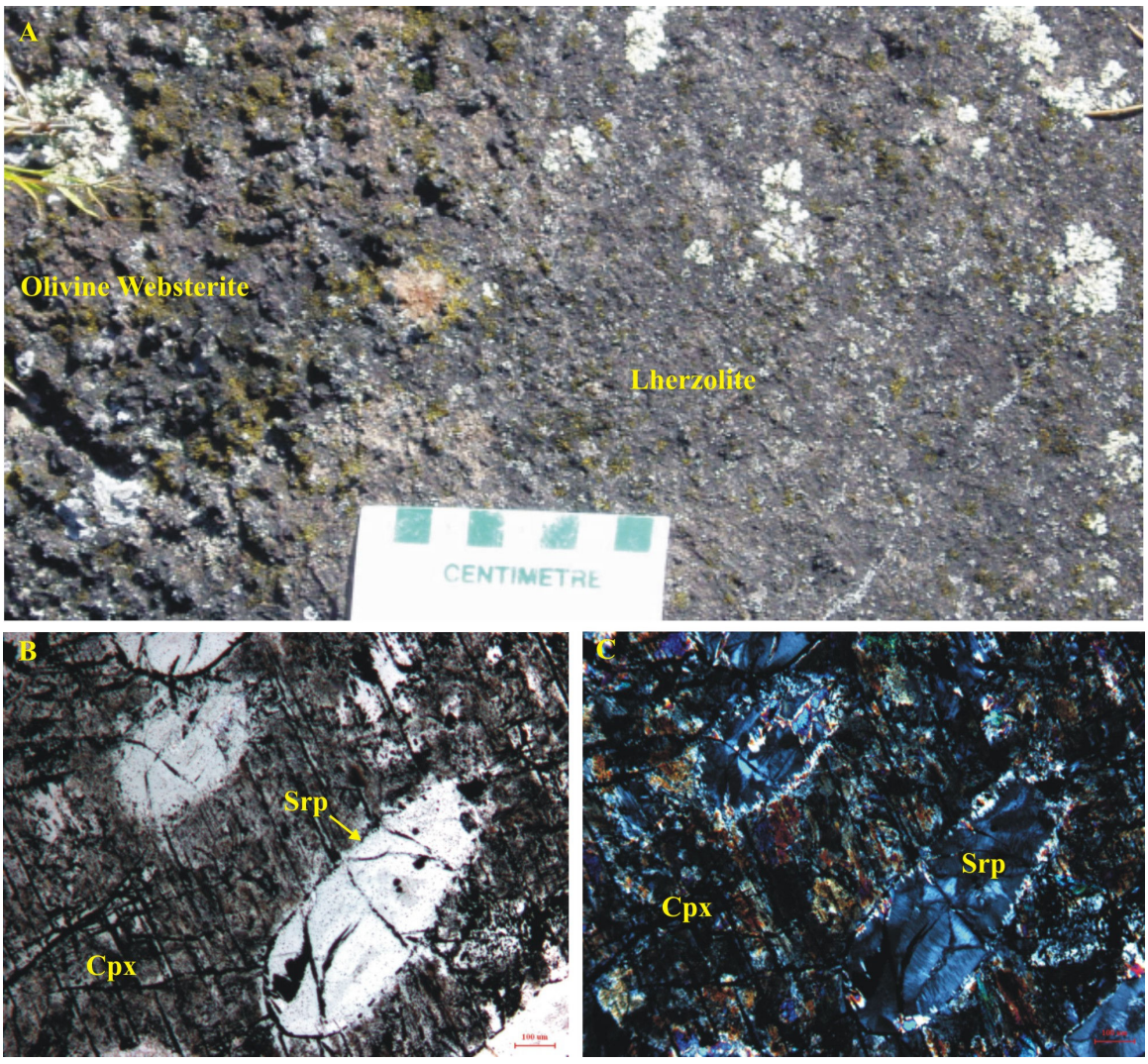

Figure 9: Photographs and photomicrographs of the megadendritic metaperidotite zone of the ultramafic series from the Chrome body of the Bird River sill. A) Photograph of the rough textured olivine websterite interlayed with lherzolite. B) and C) Photomicrographs of serpentine pseudomorphs after olivine (Srp) poikilotically enclosed by clinopyroxene (Cpx); ppl transmitted light (left) and cpl transmitted light (right).

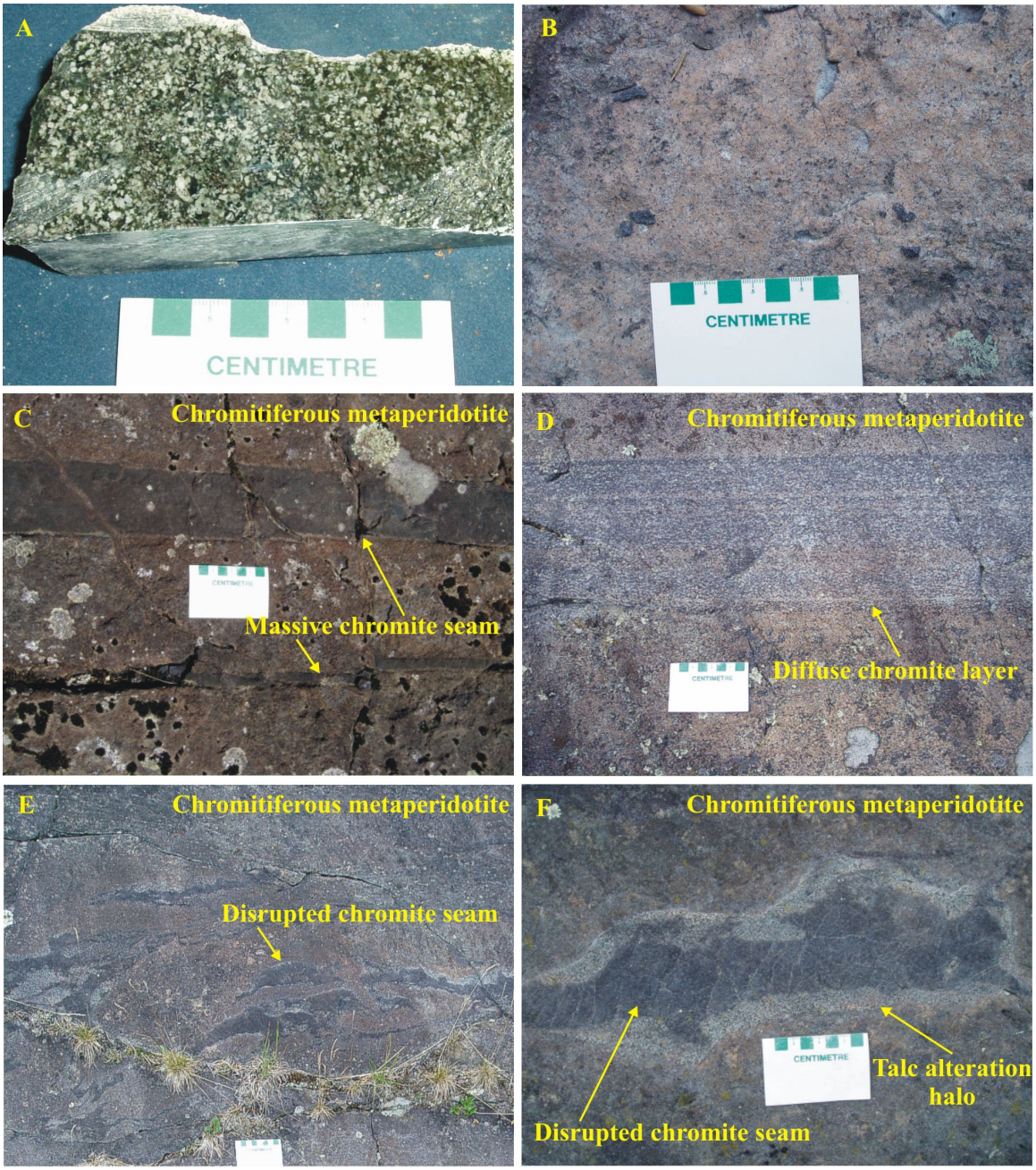

Figure 10: Photographs of the layered metaperidotite zone, massive metaperidotite zone and chromitiferous metaperidotite zone of the ultramafic series from the Chrome body of the Bird River sill. A) Channel sample of troctolite from the layered metaperidotite zone. B) Smooth textured metaperidotite from the massive metaperidotite zone. C) Massive chromite seams from the chromitiferous peridotite zone. D) Diffuse chromite layer from the chromitiferous metaperidotite zone. E) Disrupted chromite seams from the chromitiferous metaperidotite zone. F) Talc alteration halo enclosing a portion of a disrupted chromitite seam from the chromitiferous metaperidotite zone.

layer diffuse layer suite, upper main chromitites and upper chromitites.

Mineralization on the Page body is similar to that on the Chrome body but differs in that it contains chromite "pebbles". The pebbles and chromitite seams are laterally continuous across the length of the Page body. Chromite mineralization and mechanisms for the disrupted chromitite seams and pebbles is discussed in section 5.1 Chromium Mineralization.

3.2.3 Transition Series

The transition series, which separates the lower ultramafic series from the upper mafic series, was observed only on the Chrome body and ranges from 1 to 5 m in thickness. Fault contacts between the lower ultramafic series and upper mafic series were observed on the Page, National-Ledin and Peterson block bodies.

The transition series is comprised of interlayered peridotite and gabbro. It is recognized on outcrop by its smooth, brownish buff weathered surface and consists of a narrow layer marked by gradational changes in the proportions of serpentine pseudomorphs after cumulous olivine and plagioclase (Scoates, 1983). Serpentine pseudomorphs after olivine decreases in abundance upwards and original cumulus plagioclase increases in abundance upwards (Scoates, 1983).

3.2.4 Mafic Series

The mafic series varies from 100 to 600 m in thickness on the Chrome, Page, Peterson Block and National-Ledin bodies. Based on mineralogy, the mafic series is divided into four zones (Figure 6): 1) lower mafic series, 2) lower central mafic series, 3) upper central mafic series, and 4) upper mafic series. The mafic series is host to minor amounts of Ni-Cu-PGE mineralization which is discussed in Chapter 5: Bird River Sill Cr-Ni-Cu-PGE Mineralization.

Trueman (1971) compared the mafic series of the Chrome and Page bodies and attempted to correlate the units between the two bodies. It was shown that the Page body mafic series is not as thick as that of the Chrome body and does not possess many of the layers defined in the Chrome body. In the same study, Trueman (1971) identified cryptic variations of anorthite content in the plagioclase of the gabbroic rocks to indicate

crystallization of the gabbros proceeding from both the roof and floor of the magma chamber inwards.

Zone 1 and Zone 4: Lower and Upper Mafic Series

The lower mafic series is comprised of gabbro, anorthositic gabbro and anorthosite (Figure 6). The upper mafic series is similar to the lower mafic series and is comprised of quartz gabbro, anorthosite and anorthositic gabbro. These units were observed on the Chrome and Page bodies. The lower mafic series is exposed at the National-Ledin body but the upper mafic series is not. The Peterson Block body does not have any exposures of these units.

The rocks range from medium grained to pegmatitic with plagioclase crystals reaching several centimetres in length. Scoates (1983) identified a xenolith-bearing zone within the lower mafic series which is continuous across the Chrome body. This zone is reported to consist of angular to rounded blocks of coarse-grained to pegmatitic anorthositic gabbro in a medium-grained gabbro matrix. The larger fragments range from metre-sized rectangular blocks with sharply angular corners to irregularly-shaped masses with smooth curved outlines (Scoates, 1983). The fragments are believed to be disrupted pre-consolidated material that descended from above representing rocks that originally crystallized near the intrusion roof; this supports the model of Trueman (1980) for the gabbro crystallization sequence. No pegmatitic anorthositic gabbro xenoliths were identified in the current study but ultramafic xenoliths were identified on the Page body, approximately 1 metre above the faulted mafic-ultramafic series contact. The fragments consist of round medium-grained, magnetic, peridotite set in a medium- to coarse- grained gabbro matrix (Figure 11A). The nature of these xenoliths suggests they are fragments of disrupted pre-consolidated ultramafic layers and did not form near the intrusion roof like that of the anorthositic xenoliths reported to exist on the Chrome body.

Petrography of the gabbroic rocks indicates that they are composed dominantly of primary plagioclase with varying amounts of pyroxene, hornblende and replacement products actinolite-tremolite, clinoamphibole, clinozoisite, albite and chlorite. Plagioclase forms coarse-grained, euhedral to subhedral, zoned crystals and exhibits saussurization to clinozoisite and minor albite along grain boundaries and fractures

(Figure 11B). Pyroxene and hornblende form coarse- to medium-grained subhedral to anhedral crystals. Both exhibit moderate to extensive replacement by blades of actinolite-tremolite, fine-grained clinoamphibole and fine-grained chlorite. Trace amounts to 5% of interstitial quartz are present throughout.

Trace amounts of chalcopyrite, pyrite and minor amounts of ilmenite are present in both the lower and upper mafic series. Chalcopyrite and pyrite occur as fine disseminations within pyroxene and associated replacement products. Ilmenite forms anhedral masses and is interstial to primary pyroxene crystals (Figure 11C). Chalcopyrite is commonly present with the ilmenite masses.

Zone 2: Lower Central Mafic Series

The lower central mafic series is composed of hornblende gabbro. Hornblende gabbro was not observed in this study but is described in detail by Trueman (1971), who reported that it forms two layers in sharp contact with the anothositic gabbros of the lower mafic series on the Chrome body. The hornblende gabbro consists largely of hornblende with lesser amounts of plagioclase laths enclosed in clinoamphibole (Trueman, 1971). The metamorphic assemblage consists of clinozoisite, albite and chlorite that formed at the expense of hornblende and plagioclase (Trueman, 1971).

Zone 3: Upper Central Mafic Series

The upper central mafic series is composed of diorite, quartz gabbro and tonalite. The diorite and quartz gabbro is present in the Chrome body mafic series but is absent from the Page body and either absent or not exposed on the Peterson Block and National-Ledin bodies. Scoates (1983) demonstrated an increase in quartz content stratigraphically upward from anorthosite into diorite, quartz gabbro to tonalite. This is succeeded by a decrease in quartz content stratigraphically upward from tonalite to quartz gabbro which ends in fault contact with the medium grained anorthositic gabbro of the upper mafic series (Scoates, 1983).

Petrographic analysis indicates that the diorite, quartz gabbro and tonalite consist predominantly of primary plagioclase with 5 to 25% quartz and minor to trace amounts of primary pyroxene. Plagioclase and pyroxene crystals retain the same habit as described above in the lower and upper mafic series with moderate to extensive alteration. Quartz

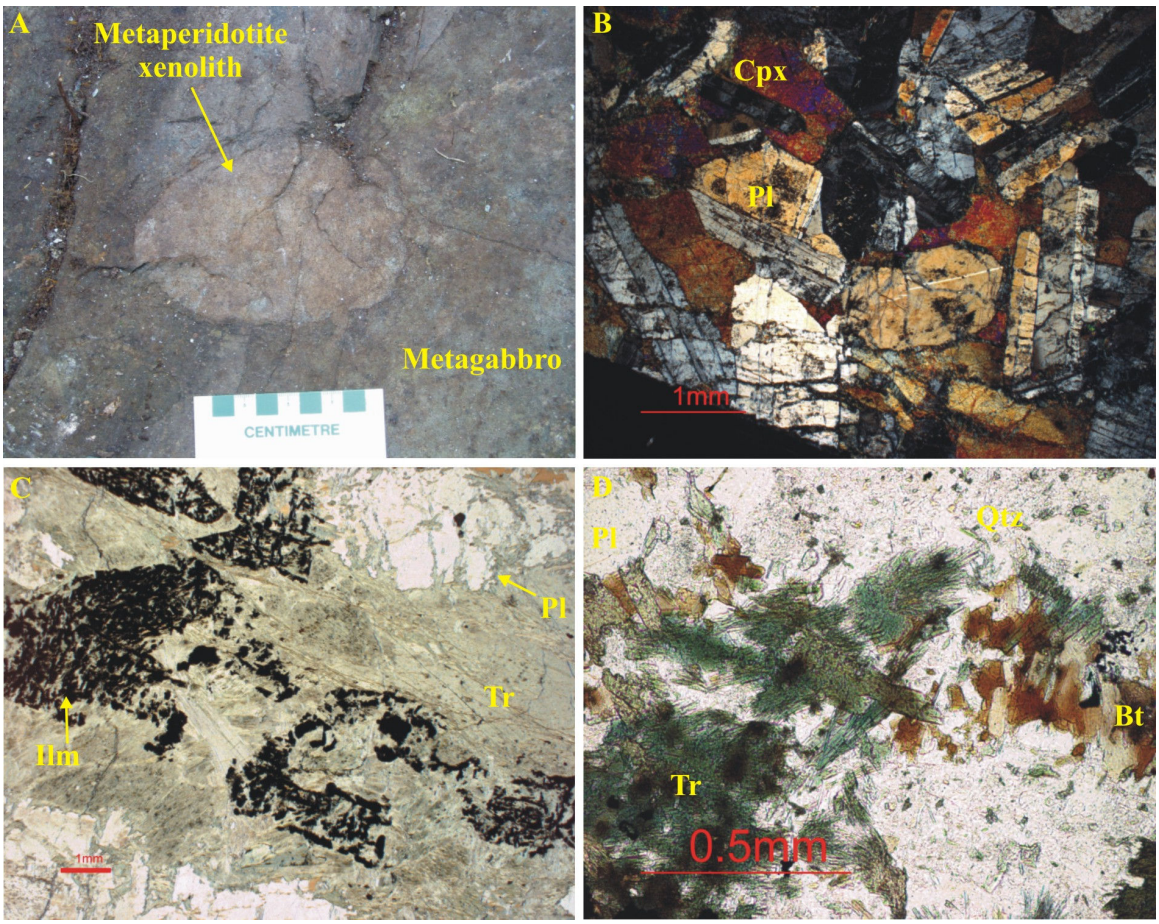

Figure 11: Photographs and photomicrographs of the mafic series from the Page and Chrome bodies of the Bird River sill. A) Photograph of a metaperidotite xenolith in the mafic series, Page body, Bird River sill. B) Microphotograh of anorthositic metagabbro with subhedral to euhedral, twinned plagioclase (Pl) crystals, Chrome body, Bird River sill; cpl transmitted light. C) Microphotograph of metagabbro with ilmenite (Il) surrounded by tremolite (Toz), Chrome body of the Bird River sill; ppl transmitted light. D) Microphotograph of metagabbro with tremolite and biotite (Bt) alteration in tonalite, Chrome body, Bird River sill; ppl transmitted light.

is present as subhedral to anhedral crystals with irregular interlocking boundaries interstitial to plagioclase and pyroxene. Tremolite, clinozoisite, chlorite, biotite and clinoamphibole are present and formed at the expense of the plagioclase, pyroxene and hornblende (Figure 11D). Minor amounts of ilmenite are disseminated throughout tremolite and trace amounts of chalcopyrite, pyrrhotite and pyrite form anhedral to subhedral disseminations within tremolite, clinozoisite and chlorite.

3.3 Quartz-feldspar porphyry intrusions

Quartz-feldspar porphyry dykes were observed in drill core intruding the lower ultramafic series of the Page body. These types of intrusions were not observed elsewhere on the BRS but have been reported to cross-cut the Maskwa-Dumbarton body. The dykes are dark grey, fine-grained, homogeneous and exhibit whitish to light green mottled patches. They are characterized in hand sample by the presence of quartz eyes approximately 4-5 mm in size. They have sharp, sheared contacts with the ultramafic rocks of the BRS.

Petrographic analysis indicates that the dykes are composed of quartz and feldspar phenocrysts embedded in a fine-grained groundmass of feldspar, quartz and biotite. Minor chlorite alteration is concentrated along fractures. Many of the dykes contain significant amounts of disseminated to massive sulphide mineralization consisting predominantly of pyrrhotite with minor chalcopyrite. Sulphide mineralization is addressed in detail in Chapter 5: Bird River sill Cr-Ni-Cu-PGE Mineralization.

3.4 Structural relationships between the Bird River sill and adjacent Bird River greenstone belt formations

Previous studies have treated the BRS as a single layered intrusion that was block faulted due to tectonism and granitoid intrusions. Davies (1952) was one of the first to introduce the block faulted model (Figure 12). Ensuing work by Juhas (1973), Trueman (1971), Scoates (1983) and Theyer (1985) also applied this model. Displacements were believed to follow north-northwest-trending shear zones that produced offsets of up to 1525 m (Bannatyne and Trueman, 1982).

There is no evidence from the field investigation in this study and that of Duguet et al. (2006 and 2007) or from examination of the total field magnetic survey to support the existence of the major north-northwest trending shear zones which accommodate the block faulted model. By contrast, this study identified an east-west trending shear zone south of the BRS Page body in the Lamprey Falls Formation (Figure 5). This shear zone has a near vertical dip and is mineralized with approximately 10% blebby pyrrhotite and minor amounts of fine disseminated chalcopyrite. It corresponds with the Peterson Creek Shear Zone defined by Duguet et al. (2006) (Figure 3). The pillowed basalts of the Lamprey Falls Formation approximately 5-8 m north of the shear zone exhibit significant brecciation (Figure 13A). Petrographic analysis indicates that the brecciated pillow selvages are contained in an epidote matrix.

Two other major shear zones are present north of the Page body and south of the Chrome and National-Ledin bodies (Figure 5). The location and extent of these are from Duguet et al. (2006 and 2007). The shear zone north of the Page body trends roughly east-west turning southward over the west end of the Page body and truncates the Maskwa Lake batholith and Lamprey Falls Formation (Figure 3). The shear zone located south of the Chrome and National-Ledin bodies of the Bird River sill truncates the Maskwa Lake batholith and Peterson Creek Formation. It is present along the Lamprey Falls Formation and Peterson Creek Formation contact in the western half of the Bird River greenstone belt (Figure 3).

Within the Chrome, Page and National-Ledin bodies of the BRS there are numerous steeply dipping faults which pre-date the major east-west trending shear zones and are inferred to pre-date the deposition of the overlying Peterson Creek Formation (Figure 5). The location and extent of the shear zones were determined from field measurements (Figure 13B) and offsets of marker horizons (i.e. offsets in chromite layers). The shear zones trend in three general directions: north-south, north-northwest and east-west. The north-south and north-northwest-trending shear zones produced clearly visible horizontal displacements ranging from a few millimetres up to several metres. Cross-cutting textures observed in the field and well documented by Trueman (1971) and Davies (1955) involve east-west trending faults being truncated by the north-south and north-

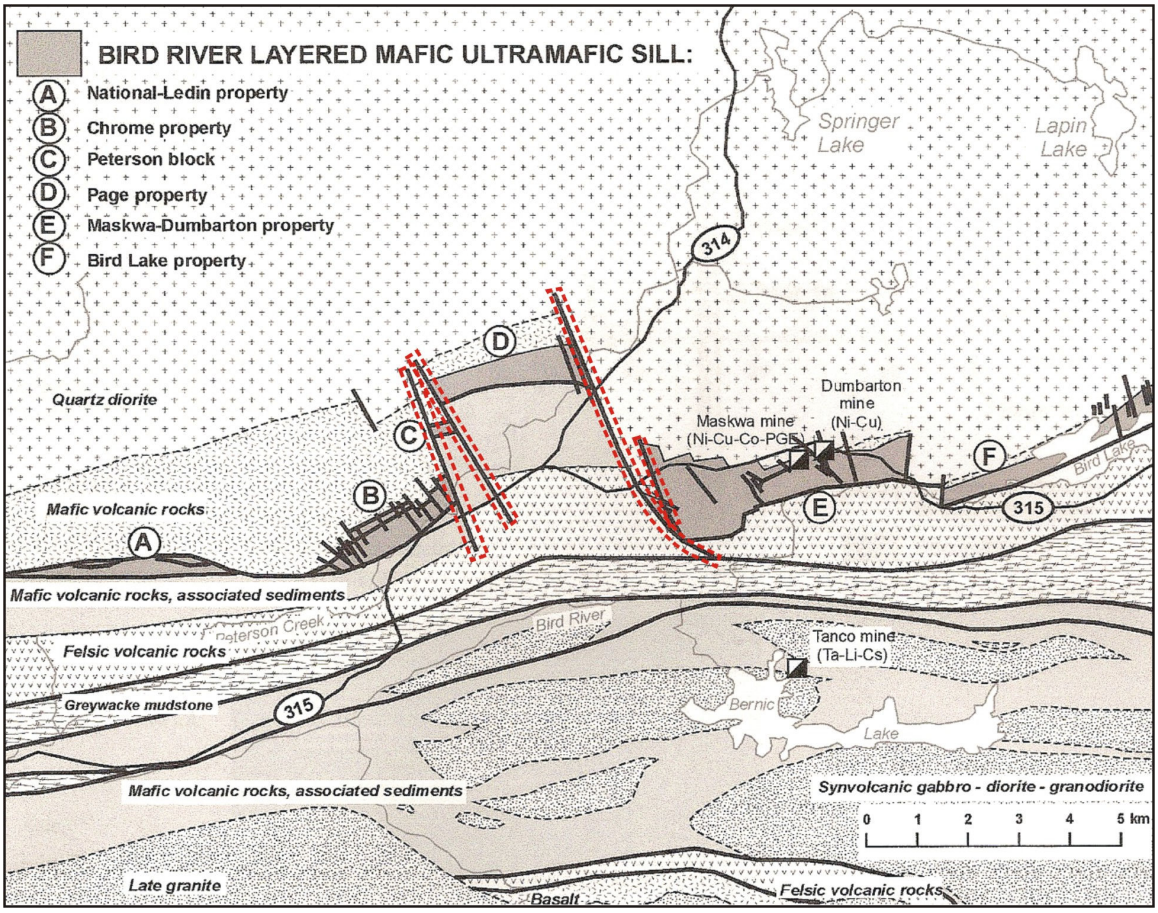

Figure 12: Simplified geological map of the Bird River sill and adjacent Bird River greenstone belt formations illustrating the block faulted model. Map from Theyer et al. (2001). The location of the interpreted major north-northwest trending faults believed to have accommodated the large displacements between the Bird River sill bodies are highlighted in red.

Figure 13: Photographs of brecciated pillowed basalt from the Lamprey Falls Formation (A) and an east-west trending shear zone, Chrome body, Bird River sill (B).

northwesterly trending faults. In other locations, the north-north-westerly faults terminate against the easterly trending faults. Trueman (1971) suggested that the easterly faulting postdates the northerly faults.

As previously discussed, the BRS intrudes the metabasalts of the Lamprey Falls Formation. The intrusive contact was observed on the north-eastern end of the BRS Chrome body (Figure 14A). The intrusive contact between the BRS and Lamprey Falls Formation in this location trends roughly north-south (Figure 15 and Figure 16). Within the marginal metagabbro, at the contact with the Lamprey Falls Formation, a 10-15 cm wide band exhibits a decrease in grain size with proximity to the Lamprey Falls Formation, which is interpreted to represent a chill margin. The pyroxenite xenoliths introduced above are present within the marginal metagabbro near the intrusive contact (Figure 16). A north-south trending shear zone is present within the BRS marginal metagabbo approximately 6-8 m east of the intrusive contact. This shear zone is illustrated in grid map A (Figure 15) and grid map B (Figure 16). In grid map A the shear zone is approximately 0.5-1 m wide but in grid map B (Figure 16) the shear zone is wider and contains numerous centimetre-wide chlorite-filled fractures both within the shear zone and directly adjacent to it.

In the eastern portion of the Chrome body, the block faulted model proposed that the contact between the BRS and Lamprey Falls Formation trends east-west and that the eastern portion of the Chrome body is bound by a major north-west trending fault (Figure 14B). This study has shown that the BRS-Lamprey Falls Formation intrusive contact trends north-south in the eastern portion of the Chrome body. Furthermore, the Chrome body does not terminate at a fault but extends further northeast for another 500 m.

In conclusion, this study in conjunction with that of Duguet et al. (2006 and 2007), failed to find evidence supporting the existence of the major north-northwest trending faults which accommodate the block faulted model. The new data from this study indicates that the separate bodies of the BRS likely represent several individual intrusions.

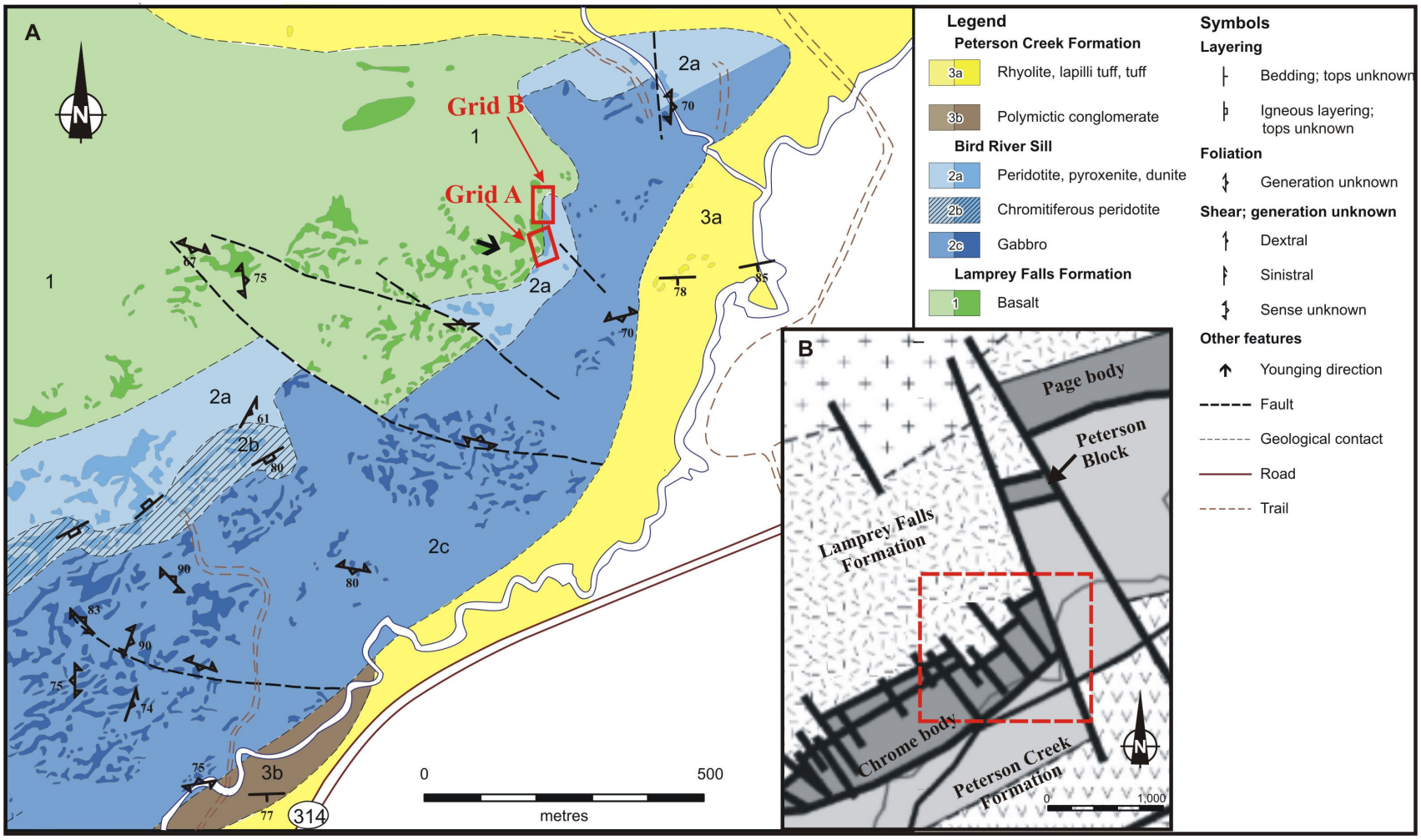

Figure 14: Simplified geological maps of the northeastern portion of the Chrome intrusion and the central bodies of the Bird River sill. Map A (Mealin, 2006) illustrates the separate intrusion model and Map B illustrates the block faulted model (Theyer et al., 2001). The highlighted area in Map B corresponds to Map A. The intrusive contact between the Bird River sill and Lamprey Falls Formation illustrated in grids A and B (Figure 15 and Figure 16) are highlighted.

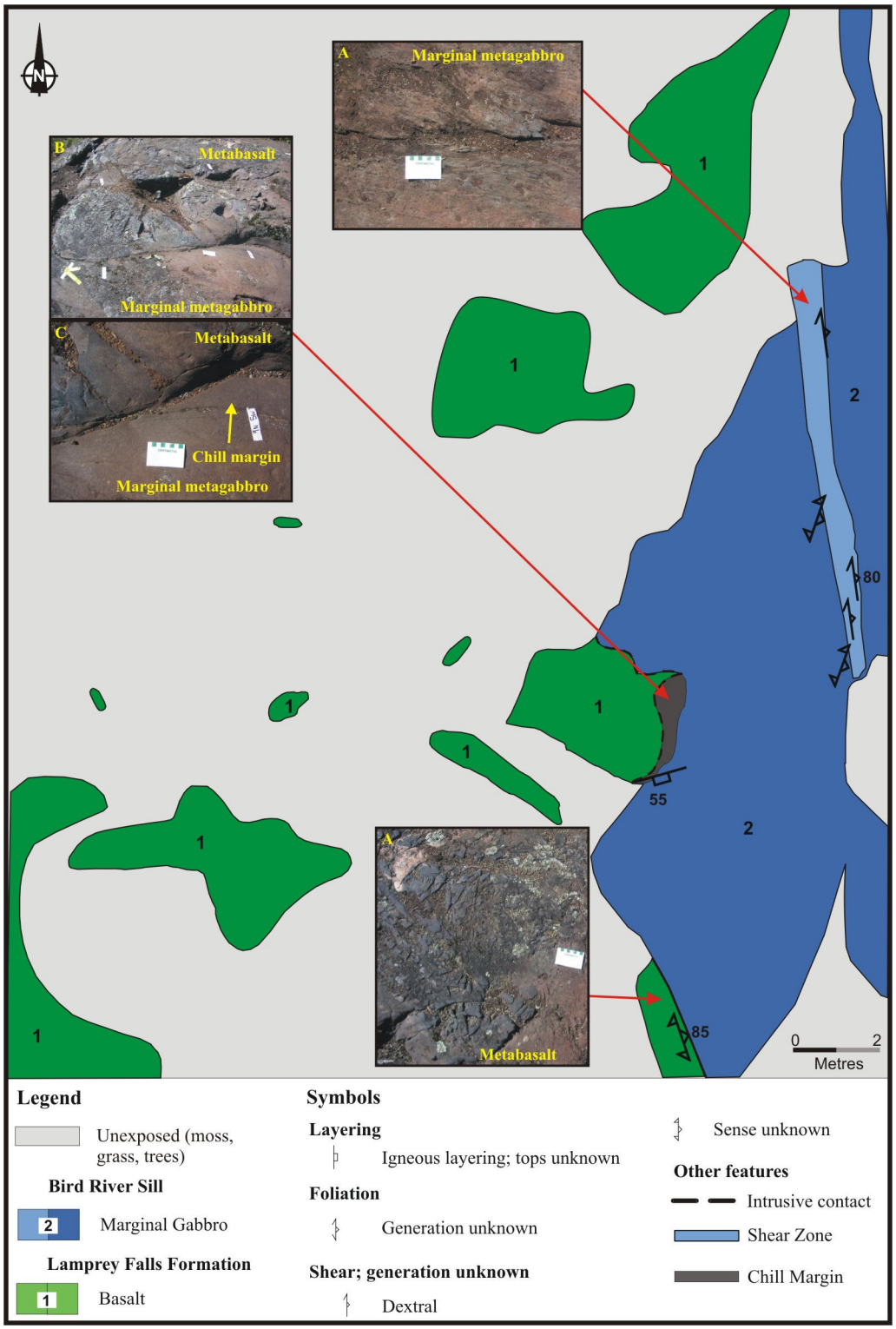

Figure 15: Detailed geological map and photographs of grid map A from Figure 14 showing the intrusive contact between the Chrome body of the Bird River sill and Lamprey Falls Formation. A) North trending shear zone that truncates the marginal metagabbro of the Chrome body. B) and C) Intrusive contact between the marginal metagabbro of the Chrome body and the metabasalts of the Lamprey Falls Formation. The chill margin is visible in B) within the Bird River sill at the contact with the Lamprey Falls Formation. D) Metabasalts of the Lamprey Falls Formation.

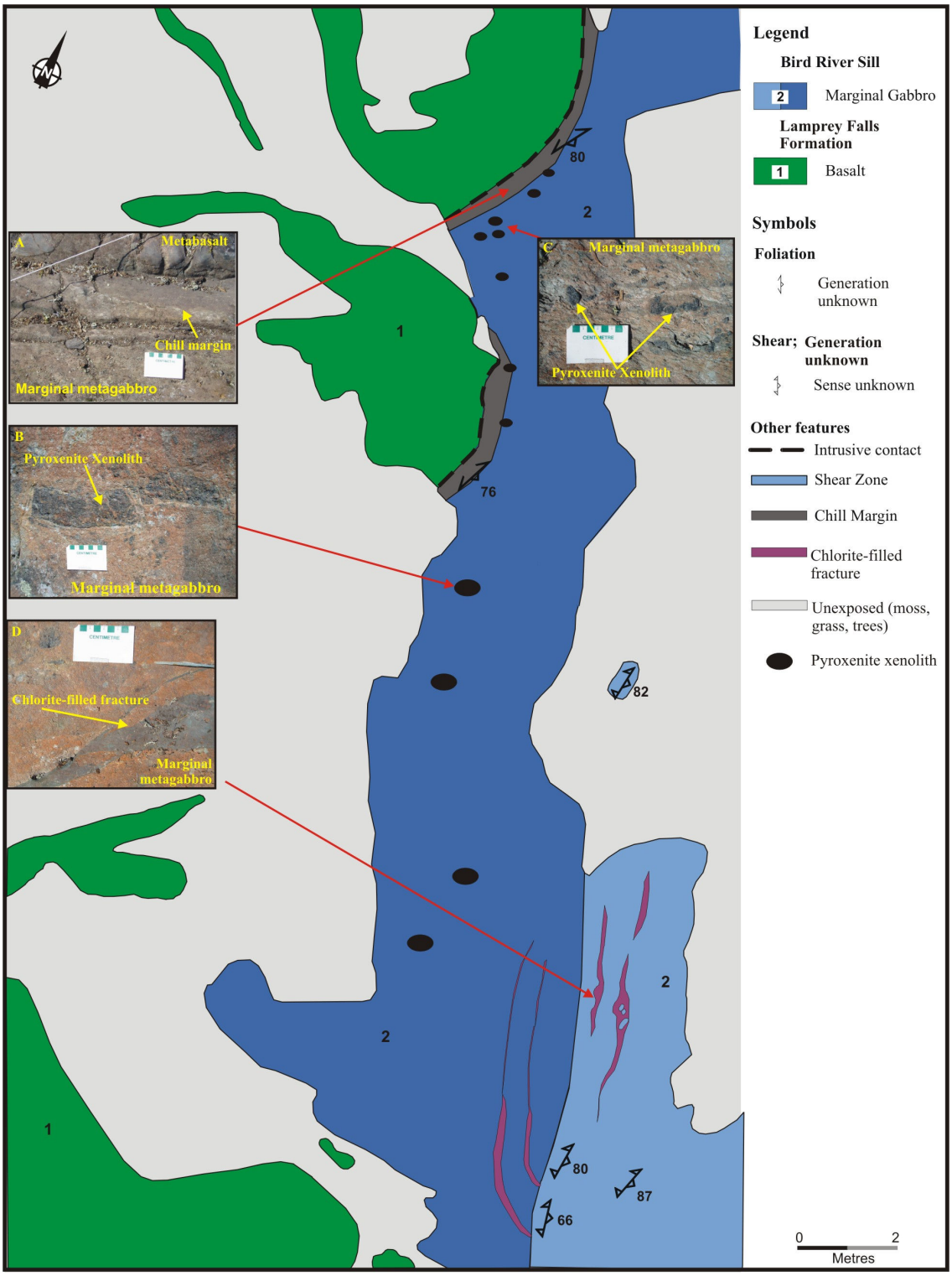

Figure 16: Detailed geological map and photographs of grid map B from Figure 14 showing the intrusive contact between the Chrome body of the Bird River sill and Lamprey Falls Formation. A) Intrusive contact between the marginal metagabbro of the Chrome body and metabasalts of the Lamprey Falls Formation. The chill margin is visible within the Chrome body along the contact with the Lamprey Falls Formation. B) and C) Pyroxenite xenoliths within the marginal metagabbro of the Chrome body present near the intrusive contract. D) Chlorite-filled fractures within the marginal metagabbro of the Chrome body.

Chapter 4: Lithogeochemistry of the Bird River sill and adjacent Bird River greenstone belt formations

The lithogeochemistry of samples from the mafic-ultramafic series of the BRS and metagabbros from the Lamprey Falls Formation were determined to:

1. Identify whether the metabasalts located south of the BRS Page body are part of the Lamprey Falls Formation or the Peterson Creek Formation;
2. Delineate the relationship of the metagabbros located within the Lamprey Falls Formation to the BRS;
3. Examine the geochemistry of the separate bodies of the BRS to identify similarities and/or differences between the separate intrusions; and,
4. Evaluate the single versus multiple magma injection emplacement models through the examination of major and trace element chemostratigraphic trends.

As discussed in Chapter 3, the BRS has undergone significant greenschist facies metamorphism. The lack of primary mineralogy in the ultramafic series of the BRS prevented the use of electron microprobe analyses to determine primary mineral compositions. This section is based on whole-rock analyses in which trace and major elements that are typically immobile in greenschist facies environments were utilized for interpretation. It is important to note that it is assumed that no major addition or removal of these relatively immobile elements has taken place.

4.1 Geochemistry of the Lamprey Falls and Peterson Creek Formations

The metavolcanic rocks of the Lamprey Falls Formation have an andesitic/basaltic composition and the metavolcanic samples from the Peterson Creek Formation range in composition from andesitic to rhyodacitic/dacitic (Figure 17A). Rocks from both the formations have a tholeiitic affinity (Figure 17B). The primitive mantle-normalized trace element patterns of the samples from the Lamprey Falls Formation are flat (Figure 17C) and geochemically akin to a modern back-arc-basin tectonic setting (Gilbert, 2005). By contrast, the trace element patterns of the samples from the Peterson Creek Formation

have a negative slope with a strong negative Nb anomaly relative to Th and La and are interpreted to be akin to a modern arc tectonic setting (Figure 17D).

The mafic volcanic sample collected from the metabasalts south of the BRS Page body is plotted on Figure 17 for comparison. This metabasalt plots in the subalkaline field, has an andesitic/basaltic composition and a tholeiitic affinity which coincides exactly with that of the metabasalts from the Lamprey Falls Formation. The trace elements of the metabasalts south of the Page body display a flat primitive-mantle normalized pattern indicating a similar tectonic setting to that of the Lamprey Falls Formation.

Data presented above indicates the metabasalts located south of the BRS Page body have an appearance, tectonic setting and composition similar to the metabasalts of the Lamprey Falls Formation and both have a composition that is distinctly different from that of the Peterson Creek Formation. Therefore, it is proposed that the metabasalts located south of the Page body belong to the mafic flows of the Lamprey Falls Formation and thus the Page body of the BRS is not in direct contact with the Peterson Creek Formation. This suggests the Page body was emplaced at a lower stratigraphic level within the Lamprey Falls Formation compared to that of the Chrome, Peterson Block and National-Ledin bodies. This new information, coupled with the confirmation of BRS detritus in the polymictic conglomerates south of the Chrome, Peterson Block and National-Ledin bodies of the Bird River sill supports the model of Trueman (1980) that the BRS intruded the Lamprey Falls Formation, which was uplifted, eroded and then overlain by the metasedimentary sequences of the Peterson Creek Formation.

4.2 Geochemistry of the mafic series of the Bird River sill and metagabbroic intrusions from the Lamprey Falls Formation

As discussed in section 3.1 General Geology, numerous metagabbroic intrusions are present north of the BRS in the Lamprey Falls Formation (Figure 5; unit 1b). Trueman (1971) identified these as faulted segments of a narrow sill that is separate from the BRS; which suggests they are possibly Lamprey Falls Formation hypabyssal gabbros. Juhas

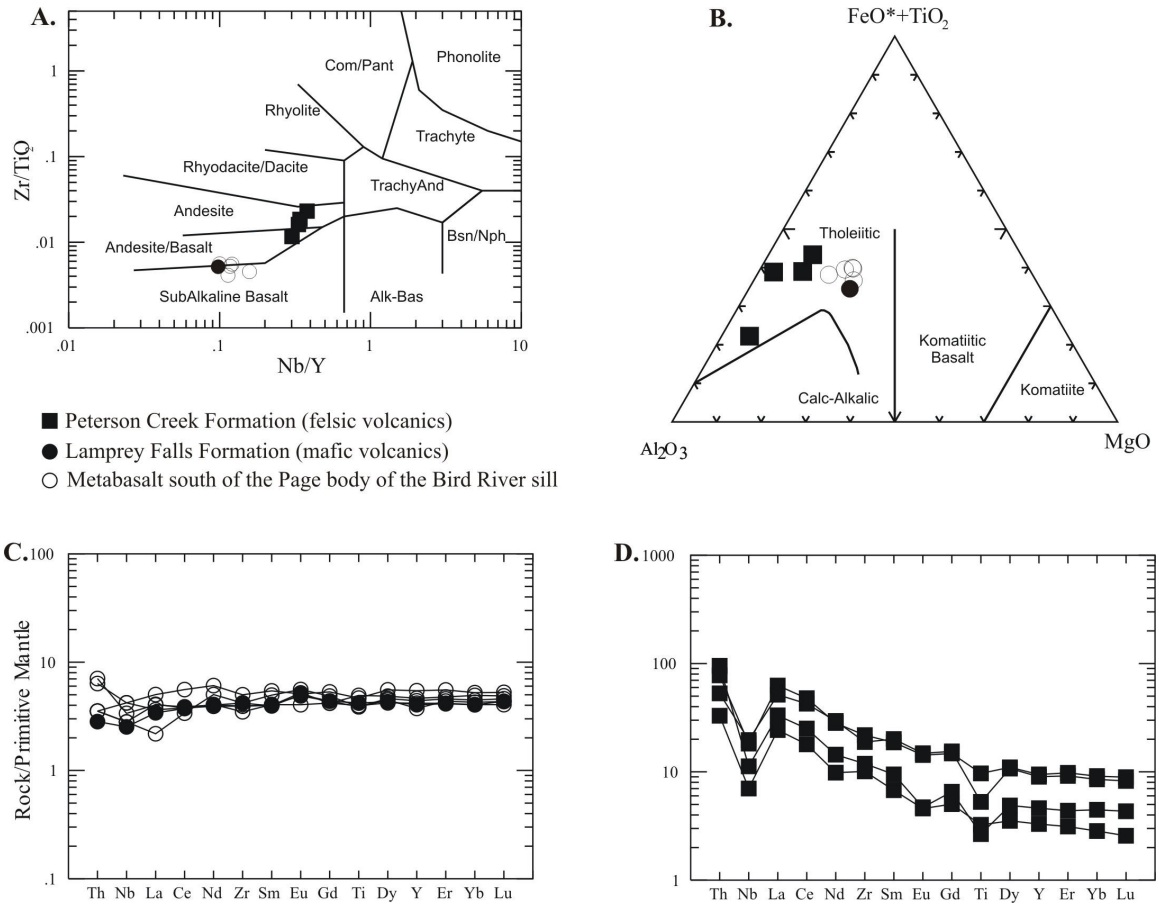

Figure 17: Trace element plots of the volcanic samples from the Lamprey Falls Formation, Peterson Creek Formation and metabasalts located south of the Bird River sill Page body. A) Alkalinity igneous rock classification diagram (Winchester and Floyd, 1977). B) Jensen cation plot (Jensen, 1976). C) Primitive mantle-normalized trace element diagram of the mafic volcanics from the Lamprey Falls Formation and metabasalts located south of the Page body. D) Primitive mantle-normalized trace element diagram of the felsic volcanics from the Peterson Creek Formation. Mantle normalizing values are from Sun and McDonough (1989). The Lamprey Falls Formation mafic volcanic data is from Gilbert (2006) and the Peterson Creek Formation felsic volcanic data is from Duguet et al. (2006). Geochemical data is located in Appendix B.

(1973) believed the metagabbros hosted in the Lamprey Falls Formation are genetically related to the BRS. Juhas (1973) identified the metamorphosed mafic-ultramafic intrusive bodies northwest of the BRS Maskwa-Dumbarton body (east of the study area) as potentially representing remnants of a feeder dyke. Nageri (1991) showed that the potential feeder dyke is actually less deformed, possesses a lower grade metamorphism, appears to cross-cut the BRS and has different chemical compositions and differentiation trends from those of the BRS. He concluded that the potential feeder dyke located northwest of the BRS Maskwa-Dumbarton body is a later and entirely separate intrusion. To date, the relationship between the BRS and the metagabbros west of the discredited feeder dyke is still unresolved.

Two Lamprey Falls Formation metagabbro samples were collected in this investigation for whole-rock lithogeochemistry to compare with metabasalts from the Lamprey Falls Formation and the mafic series of the BRS. The primitive mantle-normalized trace element patterns of the Lamprey Falls Formation metagabbros are very flat, with a weak negative Nb anomaly (Figure 18A). The trend is similar to the trace element pattern of the mafic volcanics from the Lamprey Falls Formation (Figure 17C).

The primitive mantle-normalized trace element patterns of the mafic series from the Chrome and Page bodies of the BRS reflects the cumulate nature of the BRS and illustrates the fractionation of trace elements amongst the cumulate phases (Figure 18B and C). Positive Eu peaks are attributed to the presence of plagioclase and the negative Nb anomalies are attributed to the fractionation of a Ti-phase cumulate. The nature of the negative Nb anomalies is discussed in detail in section 4.4. The Lamprey Falls Formation metagabbros do not appear to contain cumulate phases like that of the BRS mafic series. The flat primitive mantle-normalized trace element pattern of the Lamprey Falls Formation metagabbros indicates they likely represent coarse-grained flows genetically related to the mafic volcanics of the Lamprey Falls Formation.

4.3 Bird River sill geochemistry

To recap, two models have been proposed to explain the separate segments that collectively make-up the BRS: 1) earlier models proposed that the BRS bodies represent displaced blocks along north-northwest trending faults of an originally single continuous

intrusion, and 2) this study proposes that the BRS segments represent separate intrusions. The purpose of this section is to compare the major and trace element geochemistry of samples from the Chrome, Page, National-Ledin and Peterson Block bodies of the BRS to identify similarities and/or differences between the individual BRS intrusions.

4.3.1 Major and trace element geochemistry

Major element oxides for the marginal olivine metagabbro, mafic series and ultramafic series of the BRS are presented in a Jensen cation plot in Figure 19. The ultramafic series of the Chrome, Page and Peterson Block bodies are geochemically similar to komatitic basalts. The relationship between the ultramafic series and mafic series was established by Peck and Theyer (1998) who concluded the mafic series of the BRS crystallized from magmas that were cogenetic with the ultramafic series. In the Jensen cation plot, a continuous trend is exhibited from the ultramafic series of the Chrome body to the mafic series (Figure 19A). The marginal olivine metagabbro samples plot between the ultramafic and mafic series which suggests the marginal olivine metagabbro represents a component of the primitive melt that formed the Chrome body. The mafic series of the National-Ledin body roughly corresponds with that of the Chrome body but is depleted in Al_2O_3. A compositional break is exhibited between the ultramafic series and mafic series of the Page body (Figure 19B). This is attributed to the lack of representative samples across the stratigraphy of the Page body. A sample from the ultramafic series of the Peterson Block body is enriched in Al_2O_3 compared to that of the Page body.

The primitive-mantle normalized trace element patterns of the chill margin from the marginal olivine metagabbro of the Chrome body are slightly depleted in LREE, Zr, Th and Nb and are enriched in Eu and Ti (Figure 20A). The positive Eu peak is attributed to the presence of plagioclase which was confirmed optically in the marginal olivine metagabbro adjacent to the chill margin. The trace element patterns of the ultramafic series from the Chrome body are generally flat and depleted in Th and Nb (Figure 20). The positive Eu anomaly in zone 2 is attributed to the presence of plagioclase in the troctolite layers and the positive Eu anomaly in zone 3 is attributed to the presence of plagioclase-bearing peridotite suites. The positive Zr anomalies correspond to units that

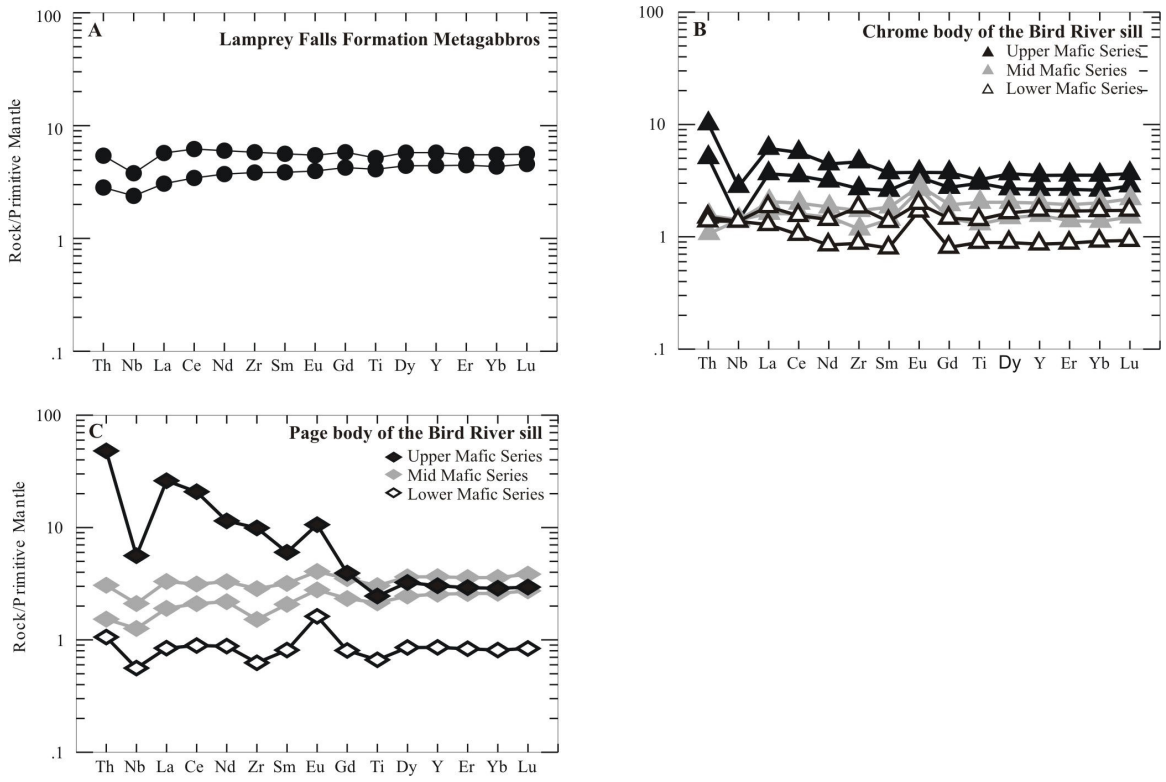

Figure 18: Primitive-mantle normalized trace element diagrams of the metagabbros from the Lamprey Falls Formation and the mafic series from the Chrome and Page bodies of the Bird River sill. A) Primitive mantle-normalized trace element diagram for the Lamprey Falls Formation metagabbros. B) and C) Primitive mantle-normalized trace element diagrams for the mafic series of the Chrome and Page bodies of the Bird River sill, respectively. Mantle normalizing values from Sun and McDonough (1989). Geochemical data is located in Appendix B.

contain pyroxenite layers. Therefore Zr may have fractionated into pyroxene and thus the Zr peaks may be attributed to clinopyroxene content.

The lower ultramafic series, mid ultramafic series and chromitiferous metaperidotite of the Page body approximately correspond to zone 1, zone 3 and zone 4 of the Chrome body ultramafic series, respectively. In general, the primitive-mantle normalized trace element patterns of the ultramafic series from the Page body are flat and contain elevated values of Th and Nb compared to that of the Chrome body (Figure 21). One sample from the mid ultramafic series of the Page body is slightly enriched in light rare earth elements (LREE). This could be attributed to the presence of a cumulate phase which concentrated LREE. Overall, the major and trace elements of the separate BRS intrusions are similar which suggests that the separate BRS intrusions shared a common magma source.

Negative Nb anomalies and elevated Th and La concentrations are present in the trace element patterns of the mafic series from the Chrome and Page bodies (Figure 18B and C). These negative Nb anomalies may indicate arc magmas, contamination of the melt through assimilation of wall rock or the crystallization of a Ti-phase cumulate. The samples from the olivine metagabbro chill margin of the Chrome body and several samples from the ultramafic series of the Page body contain elevated Nb values and depleted Th concentrations. The depleted concentration of Th indicates that these are not arc magmas (Winter, 2001). The elevated Nb values in the chill margin of the Chrome body indicates that Nb was likely concentrated in the crystallization of a Ti-phase cumulate thus resulting in negative Nb anomalies in gabbroic samples that do not contain the Ti-phase cumulate.

4.3.2 Chemostratigraphic variations in the Chrome body of the Bird River sill

The purpose of this section is to evaluate the single versus multiple magma injection emplacement models for the Chrome body of the BRS. To recap, the various emplacement models are: 1) the BRS is the result of two different magma pulses (Bateman, 1943); 2) the BRS has a complex multi-magmatic injection origin (Osborne, 1949), and; 3) the BRS was emplaced through a single magmatic injection where the layers formed via subsequent crystal fractionation and gravitational settling (Springer, 1948 and 1949, Juhas, 1973, Trueman, 1971 and Scoates, 1983).

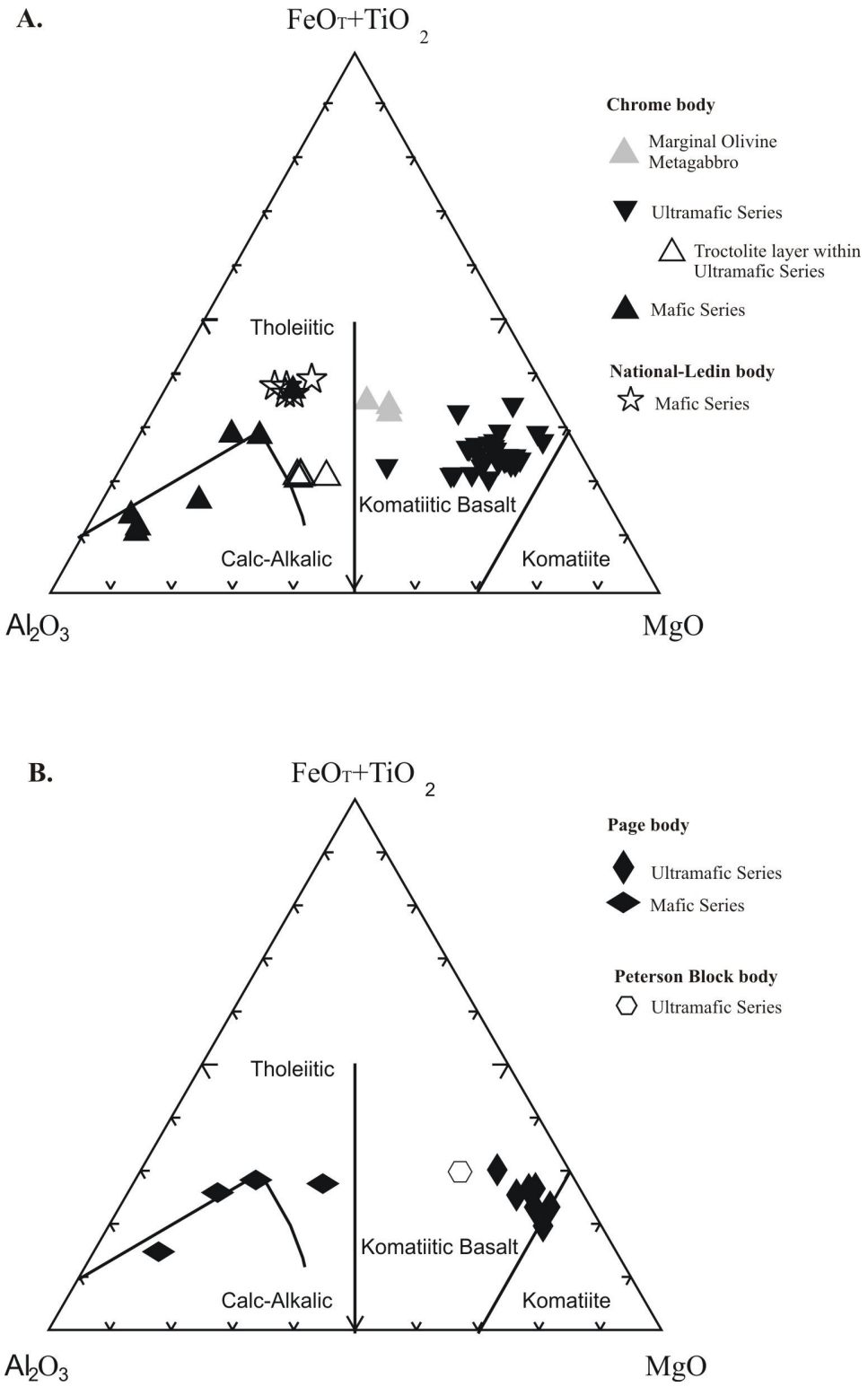

Figure 19: Ternary Al_2O_3-FeO+TiO_2-MgO whole-rock oxide Jensen cation plots (Jensen, 1976) for A) the Chrome body of the Bird River sill, and B) the Page and Peterson Block bodies of the Bird River sill. Geochemical data is located in Appendix B.

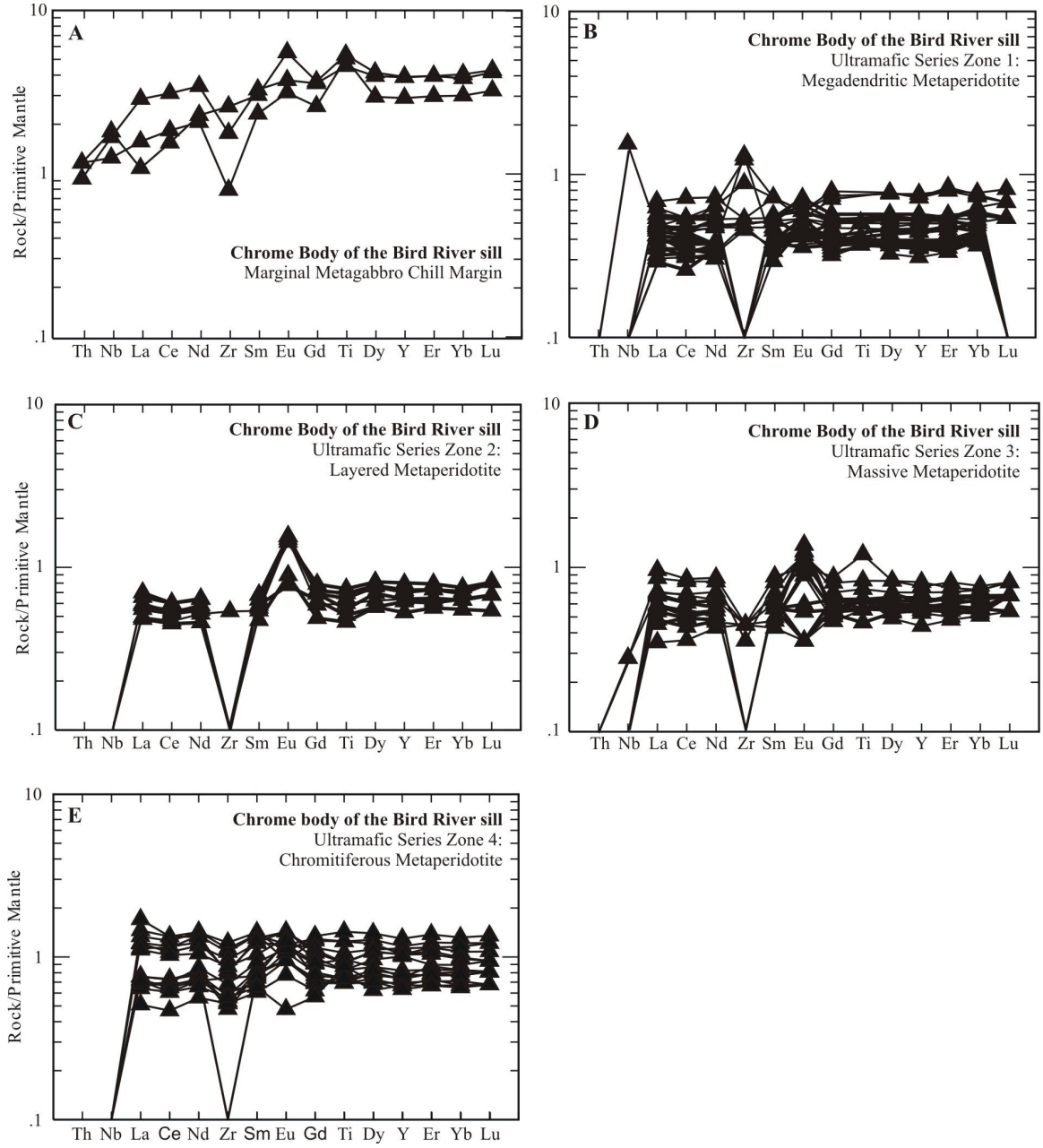

Figure 20: Primitive-mantle normalized trace element plots for the chill margin and ultramafic series of the Chrome body, Bird River sill. Mantle normalizing values are from Sun and McDonough (1989). Geochemical data is located in Appendix B.

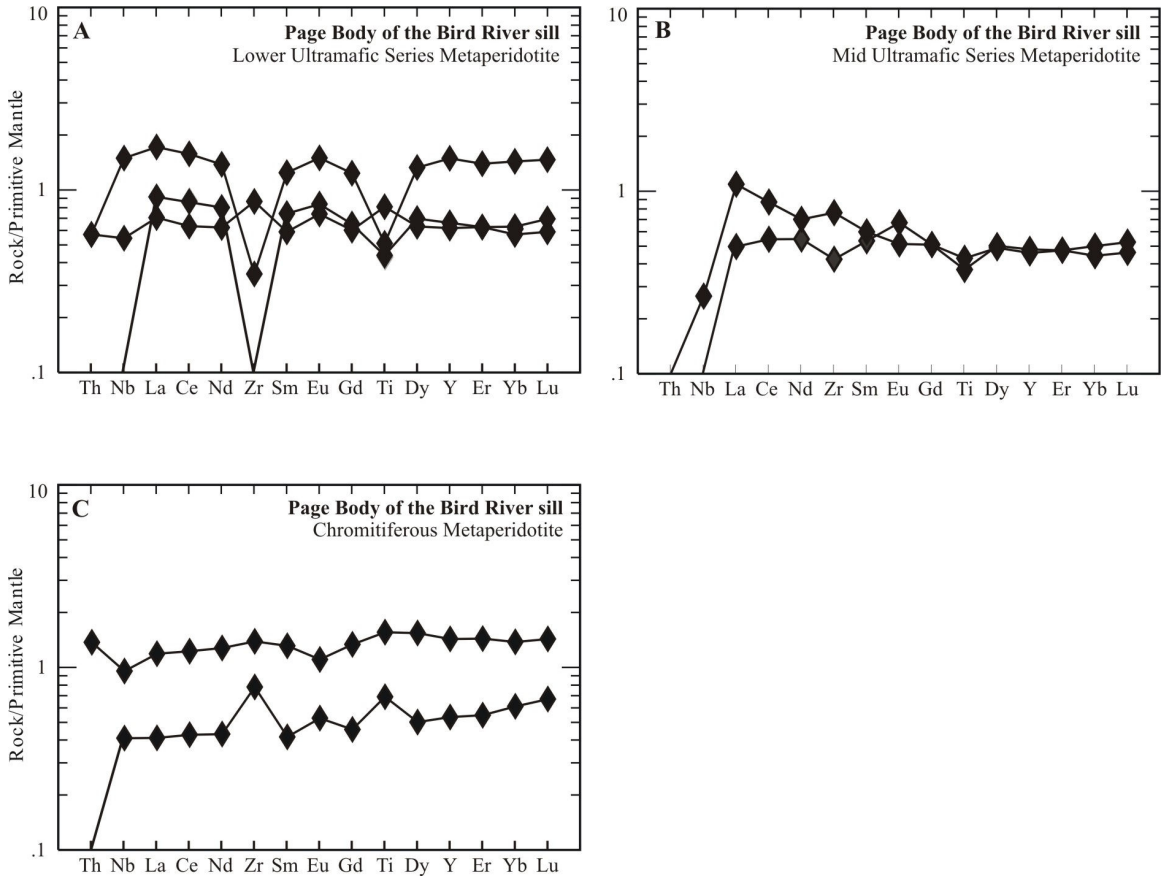

Figure 21: Primitive-mantle normalized trace element plots for the ultramafic series of the Page body, Bird River sill. Mantle normalizing values are from Sun and McDonough (1989). Geochemical data is located in Appendix B.

Channel cuts by Theyer (1985) across the stratigraphy of the ultramafic series of the BRS Chrome body provided an excellent opportunity to examine the processes involved in the emplacement and crystallization of one of the BRS bodies. The following discussion solely examines the Chrome body and not the BRS as a whole. The mafic series is not examined here because it has already been established by Peck and Theyer (1998) that the gabbroic portion of the BRS crystallized from residual liquids that were formed through crystallization of the underlying ultramafic series.

The Mg# (Mg/Mg+FeO) indicates the primitiveness of the magma. The Mg# within the ultramafic series of the Chrome intrusion decreases stratigraphically upwards from the base of the Chrome body through the megadendritic peridotite zone into the layered peridotite zone (Figure 22). There is an abrupt shift to more primitive magma (higher Mg#) at the stratigraphic top of the layered peridotite zone. This reversal is interpreted to represent two cyclic units which likely crystallized from separate pulses of magma. The trend exhibited here is similar to that of the Fox River sill, a mafic-ultramafic intrusion located several hundred kilometres north of the BRS, where two cyclic units which crystallized from separate pulses of magma are indicated by a reversal in Mg # (Peck et al., 2002) of the same magnitude displayed by the BRS.

Chemostratigraphic trends of select trace elements La, Ce and Nd through the ultramafic series of the BRS Chrome body are presented on Figure 23. In general, there is a gradual increase in the concentrations of these trace elements stratigraphically upwards with a distinct increase in concentration in the upper portion of the chromitiferous peridotite zone. It is important to note that the nature of the trends is questionable because absolute trace element concentrations are largely dependent on how they became incorporated into the final solidified rock. Late-stage processes such as compaction and deformation of the crystal mush could have caused displacement or migration of the incompatible trace elements (Wilson and Chunnett, 2006). The trends can also be attributed to variable proportions of trapped liquid in each unique sample. Single element plots can be useful indicators of magma mixing but are required to be used with trace element ratio plots to account for their inherent uncertainty.

Two equally incompatible trace elements will have a ratio that increases in concentration in the liquid at the same rate and hence the ratio will remain constant and

independent of amount of trapped liquid. This eliminates the complication and confusion in single element trends where the amount of trapped liquid is unknown (Cawthorn and McCarthy, 1985). Magma addition is represented by a change in the ratio but if the new magma is from a common magma chamber, a break in the ratio may not be produced although it may be observed in a single element plot (Cawthorn and McCarthy, 1985). Common incompatible trace element ratios used for this type of study are Ta/Nb, Th/Nb, Rb/La Ba/Th, La/Sm and Ce/Sm. For the BRS, the concentrations of Rb, Th, Nb and Ta are near or below detection limit therefore the element ratios La/Sm and Ce/Sm are utilized for this investigation.

The La/Sm and Ce/Sm trace element ratios display a significant amount of scatter which makes the interpretation of these trends difficult (Figure 24). It is clear that there is not a consistent ratio throughout the stratigraphy in either the La/Sm or Ce/Sm plots. La/Sm appears to range from approximately 1 to 2 and the Ce/Sm appears to range from approximately 3 to 5. In a study on the Merensky Reef of the Bushveld Complex, the small changes in incompatible trace element ratios Ta/Nb and Th/Nb, which are comparable to the changes exhibited by the trace element ratios of the BRS, are attributed to interactions between different magmas (Wilson and Chunnett, 2006). A study on the Xinjie layered intrusion of Southwest China similarly interpreted the small changes exhibited by Rb/La and Ba/Th near the pyroxenite-peridotite contact as suggestive of a new magma addition into the magma chamber (Zhong et al., 2004).

It is proposed that the reversal reflected in the Mg# and the small changes in the trace element ratios indicate the Chrome body was emplaced through at least two magmatic injections. Emplacement through a single injection with subsequent crystal fractionation should yield a constant trace element ratio and a gradual decrease in Mg# stratigraphically upwards. The trends exhibited by the ultramafic series of the Chrome body are more akin to those of the Merensky Reef and Xinjie intrusion, both of which are attributed to interaction between different magmas. It is important to note that there appears to be a relationship between REE content (i.e. La) and P_2O_5 (Figure 25). This is attributed to the presence of a cumulate phase, possibly apatite. The concentration of REE in apatite could also affect the La/Sm and Ce/Sm ratios.

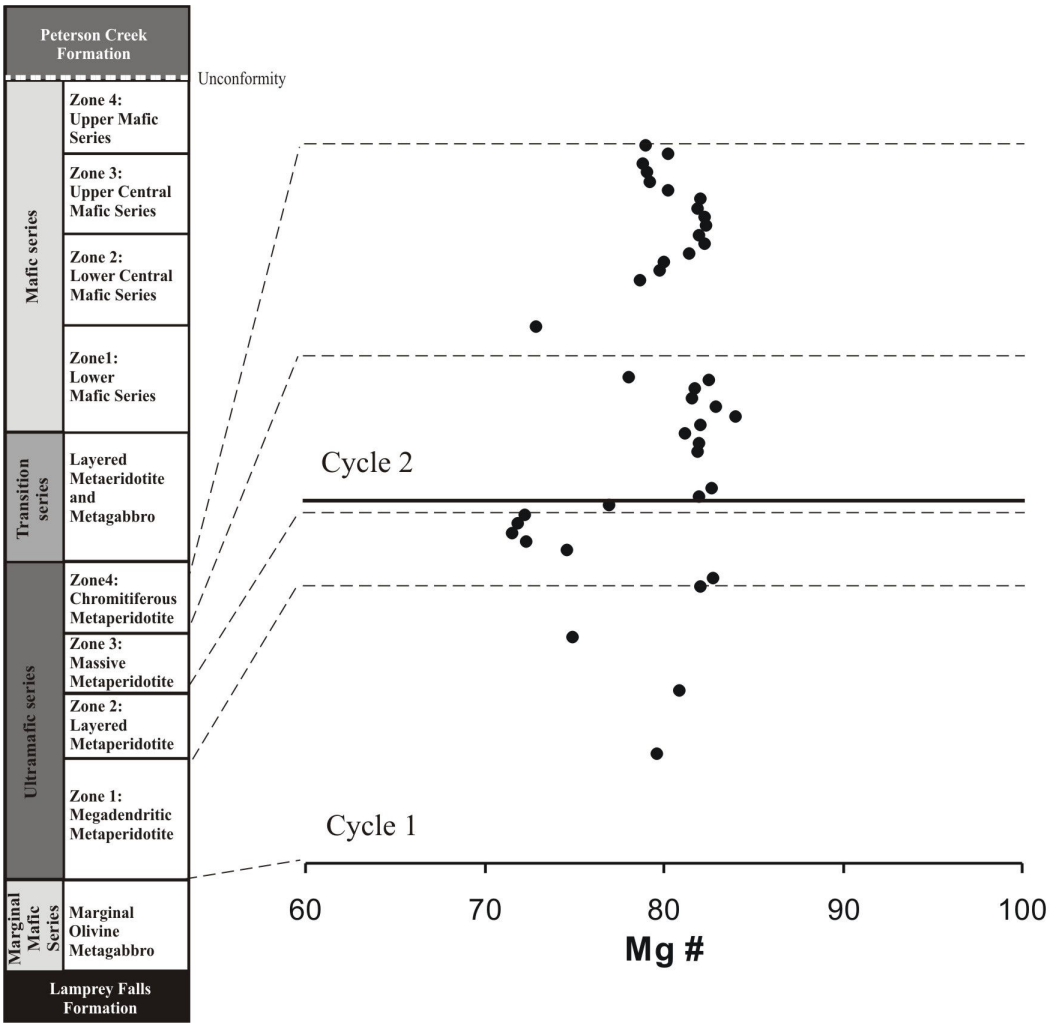

Figure 22: Mg# chemostratigraphic variations through the ultramafic series of the Chrome body, Bird River sill. Stratigraphy modified from Trueman (1971) and Scoates (1983). Geochemical data are located in Appendix B.

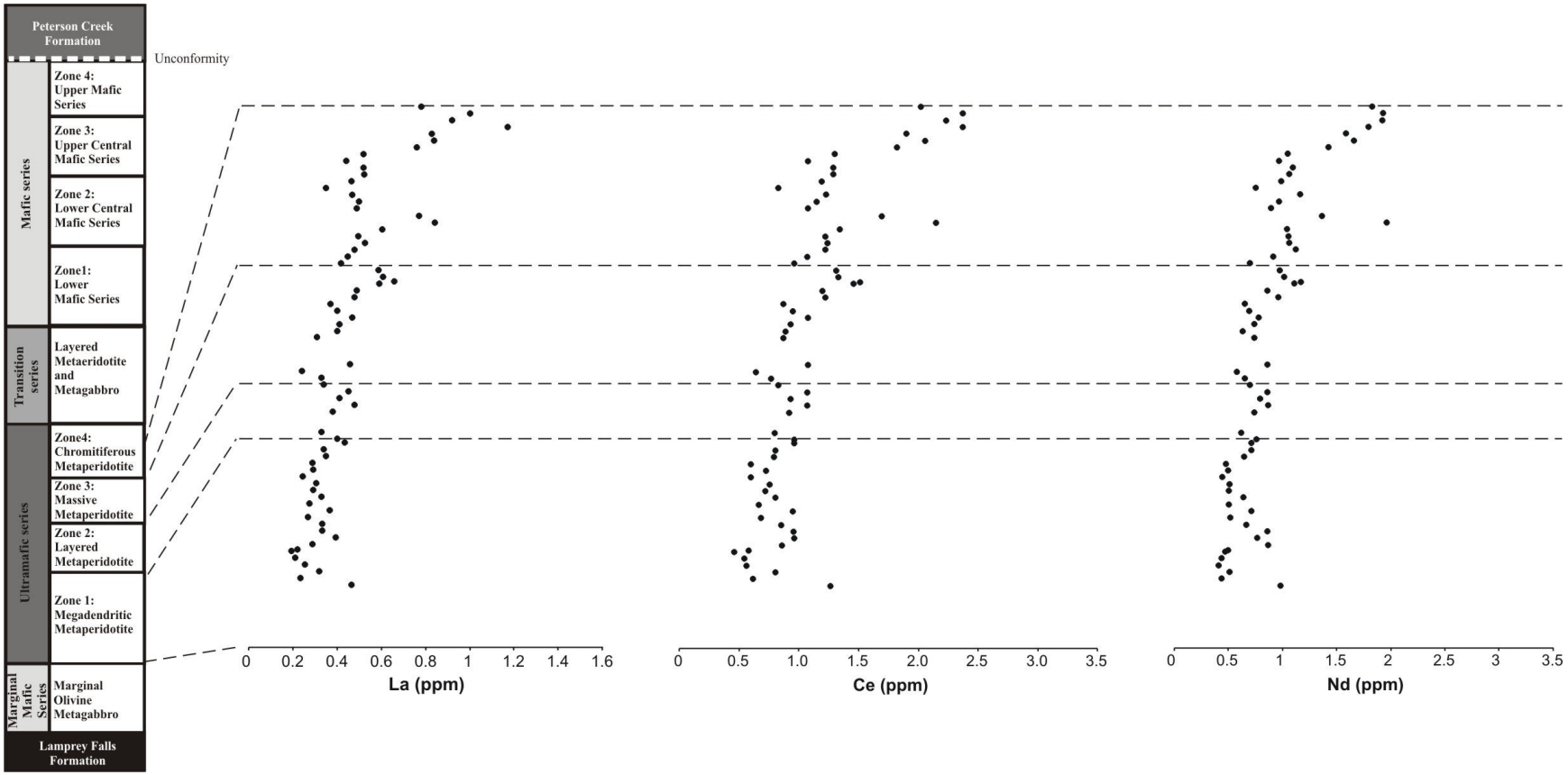

Figure 23: La, Ce and Nd variation with stratigraphy through the ultramafic series of the Chrome body, Bird River sill. Stratigraphy modified from Trueman (1971) and Scoates (1983). Geochemical data are located in Appendix B.

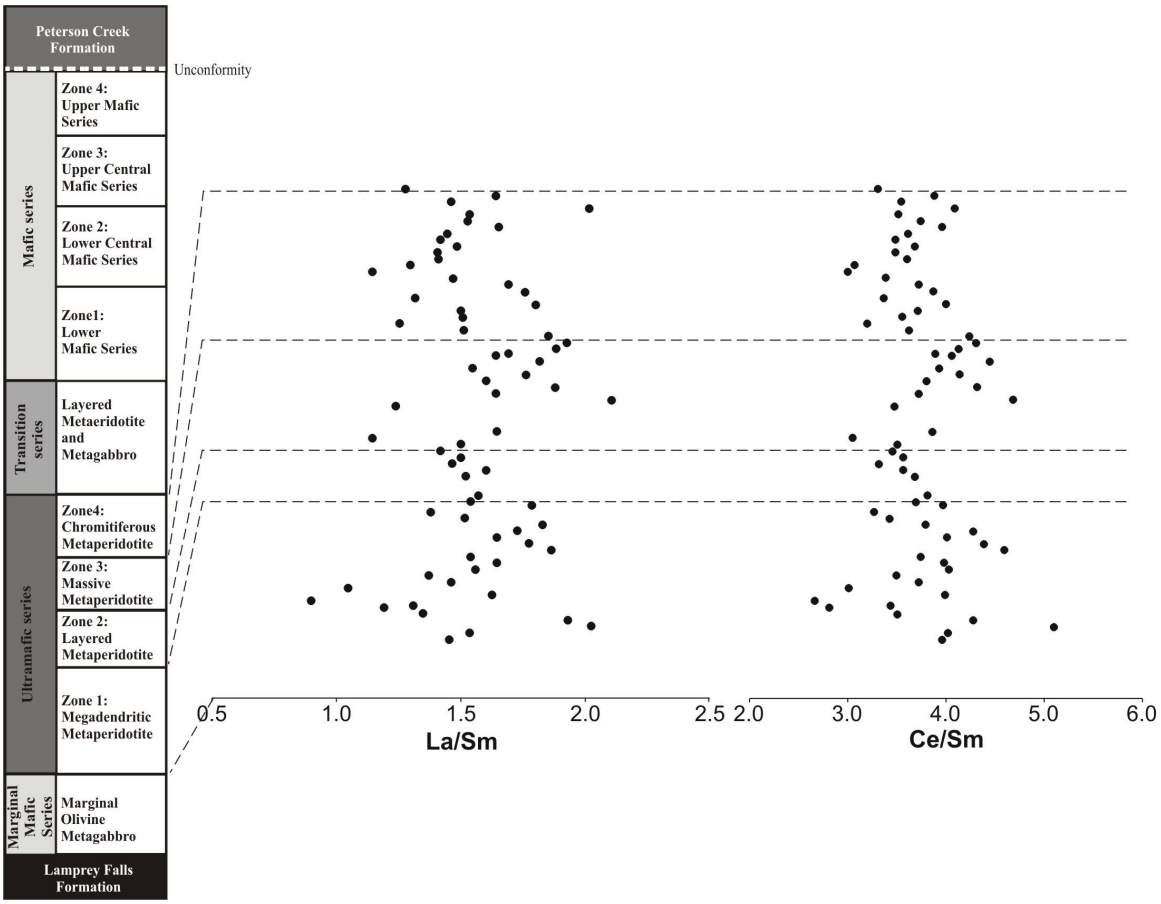

Figure 24: La/Sm and Ce/Sm variations with stratigraphy through the ultramafic series of the Chrome body, Bird River sill. Stratigraphy modified from Trueman (1971) and Scoates (1983). Geochemical data are located in Appendix B.

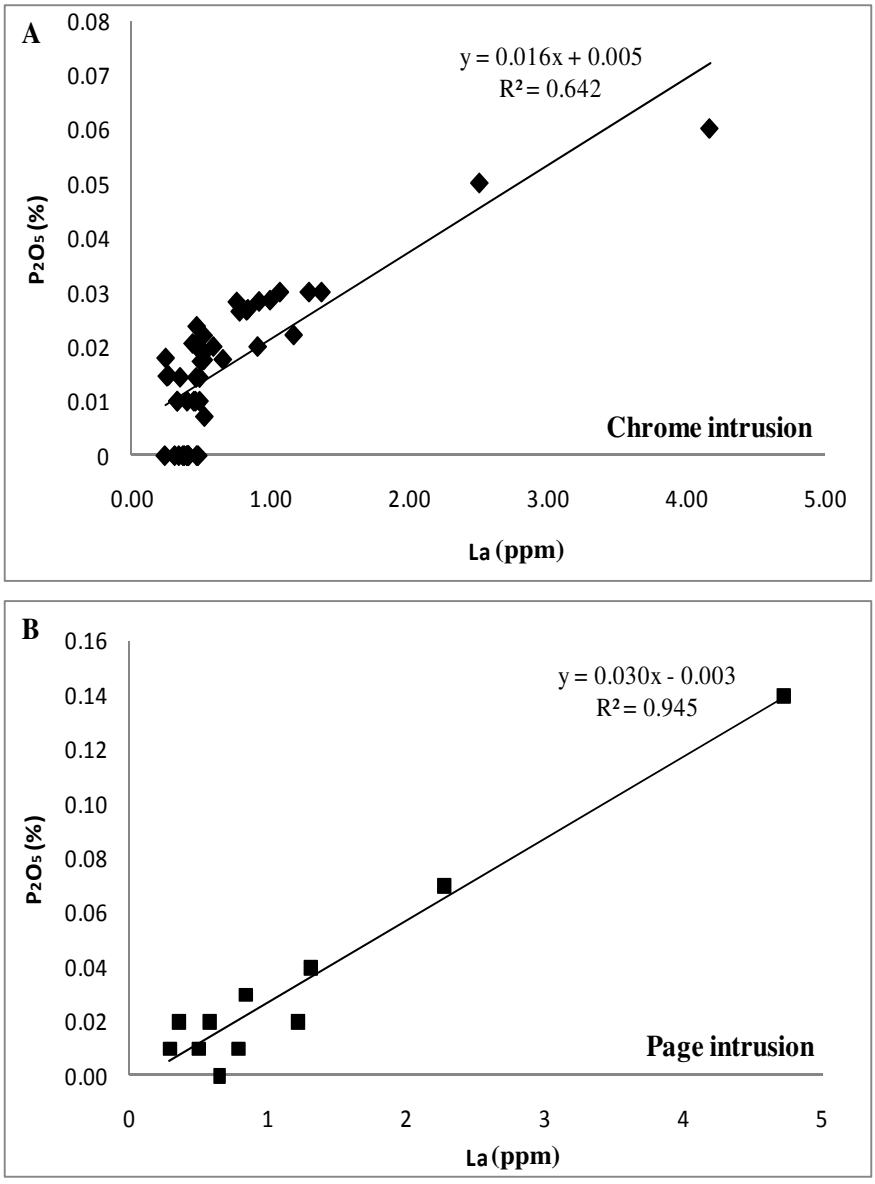

Figure 25: P_2O_5 versus La concentration of mafic and ultramafic samples from the Chrome and Page bodies of the Bird River sill. Geochemical data are located in Appendix B.

Chapter 5: Bird River Sill Cr-Ni-Cu-PGE Mineralization

The model that each BRS body is an individual intrusion implies each body may contain its own style of Ni-Cu-PGE and Cr mineralization. It is therefore necessary to consider each body separately. Due to lack of exposure and available samples from the National-Ledin and Peterson Block bodies, this section focuses on the Chrome and Page bodies. Previous studies have focussed on the chromitiferous zone of the Chrome intrusion. For this study, observations from previous studies were verified but emphasis is on the Page body and the lower Ni-Cu-PGE enriched horizon of the Chrome body.

5.1 Chromium Mineralization

Stratiform chromite deposits are common features of mafic-ultramafic layered intrusions. Within the western half of the BRS, chromite mineralization was observed in the ultramafic series of the Chrome and Page bodies. Chromite in the mafic series of the BRS was not observed in this study but occurrences have been documented (Scoates, 1983 and Bannatyne and Trueman, 1982).

5.1.1 Chrome body chromium mineralization

Chromium, present in chromite, is present in minor to trace amounts throughout the megadendritic metaperidotite zone to the top of the massive metaperidotite zone (Figure 26). There is a large increase in concentration in the chromitiferous zone where massive chromite seams are present. The results of this study are consistent with those of Theyer (1985).

Throughout the ultramafic series, chromite occurs as cumulate grains interstial to serpentinized olivine cumulate grains, chlorite and tremolite (originally pyroxene) (Figure 27A and B). Relict clinopyroxene is observed to poikilitically enclose cumulate grains of serpentinized olivine and chromite (Figure 27C). The chromite grains are euhedral to subhedral with subrounded edges and range from 0.1 to 1 mm in diameter. They contain numerous inclusions comprised of serpentinized olivine, chalcopyrite, pyrrhotite and pyrite. Sulphide inclusions are generally located within larger silicate inclusions at silicate-chromite boundaries (Figure 27D). Chromite grains exhibit

irregular fractures with chalcopyrite and/or serpentine along those fractures. The rims of several chromite grains were identified with the aid of SEM-EDS analyses to be enriched in Fe and depleted in Al; likely the result of Fe exchange with surrounding silicates during greenschist facies metamorphism. Halos with similar Fe-enrichment and Al-depletion are also present along fractures (Figure 28A and B).

In the chromitiferous metaperidotite zone, chromite forms a series of near monomineralic chromitite seams (>85% chromite) and chromitiferous peridotite layers (<85% chromite) which are laterally continuous across the Chrome body. These layers have previously been divided into six distinctive suites and are, from the lowest stratigraphic level upward (Scoates, 1983):

1.) Lower chromitites - composed of two or three partly discontinous and partly disrupted massive chromitite layers;
2.) Disrupted layer suite - composed of a serpentinized olivine cumulate layer that contains numerous disrupted massive chromitite seams;
3.) Lower main suite - composed of a narrow massive chromitite layer and a coarse-grained to pegmatitic peridotite;
4.) Banded and diffuse layer suite - composed of a sequence of diffuse (chromitiferous peridotite) and massive chromitite horizons separated by serpentinized olivine cumulate layers;
5.) Upper main chromitite - composed of two massive chromitite layers and one diffuse chromitite horizon separated by serpentinized olivine cumulate layers; and,
6.) Upper chromitites - composed of two pairs of massive chromitite horizons separated by serpentinized olivine cumulate layers.

Chromitite seams of the disrupted layer suite are of particular interest for comparison with a similar suite in the Page body. Chromitite in this layer form irregular, segmented and commonly bifurcated seams (Figure 28Figure 27C and D). Deformation is synmagmatic in origin and has previously been interpreted to be the result of gravitational instability of denser chromitite overlying a partially crystallized cumulus olivine crystal mush analogous to that of sedimentary load cast and “drop and sag” structures (Scoates et al., 1989).

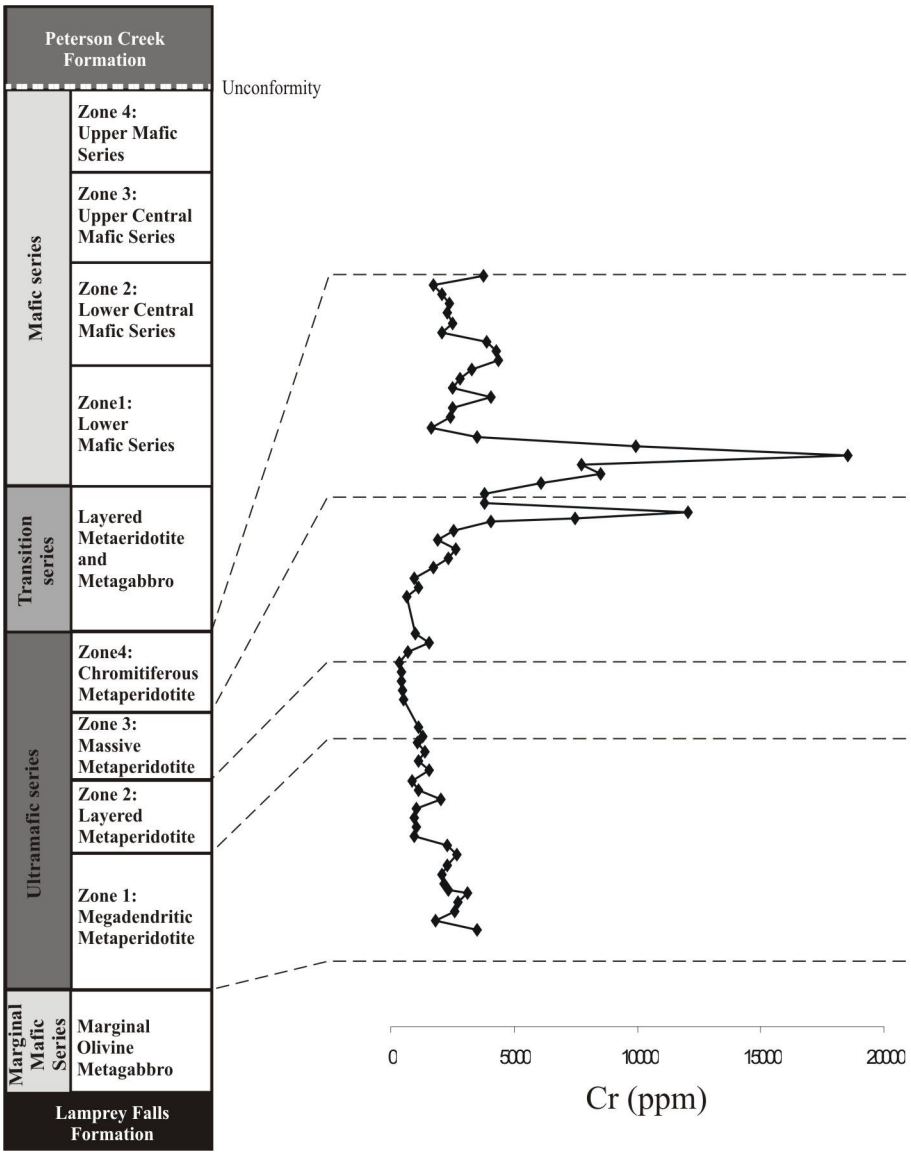

Figure 26: Chemostratigraphic variations of Cr through the ultramafic series of the Chrome body, Bird River sill. Stratigraphy modified from Trueman (1971) and Scoates (1983). Geochemical data are located in Appendix B.

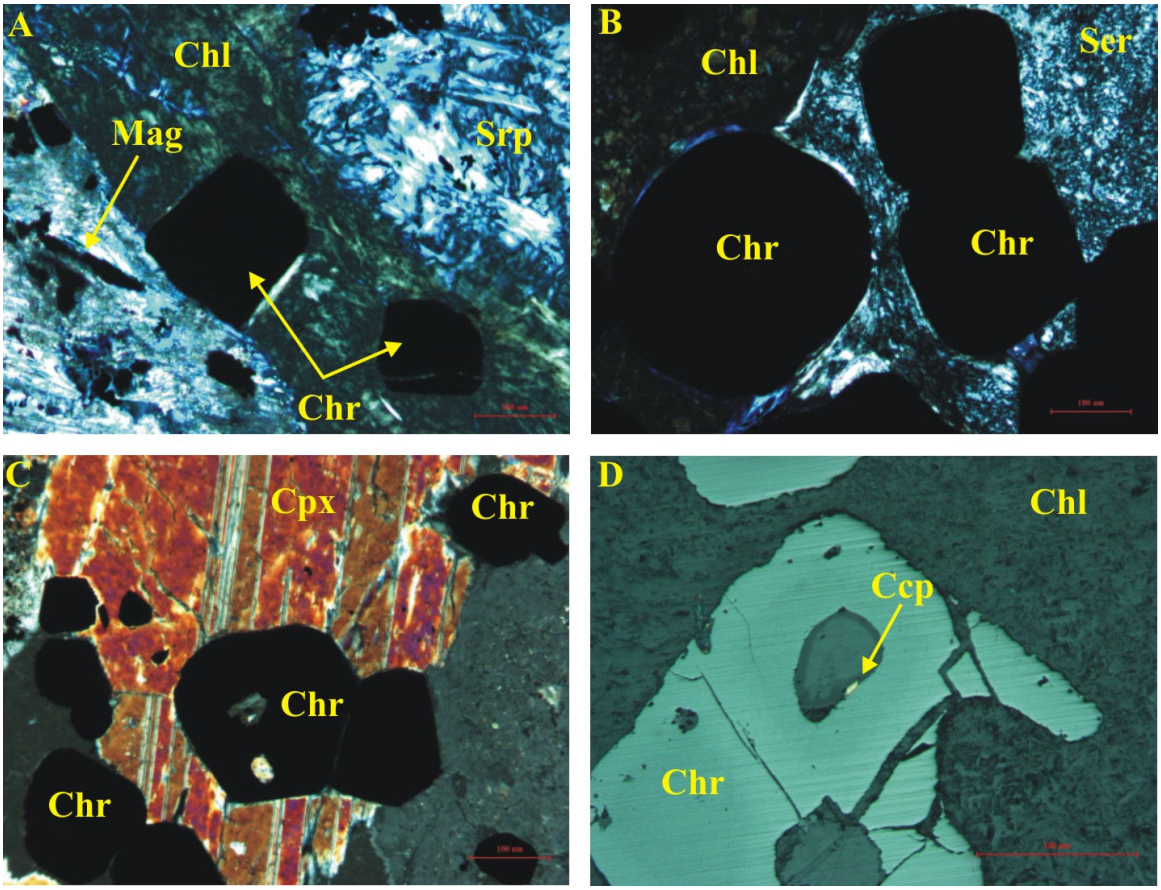

Figure 27: Photomicrographs of chromite mineralization from the Chrome body of the Bird River sill. A) Magnetite (Mag) and euhedral chromite grains (Chr) embedded in chlorite (Chl) interstial to serpentinized olivine (Srp); transmitted cpl. B) Subhedral chromite grains embedded in serpentine; transmitted cpl. C) Subhedral chromite grains enclosed in clinopyroxene (Cpx); transmitted cpl. D) Fractured, subhedral chromite grain with serpentine and chalcopyrite (Ccp) inclusions; reflected ppl.

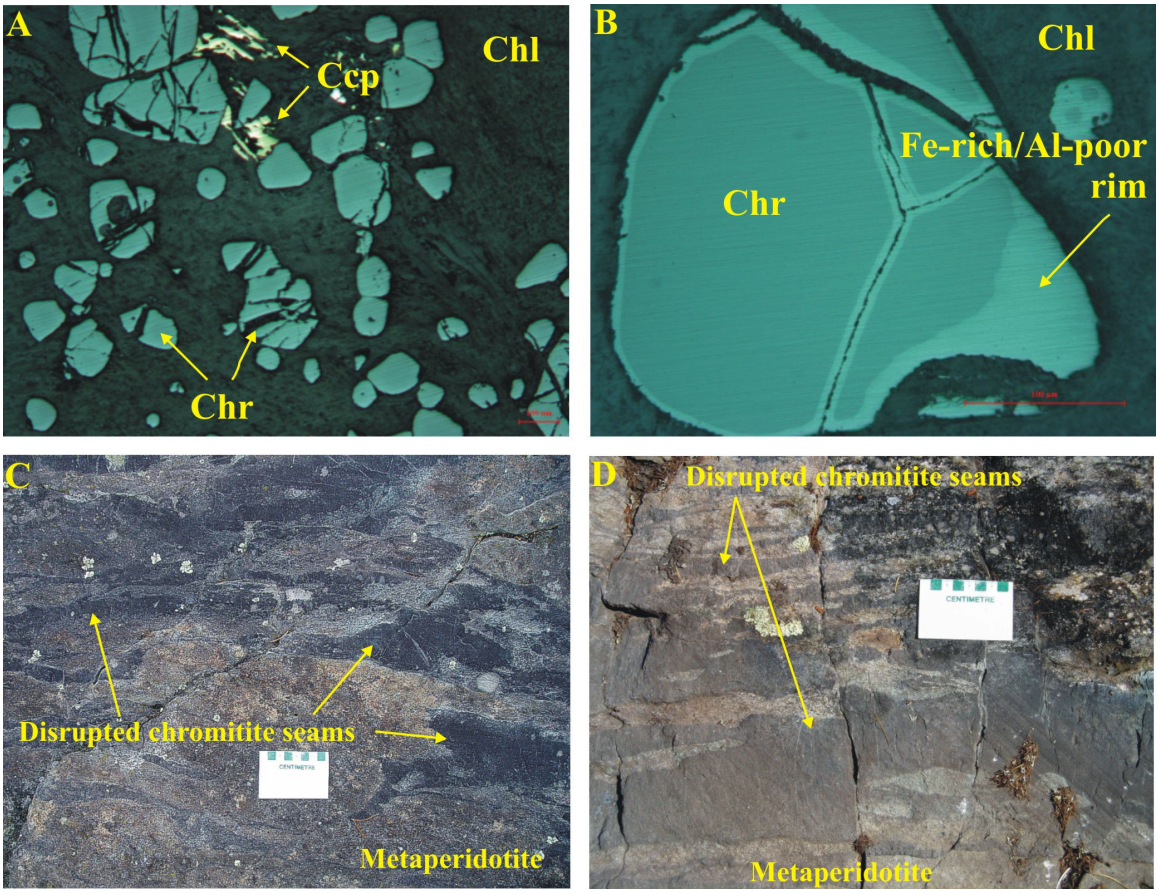

Figure 28: Photomicrographs and photographs of chromite mineralization from the Chrome body of the Bird River sill. A) Chalcopyrite interstitial to fractured chromite grains; reflected ppl. B) Subhedral chromite grain with Fe-rich/Al-poor rims and fracture halos; reflected ppl. C) and D) Photographs of the disrupted chromitite suite from the chromitiferous metaperidotite zone of the Chrome body, Bird River sill.

5.1.2 Page body chromium mineralization

Similar to that of the Chrome body, chromite in the Page body occurs in trace amounts in the lower portion of the ultramafic series and forms massive chromite layers in the upper ultramafic series near the mafic-ultramafic contact. In the lower portion of the ultramafic series, chromite is present as euhedral to subhedral grains and ranges from 0.1 to 0.5 mm in size. They are interstial to serpentinized olivine cumulate grains and embedded in talc, chlorite, tremolite, serpentine and relict clinopyroxene (Figure 29A). Very few silicate inclusions are present and no sulphide inclusions were observed in these chromite grains. SEM-EDS analyses identified Fe-enriched and Al-depleted rims along chromite grain boundaries and similar halos along fractures. In addition to this, magnetite, likely derived from the serpentinization of olivine, commonly forms ragged coatings on the chromite grains (Figure 29B). At the greenschist-amphibolite facies transition, magnetite begins to replace the original chromite (Barnes, 2000) therefore the magnetite coatings on the chromite grains are indicative of greenschist facies metamorphism.

Chromium mineralization in the upper ultramafic series of the Page body is similar to that of the chromitiferous metaperidotite zone of the Chrome body but contains a unique feature; chromite "pebbles" which occur stratigraphically above many of the disrupted chromite seams. The chromite pebbles are laterally continuous across the Page body. Figure 30 is a schematic from Theyer et al. (2001) that illustrates typical disrupted chromite seams with chromite pebbles in the eastern portion of the Page body.

In this study it was observed that the characteristics of the chromite pebbles differ significantly from east to west. In the east, pebbles are round and composed of dense chromite (>85% chromite) which range from a few millimetres up to 5 cm in diameter and are arranged in layers (Figure 31A). Elongate pebbles are oriented with the long-axis concordant to layering. Chromite pebbles present in the central area of the Page body differ from those in the east in respect to composition and size. The composition of the chromite pebbles varies from dense chromite (>85% chromite) to chromite-rich metaperidotite (<85% chromite) (Figure 31B and C). Chromite pebbles in the central area of the Page body retain their orientation within well defined layers but are generally

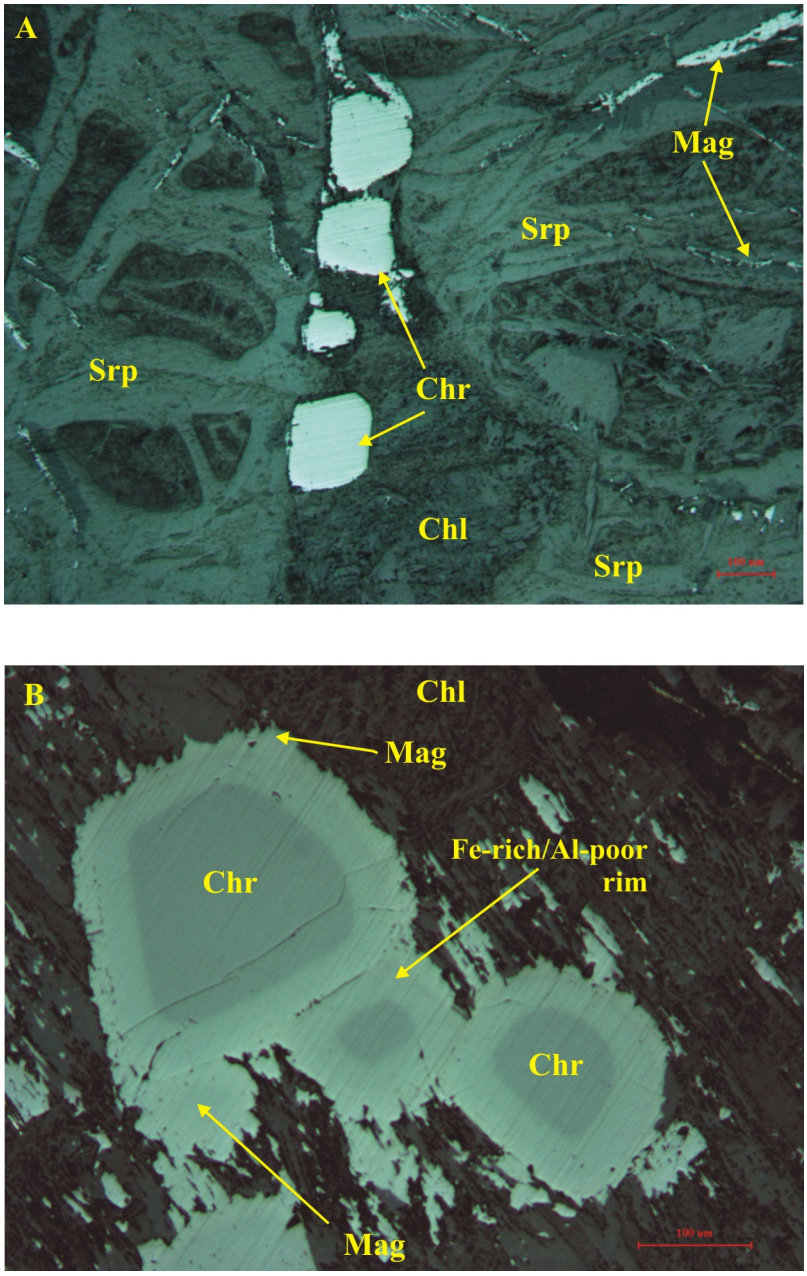

Figure 29: Photomicrographs of chromite mineralization from the Page body of the Bird River sill. A) Chromite cumulate grains (chr) embedded in chlorite (chl) interstital to serpentinized olivine cumulate grains (srp) and magnetite (mag); reflected ppl. B) Chromite cumulate grains with Fe-rich/Al-poor rims and magnetite coating. Chromite grains are embedded in chlorite; reflected ppl.

larger than those in the east. In the western portion of the Page body, there is a larger abundance of chromite-rich metaperidotite pebbles and fewer dense chromite pebbles. The size of the chromite pebbles is much larger in the west and ranges from 2 cm up to 15 cm diameter blocks. The chromite pebbles and blocks are also more angular and occur sporadically, in random orientation, throughout different stratigraphic positions in the ultramafic series, i.e. there is no clearly defined chromitiferous metaperidotite zone in the west end of the Page body (Figure 31D, E and F).

The formation of the chromite pebbles/blocks cannot be reconciled with an analogous mechanism that produces sedimentary load cast and "drop and sag" structures. Chromite pebbles occur stratigraphically above coinciding disrupted chromitite seams (Figure 30) and if the formation of the pebbles were similar to sedimentary load structures, the pebbles would be expected to form stratigraphically below these chromitite seams. Also, in many locations, chromite pebbles are present in the absence of chromitite seams. Theyer et al. (2001) proposed chromite pebbles represent autoliths derived from the debris of rigid chromitite layers that were disrupted and fragmented in a turbulent magmatic environment. Magmatic turbulence is supported by the occurrence of a chromitite pebble that indented and partially adhered to a second pebble (Theyer et al., 2001). The observed increase in size, angularity and sporadic occurrence of the chromite pebbles/blocks westward is interpreted by the author to indicate the origin of disruption of the chromite layers is in the west. The smaller pebbles present in the east are believed to have been transported away from the source in a turbulent environment and were subsequently rounded through resorption of boundaries via increased interaction with magma while the large angular blocks in the west remained close to the feeder.

5.1.3 Comparison of chromium mineralization between the Chrome and Page bodies of the Bird River sill

The Chrome and Page bodies of the BRS are similar in that they contain a chromitiferous metaperidotite zone located near the mafic-ultramafic contact. This is a common occurrence in many mafic-ultramafic intrusions. For example, the chromite layers of the world renowned Bushveld complex occur near an ultramafic-mafic contact within the critical zone (Barnes and Maier, 2002). In respect to the BRS block faulted model (Figure 12), the fact the basic stratigraphy and occurrence of chromite layers

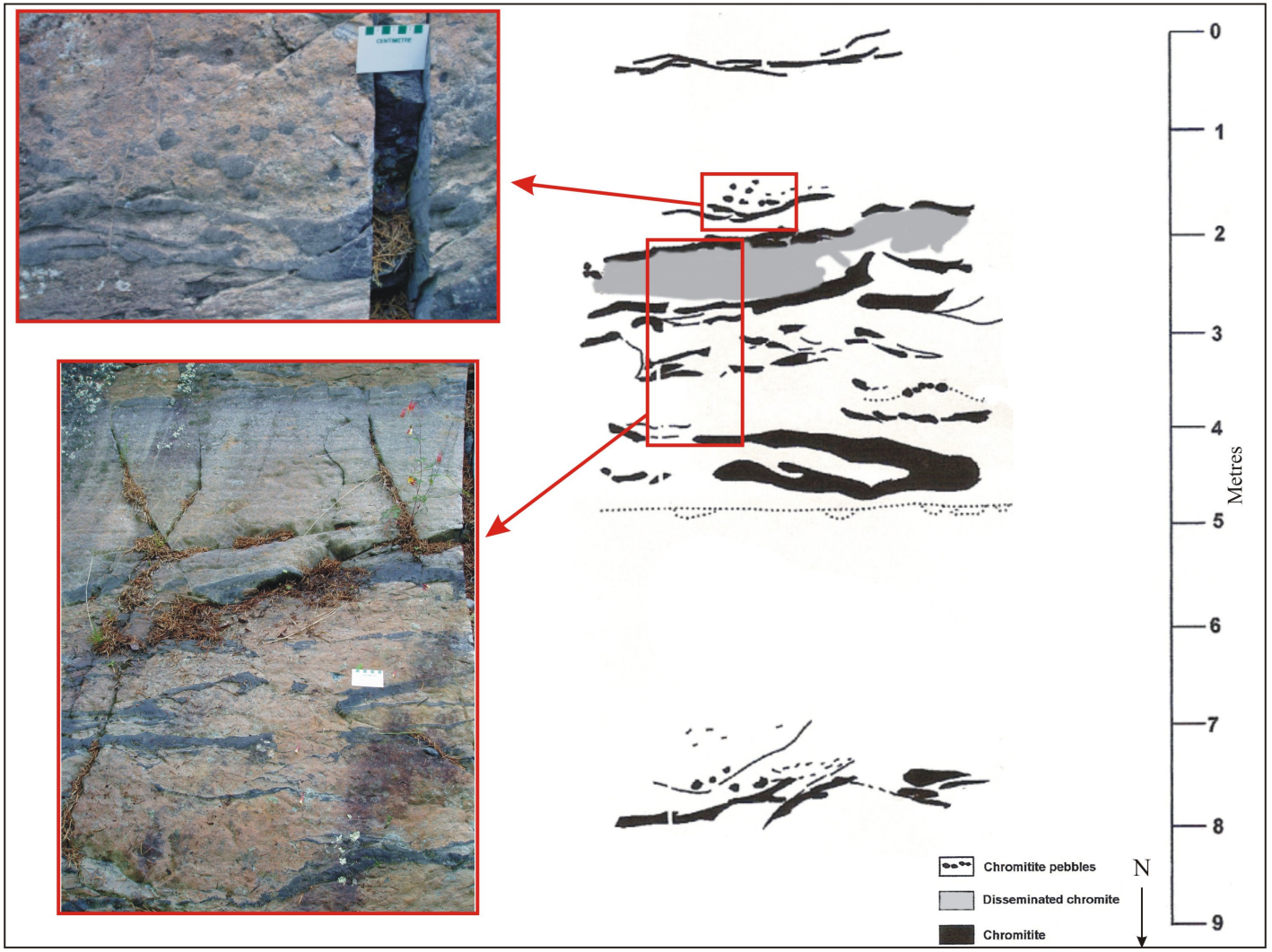

Figure 30: Detailed geological schematic of a chromitiferous metaperidotite exposure on the east end of the Page body, Bird River sill. Schematic from Theyer et al. (2001).

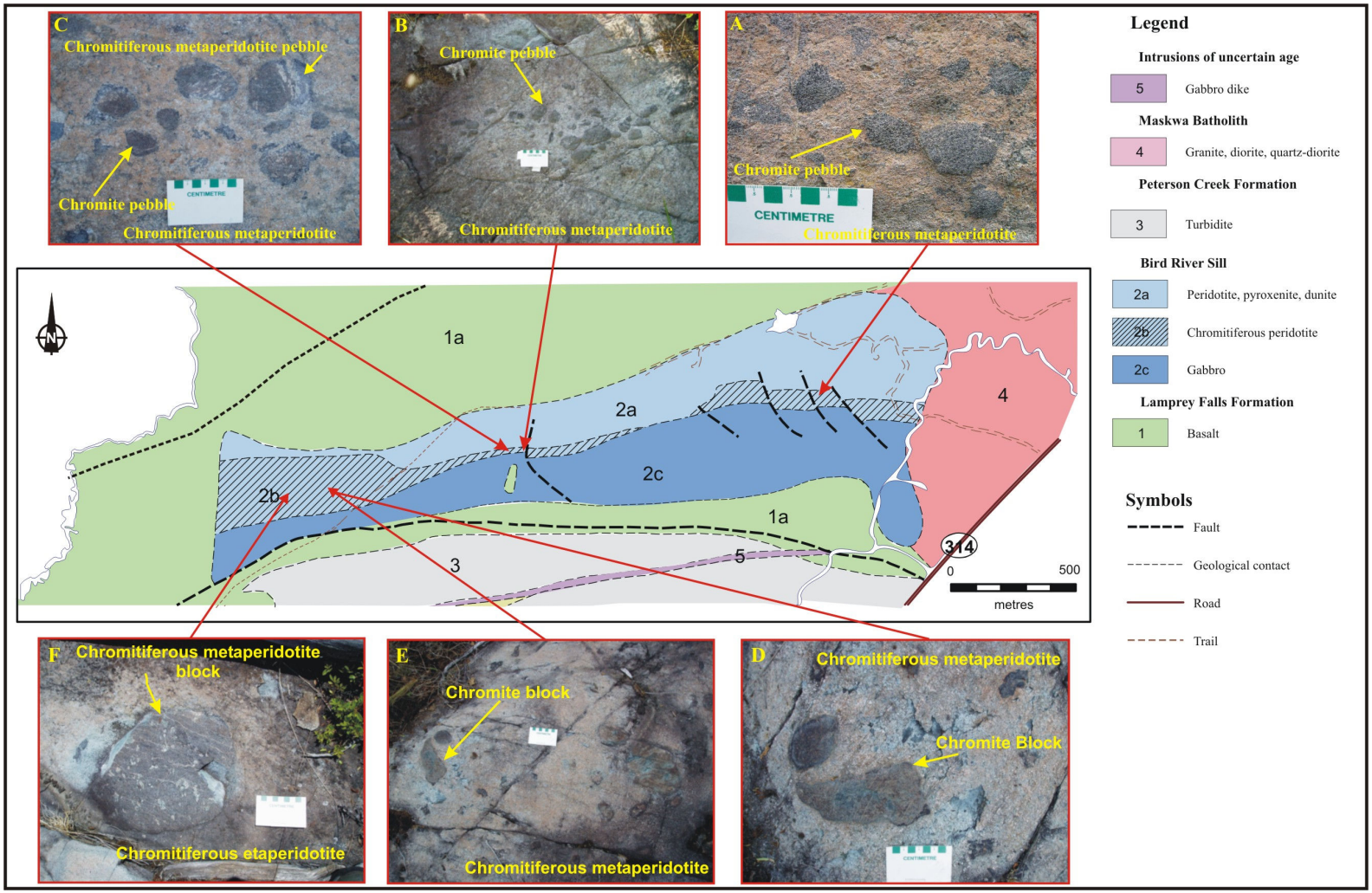

Figure 31: Simplified geological map of the Page body of the Bird River sill with photographs illustrating variations in chromite pebble characteristics from east to west. A) Round, dense chromite pebbles. B) Round, dense chromite pebble layer. C) Chromite and chromitiferous metaperidotite pebbles. D) and E) Angular, dense chromite blocks. F) Large chromitiferous metaperidotite block.

corresponds between the separate bodies of the BRS does not necessarily indicate they were once part of a single intrusion. Chromite layers have been shown to be laterally continuous within the separate Chrome and Page bodies but can not be correlated between the BRS bodies. Chromite pebbles are absent in the BRS bodies outside of the Page body. It is in the opinion of the author that the presence and lateral continuity of the chromite pebbles distinguishes the Chrome and Page bodies and thus they are not displaced segments of an originally single intrusion. The presence and lateral continuity of the chromite pebbles further supports the separate intrusion model proposed by this study.

5.2 Nickel and Copper Sulphide Mineralization

Ni-Cu sulphide mineralization was observed on the Chrome body, Page body and within the Lamprey Falls Formation in close proximity to the northern margin of the BRS. The sulphide mineralogy of these occurrences is similar to that of the Maskwa-Dumbarton body of the BRS described by Juhas (1973). This section describes the Ni-Cu and associated Fe-, Zn- and Pb-sulphide occurrences in the western half of the BRS. Common oxide minerals, magnetite and ilmenite, are discussed at the end of this section.

5.2.1 Chrome body Ni-Cu sulphide mineralization

Trace amounts of Ni-Cu sulphide minerals are present throughout the mafic and ultramafic series of the Chrome body. In the mafic series and marginal olivine metagabbro, sulphide mineralization was observed in layered gabbroic horizons and within east- and northwest-trending shear zones. Mineralization consists of very fine-grained disseminations of chalcopyrite and pyrrhotite within tremolite, clinozoisite and chlorite. In the ultramafic series, sulphide mineralization ranges from trace to 10%. The higher concentrations are contained in two significantly enriched horizons in the upper portion of the megadendritic peridotite zone and lower half of the chromitiferous zone (Figure 32). The dominant sulphide species in the ultramafic series are pentlandite, chalcopyrite, pyrrhotite and sphalerite with trace amounts of gersdorffite. The sulphide minerals are present within serpentine, tremolite, pyroxene and as inclusions in chromite.

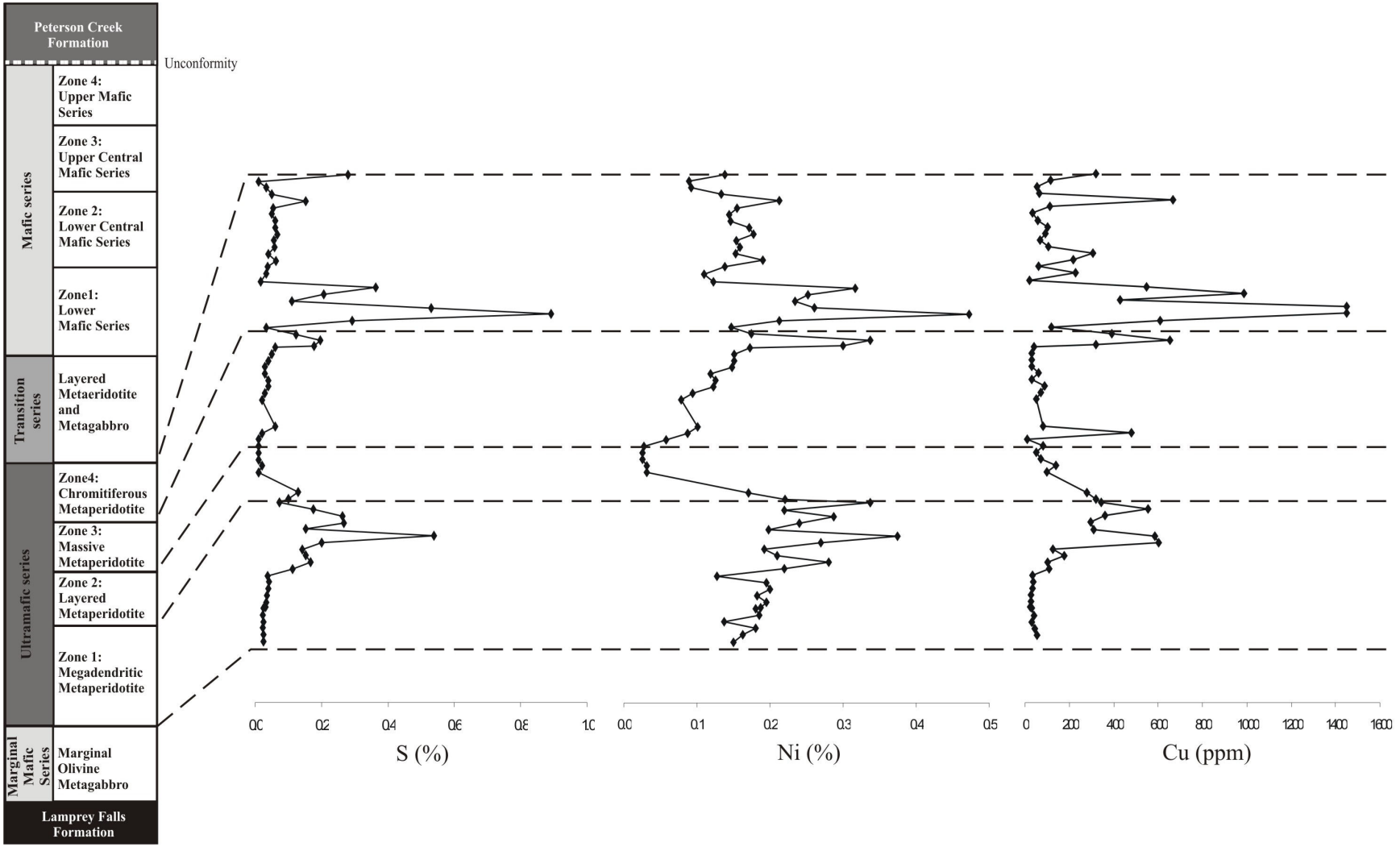

Figure 32: Chemostratigraphic variations of S, Ni and Cu through the ultramafic series of the Chrome body, Bird River sill. Stratigraphy modified from Trueman (1971) and Scoates (1983). Geochemical data are located in Appendix B.

SEM-EDS analyses indicate that gersdorffite is Co-bearing and thus is interpreted to represent an intermediate composition in the cobaltite-gersdorffite solid solution series.

As a result of metamorphism it is difficult to determine from petrographic analysis the nature of the sulphide mineralization present within the east- and northwest-trending shear zones in the mafic series and ultramafic series of the Chrome body. The Cu/Pd of the shear zones samples are below that of primitive mantle and within the Cu/Pd range of the other samples from the mafic-ultramafic series of the Chrome body (Figure 33). It is likely the sulphide mineralization present within the shear zones pre-date the deformation and are the same as that of the disseminated mineralization observed throughout the Chrome body. Remobilization, if any, is local and small scale.

5.2.2 Page body Ni-Cu sulphide mineralization

Four styles of sulphide mineralization were observed on the Page body: 1) trace to minor amounts of fine to blebby disseminated sulphide minerals, 2) sulphide mineralization along fractures, 3) massive to semi-massive sulphide mineralization, and 4) sulphide mineralized quartz-feldspar porphyry dykes. Laterally continuous Ni-Cu enriched horizons have not delineated on the Page body but there is an increase in sulphide content associated with the chromitiferous metaperidotite zone (Theyer et al., 2001). Overall, the dominant style of sulphide mineralization is fine to blebby disseminated sulphide minerals. Trace amounts to minor amounts of chalcopyrite, pyrrhotite, sphalerite, pyrite, gersdorffite, millerite and niccolite are present within the ultramafic series and mafic series of the Page body. The marginal olivine metagabbro contains minor amounts of fine to blebby disseminated chalcopyrite and pyrrhotite. Cu/Pd of the disseminated sulphide samples is consistent with that of the Chrome body (Figure 33).

The second style of mineralization consists of sulphides along fractures. Numerous sulphide-bearing fractures filled with carbonate minerals, serpentine and chlorite are present and truncate the disseminated sulphide mineralization discussed above. The dominant sulphide in the fractures is chalcopyrite but sphalerite, pyrite and pyrrhotite were observed in a few polished thin sections. Although many fractures contain sulphides, there are many that truncate the metamorphic mineral assemblage which

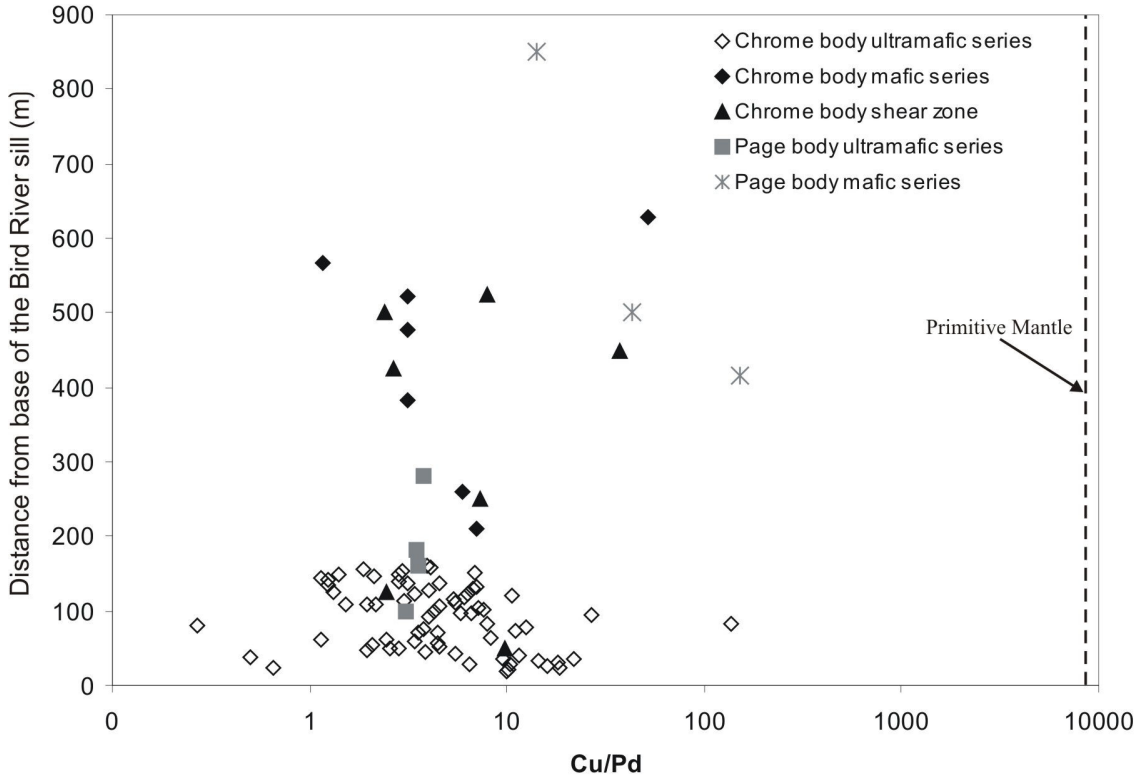

Figure 33: Cu/Pd in the mafic and ultramafic series of the Chrome and Page bodies of the Bird River sill. Stratigraphic height is relative to the base of the respective intrusion. Primitive mantle value is from Barnes and Maier (1999). Geochemical data are located in Appendix B.

appear not to contain any sulphide mineralization. These fractures are chlorite and calcite filled similar to the mineralized fractures.

Massive sulphide mineralization was observed in drill core. This zone, approximately 30 cm thick, is present at the contact between peridotite and a mineralized quartz-feldspar porphyry dyke approximately 15 m above the intrusive BRS-Lamprey Falls Formation contact. Sulphide mineralization consists of massive pyrrhotite with pentlandite exsolution and blebs of chalcopyrite. Anhedral inclusions of magnetite are enclosed in pyrrhotite. Semi-massive sulphide mineralization is present in a 15 m horizon located approximately 10 m stratigraphically above the intrusive BRS-Lamprey Falls Formation contact. Mineralization in this horizon consists of semi-massive net-textured sulphide minerals, stringers and coarse to fine blebby disseminations. Pyrrhotite and chalcopyrite are the dominant sulphide minerals but pentlandite, gersdorffite and pyrite are also present.

The fourth style of sulphide mineralization consists of mineralized quartz-feldspar porphyry dykes. These dykes truncate the lower ultramafic series of the Page body. Similar dykes are reported throughout the Maskwa-Dumbarton body of the BRS. Up to 30% of blebby disseminated sulphides composed of chalcopyrite, pyrrhotite, sphalerite and pyrite with abundant inclusions of quartz, feldspar and biotite are present. Sulphide minerals commonly exhibit a chlorite halo.

5.2.3 Lamprey Falls Formation Ni-Cu sulphide mineralization

Minor amounts of chalcopyrite, pyrrhotite and pyrite are present in chlorite- and quartz-filled fractures which cross-cut the Lamprey Falls Formation adjacent to the northern boundaries of the Chrome and Page bodies of the BRS. North of the Peterson Block body there are large quartz-filled fractures which contain significant amounts of sphalerite and galena with minor amounts of pyrrhotite, chalcopyrite, ilmenite, magnetite and hematite. In this study, galena was observed exclusively in the quartz-filled fractures north of the Peterson Block body but galena has been reported by Juhas (1973) in areas near the Maskwa-Dumbarton body of the BRS.

5.2.4 Sulphide and oxide mineralogy

Pyrrhotite

Pyrrhotite is the dominant sulphide in the BRS and is present in the ultramafic and mafic series. It occurs as massive mineralization, fine to blebby anhedral disseminations and as large, aggregates intergrown with chalcopyrite (Figure 34A). Pyrrhotite commonly exhibits pentlandite exsolution along fractures and grain boundaries (Figure 34B). Numerous anhedral to euhedral (bladed) inclusions of silicates, magnetite and other sulphides (discussed below) are present throughout. In locations where pyrrhotite is present with chromite, pyrrhotite occurs interstitial to the chromite grains. In the massive sulphide horizon of the Page body, pyrrhotite exhibits extensive pyrite and/or marcasite replacement.

Chalcopyrite and Covellite

Chalcopyrite is present in the mafic and ultramafic series of the BRS as anhedral, fine to blebby disseminations and is the dominant fracture-bound sulphide mineral with the exception of the quartz-filled fractures north of the Peterson Block body where sphalerite is the dominant sulphide mineral. Chalcopyrite commonly occurs in large aggregates intergrown with pyrrhotite and pentlandite and is replaced along grain boundaries by covellite. Within the chromite-bearing horizons of the Page and Chrome bodies, chalcopyrite typically occurs interstitial to chromite but is also present as small inclusions within the chromite cumulate grains (Figure 34C). Within the chromite grains, the chalcopyrite inclusions occur along the grain boundaries of larger silicate inclusions within the chromite grains.

Pentlandite

Pentlandite was observed exclusively in the ultramafic series of the Page and Chrome bodies of the BRS. Pentlandite is present as large blebs and along fractures and grain boundaries of pyrrhotite as fine blades, flames and exsolution blebs. Pentlandite exhibits replacement by pyrite and/or marcasite along fractures and grain boundaries (Figure 34D).

Sphalerite and Galena

Sphalerite is present within the ultramafic series of the Chrome and Page bodies as well as a minor constituent of fracture-bound sulphide minerals. Sphalerite is present as fine disseminations within tremolite, serpentine and clinozoisite and on the edges of pyrrhotite-chalcopyrite aggregates. It commonly contains numerous inclusions of magnetite and a few inclusions of galena. Sphalerite is the dominant fracture-bound sulphide mineral in the quartz-filled fractures that truncate the Lamprey Falls Formation to the north of the Peterson Block body. SEM-EDS analyses indicate sphalerite is coated by a Pb-oxide in the quartz-filled fractures (Figure 35A). Galena is present exclusively in the quartz-filled shear zones that cross-cut the Lamprey Falls Formation north of the Peterson Block body. Galena is present as anhedral to subhedral grains within and along grain boundaries of sphalerite.

Pyrite and Marcasite

Pyrite is present throughout the BRS. Two distinct generations of pyrite were identified. Primary pyrite is present as fine subhedral grains within silicate groundmass and as inclusions in pyrrhotite, pentlandite and chalcopyrite. Secondary pyrite is present as replacement products of pyrrhotite and pentlandite along fractures and grain boundaries with marcasite. Marcasite formed fibrous edges along the fractures and grain boundaries of the pyrrhotite and pentlandite grains.

Millerite

Trace amounts of millerite were observed exclusively in the ultramafic series of the Page body as fine disseminations in serpentine and as intergrowths with chalcopyrite (Figure 35B). Since millerite is a common hydrothermal alteration product of pentlandite it is possible that millerite is a secondary sulphide mineral formed at the expense of pentlandite.

Gersdorffite and Niccolite

Gersdorffite is present in trace amounts as fine subhedral to euhedral grains in pyrrhotite, pentlandite and chalcopyrite (Figure 34B and Figure 35B). Gersdorffite was observed exclusively in the ultramafic series of the Page and Chrome bodies. Niccolite was observed in one polished thin section from a massive ultramafic outcrop on the Page

body. Niccolite is present as fine anhedral disseminations within serpentine and is intergrown with pentlandite and chalcopyrite (Figure 34C).

Magnetite

Magnetite is the dominant opaque mineral in the ultramafic series of the BRS and is present as: 1) subhedral grains as inclusions in pyrrhotite, pentlandite and chalcopyrite, 2) anhedral to subhedral grains and pods disseminated throughout the silicate groundmass of the ultramafic series, and 3) fine, dusty grains that outline cleavage, fractures and grain boundaries of serpentinized olivine cumulate grains. Two generations of magnetite were identified. The first generation of magnetite is anhedral to subhedral grains present throughout the sulphide and silicate groundmass. The second generation of magnetite is the very fine ("dusty") grains which outline serpentinized olivine formed as a result of Fe released through the serpentinization of the primary ultramafic mineral assemblage. The dusty magnetite outline aids in the preservation and recognition of primary cumulate textures.

Ilmenite

Ilmenite is present as fine disseminations throughout the mafic series of the Chrome and Page bodies where it is commonly bound and replaced by rutile (Figure 35D). Ilmenite is also present as a fracture filling mineral in the quartz-filled shear zones that cross-cut the Lamprey Falls Formation north of the Chrome, Page and Peterson Creek bodies of the BRS.

5.2.5 Discussion on the origin of the Bird River sill Ni-Cu sulphide mineralization

Sulphide mineralization is present throughout the mafic and ultramafic series of the separate BRS bodies as fine to blebby disseminations and specifically on the Page body, stratigraphically controlled massive to semi-massive mineralized horizons. Increased Ni-Cu concentrations are associated with chromite horizons on both the Chrome and Page bodies. Fracture bound sulphides were observed in the mafic and ultramafic series of the Page body and along fractures which cross-cut the Lamprey Falls Formation north of the Chrome, Page and Peterson Block bodies. Ni-Cu sulphide mineralized quartz-feldspar porphyry dykes cross-cut the lower ultramafic series of the Page body. Overall, sulphide mineralization appears to be magmatic and stratigraphically controlled with

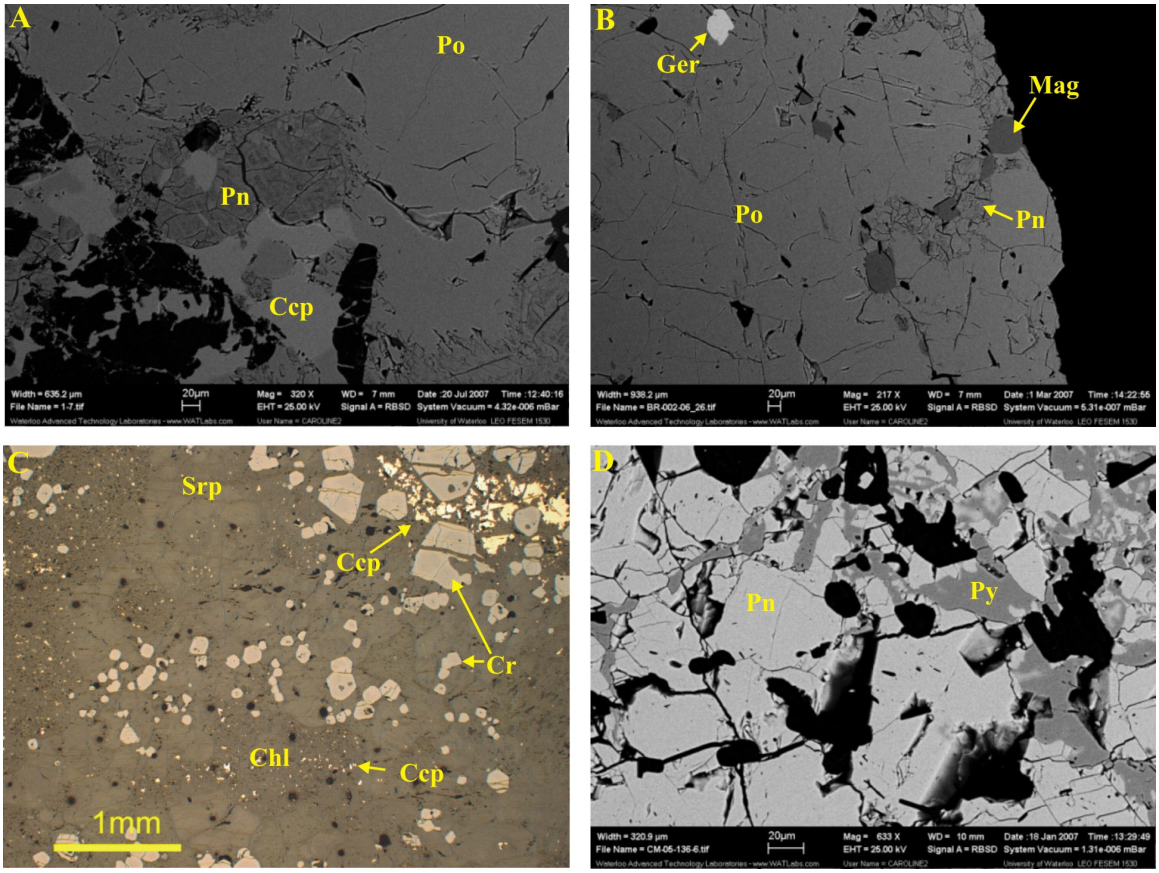

Figure 34: Photomicrgraphs and back-scattered electron images of Bird River sill sulphide and oxide mineralization. A) Semi-massive pyrrhotite (Po) and chalcopyrite (Ccp) with pentlandite (Pn) exsolution. B) Semi-massive pyrrhotite with pentlandite exsolution and disseminated grains of magnetite (Mag) and gersdorffite (Ger). C) Photomicrograph of disseminated chalcopyrite interstitial to cumulate chromite (Cr) grains in serpentine (Srp) and chlorite (Chl); reflected ppl. D) Pentlandite with pyrite (Py) replacement.

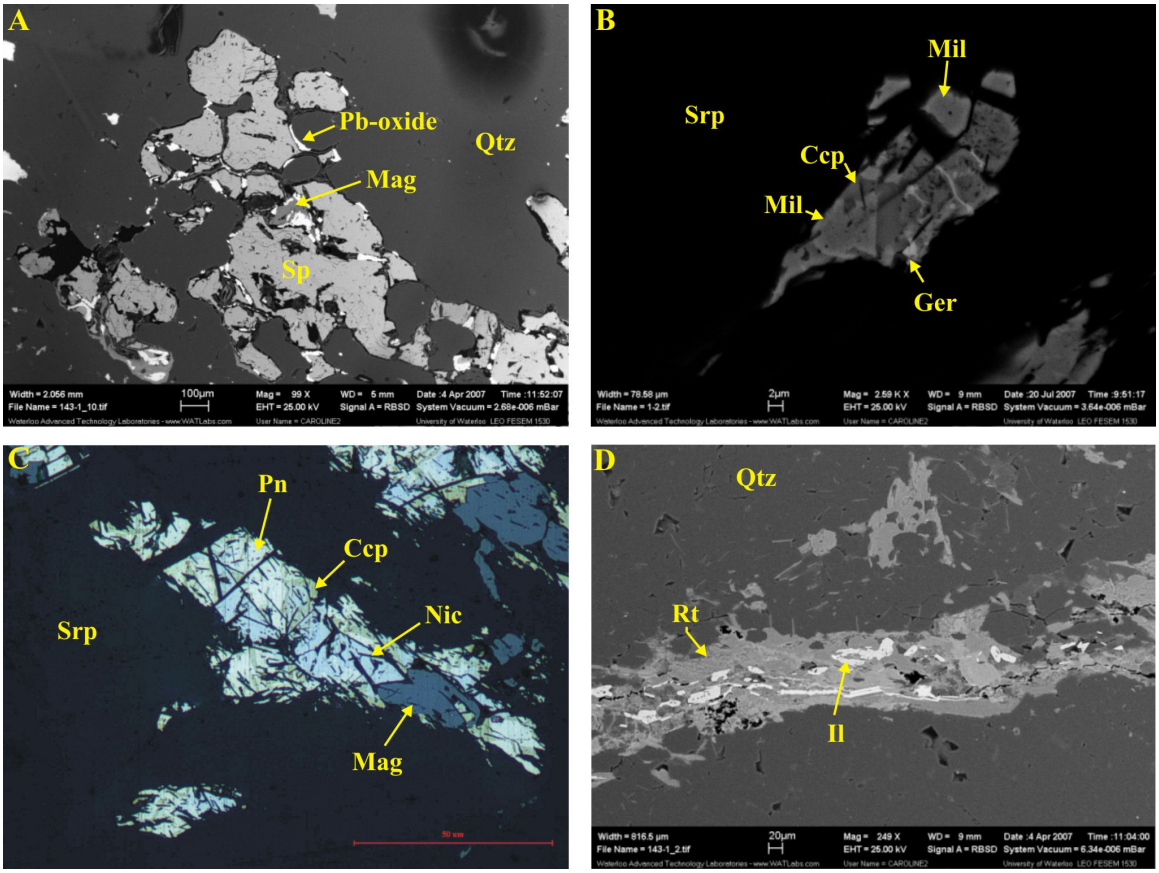

Figure 35: Photomicrographs and back-scattered electron images of Bird River sill sulphide and oxide mineralization (continued). A) Quartz-filled fracture with sphalerite (Sp), Pb-oxide coatings on the sphalerite and magnetite (Mag) inclusions. B) Chalcopyrite (Ccp), millerite (Mil) and gersdorffite (Ger) agglomerate in serpentine (Srp) groundmass. C) Chalcopyrite, pentlandite (Pn), magnetite and niccolite (Nic) agglomerate in serpentine groundmass; reflected ppl. D) Ilmentite (Il) with rutile (Rt) replacement in quartz-filled shear zone.

remobilization of Ni-Cu sulphides associated with late felsic magmatism and along shear zones and fractures within the BRS and Lamprey Falls Formation. This study agrees with previous investigations which also concluded that sulphide mineralization in the BRS is magmatic in origin.

5.3 Platinum-Group Element Mineralization

Previous investigations on PGE mineralization in the BRS have largely focussed on the chromitiferous zone of the Chrome body. To further and compliment these works, this investigation examined PGE mineralization from both the Chrome and Page bodies and the quartz-feldspar porphyry dykes that truncate the lower ultramafic series of the BRS. SEM-EDS images and semi-quantitative analyses of PGE are presented in Appendix C.

5.3.1 Chrome body Platinum-Group Element mineralization

Two correlations between Ni-Cu-PGE and Cr mineralization were shown by Scoates et al. (1988) in an investigation on the stratigraphically upper Ni-Cu-PGE enriched horizon present in the chromitiferous metaperidotite zone: 1) PGE are strongly correlated with Cr (+V+Zn), and, 2) Ni (+Cu+Co) is correlated with S and Se indicating a nickel sulphide factor. It was concluded that there is no association between PGE and the nickel sulphide factor (Scoates et al., 1988).

Geochemical data from this study indicates Pt-Pd enriched horizons are present within the ultramafic series of the Chrome body and correspond with the two Ni-Cu enriched horizons discussed above in section 5.2.1 (Figure 36). The upper Ni-Cu-PGE enriched horizon present in the chromitiferous metaperidotite zone corresponds with Cr enrichment whereas the lower Ni-Cu-PGE enriched horizon present in the megadendritic metaperidotite zone does not correspond to Cr enrichment (Figure 36). This data is consistent with that of Theyer (1985). It is interesting that the lower Ni-Cu-PGE enriched horizon corresponds with significant concentrations of As but the upper Ni-Cu-PGE enriched horizon is only associated with moderate increases in As and the highest concentrations of As occur stratigraphically above the upper Ni-Cu-PGE enriched horizon. This suggests that arsenide PGM species (i.e. sperrylite ($PtAs_2$)) are not as

abundant in the Cr-rich upper PGE enriched horizon compared to PGM occurrences outside of the chromite layers.

Thirteen PGM and one sulphurarsenide mineral containing PGE were identified in the stratigraphically lower Ni-Cu-PGE enriched horizon of the Chrome body with the aid of SEM-EDS analyses. PGM include (in order of abundance): merenskyite ($PdTe_2$), borovskite (Pd_3SbTe_4), hollingworthite (RhAsS), kotulskite (Pd(Te,Bi)) and sperrylite ($PtAs_2$). The PGE-bearing sulphurarsenide mineral is gersdorffite. Previous investigations have identified PGM in the upper Ni-Cu-PGE enriched horizon of the Chrome body and within other PGE enriched horizons not identified in this investigation. PGM include: sperrylite ($PtAs_2$), kotulskite (Pd(Te,Bi)), merenskyite ($PdTe_2$), laurite (RuS_2), hollingworthite (RhAsS), irarsite (IrAsS), keithconnite ($Pd_{3-X}Te$), and mertieite II (Pd_8Sb_3) (Scoates et al., 1988). PGM have also been identified as inclusions in cumulous chromite and include PGE alloys ($(Ru,Os,Ir)S_2$), laurite (RuS_2) and rutheniridosimine (Ir,Os,Ru) (Talkington et al., 1983). It was concluded that these PGM inclusions in chromite were either trapped or formed during chromite precipitation (Talkington et al., 1983).

PGM identified in this study in the lower Ni-Cu-PGE enriched horizon of the Chrome body range from <5 to 10 µm in size and are dominantly round, anhedral discrete grains (Figure 37A). Two PGM exhibit more complex structures. The first is a branching subhedral sperrylite grain bound by subhedral hollingworthite (Figure 37B) and the second is a euhedral sulphurarsenide grain with a core that has a composition similar to hollingworthite (Figure 37C). PGM reported from other studies range from <5 to 20 µm in size and are polyhedral, round discrete grains (Talkington et al., 1983 and Scoates et al., 1988)

Majority of the PGM identified in this study occur as disseminated grains in pentlandite. Three are present at the boundaries of the sulphide mineral with silicate gangue. The smallest PGM (~1.5 µm in size) occur within silicate gangue near sulphide boundaries. PGM reported from other studies are present within silicate gangue (with the exception of the chromite inclusions and a few are associated with sulphides) (Scoates et al., 1988).

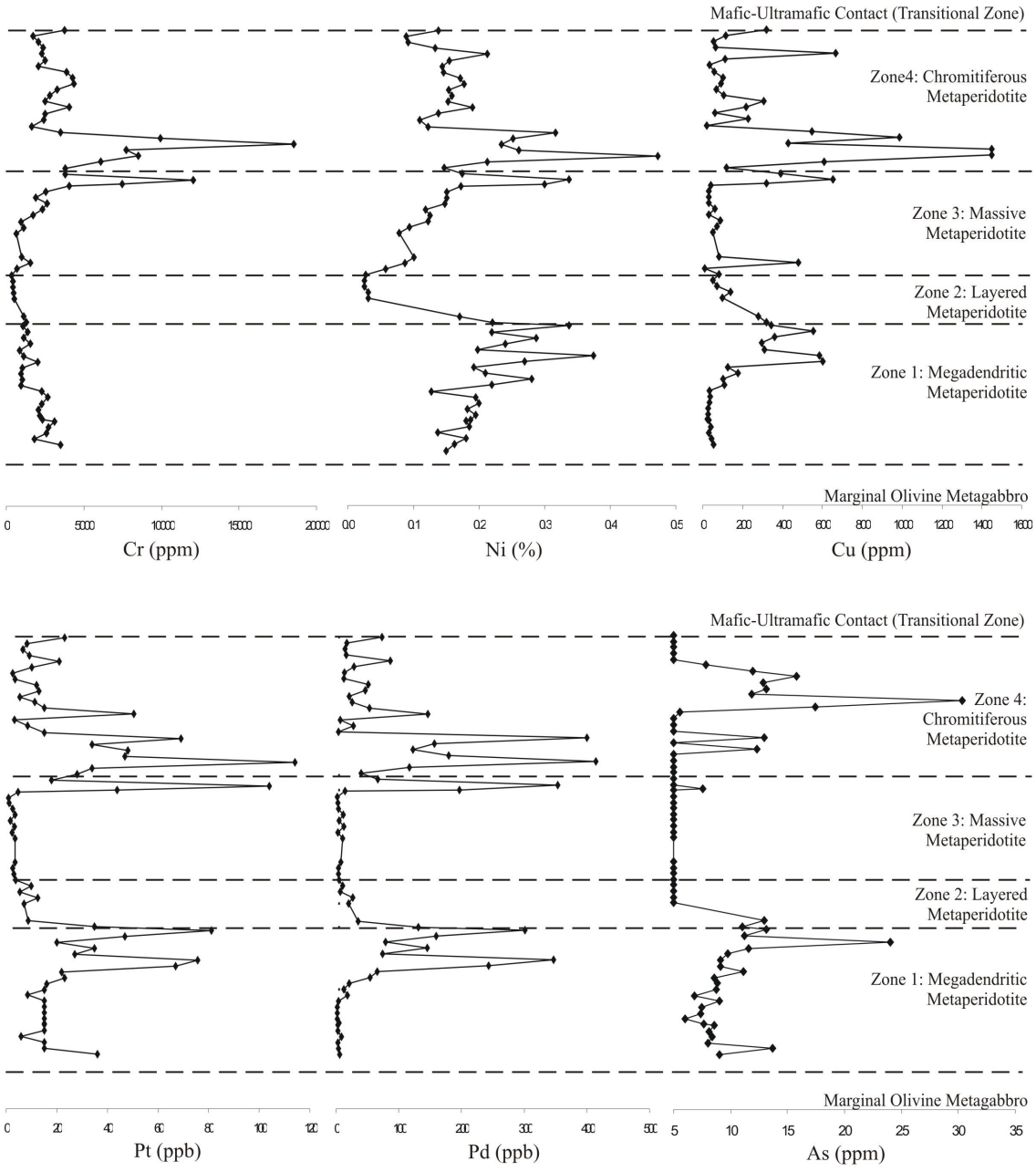

Figure 36: Chemostratigraphic variations of Pt, Pd and As through the ultramafic series of the Chrome body, Bird River sill. For comparison purposes the chemostratigraphic variations of Cr, Ni and Cu from Figure 32 are included. Geochemical data are located in Appendix B.

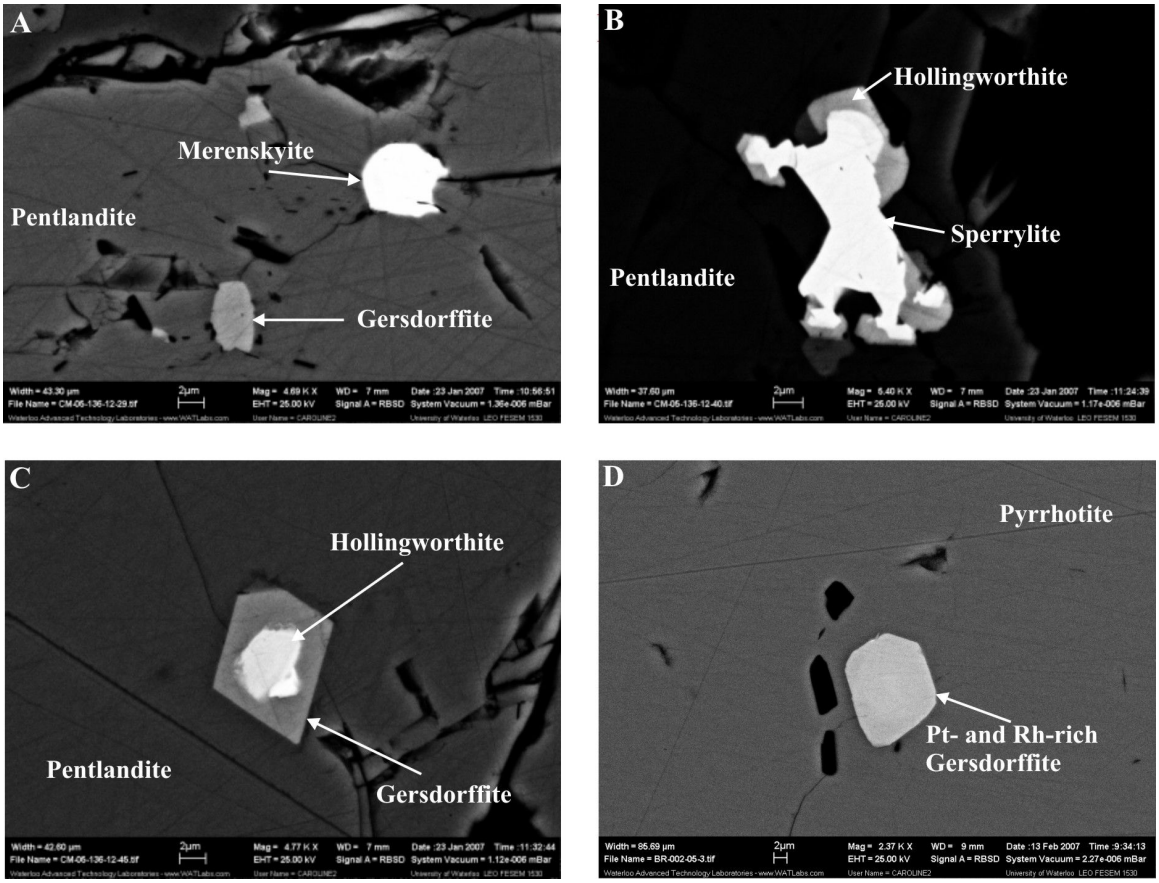

Figure 37: Back-scattered electron images of Platinum-Group Minerals and suphurarsenide minerals from the Chrome body of the Bird River sill. A) Merenskyite and gersdorffite inclusions in pentlandite. B) Pentlandite with a branching sperrylite inclusion with hollingworthite formed along it's grain boundaries. C) Pentlandite with a gersdorffite inclusion that contains a core that has a similar composition to that of hollingworthite. D) Pyrrhotite with a Pt- and Rh-rich gersdorffite inclusion.

Previous studies have concluded that PGE are strongly correlated with chromium and there is no correlation between PGE and the Ni sulphide factor (Scoates et al., 1988). Results from this study indicate that the upper PGE enriched horizon does occur in the same horizon as the massive chromite mineralization but in a plot of Pt+Pd versus chromium there is no direct correlation between the two but there is a weak correlation between Pt+Pd and Ni+Cu (Figure 38A and B). In regards to the lower PGE enriched horizon (where massive chromite layers are absent) there is a very strong correlation between Pt+Pd and Ni+Cu (Figure 38C). This suggests that PGE mineralization is associated with Ni-Cu sulphide mineralization.

5.3.2 Page body Platinum-Group Element mineralization

PGE are present in PGE-bearing sulphurarsenide minerals and as discrete PGM. Five PGM and two Ag minerals were identified and include: kotulskite (Pd(Te,Bi)), merenskyite ($PdTe_2$), stutzite ($Ag_{5-x}Te_3$) and keithconnite (Pd_3Te). PGM range in size from 2 to 40 µm and the Ag minerals, stutzite, are approximately 5 µm in size. PGM are present as round, anhedral inclusions in pentlandite and pyrrhotite.

The most common occurrence of PGE is within sulphurarsenide minerals. Pt, Rh and Pd are commonly present in Co-bearing gersdorffite (Figure 39A). As discussed previously, the sulphurarsenide mineral gersdorffite represents an intermediate composition of the cobaltite-gersdorffite solid solution series. Gersdorffite minerals tend to be subhedral to euhedral (cubic to hexagonal) and range from 10 to 60 µm in size. Several grains exhibit zoning from Pt- and Rh-rich cores to Pt- and Rh-depleted rims (Figure 39B). Seven of the 12 PGE-bearing gersdorffite grains are hosted within semi-massive sulphides comprised of pyrrhotite, pyrite, chalcopyrite and pentlandite. The remaining five grains occur at the edges of pyrrhotite, pentlandite and chalcopyrite in contact with chlorite or serpentine. There is a strong correlation between Pt+Pd and Ni+Cu in the Page body similar to that of the lower PGE enriched horizon of the Chrome body (Figure 38C).

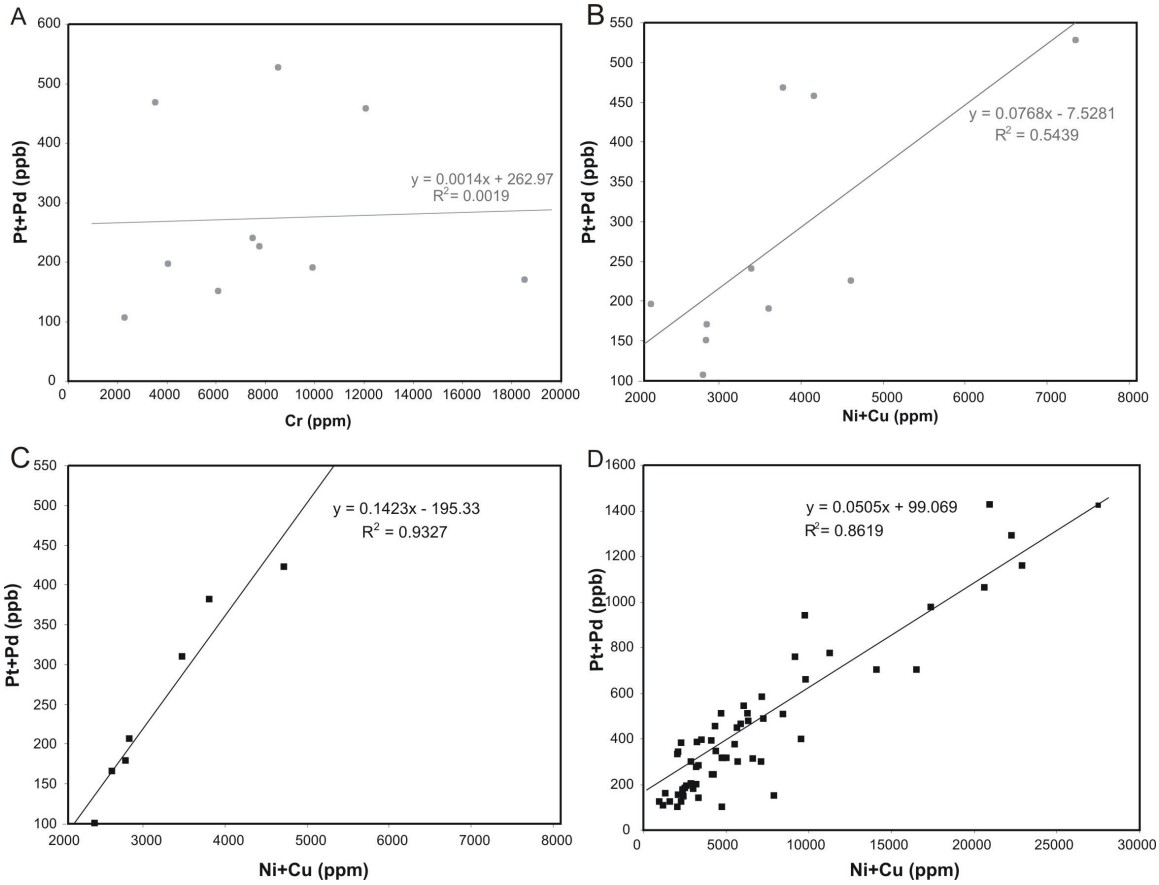

Figure 38: Pt+Pd versus Cr and Ni+Cu of Platinum-Group Element mineralized samples from the Chrome and Page bodies of the Bird River sill. A) Pt+Pd versus Cr of PGE mineralized chromitiferous metaperidotite from the upper PGE enriched horizon of the Chrome body. B) and C) Pt+Pd versus Ni+Cu of PGE mineralized chromitiferous metaperidotite from the upper PGE enriched horizon and the lower PGE enriched horizon of the Chrome body. D) Pt+Pd versus Ni+Cu of PGE mineralized metaperidotite from the lower ultramafic series of the Page body. Data for the Page body is a combination of analyses from this study and assays of drillcore provided by Gossan Resources Ltd. Only the samples that contain anomalously high concentrations of PGE (Pt+Pd > 100 ppb) are used in these graphs. Geochemical data is located in Appendix B.

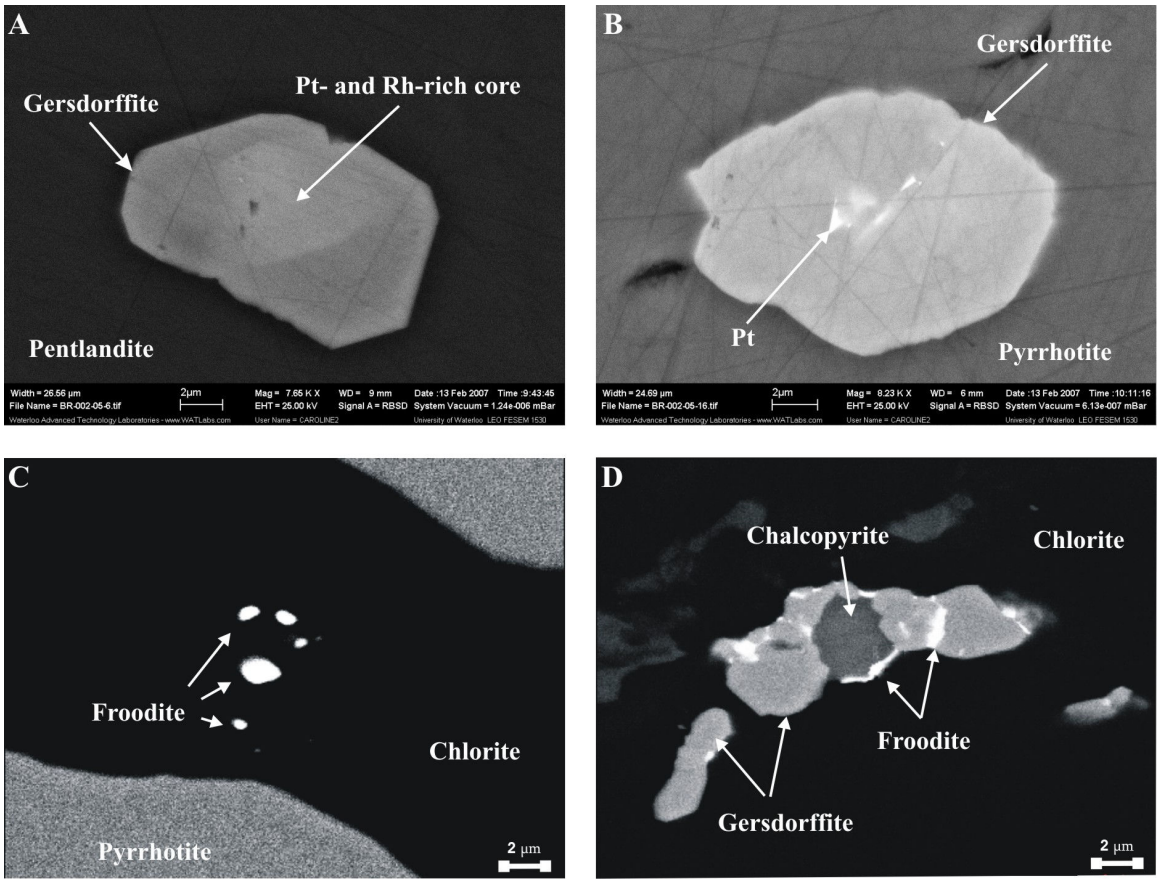

Figure 39: Back-scattered electron photomicrographs of Platinum-Group Minerals and sulphurarsenide minerals from the Page body of the Bird River sill and from the quartz-feldspar porphyritic dyke which truncates the lower ultramafic series of the Bird River sill. A) Pentlandite with a gersdorffite inclusion that contains a Pt- and Rh-rich core. B) Pyrrhotite with a gersdorffite inclusion that contain Pt disseminations. C) Froodite grains within a chlorite groundmass in close proximity to pyrrhotite. D) Froodite intergrown with chalcopyrite and gersdorffite in a chlorite groundmass.

In summary, both of the BRS bodies exhibit a strong association between PGE mineralization and Ni-Cu sulphide mineralization but do not appear to correlate with chromium. PGE in the Page body are predominately present in PGE-bearing sulphurarsenides whereas the occurrence of PGE in the Chrome body is dominated by As and Te PGM species. PGE are commonly present as inclusions in sulphide minerals pentlandite, chalcopyrite and pyrrhotite or along/near contacts between sulphide and silicate minerals (chlorite and serpentine). PGM identified within silicate gangue are interpreted to represent small-scale remobilization possibly related to greenschist facies metamorphism (Scoates et al., 1988).

5.3.3 Quartz-feldspar porphyry dyke Platinum-Group Element mineralization

Six PGM (froodite ($PdBi_2$)) and 1 unidentified PGM species were identified with the aid of SEM-EDS in the quartz-feldspar porphyry dyke which cross-cuts the lower ultramafic series of the Page body. By contrast to the PGM occurrences in the Page body, the PGM present in the quartz-feldspar porphyry dyke typically form small (1 to 5 µm in size), anhedral grains within a chlorite groundmass. However, the PGM are in close proximity to the sulphide minerals chalcopyrite, pyrrhotite and pentlandite (Figure 39C and D). A few of the PGM occur within fine sulphide blebs in isolated sulphide masses within a chlorite groudmass. For example, Figure 39D illustrates froodite intergrown with gersdorffite enclosing chalcopyrite in a chlorite groundmass. In addition to the PGM species, Pt and Ag content were identified in chalcopyrite and pentlandite, respectively. The PGE-rich sulphides occur as small isolated sulphide minerals within the host silicate.

5.3.4 Discussion on the origin and remobilization of the Bird River sill Platinum-Group Element mineralization

PGE primitive-mantle normalized profiles from the Chrome and Page bodies along with the PGE profile of a mineralized quartz-feldspar porphyry dyke are presented in Figure 40. The PGE profile of the Maskwa West deposit from the Maskwa-Dumbarton body of the BRS (east of the study area) is also included. For comparison, the profiles of two well known deposits, the Bushveld Complex and Lac des Iles, are included. The

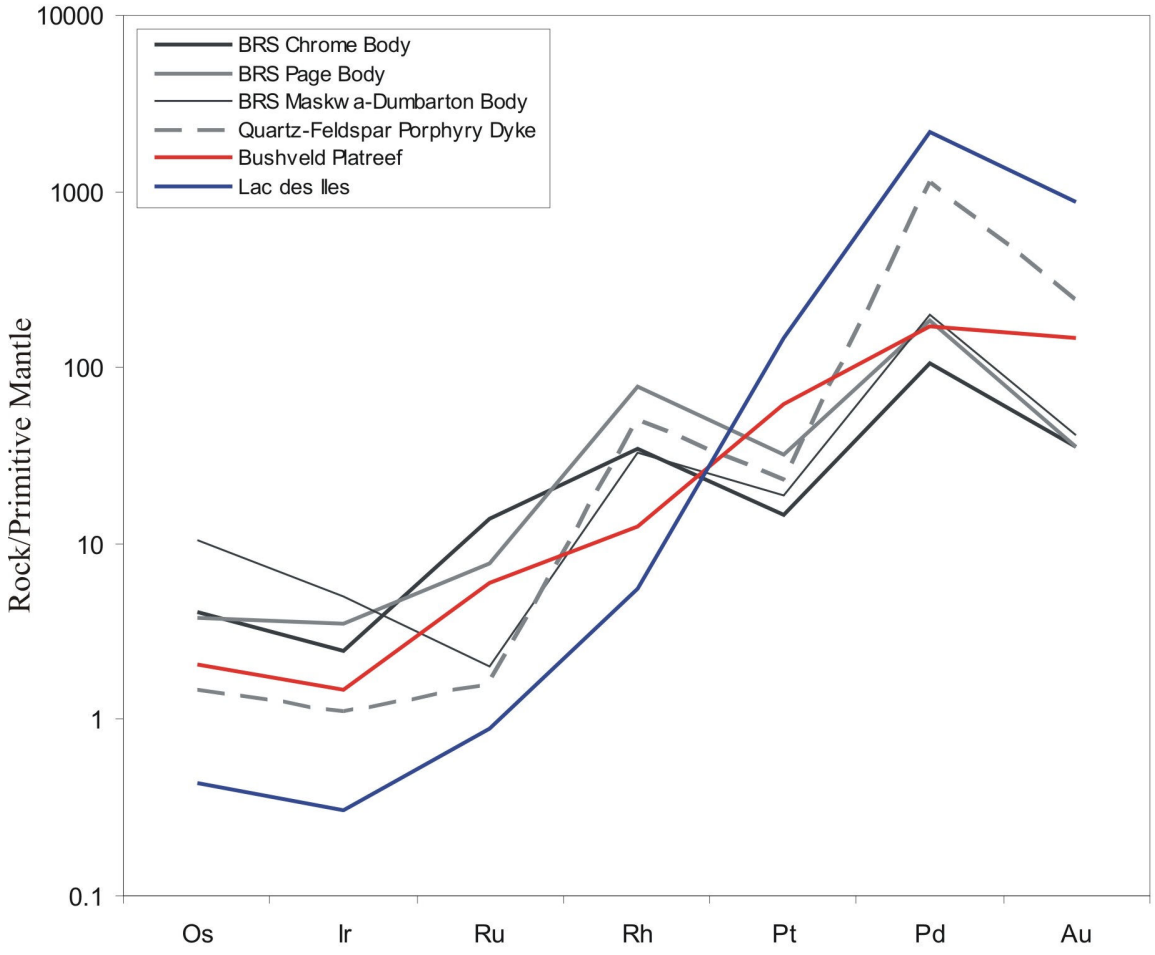

Figure 40: Primitive-mantle normalized Platinum-Group Element profiles of the Chrome, Page and Maskwa-Dumbarton bodies of the Bird River sill and a mineralized quartz-feldspar porphyry dyke. Platinum-Group Element profiles of the Bushveld Complex Platreef and Lac des Iles are included for comparison. Bushveld Platreef data are from Barnes and Maier (2002) and Lac des Iles data are from Hinchey et al. (2005). Geochemical data is located in Appendix B.

Bushveld Complex is interpreted to be a magmatic PGE profile (Barnes and Maier, 2002). The Chrome, Page and Maskwa-Dumbarton BRS bodies have similar trends to that of the Bushveld Complex and thus are also interpreted to be magmatic. Lac des Iles illustrates the profile for a magmatic deposit with PGE enrichment by fluids (Hinchey et al, 2005). The profile of the mineralized quartz-feldspar porphyry dyke is enriched in Pd and depleted in the more immobile PGE (Ru, Os and Ir), similar to Lac des Iles and thus is also interpreted to have been enriched by fluids. Overall, the PGE profiles indicate that PGE mineralization is magmatic in origin and that remobilization occurred in association with late felsic magmatism.

In section 5.2 Nickel and Copper Mineralization, the presence of sulphide mineralized shear zones and fractures were identified in the BRS and Lamprey Falls Formation. Samples from these locations were analyzed for Pt and Pd to examine whether PGE have also been enriched. The results are presented in Table 3 and sample locations are identified in Figure 41.

Table 3: Pt, Pd, Cu, Ni and Co content of mineralized shear zones and fractures in the Bird River sill and Lamprey Falls Formation.

Formation	Sample ID	Pt (ppb)	Pd (ppb)	Pd/Pt	Cu (ppm)	Ni (ppm)	Co (ppm)
Lamprey Falls Formation	CM-06-040-1	10.0	10.8	1.08	30.0	90.0	---
	CM-06-086-1	7.80	11.0	1.41	240	140	60.0
	CM-06-052-1	12.4	13.5	1.09	4920	440	190
	CM-06-054-1	---	---	---	20.0	---	---
Bird River Sill (Peterson Block)	CM-06-069-2	56.7	164	2.89	20.0	640	30.0
	CM-06-065-1	---	---	---	50.0	80.0	---
Bird River Sill (Chrome body)	CM-05-005-2	170	661	3.88	409	150	39.6
	CM-05-006-1	4.03	1.32	0.33	151	64.3	---
	CM-05-028-1	3.78	1.80	0.48	---	32.8	---
	CM-05-031-1	122	216	1.77	968	244	29.1
	CM-05-046-1	157	681	4.34	384	4392	190
	CM-05-055-1	62.4	189	3.04	607	1532	133
	CM-05-124-1	18.8	20.6	1.10	138	126	31.5
Bird River Sill (Page body)	CM-06-037-1	6.30	4.90	0.78	70.0	120	---

--- below detection limit

The mineralized shear zone samples from the Lamprey Falls Formation and Page body of the BRS are not enriched in PGE (Pt+Pd < 100 ppb) but several samples from shear zones in the Chrome and Peterson Block bodies of the BRS are enriched in PGE with Pt+Pd values ranging from 220 ppb to 831 ppb. On average, the Pd/Pt ratio of the magmatic PGE mineralization from the Chrome, Page and Maskwa-Dumbarton bodies of

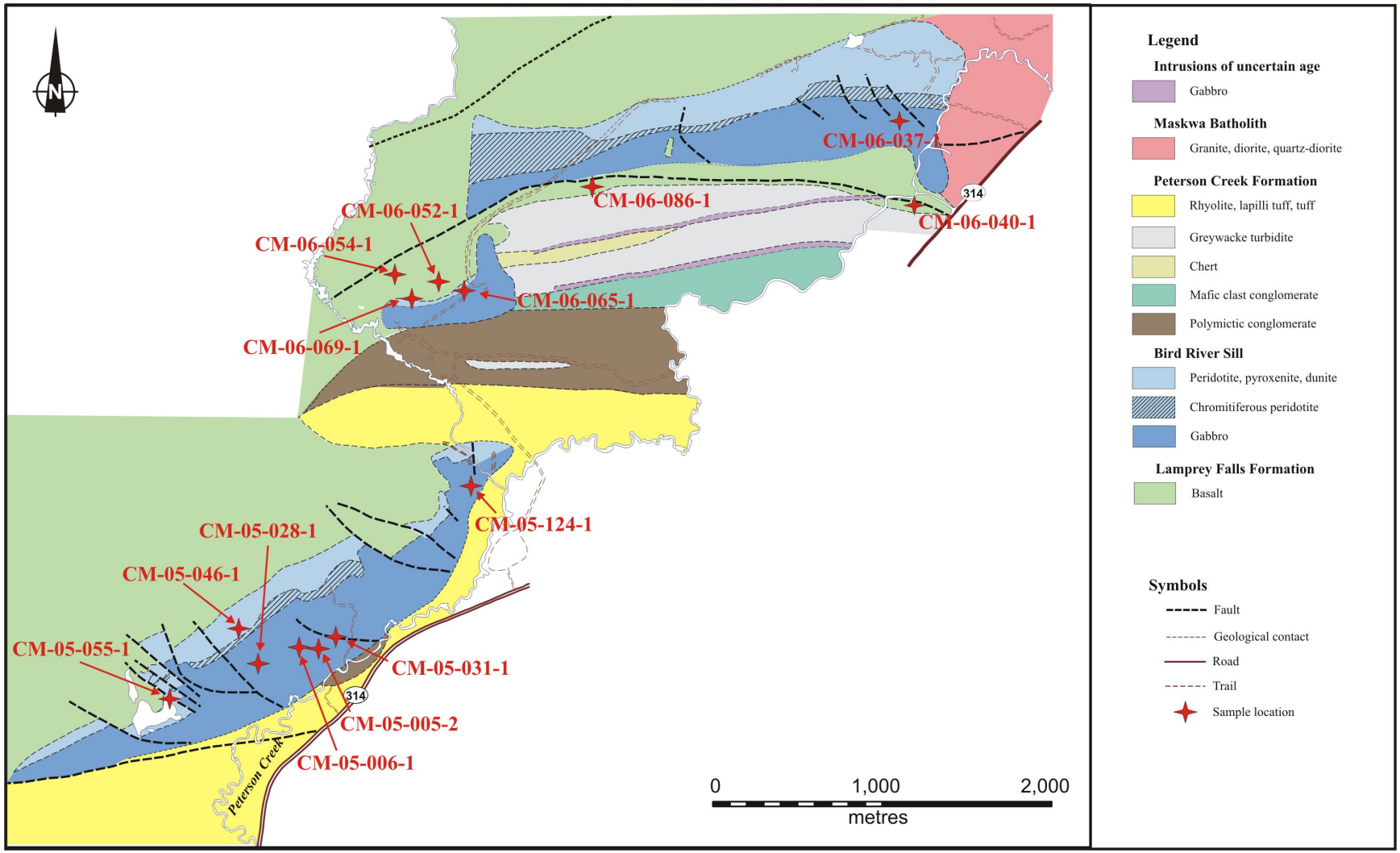

Figure 41: Simplified geological map of the Chrome, Peterson Block and Page bodies of the Bird River sill illustrating the sample locations for the Platinum-Group Element remobilization investigation.

the BRS range from 3.34 to 6.16 and the PGE enriched quartz-feldspar porphyry dyke has a ratio of 28. The Pd/Pt ratio of PGE mineralized samples (Pt+Pd >100 ppb) from the shear zones range from 1.77 to 4.34 which is consistent with that of the magmatic PGE mineralization. This suggests that PGE have not been enriched along these shear zones or fractures.

5.4 Sulphur Isotopes

To determine the nature of the sulphur source to the BRS, the sulphur isotopes of ten samples were analyzed. These include: five samples from the ultramafic series of the Page body (metaperidotite), two samples from the ultramafic series of the Chrome body (metaperidotite), one sample from the Lamprey Falls Formation north of the BRS Peterson Block body (Ni-Cu mineralized fracture), one sample from the Maskwa West deposit (meta-anorthosite) and one sample from the Dumbarton deposit (iron formation hosted by the Lamprey Falls Formation). The iron formation sample was submitted to determine sulphur isotope ratios of the host rock for comparison with BRS values. Results are summarized in Table 4.

Sulphur isotope ratios for the Page body range from $\delta^{34}S$ -0.17 to +0.43 and average +0.07. Chrome body values range from $\delta^{34}S$ -1.06 to -1.46 and average -1.26. Galaxy occurrence, Maskwa West deposit and the Dumbarton deposit $\delta^{34}S$ values are +1.28, -0.94 and -5.88, respectively. Magmas formed by partial melting of the mantle should have $\delta^{34}S$ values around zero (Ohmoto and Rye, 1979) and the samples from the Chrome, Page, and Maskwa-Dumbarton bodies of the BRS and the Galaxy occurrence from the Lamprey Falls Formation all have values near zero which could indicate a magmatic source of sulphur. On the other hand, the Dumbarton iron formation which represents a possible source of sulphur that could have been assimilated by the BRS contains a $\delta^{34}S$ that is slightly but nevertheless distinctly more negative than the values from the BRS.

Table 4: Bird River sill and Lamprey Falls Formation sulphur isotope analytical results.

	Sample ID:	Sample Description:	Mineral Separates:	$\delta^{34}S$:	Repeat:		Average:
Page body (Bird River sill)	BR-05-02-5 BR-05-02-7a BR-05-02-7b BR-06-016-48a BR-06-016-48b	metaperidotite	po, pn po, pn ccp po, pn ccp	-0.12 -0.17 0.03 0.16 0.43			0.07
Chrome body (Bird River sill)	CM-05-136-12 CM-05-145	metaperidotite	bulk sulfur bulk sulfur	-1.06 6.13	-1.46		-1.26
Maskwa-Dumbarton body (Maskwa deposit - Bird River sill)	40307	meta-anorthosite	bulk sulfur	-0.94			-0.94
Galaxy occurrence (Lamprey Falls Formation)	CM-06-052-1	quartz-and chlorite-filled fracture in metabasalt	bulk sulfur	1.71	0.84		1.28
Dumbarton deposit (Lamprey Falls Formation)	38450	iron formation	po, pn	-5.43	-6.09	-6.11	-5.88

Although the source of sulphur cannot be unambiguously determined based on sulphur isotopes alone, it is interesting to note that the BRS Page body and the Galaxy occurrence both contain positive $\delta^{34}S$ values. The Chrome body and Maskwa West deposit both contain negative $\delta^{34}S$ values. Through field observations it is known that the Maskwa-Dumbarton body of the BRS cross-cuts the Dumbarton iron formation (Juhas, 1973) and the iron formation associated with the Dumbarton mine contains moderately negative $\delta^{34}S$ values more consistent with sedimentary sulphides. If sulphur source to the Maskwa-Dumbarton body is at least partially external through assimilation of the Dumbarton iron formation negative $\delta^{34}S$ values would be expected. The same would be true for the BRS Chrome body; if sulphur source to the Chrome body is partially external, negative $\delta^{34}S$ would be expected. It is possible that the Chrome and Maskwa-Dumbarton bodies assimilated external sulphur sources thus explaining their negative $\delta^{34}S$ values whereas the BRS Page body may not have assimilated external sulphur and its sulphur source is solely magmatic thus explaining the Page body's positive $\delta^{34}S$ values. However, the sulphur isotope difference between the Page and Chrome bodies suggests that these are likely separate intrusions.

Chapter 6: Summary, Interpretation and Conclusions

The purpose of this investigation is to develop a petrogenetic model for the emplacement of the western half of the BRS and to establish the controls on Ni-Cu-PGE and Cr mineralization. Pertinent data developed in the preceding chapters are summarized in this chapter and a petrogenetic model for the emplacement of the BRS is presented.

6.1 Summary

6.1.1 Relationships between the Bird River sill and adjacent Bird River greenstone belt formations

The BRS intrudes the metavolcanic sequence of the Lamprey Falls Formation and is overlain by the metasedimentary rocks of the Peterson Creek Formation. The BRS and Lamprey Falls Formation have been tilted southward and thus have southward younging directions. It was shown that the metabaslts south of the BRS Page body have a similar appearance and geochemistry to the metabasalts of the Lamprey Falls Formation and are interpreted to belong to the Lamprey Falls Formation. Therefore, by contrast to the other BRS bodies, the Page body is not in direct contact with the overlying metasedimentary rocks of the Peterson Creek Formation. This suggests that the Page body was emplaced at a lower stratigraphic level within the Lamprey Falls Formation compared to that of the Chrome, Peterson Block and National-Ledin bodies.

Previous studies have treated the BRS as a single layered intrusion that was block faulted. Displacements were believed to follow north-northwest trending faults that cross-cut the BRS, Lamprey Falls Formation and Peterson Creek Formation and produce offsets of up to 1525 m (Bannatyne and Trueman, 1982). There is no evidence from this investigation that supports the existence of the major north-northwest trending faults which accommodate the block faulted model. By contrast, this study identified a mineralized east-west trending shear zone south of the BRS Page body in the Lamprey Falls Formation. This shear zone truncates the Lamprey Falls Formation and Peterson Creek Formation and is laterally continuous across the Bird River greenstone belt. It corresponds with part of the Peterson Creek Shear Zone defined by Duguet et al. (2006).

This study also identified north-south trending intrusive contacts in a location corresponding with one of the faults from the block faulted model. It is thus concluded that the separate bodies of the BRS are not displaced segments of a single intrusion but represent separate, individual intrusions.

6.1.2 Stratigraphy

The separate BRS intrusions have a similar stratigraphy which includes four basic units. Starting from the base these are a marginal mafic series (marginal olivine metagabbro), an ultramafic series, a transition series and an upper mafic series. The ultramafic series is host to all significant Cr-Ni-Cu-PGE mineralization and is further subdivided into a lower megadendritic metaperidotite zone (layered olivine websterite and lherzolite), layered metaperidotite zone (peridotite interlayered with troctolite), massive metaperidotite zone and a chromitiferous metaperidotite zone (Scoates, 1983). The lower ultramafic series of the Page body is truncated by mineralized quartz-feldspar porphyry dykes. It was established by Peck and Theyer (1998) that the mafic series of the BRS crystallized from residual liquids that were formed through crystallization of the underlying ultramafic series.

A chill margin is visible at the intrusive contact between the BRS and Lamprey Falls Formation in the marginal olivine metagabbro of the Chrome body. Based on geochemistry, it was interpreted that the marginal metagabbro represents a component of the primitive melt that formed the Chrome body. This marginal metagabbro unit contains numerous pyroxenite clasts near the intrusive contact. The pyroxenite clasts are believed to represent remnants of a disrupted ultramafic unit that crystallized prior to the Chrome intrusion.

6.1.3 Major and trace element geochemistry

Geochemically, the major and trace element abundances in the mafic and ultramafic series of the Chrome, Page, Peterson Block and National-Ledin bodies are similar and geochemically similar to both modern back-arc-basin basalts and MORB. The strong similarity between the separate intrusions suggests the separate intrusions shared a common magma source.

Stratigraphic variations in major and trace elements were examined to evaluate the single versus multiple magma injection emplacement models for the Chrome body of the BRS. To recap, the various models are: 1) the mafic-ultramafaic units of the BRS are the result of two different magma pulses (Bateman, 1943); 2) the BRS has a complex multi-injection origin (Osborne, 1949 and Theyer, 1985 and 1991), and; 3) the BRS was emplaced through a single magmatic injection where the layers formed via subsequent crystal fractionation and gravitational settling (Springer, 1948 and 1949, Juhas, 1973, Trueman, 1971 and Scoates, 1983). The reversal reflected in the Mg# and the small changes in the trace element ratios suggest the Chrome body was emplaced through at least two magmatic injections thus supporting the multiple magmatic-injection model.

6.1.4 Chromium mineralization

The chromitiferous metaperidotite zone contains massive chromite layers that are laterally continuous across the Page and Chrome bodies. In the chromitiferous peridotite zone of the Chrome body, chromite forms a series of near monomineralic chromite seams and chromitiferous peridotite layers. The chromite seams form laterally continuous layers and disrupted chromite suites where chromite is present as irregular, segmented and commonly bifurcated seams. Deformation is synmagmatic in origin and interpreted to be caused by gravitational instability of denser chromite overlying a partially crystallized olivine mush (Scoates et al., 1989).

Chromium mineralization of the Page body is similar to that of the Chrome body but contains a unique feature, chromite “pebbles” which occur stratigraphically above many of the disrupted chromite seams. The chromite pebbles are laterally continuous across the Page body but differ in composition, size, angularity and stratigraphic position from the east end of the Page body to the west end. In the east, chromite pebbles are small, round and arranged in layers where the elongate axis of the more oval shaped chromite pebbles are concordant with layering. The chromite pebbles present in the west end of the Page body are much larger, more angular and occur sporadically in random orientation throughout different stratigraphic positions in the ultramafic series, i.e. there is no clearly defined chromitiferous zone in this portion of the Page body. Theyer et al. (2001) proposed that chromite pebbles represent autoliths derived from the debris of rigid

chromite layers that were disrupted and fragmented in a turbulent magmatic environment. New observations from this study suggest that the origin of that disruption is in the west end of the Page body. It is believed that the larger, more angular chromite blocks stayed close to the source of disruption whereas smaller debris were transported eastward. None-the-less, the presence and lateral continuity of the chromite pebbles distinguishes the Page body from the Chrome body and further supports the separate intrusion model proposed by this study.

6.1.5 Ni-Cu sulphide mineralization

Sulphide mineralization is present throughout the mafic and ultramafic series of the separate BRS bodies as fine to blebby disseminations and specifically on the Page body, stratigraphically controlled massive to semi-massive mineralized horizons. Increased Ni-Cu concentrations are associated with the chromite horizons on both the Chrome and Page bodies. Fracture bound sulphides were observed in the mafic and ultramafic series of the Page body and along fractures that cross-cut the Lamprey Falls Formation north of the Chrome, Page and Peterson Block bodies. Ni-Cu sulphide mineralized quartz-feldspar porphyry dykes that cross-cut the lower ultramafic series of the Page body were also identified. Overall, sulphide mineralization appears to be magmatic and stratigraphically controlled with remobilization of Ni-Cu sulphides associated with late felsic magmatism and along shear zones and fractures within the BRS and Lamprey Falls Formation.

6.1.6 Platinum-Group Element mineralization

PGE in the Chrome and Page bodies of the BRS exhibit a strong association with Ni-Cu sulphide mineralization but do not appear to be correlated with chromium. PGE in the Page body are predominantly present in PGE-bearing sulphurarsenides whereas the occurrence of PGE in the Chrome body is dominated by As and Te PGM species. PGE are present as inclusions in sulphide minerals (pentlandite, chalcopyrite, pyrrhotite) or along/near contacts between sulphide minerals and silicate minerals (chlorite and serpentine). PGE present within silicate gangue are interpreted to represent small-scale remobilization possibly related to greenschist facies metamorphism (Scoates et al., 1988).

The PGE primitive-mantle normalized profiles of the Chrome, Page and Maskwa-Dumbarton bodies of the BRS indicate that PGE mineralization is magmatic in origin. The PGE profile of a mineralized quartz-felspar porphyry dyke that truncates the lower ultramafic series of the Page body suggests PGE were enriched along this dyke and thus PGE remobilization is associated with late felsic magmatism. There is no evidence to suggest that PGE were enriched along any of the Ni-Cu sulphide mineralized shear zones that cross-cut the BRS and Lamprey Falls Formation in the study area.

6.1.7 Sulphur isotopes

Due to the small range in $\delta^{34}S$ values the source of sulphur to the BRS cannot be unambiguously determined based on sulphur isotopes alone. None-the-less, it is interesting that the Page body of the BRS contains a positive $\delta^{34}S$ value near zero which suggests a magmatic source of sulphur for the BRS. The Chrome and Maskwa-Dumbarton bodies also contain $\delta^{34}S$ values near zero but their values are distinctly negative. It is shown in Juhas (1973) that the Maskwa-Dumbarton body cross-cuts the Dumbarton deposit (iron formation within the Lamprey Falls Formation) which contains a $\delta^{34}S$ of -5.88. If sulphur source to the Maskwa-Dumbarton body of the BRS is at least partially external through assimilation of the Dumbarton iron formation negative $\delta^{34}S$ values would be expected. The same is true for the Chrome body. However, the distinct isotope difference between the Chrome and Page bodies of the BRS suggests these are separate intrusions and further supports the model proposed by this study.

6.2 A model for the emplacement of the Bird River sill

The following model is proposed to best reconcile the above observations: The Page, Peterson Block and Chrome bodies are separate intrusions that are a part of a single conduit system which were emplaced through multiple magmatic-injections. The intrusions are interpreted to share a common magma source with the National-Ledin intrusion (Figure 42, Figure 43 and Figure 44). The Page intrusion is interpreted to be the stratigraphically lowest chamber and to have been the first intrusion to form (Figure 42). There is an interpreted cogenetic relationship between the National-Ledin and the other BRS intrusions but the timing relationship is unknown.

The Chrome body formed from magma being forced out of the Page intrusion along a new feeder dyke where it rose stratigraphically upwards to form the Chrome intrusion. Ultramafic clasts (i.e. the pyroxenite clasts present within the marginal olivine metagabbro on the northeastern end of the Chrome body) likely originated from the Page body or feeder dyke and were suspended in the melt and deposited at the base of the Chrome intrusion near the feeder dyke on the northeast end of the intrusion. The Peterson Block intrusion is interpreted to represent a small offshoot from the feeder dyke connecting the Page and Chrome bodies.

Crystallization of the massive chromite seams was likely the result of magma mixing between an evolved melt in the intrusions and an injection of new primitive magma (Figure 42). Following the semi-consolidation of chromite and peridotite layers, magma recharge into the Page chamber disrupted the ultramafic and chromite layers producing the ultramafic clasts and chromite 'pebbles' (Figure 43). The larger chromite pebbles and blocks remained in the west end of the Page intrusion close to the feeder dyke and the smaller chromite pebbles were deposited stratigraphically on top of existing chromite layers further east in the intrusion. The smaller chromite pebbles were rounded and partially resorbed during transport due to increased interaction with the melt.

The upper mafic series of the BRS bodies crystallized from the residual melt formed through the crystallization of the lower ultramafic series. Following the formation of the BRS intrusive complex the intrusions were uplifted, eroded and overlain by the Peterson Creek Formation. The Bird River greenstone belt later underwent significant vertical displacement and minor strike-slip movement. Deformation resulted in tilting/overturning of the BRS intrusive complex and adjacent Bird River greenstone belt formations from their original horizontal positions (Figure 44).

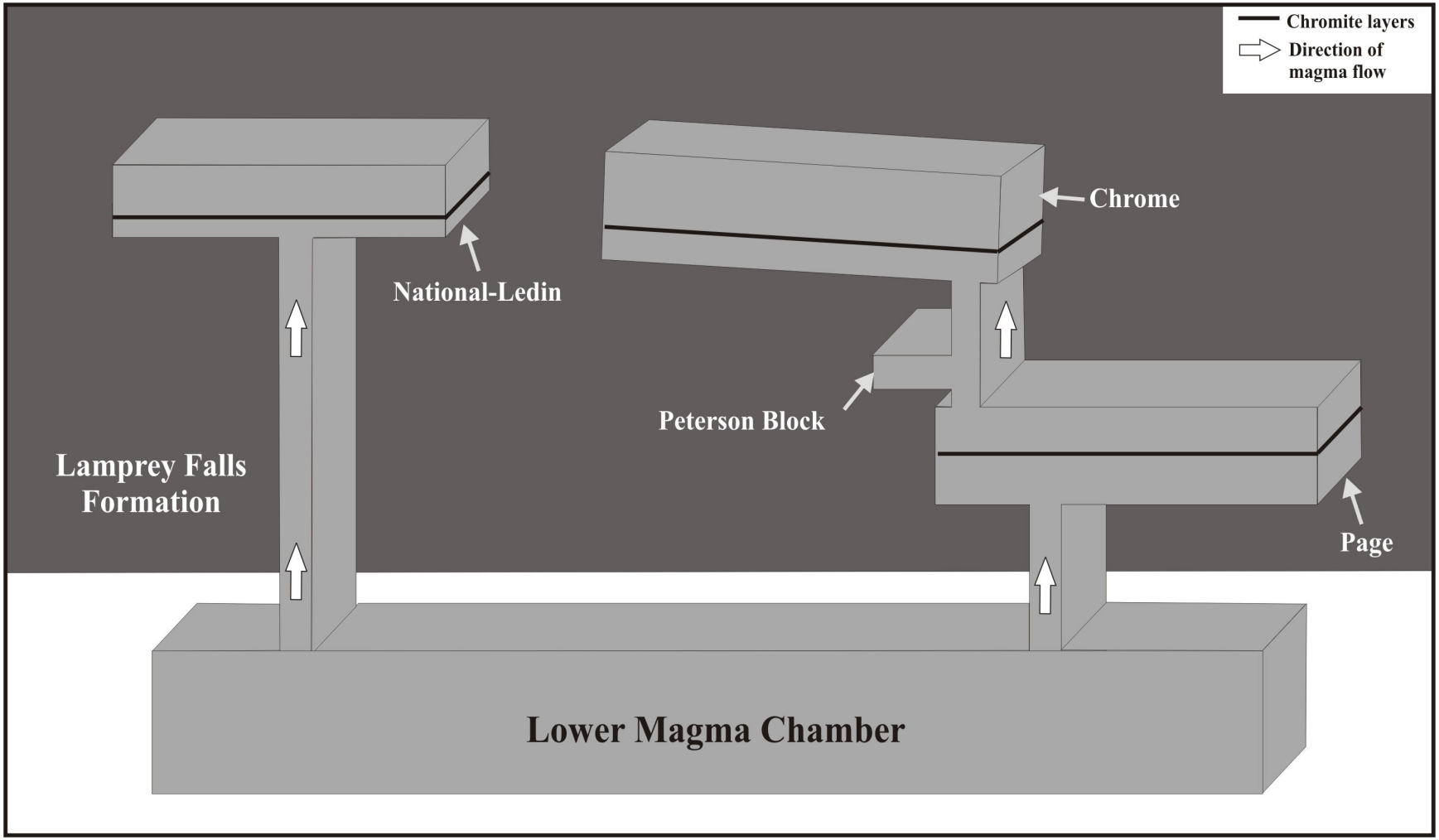

Figure 42: Part I of the Bird River sill emplacement model. Magma intrudes the Lamprey Falls Formation mafic volcanic sequence to form the Page, Peterson Block, Chrome and National-Ledin intrusions. The Chrome body formed from magma being forced out of the Page intrusion along a new feeder dyke where it rose stratigraphically upwards to form the Chrome intrusion. The Peterson Block intrusion is a small offshoot from the feeder dyke. Crystallization of the massive chromite seams was initiated by the injection of primitive magma mixing with evolved magma in the chambers.

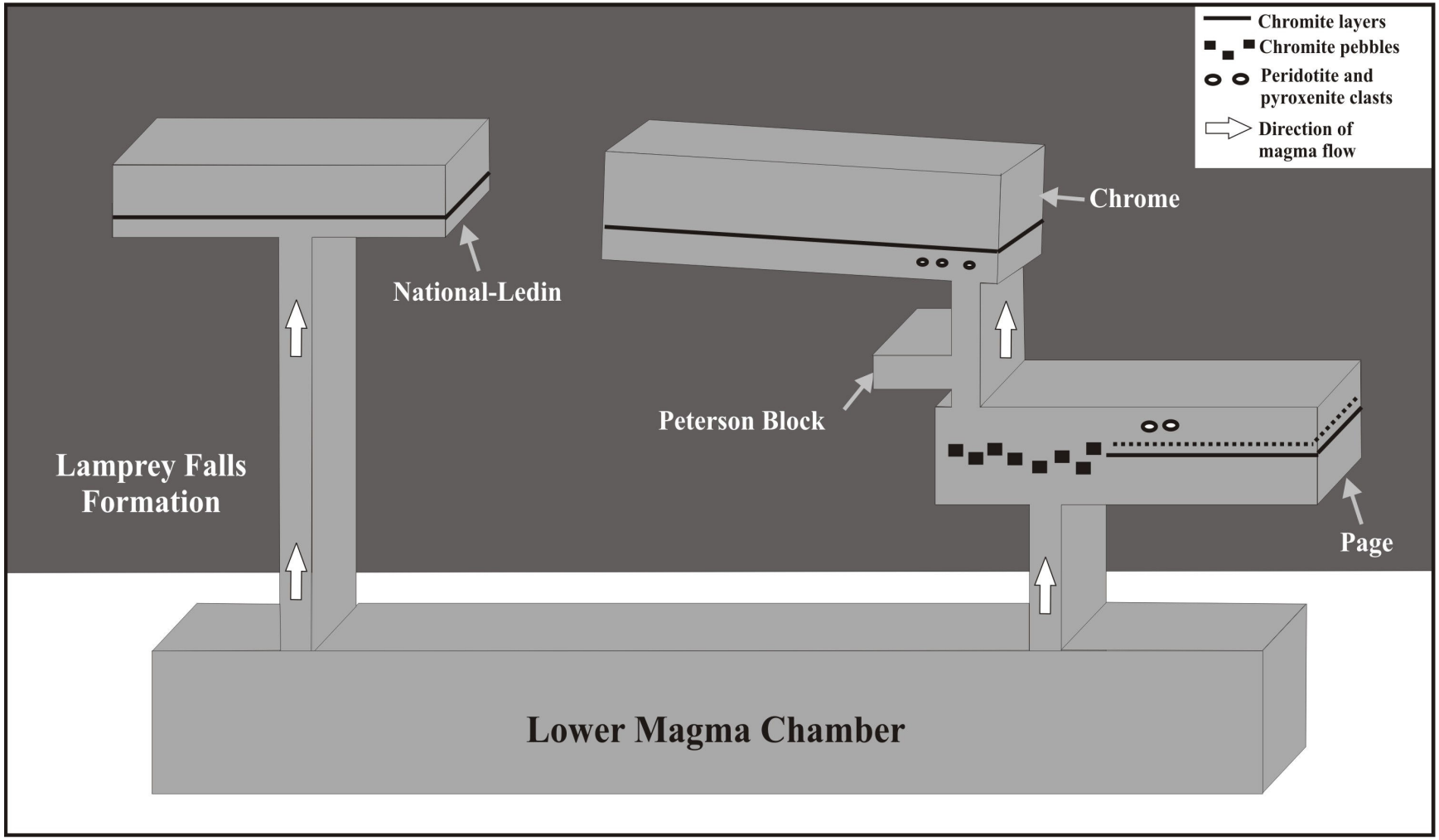

Figure 43: Part II of the Bird River sill emplacement model. Magma recharge into the Page intrusion disrupts the semi-consolidated ultramafic and chromite layers producing the chromite "pebbles" and ultramafic clasts.

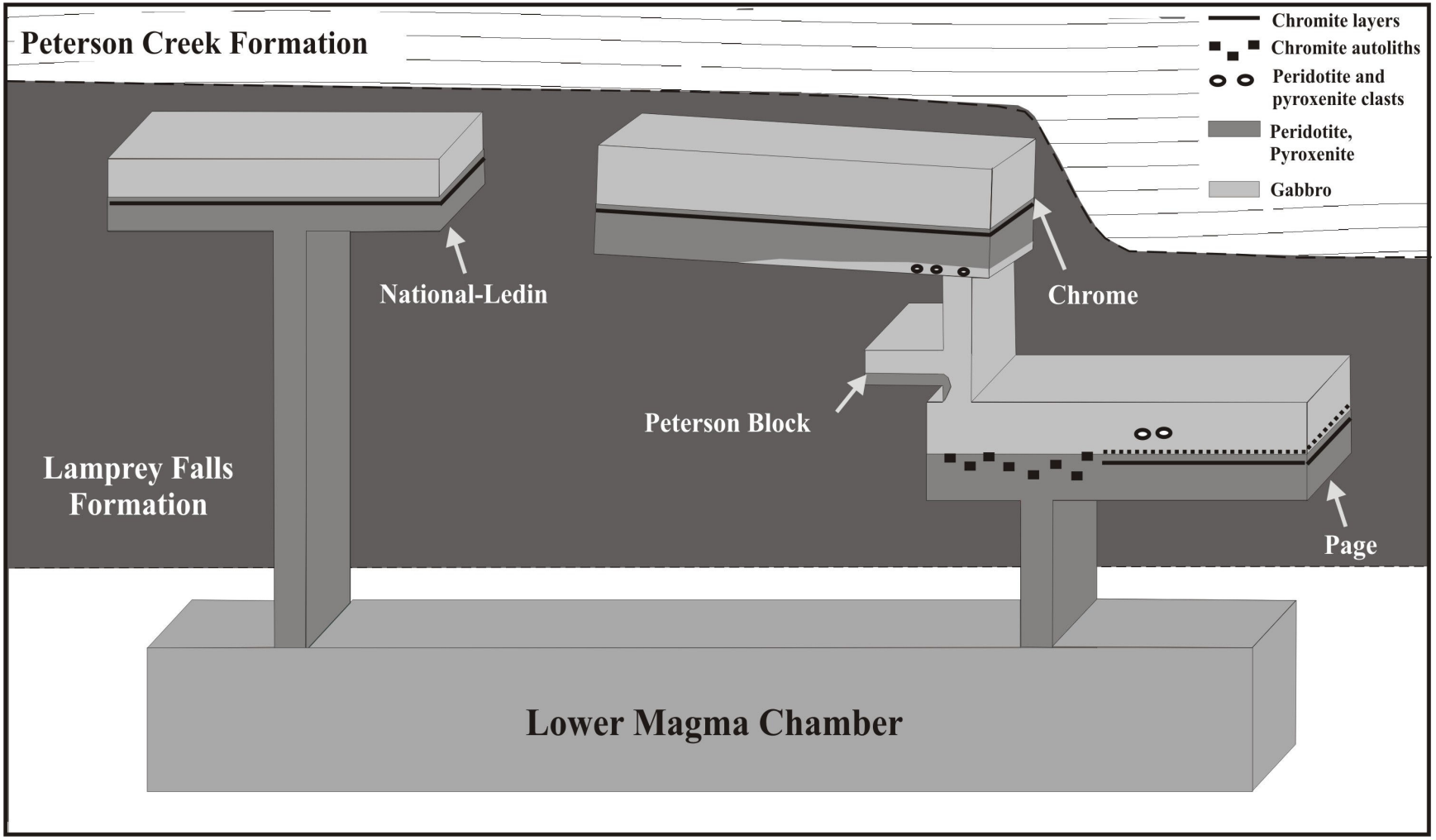

Figure 44: Part III of the Bird River sill emplacement model. The upper mafic series of the intrusions crystallized from the residual melt formed through the crystallization of the lower ultramafic series. The Bird River sill complex was then overlain by the Peterson Creek Formation and overturned from its original horizontal position.

6.3 Conclusions and Economic Implications

The BRS intrusive complex is composed of differentiated, layered, mafic-ultramafic sills which were emplaced as separate intrusions at different stratigraphic levels within the Lamprey Falls Formation. The BRS and Lamprey Falls Formation are overlain by the metasedimentary rocks of the Peterson Creek Formation and were overturned southward. The intrusions share a common magma source which is geochemically similar to both modern back-arc-basin basalts and MORB and have a complex, multiple magmatic-injection history. The metagabbroic intrusions in the Lamprey Falls Formation located north of the Chrome and National-Ledin bodies of the BRS represent coarse-grained flows genetically related to the mafic volcanics of the Lamprey Falls Formation and do not appear to be related to the BRS complex.

All significant concentrations of Ni-Cu-PGE and Cr mineralization in the western half of the BRS complex are contained in the ultramafic series of the Chrome and Page bodies. Mineralization is magmatic in origin with significant Ni-Cu and PGE remobilization associated with late felsic magmatism. Ni-Cu remobilization is also associated with mineralized shear zones that extend into the Lamprey Falls Formation. The sulphur source could not be determined unambiguously based on sulphur isotopes alone but suggests that the sulphur in the BRS is magmatic in origin and that the Chrome and Maskwa-Dumbarton bodies may have assimilated some amount of external sulphur from iron formations present within the Lamprey Falls Formation.

The findings of this investigation have considerable economic implications. The following points should be considered in the exploration for Ni-Cu-PGE and Cr deposits in the BRS:

1. The model that each BRS body is an individual intrusion implies each body may contain its own style of Ni-Cu-PGE and Cr mineralization. It is therefore necessary to consider each intrusion separately.
2. There has been significant enrichment of Ni-Cu and PGE associated with late felsic magmatism. There is also evidence that the Ni-Cu present along shear zones that extend into the Lamprey Falls Formation were remobilized from the BRS complex.

3. An unidentified magnetic anomaly of a similar magnitude, orientation and stratigraphic position as the National-Ledin and Chrome bodies of the BRS is present to the west of the National-Ledin intrusion. This may represent another intrusive body of the BRS complex and thus has potential to host Ni-Cu-PGE and Cr mineralization.
4. The Page body is interpreted to represent a turbulent magmatic environment and the stratigraphically lowest intrusion of the BRS. The melt that formed the Peterson Block and Chrome intrusions is believed to have passed through the Page intrusion. Therefore, the Page body is an excellent exploration target as it represents a turbulent environment in which significant amounts of magma have passed through.

References

Bannatyne, B.B. and Trueman, D.L. 1982. Chromite reserves and geology of the Bird River Sill, Manitoba. Manitoba Department of Energy and Mines, Mineral Resources Division, Open File Report OF82-1, 73 p.

Barnes, S.J 2000. Chromite in Komatiites: II. Modification during greenschist to mid-amphibolite facies metamorphism. Journal of Petrology, v. 41, no. 3, p. 387-409.

Barnes, S.J. and Maier, W.D. 1999. The fractionation of Ni, Cu and the noble metals in silicate and sulphide liquids. *In* Dynamic processes in magmatic ore deposits and their application to mineral exploration. Keays, R.R., Lesher, C.M., Lightfoot, P.C. and Farrow, C.E.G., (eds.). Geological Association of Canada, Short Course Notes, 13, 69-106.

Barnes, S.J. and Maier, W.D. 2002. Platinum-Group Element Distributions in the Rustenberg Layered Suite of the Bushveld Complex, South Africa. *In* The Geology, Geochemistry, Mineralogy and Mineral Beneficiation of Platinum-Group Elements, L.J. Cabri, Ed., Canadian Institute of Mining and Metallurgy Special Volume, v. 54, p 431-458.

Bateman, J.D. 1942. Chromite in Manitoba: Extent of deposits and their value in warfare. Precambrian Magazine, v. 15, no. 12.

Bateman, J.D. 1943. Bird River chromite deposits, Manitoba. Transactions of the Canadian Institute of Mining and Metallurgy, v. 46, p. 154–183.

Bateman, J.D. 1945. Composition of the Bird River chromite, Manitoba. American Mineralogist, v. 30.

Brownell, G.M. 1942. Chromite (in Manitoba): Geology and character of a discovery deposit. Precambrian Magazine, v. 15, no. 12.

Brownell, G.M. 1943. Chromite from Manitoba. University of Toronto Studies, Geological Series, no. 48, p. 101-102.

Cawthorn, R.G. and McCarthy, T.S. 1985. Incompatible trace element behaviour in the Bushveld Complex. Economic Geology, v. 80, no. 4, p. 1016-1026.

Cerny, P., Trueman, D.L., Ziehlke, D.V., Goad, B.E. and Paul, J. 1981. The Cat Lake–Winnipeg River and the Wekusko Lake pegmatite fields, Manitoba. Manitoba Energy and Mines, Mineral Resources Division, Economic Geology Report ER80-1, 215 p.

Childerhouse, A.J. 1928. Genetic Relationships in the Flin Flon, Mandy and Oiseau River Ore Deposits. M.Sc. thesis, University of Manitoba, Winnipeg, Manitoba.

Coats, C.J.A. and Buchan, R. 1979. Petrology of serpentinized metamorphic olivine, Bird River Sill, Manitoba. Canadian Mineralogist, v. 17, p. 847-855.

Coats, C.J.A., Stockford, H.R. and Buchan, R. 1979. Geology of the Maskwa West nickel deposit, Manitoba. Canadian Mineralogist, v. 17, p. 309-318.

Colony, R.J. 1920. A norite of the Sudbury-type in Manitoba. Canadian Mineralogical Journal, v. 41, p. 47.

Cooke, H.C. 1922. Geology and mineral resources of the Rice Lake and Oiseau River areas, Manitoba. Geological Survey of Canada Report, 1921, part C, p. 1-36.

Davies, J.F. 1952. Geology of the Oiseau (Bird) River area. Manitoba Mines and Natural Resources, Mines Branch, Publication 51-3, 24 p.

Davies, J.F. 1955. Geology and mineral deposits of the Bird Lake area. Manitoba Mines and Natural Resources, Mines Branch, Publication 54-1, 44 p.

Duguet, M., Gilbert, H.P. and Corkery, M.T. 2005. Preliminary results of geological mapping and structural analysis of the Bird River greenstone belt, southeastern Manitoba (parts of NTS 52L5N and 6). *In* Report of Activities 2005, Manitoba Industry, Economic Development and Mines, Manitoba Geological Survey, p. 117–124.

Duguet, M., Gilbert, H.P., Corkery, M.T. and Lin, S. 2006. Geology and structure of the Bird River Belt, southeastern Manitoba (parts of NTS 52L5N and 6). *In* Report of Activities 2006, Manitoba Science, Technology, Energy and Mines, Manitoba Geological Survey, p. 170–183.

Duguet, M., Lin, S., Gilbert, H.P. and Corkery, M.T. 2007. Structural geology and kinematic evolution of the Bird River greenstone belt, English River Subprovince, Manitoba (NTS 52L5N, 6). *In* Report of Activities 2007, Manitoba Science, Technology, Energy and Mines, Manitoba Geological Survey, p. 144-154.

Gilbert, H.P. 2005. Geological investigations in the Bird River area, southeastern Manitoba (parts of NTS 52L5N and 6N). *In* Report of Activities 2005, Manitoba Industry, Economic Development and Mines, Manitoba Geological Survey, p. 125–139.

Gilbert, H.P. 2006. Geological investigations in the Bird River area, southeastern Manitoba (parts of NTS 52L5N and 6). *In* Report of Activities 2006, Manitoba Science, Technology, Energy and Mines, Manitoba Geological Survey, p. 184–205.

Gilbert, H.P. 2007. Stratigraphic investigations in the Bird River greenstone belt, Manitoba (parts of NTS 52L5N, 6). *In* Report of Activities 2007, Manitoba Science, Technology, Energy and Mines, Manitoba Geological Survey, p. 129-143.

Hinchey, J.G., Hattori K.H. and Lavigne, J.A. 2005. Geology, Petrology and Controls on PGE Mineralization of the Southern Roby and Twilight Zones, Lac des Iles Mine, Canada. Economic Geology, v. 100, p. 43-61.

Jensen, L.S. 1976. A new method of classifying subalkalic volcanic rocks. Ontario Division of Mines, Misc. Paper 66.

Juhas, A.P. 1973. Geology and origin of copper-nickel sulphide deposits of the Bird River area of Manitoba. Ph.D. thesis, University of Manitoba, Winnipeg, Manitoba, 285 p.

Karup-Moller, S. and Brummer, J.J. 1971. Geology and sulphide deposits of the Bird River claim group, southeastern Manitoba. *In* Geoscience Studies in Manitoba, A.C. Turnock, Ed., Geological Association of Canada Special Paper, no. 9.

Kremer, P.D. 2005. Preliminary results from geological mapping of the Bernic Lake Formation, Bird River greenstone belt, southeastern Manitoba (NTS 52L6). *In* Report of Activities 2005, Manitoba Industry, Economic Development and Mines, Manitoba Geological Survey, p. 140–145.

Kremer, P.D. and Lin, S. 2006. Structural geology of the Bernic Lake area, Bird River greenstone belt, southeastern Manitoba (NTS 52L6): implications for rare element pegmatite emplacement. *In* Report of Activities 2006, Manitoba Science, Technology, Energy and Mines, Manitoba Geological Survey, p. 206–213.

McCann, W.S. 1921. The Maskwa River Copper-Nickel Deposit, southeastern Manitoba. Geological Survey of Canada Summary Report, 1920, part c, p. 19-29.

McRitchie, W.D. and Weber, W. 1971. Metamorphism and deformation in the Manigotagan Gneissic Belt, South-Eastern Manitoba. Manitoba, Department of Mines and Natural Resources, Mines Branch, v. 71-1, p. 235-271.

Mealin, C.A. 2005. Geological investigations of the Chrome property, Bird River Sill, southeastern Manitoba (parts of NTS 52L5). *In* Report of Activities 2005, Manitoba Industry, Economic Development and Mines, Manitoba Geological Survey, p. 146–149.

Mealin, C.A. 2005. Geology of the Chrome property, Bird River Sill, southeastern Manitoba (part of NTS 52L5). Manitoba Industry, Economic Development and Mines, Manitoba Geological Survey, Preliminary Map PMAP2005-8, scale 1:5000.

Mealin, C.A. 2006. Geological investigations in the Bird River Sill, southeastern Manitoba (part of NTS 52L5): geology and preliminary geochemical results. *In* Report of Activities 2006, Manitoba Science, Technology, Energy and Mines, Manitoba Geological Survey, p. 214-255.

Mealin, C.A. 2006. Geology of the Bird River Sill, southeastern Manitoba (part of NTS 52L5). Manitoba Science, Technology, Energy and Mines, Manitoba Geological Survey, Preliminary Map PMAP2006-4, scale 1:5000.

Moore, E.S. 1913. Region east of the south end of Lake Winnipeg. Geological Survey of Canada Summary Report, 1912, p. 262-270.

Murphy, L.A. and Theyer, P. 2005. Geology, structure and mineralization of the Ore Fault property, Bird River greenstone belt, southeastern Manitoba (parts of NTS 52L5NE and 52L6NW). *In* Report of Activities 2005, Manitoba Industry, Economic Development and Mines, Manitoba Geological Survey, p. 156–160.

Nageri, P.J. 1991. Relationships and significance of the subsill intrusions at Maskwa-Dumbarton, Bird River Sill, Manitoba. M.Sc. thesis, Carleton University, Ottawa, Ontario.

Natural Resources Canada 25 January 2008. Geological Survey of Canada - Cooperative Geological Mapping Strategies Across Canada: COGMAPS. 31 January 2008 <http://gsc.nrcan.gc.ca/cogmaps/proj/westernsuperior/index_e.php>.

Ohmoto, H. and Rye, R.O. 1996. Geochemistry of Hydrothermal Ore Deposits. 2nd Edition, H.L. Barnes, Ed., Elsevier, p. 21-23.

Ohnenstetter, D., Watkinson, D.H., Jones, P.C. and Talkington, R. 1986. Cryptic compositional variation in laurite and enclosing chromite form the Bird River Sill, Manitoba. Economic Geology, v. 81, p. 1159–1168.

Osborne, T.C. 1949. Petrography and petrogenesis of the Bird River chromite bearing sill. M.Sc. thesis, University of Manitoba, Winnipeg, Manitoba.

Peck, D.C., Scoates, R.F.J., Theyer, P., Desharnais, G., Hulbert, L.J. and Huminicki, M.A.E. 2002. Stratiform and Contact-type PGE-Cu-Ni Mineralization in the Fox River Sill and the Bird River Belt, Manitoba. *In* The Geology, Geochemistry, Mineralogy and Mineral Beneficiation of Platinum-Group Elements, L.J. Cabri, Ed., Canadian Institute of Mining and Metallurgy Special Volume, v. 54, p. 367-387.

Peck, D.C. and Theyer, P. 1998. PGE-copper-nickel potential of mafic-ultramafic intrusions in the Bird River greenstone belt (parts of NTS 52L). *In* Report of Activities 1998, Manitoba Energy and Mines, Manitoba Geological Survey, p. 151–160.

Peck, D.C., Theyer, P., Bailes, A.H. and Chornoby, J. 1999. Field and lithogeochemical investigations of mafic and ultramafic rocks and associated Cu-Ni-PGE mineralization in the Bird River greenstone belt (parts of NTS 52L). *In* Report of Activities 1999, Manitoba Industry, Trade and Mines, Geological Services, p. 106–110.

Scoates, R.F.J. 1983: A preliminary stratigraphic examination of the ultramafic zone of the Bird River sill (part of 52L/5NE); in Report of Activities 1983, Manitoba Department of Energy and Mines, Mineral Resources Division, p. 70-83.

Scoates, R.F.J., Eckstrand, O.R. and Cabri, L.J. 1988. Interelement correlation, stratigraphic variation and distribution of PGE in the ultramafic series of the Bird River Sill, Canada. *In* Geo-Platinum 87, H.M. Pritchard, P.J. Plotts, J.F.W. Bowles and S.J. Cribb, Ed., London and New York: Elsevier, p. 239-249.

Scoates, R.F.J., Williamson, B.L., Eckstrand, O.R. and Duke, J.M. 1989. Stratigraphy of the Bird River Sill and its chromitiferous zone, and preliminary geochemistry of the chromitite layers and PGE-bearing units, Chrome property, Manitoba. *In* Investigations by the Geological Survey of Canada in Manitoba and Saskatchewan during the 1984–1989 Mineral Development Agreements, A.G. Galley, Ed., Geological Survey of Canada, Open File 2133, p. 69–82.

Springer, G.D. 1948. Geology of the Cat Lake – Maskwa Lake area, Manitoba. Manitoba Mines and Natural Resources, Mines Branch, Publication 47-2.

Springer, G.D. 1949. Geology of the Cat Lake – Winnipeg River area, Manitoba. Manitoba Mines and Natural Resources, Mines Branch, Publication 48-7.

Springer, G.D. 1950. Geology of the Cat Lake – Winnipeg River area, Manitoba. Manitoba Mines and Natural Resources, Mines Branch, Publication 49-7.

Stansell, L.A. and Theyer, P. 2005. Sulphide fragments in waste rock at the Maskwa open pit mine, southeastern Manitoba (parts of NTS 52L6NW): investigations on petrogenesis, potential source rocks and mode of emplacement. *In* Report of Activities 2005, Manitoba Industry, Economic Development and Mines, Manitoba Geological Survey, p. 161–163.

Sun, S.S. and McDonough, W.F. 1989. Chemical and isotopic systematics of oceanic basalts: implication for mantle composition and processes. Geological Society, Special Publications, v. 42, p. 313-345.

Talkington, W. and Watkinson, D.H. 1986. Whole rock platinum-group element trends in chromite-rich rocks in ophiolitic and stratiform igneous complexes. *In* Metallogeny of basic and ultrabasic rocks, M.J. Gallagher, R.A. Ixer, C.R. Neary, H.M. Pritchard, Eds., London, The Institution of Mining and Metallurgy.

Talkington, W., Watkinson, D.H., Whittaker, P.J. and Jones, P.C 1983. Platinum-group-mineral inclusions in chromite from the Bird River Sill, Manitoba. Mineralium Deposita, v. 18, p. 245–255.

Theyer, P. 1985. Platinum-palladium distribution in ultramafic rocks of the Bird River complex, southeastern Manitoba. Manitoba Energy and Mines, Open File Report OF85-4, 46 p.

Theyer, P. 1991. Petrography, chemistry and distribution of platinum and palladium in ultramafic rocks of the Bird River Sill, SE Manitoba, Canada. Mineralium Deposita, v. 26, p. 165–174.

Theyer, P. 2000. New PGE-related results of studies on the Chrome and Page properties, Bird River Sill (NTS 52L/5). *In* Report of Activities 2000, Manitoba Industry, Trade and Mines, Manitoba Geological Survey, p. 175–178.

Theyer, P. 2002. Platinum group element investigations in the Peterson Block of the Bird River Sill (NTS 52L5NE), Manitoba. *In* Report of Activities 2002, Manitoba Industry, Trade and Mines, Manitoba Geological Survey, p. 250–254.

Theyer, P., Bruni, E. and Sundell, C. 2001. Stratigraphy, geology and mineralization of selected parts of the Page property, Bird River Sill (part of NTS 52L/5). *In* Report of

Activities 2001, Manitoba Industry, Trade and Mines, Manitoba Geological Survey, p. 126–132.

Timmins, E.A. 1985. Palemagnetism and geochronology of the Bird River greenstone belt. M.Sc. thesis, University of Windsor, Windsor, Ontario.

Trueman, D.L. 1970. Geology of the Chrome and Page properties: Bird River Sill, Manitoba. Manitoba Mines and Natural Resources, Mines Branch, Preliminary Map 1970-A-1.

Trueman, D.L. 1971. Petrological, structural and magnetic studies of a layered basic intrusion, Bird River Sill, Manitoba. M.Sc. thesis, University of Manitoba, Winnipeg, Manitoba.

Trueman, D.L. 1975. Bird River West, Manitoba. Manitoba Mines and Natural Resources, Mines Branch, Preliminary Map Series 1975-F-10.

Trueman, D.L. 1975. Bird River East, Manitoba. Manitoba Mines and Natural Resources, Mines Branch, Preliminary Map Series 1975-F-11.

Trueman, D.L. 1980. Stratigraphy, structure and metamorphic petrology of the Archean greenstone belt at Bird River, Manitoba. Ph.D. thesis, University of Manitoba, Winnipeg, Manitoba.

Tyrell, J.B. 1900. East shore, Lake Winnipeg. Geological Survey of Canada Annual Report, v. 11, Part G, p. 64-67 & 72-77.

Wang, X. 1993. U-Pb zircon geochronology study of the Bird River greenstone belt, southeastern Manitoba. M.Sc. thesis, University of Windsor, Windsor, Ontario.

Williamson, B.L. 1990. Geology of the Bird River Sill at the Chrome property, southeastern Manitoba. Geological Survey of Canada, Open File Report 2067, 44 p.

Wilson, A. and Chunnett, G. 2006. Trace Element and Platinum Group Element Distributions and the Genesis of the Merensky Reef, Western Bushveld Complex, South Africa. Journal of Petrology, v. 47, no. 12, p. 2369-2403.

Winchester, J.A. and Floyd, P.A. 1977. Geochemical differentiation of different magma series and their differentiation products using immobile elements. Chemical Geology, v. 20, p. 325–343.

Winter, J.D. An Introduction to Igneous and Metamorphic Petrology. New Jersey: Prentice Hall, 2001.

Wright, J.F. 1926. Geology and mineral deposits of the Oiseau River Map area, Manitoba. Geological Survey of Canada Summary Report, 1924, part B, p. 51-104.

Wright, J.F. 1932. Geology and mineral deposits of a part of southeastern Manitoba. Geological Survey of Canada Memoir 169.

Zhong, H., Yao, Y., Prevec, S.A., Wilson, A.H., Viljoen, M.J., Viljoen, R.P., Liu, B.G. and Luo, Y.N. 2004. Trace-element and Sr-Nd isotopic geochemistry of the PGE-bearing Xinjie layered intrusion in SW China. Chemical Geology, v. 203, p. 237-252.

Appendix A: Sample Descriptions

CHROME BODY, BIRD RIVER SILL: Samples collected from Theyer's (1985) western and central channel cuts

Sample ID:	Distance from base of the sill:	Stratigraphy:	Sample Description:	Analyses					
				ICP-MS	LECO (S)	Fire Assay (Ni-Cu-Co and Pt-Pd-Au)	ICP-MS (Pt, Pd, Rh, Os, Ir, Ru)	Sulfur Isotope	SEM
51CM-06-38	628	Upper Mafic Series	quartz metagabbro	X	X	X			
51CM-06-37	568		quartz metagabbro	X	X	X			
51CM-06-36	521.2		metagabbro	X	X	X			
51CM-06-35	477.2		metagabbro	X	X	X			
51CM-06-34	382.8		metagabbro	X	X	X			
51CM-05-1	160	Chromitiferous Peridotite Zone	chromitiferous metaperidotite	X	X	X			
51CM-05-5	158		chromitiferous metaperidotite	X	X	X			
51CM-05-9	156		metaperidotite	X	X	X			
51CM-05-13	154		metaperidotite	X	X	X			
51CM-05-17	152		metaperidotite	X	X	X			
51CM-05-21	150		metaperidotite	X	X	X			
51CM-05-25	148		metaperidotite	X	X	X			
51CM-05-29	146		chromitiferous metaperidotite	X	X	X			
51CM-05-33	144		chromitiferous metaperidotite	X	X	X			
51CM-05-37	142		chromitiferous metaperidotite	X	X	X			
51CM-05-41	140		chromitiferous metaperidotite	X	X	X			
51CM-05-46	138		chromitiferous metaperidotite	X	X	X			
51CM-05-49	136		chromitiferous metaperidotite	X	X	X			
51CM-05-53	134		massive chromite	X	X	X			
51CM-05-57	132		chromitiferous metaperidotite	X	X	X			
51CM-05-61	130		chromitiferous metaperidotite	X	X	X			
51-84-BRS-100	127.7		chromitiferous metaperidotite	X	X	X			
51-84-BRS-104	125.7		chromitiferous metaperidotite	X	X	X			
51-84-BRS-108	123.7		chromitiferous metaperidotite	X	X	X			
51-84-BRS-112	121.7		chromitiferous metaperidotite	X	X	X			
51-84-BRS-116	119.7		chromite	X	X	X			
51-84-BRS-120	117.7		chromitiferous metaperidotite	X	X	X			
51-84-BRS-124	115.7		chromitiferous metaperidotite	X	X	X			
51-84-BRS-128	113.7	Massive Peridotite Zone	chromitiferous metaperidotite	X	X	X			
51-84-BRS-132	111.7		metadunite (chromite-bearing)	X	X	X			
51-84-BRS-136	109.7		metaperidotite (chromite-bearing)	X	X	X			
51-84-BRS-139	108.2		metaperidotite	X	X	X			
51CM-06-1	107.7		metadunite	X	X	X			
51CM-06-2	105.7		metaperidotite	X	X	X			
51CM-06-3	103.7		metaperidotite	X	X	X			
51CM-06-4	101.7		metaperidotite	X	X	X			
51CM-06-5	99.7		metaperidotite	X	X	X			

CHROME BODY, BIRD RIVER SILL: Samples collected from Theyer's (1985) western and central channel cuts (continued)

Sample ID:	Distance from base of the sill:	Stratigraphy:	Sample Description:	Analyses					
				ICP-MS	LECO (S)	Fire Assay	ICP-MS	Sulfur Isotope	SEM
51CM-06-6	97.7	Massive Peridotite Zone	metaperidotite	X	X	X			
51CM-06-7	95.7		metaperidotite	X	X	X			
51CM-06-8	93.7		metaperidotite	X	X	X			
51CM-06-9	91.7		metaperidotite	X	X	X			
51CM-06-13	83.7		metaperidotite	X	X	X			
51CM-06-14	81.7		metaperidotite	X	X	X			
51CM-06-15	79.7		metaperidotite	X	X	X			
51CM-06-16	77.7	Layered Peridotite Zone	metatroctolite	X	X	X			
51CM-06-17	75.7		metatroctolite	X	X	X			
51CM-06-18	73.7		metatroctolite	X	X	X			
51CM-06-19	71.7		metatroctolite	X	X	X			
51CM-06-20	69.7		metatroctolite	X	X	X			
51CM-06-23	63.7		metaperidotite? (deformed--very fine grained)	X	X	X			
51CM-06-24	61.7		metaperidotite? (deformed--very fine grained)	X	X	X			
51-84-BRS-140	60.6	Mega-Dendritic Peridotite Zone	metaperidotite (chromite-bearing)	X	X	X			
51-84-BRS-144	58.5		metaperidotite (chromite-bearing)	X	X	X			
51-84-BRS-148	56.5		metaperidotite (chromite-bearing)	X	X	X			
51-84-BRS-152	54.5		metaperidotite (chromite-bearing)	X	X	X			
51-84-BRS-156	52.5		metadunite (chromite-bearing)	X	X	X			
51-84-BRS-160	50.5		metaperidotite (chromite-bearing)	X	X	X			
51-84-BRS-164	48.5		metapyroxenite	X	X	X			
51-84-BRS-168	46.5		metapyroxenite	X	X	X			
51-84-BRS-172	44.5		metaperidotite	X	X	X			
CM-05-136-12	43		metaperidotite					X	X
CM-05-136-11	42.6		metaperidotite				X		
51-84-BRS-176	42.5		metaperidotite (chromite-bearing)	X	X	X			
51-84-BRS-180	40.5		metaperidotite	X	X	X			
51-84-BRS-184	38.5		metaperidotite (chromite-bearing)	X	X	X			
51-84-BRS-188	36.5		metaperidotite (chromite-bearing)	X	X	X			
51-84-BRS-192	34.5		metapyroxenite	X	X	X			
51-84-BRS-196	32.5		metapyroxenite	X	X	X			
51-84-BRS-200	30.5		metaperidotite	X	X	X			
51-84-BRS-203	29.0		metaperidotite	X	X	X			
51-84-BRS-204	28.5		metaperidotite	X	X	X			
51-84-BRS-208	26.5		metaperidotite	X	X	X			

CHROME BODY, BIRD RIVER SILL: Samples collected from Theyer's (1985) western and central channel cuts (continued)

Sample ID:	Distance from base of the sill:	Stratigraphy:	Sample Description:	Analyses					
				ICP-MS	LECO (S)	Fire Assay (Ni-Cu-Co and Pt-Pd-Au)	ICP-MS (Pt, Pd, Rh, Os, Ir, Ru)	Sulfur Isotope	SEM
51-84-BRS-212	24.5		metaperidotite	X	X	X			
51-84-BRS-216	22.5	Mega-Dendritic	metaperidotite	X	X	X			
51-84-BRS-220	20.5	Peridotite Zone	metaperidotite	X	X	X			
51-84-BRS-224	18.5		metaperidotite	X	X	X			

CHROME BODY, BIRD RIVER SILL: Outcrop grab samples

Sample ID:	UTM Coordinates: (NAD 83 Zone 15)		Sample Description:	Analyses					
	Easting	*Northing*		ICP-MS	LECO (S)	Fire Assay (Ni-Cu-Co and Pt-Pd-Au)	ICP-MS (Pt, Pd, Rh, Os, Ir, Ru)	Sulfur Isotope	SEM
CM-05-005-2	318404	5592370	metagabbro			X			
CM-05-006-1	318356	5592381	metagabbro			X			
CM-05-010-1	318509	5592396	metagabbro			X			
CM-05-011-1	318334	5592278	anorthositic metagabbro			X			X
CM-05-028-1	318067	5592245	anorthositic metagabbro			X			
CM-05-031-1	318498	5592422	metagabbro			X			
CM-05-034-1	318207	5592327	metagabbro			X			
CM-05-036-1	318195	5592444	pegmatitic quartz metagabbro	X	X	X			
CM-05-040-1	317906	5592326	metagabbro			X			
CM-05-043-1	317768	5592439	metaperidotite			X			X
CM-05-046-1	317982	5592475	metaperidotite			X			
CM-05-055-1	317522	5592029	metaperidotite			X			
CM-05-063-1	318023	5592284	metagabbro			X			
CM-05-083-2	318475	5592667	metaperidotite			X			
CM-05-084-1	318442	5592626	anorthositic metagabbro	X	X	X			
CM-05-088-1	318115	5592537	chromitiferous metadunite						X
CM-05-092-1	318345	5592784	metaperidotite			X			
CM-05-099-2	318162	5592743	metapyroxenite			X			
CM-05-124-1	319312	5593286	metagabbro			X			
CM-05-134-5	319098	5593128	chill margin	X	X	X			
CM-05-135-3	319117	5593221	chill margin	X	X	X			
CM-06-122-1	319110	5593235	chill margin	X	X	X			
CM-05-145	----------	----------	metaperidotite					X	

PAGE BODY, BIRD RIVER SILL: Samples collected from outcrop and drillcore

Sample ID:	UTM Coordinates: (NAD 83 Zone 15)		Sample Description:	Analyses					
	Easting	*Northing*		ICP-MS	LECO (S)	Fire Assay (Ni-Cu-Co and Pt-Pd-Au)	ICP-MS (Pt, Pd, Rh, Os, Ir, Ru)	Sulfur Isotope	SEM
CM-06-003-1	322022	5595558	metaperidotite	X					
CM-06-015-1	321858	5595930	metaperidotite	X					
CM-06-023-2	321501	5595630	metaperidotite	X					X
CM-06-030-1	321204	5595401	metagabbro	X	X	X			
CM-06-032-1	321271	5595352	metagabbro	X	X	X			
CM-06-033-1	321558	5595629	metagabbro	X					
CM-06-035-1	321326	5595791	metaperidotite	X	X	X			
CM-06-037-1	322050	5595223	metagabbro	X	X	X			
Drill hole #2									
BR-05-002-5			massive pyrrhotite with chalcopyrite stringers					X	X
BR-05-002-6	321633	5595949	semi-massive pyrrhotite with chalcopyrite blebs				X		X
BR-05-002-7			semi-massive pyrrhotite with chalcopyrite blebs					X	X
Drill hole #10									
BR-06-010-1			metaperidotite			X			
BR-06-010-3			metaperidotite			X			
BR-06-010-4			metaperidotite			X			
BR-06-010-6			metaperidotite			X			
BR-06-010-7			metaperidotite			X			
BR-06-010-8	321681	5595876	metaperidotite			X			
BR-06-010-10			metaperidotite			X			
BR-06-010-12			metaperidotite			X			
BR-06-010-29			quartz-feldspar porphyry				X		X
BR-06-010-31			massive pyrrhotite					X	
BR-06-010-37			metagabbro	X	X	X			
BR-06-010-42			metabasalt			X			
Drill hole #16									
BR-06-016-45			metaperidotite			X			
BR-06-016-46	320489	5595562	metaperidotite			X			
BR-06-016-47			metapyroxenite			X			
BR-06-016-48			metaperidotite					X	

PETERSON BLOCK, NATIONAL-LEDIN AND MASKWA-DUMBARTON BODIES, BIRD RIVER SILL AND BIRD RIVER GREENSTONE BELT FORMATIONS:
Samples collected from outcrop and drillcore

Sample ID:	UTM Coordinates: Zone 15 NAD 83		Sample Description:	Analyses					
				ICP-MS	LECO (S)	Fire Assay (Ni-Cu-Co and Pt-Pd-Au)	ICP-MS (Pt, Pd, Rh, Os, Ir, Ru)	Sulfur Isotope	SEM
Bird River Sill Peterson Block Body									
CM-06-069-2	318996	5594430	metaperidotite	X	X	X			
Bird River Sill National-Ledin Body									
CM-06-113-1	314537	5591746	metagabbro	X	X	X			
Bird River Sill Maskwa-Dumbarton Body									
40306	----------	----------	meta-anorthosite				X		
40307	----------	----------	meta-anorthosite					X	
Lamprey Falls Formation									
CM-05-143-1	319071	5594492	quartz with galena mineralization						X
CM-06-040-1	321952	5594960	metabasalt	X	X	X	X		
CM-06-048-1	321036	5595959	metabasalt			X	X		
CM-06-052-1	319129	5594501	metabasalt with mineralized fracture			X		X	X
CM-06-054-1	318887	5594576	metabasalt			X	X		
CM-06-065-1	319268	5594796	metabasalt			X	X		
CM-06-086-1	320058	5595069	metabasalt			X	X		
CM-06-112-1	307116	5591861	metagabbro	X	X	X	X		
CM-06-123-1	313122	5593873	metagabbro	X	X	X	X		
38540	----------	----------	sulphide bearing iron formation (Dumbarton mine)					X	

Appendix B: Geochemical Data

LITHOGEOCHEMISTRY: CHROME BODY, BIRD RIVER SILL (samples collected from P.Theyer's western and central channel cuts (Theyer, 1985))

Sample ID:	Distance from base of the sill:	Stratigraphy:	Au ppb FA-MS	Pt ppb FA-MS	Pd ppb FA-MS	Cu ppm ICP-OES	Ni ppm ICP-OES	Co ppm ICP-OES	S % IR	SiO2 % FUS-ICP	Al2O3 % FUS-ICP	Fe2O3(T) % FUS-ICP	MnO % FUS-ICP	MgO % FUS-ICP	CaO % FUS-ICP	Na2O % FUS-ICP	K2O % FUS-ICP	TiO2 % FUS-ICP	P2O5 % FUS-ICP	LOI % FUS-ICP	Total % FUS-ICP	Sc ppm FUS-ICP	Be ppm FUS-ICP
51CM-06-38	628		3.00	2.40	2.50	130	40.0	---	0.07	51.7	14.1	11.7	0.16	7.30	10.6	2.02	0.15	0.70	0.06	0.89	99.4	42.0	---
51CM-06-37	568		2.00	22.7	43.0	50.0	40.0	---	0.05	51.2	19.2	9.16	0.12	5.36	11.2	2.25	0.08	0.65	0.05	0.97	100	30.0	---
51CM-06-36	521.2	Upper Mafic Series	1.00	13.8	19.1	60.0	---	---	0.03	47.3	27.6	4.43	0.05	2.28	15.0	2.18	0.09	0.28	0.03	0.98	100	11.0	---
51CM-06-35	477.2		2.00	12.4	22.1	70.0	200	40.0	0.05	45.3	20.3	10.8	0.15	8.04	10.9	1.58	0.20	0.44	0.03	2.40	100	17.0	---
51CM-06-34	382.8		1.00	22.3	22.5	70.0	50.0	---	0.06	48.0	23.6	5.5	0.10	5.72	14.4	1.55	0.03	0.22	0.02	1.10	100	24.0	---
CM-05-036-1	260									46.3	28.4	3.47	0.05	3.19	14.4	1.84	0.16	0.20	0.02	1.49	99.5	9.0	---
CM-05-084-1	210									45.5	28.9	3.81	0.05	3.20	14.6	1.74	0.35	0.32	0.03	1.64	100	13.0	---
51CM-05-1	160		3.90	23.1	73.1	285	1386	114	0.28	41.1	8.21	11.5	0.15	25.3	5.91	0.10	0.02	0.27	0.03	6.84	99.5	21.3	0.73
51CM-05-5	158		---	8.23	17.0	70.1	896	106	0.01	40.7	7.70	10.9	0.18	25.8	6.38	0.10	0.02	0.27	0.03	6.74	98.8	20.6	0.66
51CM-05-9	156		---	6.51	14.3	26.8	926	122	0.03	41.4	7.66	12.0	0.17	26.1	5.94	0.10	0.01	0.31	0.03	6.53	100	21.1	0.77
51CM-05-13	154		1.30	9.16	16.5	48.5	1334	121	0.05	39.3	6.09	12.4	0.18	27.3	5.74	0.06	0.05	0.20	0.02	8.55	100	16.0	0.50
51CM-05-17	152		7.64	21.0	86.6	595	2126	154	0.15	39.7	6.70	12.4	0.15	27.4	4.92	0.06	0.05	0.23	0.03	7.72	99.3	18.2	0.71
51CM-05-21	150		3.14	10.0	28.9	81.8	1551	121	0.05	38.3	6.48	11.9	0.16	28.2	4.70	0.06	---	0.20	0.03	9.11	99.1	17.3	0.75
51CM-05-25	148		1.46	2.65	13.5	19.1	1437	129	0.05	39.5	6.01	10.9	0.15	29.0	4.32	0.06	0.01	0.18	0.03	8.91	99.0	16.2	0.68
51CM-05-29	146		2.38	3.51	12.7	27.0	1459	126	0.06	38.3	5.30	11.4	0.16	30.1	3.44	0.03	0.01	0.15	0.02	9.93	98.9	13.1	0.58
51CM-05-33	144		2.88	12.0	51.3	58.4	1719	143	0.06	37.6	5.56	11.4	0.16	31.0	2.79	0.03	0.02	0.15	0.02	10.4	99.1	13.5	0.65
51CM-05-37	142		3.20	13.0	46.8	57.6	1772	144	0.07	37.8	5.59	11.2	0.16	30.6	3.28	0.05	0.01	0.15	0.02	10.2	99.2	13.9	0.68
51CM-05-41	140		1.35	5.50	20.6	58.2	1539	115	0.06	38.2	5.67	11.1	0.16	29.4	4.28	0.03	---	0.18	0.02	9.89	98.8	14.7	0.65
51CM-05-46	138	Chromitiferous Peridotite Zone	1.65	11.2	25.8	81.1	1586	132	0.06	37.2	5.92	11.1	0.16	30.2	3.47	0.03	---	0.16	0.01	10.6	98.8	15.4	0.76
51CM-05-49	136		3.39	15.0	53.4	244	1527	128	0.04	38.9	6.34	11.2	0.16	28.7	4.43	0.02	0.02	0.17	0.01	9.30	99.3	15.6	0.55
51CM-05-53	134		5.85	50.4	146	182	1897	141	0.06	39.0	6.79	12.1	0.17	28.1	4.41	0.05	0.02	0.21	0.02	8.61	99.4	17.1	0.73
51CM-05-57	132		1.42	3.30	7.07	49.8	1378	111	0.04	39.0	6.35	11.8	0.17	27.2	5.39	0.03	0.02	0.16	0.02	8.94	99.1	15.7	---
51CM-05-61	130		---	8.56	27.5	184	1099	113	0.03	40.0	8.62	12.1	0.16	26.1	5.03	0.05	0.03	0.19	0.01	7.55	99.9	19.4	0.54
51-84-BRS-100	127.7		1.86	15.0	4.00	16.0	1225	94.5	0.02														
51-84-BRS-104	125.7		3.76	69.0	400	527	3165	152	0.36														
51-84-BRS-108	123.7		14.1	34.0	157	997	2515	127	0.21														
51-84-BRS-112	121.7		20.0	48.0	123	421	2345	137	0.11														
51-84-BRS-116	119.7		20.0	46.9	180	1915	2608	181	0.53	38.8	7.73	15.2	0.16	23.8	5.98	0.10	0.03	0.19	0.01	7.08	99.0	19.3	0.61
51-84-BRS-120	117.7		8.97	114	414	2530	4730	168	0.89														
51-84-BRS-124	115.7		6.03	34.0	117	623	2130	131	0.29														
51-84-BRS-128	113.7		4.70	28.0	40.0	121	1473	105	0.03														
51-84-BRS-132	111.7		4.16	18.0	67.0	365	1743	116	0.12														
51-84-BRS-136	109.7		13.1	104	354	689	3375	140	0.20														
51-84-BRS-139	108.2		10.4	43.9	197	301	3001	147	0.18	36.5	5.72	14.2	0.18	29.4	2.65	0.04	---	0.26	0.02	9.69	98.7	14.5	0.65
51CM-06-1	107.7		3.00	4.60	13.9	30.0	1730	110	0.06	38.2	5.25	11.6	0.15	31.9	2.42	0.01	0.04	0.18	0.02	9.50	99.2	15.0	---
51CM-06-2	105.7		3.00	0.90	2.20	10.0	1510	100	0.05	38.1	5.83	11.8	0.14	30.8	3.37	---	---	0.14	0.01	9.19	99.3	14.0	---
51CM-06-3	103.7	Massive Peridotite Zone	2.00	1.20	2.80	20.0	1510	100	0.04	38.9	6.04	11.8	0.14	30.5	3.45	---	0.07	0.16	0.02	8.76	99.8	14.0	---
51CM-06-4	101.7		2.00	2.60	3.90	30.0	1480	100	0.03	39.0	5.76	11.1	0.15	31.2	3.06	---	---	0.12	---	9.10	99.5	13.0	---
51CM-06-5	99.7		2.00	3.50	11.6	50.0	1190	90.0	0.03	39.7	7.95	9.08	0.16	27.9	5.70	---	0.06	0.14	---	8.18	98.8	13.0	---
51CM-06-6	97.7		1.00	1.70	5.20	30.0	1250	90.0	0.04	39.1	6.97	11.1	0.16	29.7	4.11	---	0.01	0.14	---	8.49	99.8	14.0	---
51CM-06-7	95.7		2.00	3.20	12.1	80.0	1230	80.0	0.04	41.6	7.45	10.5	0.14	26.4	6.54	---	0.04	0.14	---	6.92	99.7	14.0	---
51CM-06-8	93.7		1.00	2.40	3.00	80.0	940	60.0	0.03	41.1	7.85	9.96	0.13	26.5	6.51	---	0.01	0.14	---	7.74	99.9	11.0	---
51CM-06-9	91.7		1.00	3.60	10.0	40.0	780	70.0	0.02	36.4	12.0	10.7	0.13	28.2	3.20	---	---	0.12	---	9.08	99.8	14.0	---

--- below detection limit

LITHOGEOCHEMISTRY: CHROME BODY, BIRD RIVER SILL (samples collected from P.Theyer's western and central channel cuts (Theyer, 1985)) (continued)

Sample ID:	Distance from base of the sill:	Stratigraphy:	V ppm FUS-ICP	Co ppm FUS-MS	Ni ppm FUS-MS	Cu ppm FUS-MS	Cr ppm FUS-MS	Zn ppm FUS-MS	Ga ppm FUS-MS	Ge ppm FUS-MS	As ppm FUS-MS	Rb ppm FUS-MS	Sr ppm FUS-ICP	Y ppm FUS-MS	Zr ppm FUS-ICP	Nb ppm FUS-MS	Mo ppm FUS-MS	Ag ppm FUS-MS	In ppm FUS-MS	Sn ppm FUS-MS	Sb ppm FUS-MS	Cs ppm FUS-MS	Ba ppm FUS-ICP
51CM-06-38	628		261	48.0	120	140	250	60.0	16.0	1.30	---	---	115	16.4	52.0	1.70	---	---	---	---	---	0.30	24.0
51CM-06-37	568		221	35.0	80.0	60.0	120	30.0	18.0	1.20	---	1.00	137	12.4	30.0	1.30	---	1.10	---	---	---	0.60	26.0
51CM-06-36	521.2	Upper Mafic Series	87.0	15.0	30.0	60.0	---	---	18.0	0.90	---	2.00	146	6.50	13.0	0.50	---	---	---	---	---	1.10	15.0
51CM-06-35	477.2		139	59.0	280	70.0	30.0	60.0	15.0	1.20	---	2.00	122	9.20	19.0	0.80	---	---	---	---	8.60	1.10	31.0
51CM-06-34	382.8		115	27.0	90.0	80.0	270	40.0	15.0	1.10	---	1.00	94.0	5.00	5.00	0.30	---	---	---	---	---	0.60	11.0
CM-05-036-1	260		64.0	11.0	50.0	10.0	80.0	---	17.0	0.80	---	4.00	164	4.30	10.0	0.50	---	---	---	---	---	1.50	21.0
CM-05-084-1	210		102	15.0	50.0	30.0	30.0	---	18.0	0.80	---	8.00	145	7.90	21.0	0.70	---	---	---	---	---	1.50	29.0
51CM-05-1	160		150				3740	89.5	8.24	1.21	---	---	3.40	4.70	12.0	---	---	---	---	---	---	---	11.1
51CM-05-5	158		140				1720	87.4	7.83	1.23	---	---	4.29	5.29	12.6	---	---	---	---	---	---	---	13.7
51CM-05-9	156		151				2060	86.2	8.06	1.28	---	---	3.86	5.90	13.7	---	---	---	---	---	---	---	6.71
51CM-05-13	154		112				2380	85.4	6.48	1.22	---	---	6.43	4.73	8.84	---	---	---	---	---	0.74	---	6.01
51CM-05-17	152		124				2280	76.7	7.00	1.23	---	---	3.53	5.13	10.8	---	---	---	---	---	1.09	---	5.49
51CM-05-21	150		115				2510	84.6	6.77	1.19	7.80	---	5.59	4.70	9.27	---	---	---	---	---	0.57	---	9.64
51CM-05-25	148		107				2070	74.4	6.21	1.31	11.9	---	4.57	4.59	9.81	---	---	---	---	---	1.67	---	4.76
51CM-05-29	146		85.2				3890	96.2	4.80	1.23	15.8	---	4.14	3.03	5.86	---	---	---	---	---	1.43	---	5.84
51CM-05-33	144		93.3				4290	103	5.59	1.08	12.9	---	3.99	3.16	6.72	---	---	---	---	---	1.23	---	3.12
51CM-05-37	142		92.0				4360	111	5.63	1.05	13.1	---	6.31	3.33	5.35	---	---	---	---	---	1.69	---	5.92
51CM-05-41	140	Chromitiferous Peridotite Zone	84.5				3300	84.6	6.23	1.16	11.9	---	6.87	3.42	6.44	---	---	---	---	---	0.73	---	5.58
51CM-05-46	138		84.9				2820	78.1	6.56	1.12	30.3	---	6.62	3.36	6.00	---	---	---	---	---	0.87	---	5.29
51CM-05-49	136		76.7				2490	78.5	6.35	1.15	17.4	---	4.08	3.05	5.79	---	---	---	---	1.58	---	---	15.3
51CM-05-53	134		106				4050	126	6.48	1.10	5.58	---	3.20	3.75	7.62	---	---	---	---	---	1.21	---	10.4
51CM-05-57	132		81.8				2490	81.7	6.10	1.09	---	---	6.14	3.55	---	---	---	---	---	---	---	---	15.9
51CM-05-61	130		93.0				2430	95.4	7.24	1.14	---	---	3.37	2.88	6.31	---	---	---	---	---	0.68	---	38.2
51-84-BRS-100	127.7		83.4	94.5	951.3	21.1	1622	56.0	8.12	---	---	---	8.08	3.81	5.90	---	---	---	---	---	---	---	---
51-84-BRS-104	125.7		85.7	152	2380	550	3514	49.7	6.99	1.15	13.0	---	3.50	5.74	10.5	1.03	---	---	---	---	---	---	3.38
51-84-BRS-108	123.7		154	127	1840	986	9924	116	9.65	---	---	---	4.90	3.52	---	---	---	---	---	---	---	---	6.88
51-84-BRS-112	121.7		172	137	1680	427	18514	166	11.2	---	12.3	---	2.46	3.17	---	---	---	---	---	---	0.54	---	3.68
51-84-BRS-116	119.7		114				7745	99.7	7.34	---	---	---	4.55	3.22	6.66	---	---	---	---	---	0.56	---	---
51-84-BRS-120	117.7		185	168	2220	1450	8500	91.8	9.41	1.05	---	---	4.26	3.80	14.1	---	---	---	---	---	---	---	---
51-84-BRS-124	115.7		89.1	131	1410	608	6079	74.1	8.16	1.00	---	---	4.31	2.79	---	---	---	---	---	1.33	0.57	---	---
51-84-BRS-128	113.7		69.0	105	1220	119	3796	102	7.51	---	---	---	4.67	2.01	---	---	---	---	---	---	---	---	15.0
51-84-BRS-132	111.7		83.3	116	1460	390	3810	60.0	6.94	1.08	---	---	2.92	3.02	---	---	---	---	---	---	0.53	---	---
51-84-BRS-136	109.7		165	140	2390	653	12058	109	10.4	1.07	---	---	4.97	3.10	---	---	---	---	---	---	0.61	---	---
51-84-BRS-139	108.2		143				7471	91.9	7.41	1.14	7.55	---	3.65	3.48	5.04	---	---	---	---	---	---	---	---
51CM-06-1	107.7		76.0	116	1670	40.0	4050	70.0	6.00	1.10	---	---	3.00	3.70	4.00	0.20	---	---	---	---	---	0.40	4.00
51CM-06-2	105.7		59.0	109	1630	30.0	2570	50.0	5.00	1.10	---	---	4.00	3.00	5.00	---	---	---	---	---	---	0.30	---
51CM-06-3	103.7	Massive Peridotite Zone	56.0	106	1620	30.0	1910	50.0	5.00	1.10	---	---	3.00	3.20	5.00	0.20	---	---	---	---	---	0.20	3.00
51CM-06-4	101.7		64.0	115	1610	30.0	2640	70.0	6.00	1.10	---	---	3.00	2.60	---	---	---	---	---	---	---	0.30	---
51CM-06-5	99.7		70.0	107	1450	60.0	2350	80.0	7.00	1.20	---	---	4.00	2.80	---	---	---	---	---	---	---	0.20	8.00
51CM-06-6	97.7		75.0	110	1390	30.0	1720	70.0	6.00	1.10	---	---	4.00	2.70	---	---	---	---	---	---	---	0.20	6.00
51CM-06-7	95.7		55.0	106	1470	90.0	950	60.0	7.00	1.20	---	---	4.00	2.50	---	---	---	---	---	---	---	0.10	---
51CM-06-8	93.7		57.0	92.0	1240	70.0	1140	60.0	6.00	1.10	---	---	4.00	2.00	---	---	---	---	---	---	---	---	10.0
51CM-06-9	91.7		50.0	104	1000	50.0	630	60.0	8.00	1.00	---	---	---	2.60	---	---	---	---	---	---	---	0.20	6.00

--- below detection limit

LITHOGEOCHEMISTRY: CHROME BODY, BIRD RIVER SILL (samples collected from P.Theyer's western and central channel cuts (Theyer, 1985)) (continued)

Sample ID:	Distance from base of the sill:	Stratigraphy:	La ppm FUS-MS	Ce ppm FUS-MS	Pr ppm FUS-MS	Nd ppm FUS-MS	Sm ppm FUS-MS	Eu ppm FUS-MS	Gd ppm FUS-MS	Tb ppm FUS-MS	Dy ppm FUS-MS	Ho ppm FUS-MS	Er ppm FUS-MS	Tm ppm FUS-MS	Yb ppm FUS-MS	Lu ppm FUS-MS	Hf ppm FUS-MS	Ta ppm FUS-MS	W ppm FUS-MS	Tl ppm FUS-MS	Pb ppm FUS-MS	Bi ppm FUS-MS	Th ppm FUS-MS	U ppm FUS-MS
51CM-06-38	628		4.17	10.0	1.29	6.03	1.65	0.63	2.22	0.42	2.68	0.56	1.70	0.26	1.74	0.27	1.50	0.14	---	---	---	---	0.86	0.21
51CM-06-37	568		2.51	6.24	0.85	4.24	1.15	0.57	1.64	0.30	1.97	0.42	1.27	0.19	1.28	0.21	0.90	0.10	---	---	---	---	0.43	0.13
51CM-06-36	521.2	Upper Mafic Series	1.07	2.80	0.38	2.01	0.63	0.44	0.86	0.17	1.08	0.22	0.66	0.10	0.67	0.11	0.40	0.03	---	---	---	---	0.09	0.06
51CM-06-35	477.2		1.37	3.48	0.48	2.47	0.81	0.47	1.14	0.22	1.48	0.31	0.92	0.14	0.98	0.16	0.60	0.06	---	---	---	---	0.13	0.16
51CM-06-34	382.8		0.47	1.38	0.22	1.22	0.40	0.25	0.58	0.12	0.79	0.17	0.51	0.08	0.52	0.08	0.20	---	---	---	---	---	---	0.03
CM-05-036-1	260		0.91	1.85	0.23	1.17	0.36	0.29	0.49	0.10	0.67	0.14	0.43	0.07	0.46	0.07	0.30	0.02	---	---	---	---	0.13	0.28
CM-05-084-1	210		1.28	2.78	0.38	1.97	0.62	0.34	0.89	0.18	1.23	0.27	0.83	0.13	0.86	0.13	0.60	0.04	---	0.05	6.00	---	0.12	0.11
51CM-05-1	160		0.78	2.02	0.31	1.83	0.61	0.16	0.75	0.14	0.89	0.19	0.55	0.08	0.53	0.08	0.39	---	---	---	---	---	---	---
51CM-05-5	158		1.00	2.37	0.35	1.93	0.61	0.20	0.77	0.15	0.94	0.19	0.59	0.09	0.60	0.09	0.38	---	---	---	---	---	---	---
51CM-05-9	156		0.92	2.23	0.34	1.92	0.63	0.18	0.80	0.16	1.03	0.22	0.66	0.10	0.65	0.10	0.44	---	---	---	---	---	---	---
51CM-05-13	154		1.17	2.37	0.34	1.80	0.58	0.24	0.66	0.12	0.79	0.17	0.52	0.08	0.49	0.07	0.28	---	---	---	---	---	---	---
51CM-05-17	152		0.83	1.90	0.28	1.59	0.54	0.20	0.68	0.13	0.82	0.18	0.55	0.08	0.57	0.09	0.33	---	---	---	---	---	---	---
51CM-05-21	150		0.84	2.06	0.30	1.66	0.55	0.24	0.63	0.12	0.80	0.17	0.50	0.07	0.48	0.07	0.29	---	---	---	---	---	---	---
51CM-05-25	148		0.76	1.82	0.26	1.42	0.46	0.22	0.59	0.11	0.71	0.15	0.43	0.07	0.44	0.07	0.27	---	---	---	---	---	---	---
51CM-05-29	146		0.52	1.30	0.19	1.05	0.36	0.16	0.44	---	0.54	0.11	0.35	0.05	0.33	0.05	0.20	---	---	---	---	---	---	---
51CM-05-33	144		0.44	1.08	0.17	0.97	0.31	0.16	0.41	---	0.51	---	0.34	0.05	0.35	0.05	0.20	---	---	---	---	---	---	---
51CM-05-37	142		0.52	1.29	0.20	1.10	0.35	0.16	0.42	---	0.59	0.13	0.38	0.06	0.38	0.06	---	---	---	---	---	---	---	---
51CM-05-41	140		0.52	1.29	0.19	1.06	0.37	0.20	0.55	---	0.64	0.14	0.42	0.06	0.41	0.06	0.20	---	---	---	---	---	---	---
51CM-05-46	138	Chromitiferous Peridotite Zone	0.47	1.19	0.18	0.99	0.33	0.18	0.48	---	0.57	0.12	0.38	0.06	0.40	0.06	---	---	---	---	---	---	---	---
51CM-05-49	136		0.35	0.83	0.13	0.76	0.27	0.13	0.37	---	0.46	0.10	0.32	0.05	0.33	0.05	---	---	---	---	---	---	---	---
51CM-05-53	134		0.47	1.23	0.21	1.16	0.41	0.19	0.54	0.10	0.64	0.13	0.40	0.06	0.41	0.06	0.21	---	1.42	---	---	---	---	---
51CM-05-57	132		0.50	1.15	0.17	0.97	0.34	0.21	0.46	---	0.61	0.12	0.37	0.06	0.38	0.06	---	---	---	---	13.3	---	---	---
51CM-05-61	130		0.49	1.08	0.16	0.89	0.29	0.08	0.34	---	0.52	0.11	0.32	---	0.32	0.05	---	---	---	---	---	---	---	---
51-84-BRS-100	127.7		0.77	1.70	0.25	1.37	0.44	0.17	0.59	0.10	0.66	0.14	0.41	0.06	0.40	0.06	---	---	---	---	---	---	---	---
51-84-BRS-104	125.7		0.84	2.15	0.35	1.97	0.64	0.16	0.85	0.15	0.97	0.20	0.58	0.09	0.53	0.08	0.32	---	---	---	5.96	---	---	---
51-84-BRS-108	123.7		0.61	1.35	0.20	1.04	0.34	0.15	0.48	---	0.55	0.12	0.38	0.06	0.38	0.05	---	---	---	---	9.76	---	---	---
51-84-BRS-112	121.7		0.49	1.22	0.19	1.05	0.33	0.22	0.44	---	0.49	0.10	0.31	---	0.30	0.05	---	---	---	---	---	---	---	---
51-84-BRS-116	119.7		0.53	1.24	0.19	1.06	0.35	0.11	0.47	---	0.58	0.12	0.35	0.05	0.35	0.05	0.21	---	---	---	8.68	---	---	---
51-84-BRS-120	117.7		0.48	1.22	0.19	1.12	0.38	0.10	0.54	0.10	0.65	0.14	0.43	0.07	0.43	0.06	0.41	---	---	---	---	---	---	---
51-84-BRS-124	115.7		0.45	1.07	0.16	0.91	0.30	0.09	0.40	---	0.47	---	0.30	---	0.31	0.05	---	---	---	---	---	---	---	---
51-84-BRS-128	113.7		0.42	0.96	0.13	0.70	0.23	0.14	0.29	---	0.33	---	0.22	---	0.22	---	---	---	---	---	---	---	---	---
51-84-BRS-132	111.7		0.59	1.31	0.19	0.98	0.31	0.15	0.44	---	0.49	0.10	0.31	---	0.34	0.05	---	---	---	---	---	---	---	---
51-84-BRS-136	109.7		0.61	1.33	0.19	1.02	0.32	0.13	0.42	---	0.53	0.11	0.35	0.05	0.34	0.05	---	---	---	---	---	---	---	---
51-84-BRS-139	108.2		0.66	1.51	0.21	1.17	0.39	0.17	0.52	---	0.61	0.13	0.39	0.06	0.38	0.06	---	---	---	---	---	---	---	---
51CM-06-1	107.7		0.59	1.46	0.20	1.11	0.36	0.20	0.48	0.09	0.61	0.12	0.36	0.05	0.36	0.06	0.20	---	---	---	---	---	---	0.02
51CM-06-2	105.7		0.49	1.20	0.16	0.86	0.27	0.18	0.36	0.07	0.49	0.10	0.30	0.05	0.31	0.05	0.10	---	---	---	---	---	---	---
51CM-06-3	103.7	Massive Peridotite Zone	0.48	1.22	0.18	0.96	0.31	0.21	0.42	0.08	0.52	0.11	0.34	0.05	0.36	0.06	0.20	0.01	---	---	---	---	---	0.21
51CM-06-4	101.7		0.37	0.87	0.12	0.65	0.21	0.16	0.32	0.06	0.42	0.09	0.28	0.04	0.28	0.04	0.10	---	---	---	---	---	---	---
51CM-06-5	99.7		0.40	0.95	0.13	0.69	0.25	0.10	0.38	0.07	0.47	0.10	0.32	0.05	0.33	0.05	0.10	---	0.60	---	---	0.10	---	0.05
51CM-06-6	97.7		0.47	1.08	0.14	0.78	0.25	0.21	0.32	0.06	0.44	0.09	0.27	0.04	0.27	0.05	---	---	---	---	---	0.10	---	0.02
51CM-06-7	95.7		0.41	0.93	0.13	0.74	0.25	0.09	0.33	0.06	0.42	0.09	0.27	0.04	0.28	0.05	0.10	---	1.20	---	---	---	---	0.03
51CM-06-8	93.7		0.40	0.89	0.12	0.63	0.19	0.06	0.30	0.06	0.36	0.08	0.23	0.04	0.25	0.04	0.10	0.02	---	---	---	0.10	---	0.02
51CM-06-9	91.7		0.31	0.87	0.13	0.74	0.25	0.06	0.34	0.07	0.45	0.10	0.29	0.05	0.31	0.05	0.20	---	---	---	---	---	---	0.03

--- below detection limit

LITHOGEOCHEMISTRY: CHROME BODY, BIRD RIVER SILL (samples collected from P.Theyer's western and central channel cuts (Theyer, 1985)) (continued)

Sample ID:	Distance from base of the sill:	Stratigraphy:	Au ppb FA-MS	Pt ppb FA-MS	Pd ppb FA-MS	Cu ppm ICP-OES	Ni ppm ICP-OES	Co ppm ICP-OES	S % IR	SiO2 % FUS-ICP	Al2O3 % FUS-ICP	Fe2O3(T) % FUS-ICP	MnO % FUS-ICP	MgO % FUS-ICP	CaO % FUS-ICP	Na2O % FUS-ICP	K2O % FUS-ICP	TiO2 % FUS-ICP	P2O5 % FUS-ICP	LOI % FUS-ICP	Total % FUS-ICP	Sc ppm FUS-ICP	Be ppm FUS-ICP
51CM-06-13	83.7	Massive Peridotite Zone	3.00	3.60	7.50	60.0	1010	70.0	0.06	43.0	8.71	9.15	0.14	25.5	6.84	---	---	0.12	0.01	6.93	100	14.0	---
51CM-06-14	81.7		15.0	2.70	3.60	490	870	60.0	0.02	44.7	9.53	8.7	0.13	23.1	8.38	0.06	0.01	0.12	---	5.57	100	14.0	---
51CM-06-15	79.7		---	3.10	3.70	---	580	50.0	0.01	41.6	14.3	9.72	0.15	19.0	9.56	0.14	0.04	0.10	0.01	5.48	100	15.0	---
51CM-06-16	77.7	Layered Peridotite Zone	---	3.80	4.80	60.0	270	30.0	0.01	44.7	18.9	7.77	0.12	11.8	12.3	1.06	0.12	0.13	---	3.46	100	20.0	---
51CM-06-17	75.7		---	9.80	10.7	40.0	250	--	0.01	46.2	18.1	7.72	0.13	11.5	11.7	1.45	0.14	0.16	0.01	3.12	100	26.0	---
51CM-06-18	73.7		---	5.50	6.30	70.0	250	30.0	0.01	45.3	18.4	7.74	0.12	11.4	12.7	1.20	0.10	0.14	---	3.17	100	23.0	---
51CM-06-19	71.7		1.00	12.4	27.0	120	310	--	0.02	45.2	18.3	7.69	0.12	11.7	12.7	1.04	0.09	0.15	---	3.35	100	22.0	---
51CM-06-20	69.7		3.00	7.00	19.7	70.0	310	30.0	---	44.2	17.4	8.05	0.12	13.8	11.9	0.68	0.07	0.12	---	3.89	100	19.0	---
51CM-06-23	63.7		5.00	8.80	35.1	290	1710	110	0.13	39.2	6.02	10.9	0.14	30.4	3.97	---	0.09	0.10	0.01	9.28	100	15.0	---
51CM-06-24	61.7		14.0	35.0	131	320	2210	130	0.10	39.6	6.37	11.2	0.15	29.8	4.23	---	0.03	0.11	0.01	8.69	100	16.0	---
51-84-BRS-140	60.6	Mega-Dendritic Peridotite Zone	1.16	81.0	301	345	3375	168	0.07														
51-84-BRS-144	58.5		1.70	47.0	160	545	2200	122	0.17														
51-84-BRS-148	56.5		1.28	20.0	79.0	352	2875	136	0.26														
51-84-BRS-152	54.5		1.79	35.0	145	302	2400	128	0.27														
51-84-BRS-156	52.5		1.22	27.0	74.0	339	1983	102	0.15														
51-84-BRS-160	50.5		16.1	75.6	347	882	3744	192	0.54	35.4	3.51	17.4	0.15	30.2	2.29	0.02	0.05	0.11	0.02	9.99	99.1	11.2	---
51-84-BRS-164	48.5		2.94	67.0	243	691	2700	122	0.20														
51-84-BRS-168	46.5		1.38	22.0	66.0	130	1925	110	0.14														
51-84-BRS-172	44.5		1.32	23.0	54.0	210	2100	112	0.15														
51-84-BRS-176	42.5		1.30	16.0	21.0	115	2800	139	0.17														
51-84-BRS-180	40.5		1.31	15.0	12.0	137	2200	114	0.11														
51-84-BRS-184	38.5		1.37	8.46	18.3	9.12	1276	108	0.04	37.7	2.71	13.9	0.12	34.3	0.69	0.01	0.03	0.09	0.01	9.95	99.6	15.6	---
51-84-BRS-188	36.5		3.48	15.0	4.00	38.0	1950	110	0.04														
51-84-BRS-192	34.5		3.26	15.0	2.00	44.0	2000	111	0.04														
51-84-BRS-196	32.5		2.69	15.0	2.00	29.0	1825	108	0.03														
51-84-BRS-200	30.5		3.20	15.0	2.00	36.0	1950	113	0.03														
51-84-BRS-203	29.0		3.37	15.0	5.00	32.0	1875	111	0.03														
51-84-BRS-204	28.5		4.04	15.0	3.00	31.0	1800	114	0.03														
51-84-BRS-208	26.5		3.69	15.0	3.00	48.0	1850	113	0.02														
51-84-BRS-212	24.5		---	5.85	8.34	5.41	1369	104	0.02	38.2	2.68	14.3	0.13	32.5	0.94	0.04	0.04	0.08	0.01	10.1	99.0	14.1	---
51-84-BRS-216	22.5		2.43	15.0	3.00	55.0	1800	119	0.02														
51-84-BRS-220	20.5		4.28	15.0	4.00	41.0	1625	112	0.03														
51-84-BRS-224	18.5		20.0	36.0	6.00	60.0	1500	136	0.02														

--- below detection limit

LITHOGEOCHEMISTRY: CHROME BODY, BIRD RIVER SILL (samples collected from P.Theyer's western and central channel cuts (Theyer, 1985)) (continued)

Sample ID:	Distance from base of the sill:	Stratigraphy:	V ppm FUS-ICP	Co ppm FUS-MS	Ni ppm FUS-MS	Cu ppm FUS-MS	Cr ppm FUS-MS	Zn ppm FUS-MS	Ga ppm FUS-MS	Ge ppm FUS-MS	As ppm FUS-MS	Rb ppm FUS-MS	Sr ppm FUS-ICP	Y ppm FUS-MS	Zr ppm FUS-ICP	Nb ppm FUS-MS	Mo ppm FUS-MS	Ag ppm FUS-MS	In ppm FUS-MS	Sn ppm FUS-MS	Sb ppm FUS-MS	Cs ppm FUS-MS	Ba ppm FUS-ICP
51CM-06-13	83.7	Massive Peridotite Zone	60.0	97.0	1190	80.0	1000	60.0	7.00	1.10	---	---	3.00	2.80	---	---	---	---	---	---	---	0.10	10.0
51CM-06-14	81.7		65.0	99.0	1210	480	1570	60.0	8.00	1.30	---	---	37.0	2.40	---	---	---	---	---	---	---	0.20	7.00
51CM-06-15	79.7		55.0	77.0	790	---	700	60.0	10.0	1.20	---	---	172	2.50	---	---	---	---	---	---	---	0.20	10.0
51CM-06-16	77.7	Layered Peridotite Zone	74.0	53.0	410	80.0	350	40.0	13.0	1.10	---	2.00	277	2.90	6.00	---	---	---	---	---	---	0.20	23.0
51CM-06-17	75.7		91.0	49.0	370	50.0	420	40.0	12.0	1.20	---	2.00	216	3.60	---	---	---	---	---	---	---	0.30	34.0
51CM-06-18	73.7		83.0	52.0	360	70.0	420	40.0	12.0	1.30	---	1.00	240	3.20	---	---	---	---	---	---	---	0.20	25.0
51CM-06-19	71.7		82.0	57.0	460	140	460	40.0	13.0	1.30	---	1.00	221	3.30	---	---	---	---	---	---	---	0.40	21.0
51CM-06-20	69.7		66.0	64.0	510	100	500	40.0	12.0	1.20	---	2.00	205	2.90	---	---	---	---	---	---	---	0.10	18.0
51CM-06-23	63.7		52.0	104	1600	280	1130	50.0	5.00	1.20	13.0	2.00	3.00	2.40	---	---	---	---	---	---	---	0.30	4.00
51CM-06-24	61.7		54.0	134	2090	320	1280	60.0	6.00	1.20	11.0	---	---	2.80	---	---	---	---	---	---	---	0.30	---
51-84-BRS-140	60.6	Mega-Dendritic Peridotite Zone	66.0	168	2500	747	1090	65.8	6.14	1.22	13.2	---	4.41	2.39	---	---	---	---	---	1.20	0.62	---	18.8
51-84-BRS-144	58.5		64.5	122	1780	554	1389	60.2	5.48	1.20	11.2	---	---	2.40	---	---	2.15	---	---	---	0.52	---	3.04
51-84-BRS-148	56.5		58.1	136	1920	362	1123	56.9	5.18	1.22	24.0	---	2.82	2.42	---	---	---	---	---	1.06	0.64	---	4.00
51-84-BRS-152	54.5		56.6	128	1740	296	1574	68.3	4.41	1.13	11.6	---	3.06	1.65	---	---	2.75	---	---	---	0.55	---	---
51-84-BRS-156	52.5		41.3	102	1390	310	870	50.3	4.55	1.08	9.77	---	3.23	1.64	---	---	2.55	---	---	1.08	---	---	---
51-84-BRS-160	50.5		43.6				1114	63.6	3.92	1.14	9.13	---	3.08	1.41	5.46	---	2.40	---	---	1.03	---	---	4.38
51-84-BRS-164	48.5		49.0	122	1720	603	2038	80.8	4.33	1.05	9.14	---	2.90	1.61	---	---	2.22	---	---	---	0.57	---	5.41
51-84-BRS-168	46.5		45.2	110	1470	124	1055	55.7	4.00	1.05	11.1	---	2.91	1.79	---	---	3.04	---	---	1.47	0.54	---	3.40
51-84-BRS-172	44.5		43.4	112	1480	178	944	46.5	4.06	1.04	8.59	---	4.01	2.13	---	---	2.81	---	---	1.19	1.15	---	10.4
51-84-BRS-176	42.5		43.1	139	1740	101	1024	53.0	3.73	1.11	8.82	---	2.75	1.73	---	---	3.06	---	---	1.32	0.62	---	---
51-84-BRS-180	40.5		34.8	114	1540	109	944	49.7	4.17	1.06	8.79	---	3.64	2.36	---	---	2.35	---	---	---	0.63	---	3.32
51-84-BRS-184	38.5		43.3				2292	37.4	3.31	1.24	6.81	---	---	2.01	---	---	2.57	---	---	1.27	---	---	---
51-84-BRS-188	36.5		56.4	110	1430	36.9	2673	56.5	3.94	1.40	9.04	---	3.31	2.28	---	---	3.55	---	---	2.07	---	---	---
51-84-BRS-192	34.5		61.1	111	1400	34.0	2278	49.3	3.81	1.25	7.45	---	2.74	3.30	9.87	---	3.02	---	---	1.33	---	0.72	7.54
51-84-BRS-196	32.5		49.3	108	1380	25.9	2066	44.0	3.97	1.30	7.39	---	4.49	2.59	---	---	2.64	---	---	1.12	1.13	---	5.46
51-84-BRS-200	30.5		58.4	113	1390	28.1	2175	39.4	3.44	1.19	5.97	---	---	3.27	13.8	---	2.04	---	---	---	0.71	---	3.78
51-84-BRS-203	29.0		50.8	111	1410	24.6	2314	50.0	3.96	1.23	7.63	---	---	2.04	---	---	2.23	---	---	1.02	---	---	---
51-84-BRS-204	28.5		58.6	114	1520	30.5	3101	50.9	3.27	1.24	8.54	---	---	1.71	---	---	2.39	---	---	---	---	---	---
51-84-BRS-208	26.5		53.5	113	1350	40.8	2740	48.0	3.49	1.30	8.09	---	2.20	1.77	5.1	---	3.38	---	---	1.55	1.63	---	4.13
51-84-BRS-212	24.5		46.2				2603	48.7	3.16	1.24	8.36	---	2.03	1.60	---	---	2.88	---	---	1.29	5.83	---	---
51-84-BRS-216	22.5		56.5	119	1210	45.1	1812	---	3.57	1.26	8.03	---	2.09	2.27	14.6	1.1	3.12	---	---	1.61	---	---	---
51-84-BRS-220	20.5		51.8	112	1230	54.8	3484	38.2	3.79	1.26	13.7	---	2.73	1.61	---	---	3.45	---	---	1.88	---	---	---
51-84-BRS-224	18.5		205	136	1190	58.3	28478	116	8.50	1.13	9.01	---	3.23	3.45	5.98	---	3.57	---	---	1.89	---	---	5.13

--- below detection limit

LITHOGEOCHEMISTRY: CHROME BODY, BIRD RIVER SILL (samples collected from P.Theyer's western and central channel cuts (Theyer, 1985)) (continued)

Sample ID:	Distance from base of the sill:	Stratigraphy:	La ppm FUS-MS	Ce ppm FUS-MS	Pr ppm FUS-MS	Nd ppm FUS-MS	Sm ppm FUS-MS	Eu ppm FUS-MS	Gd ppm FUS-MS	Tb ppm FUS-MS	Dy ppm FUS-MS	Ho ppm FUS-MS	Er ppm FUS-MS	Tm ppm FUS-MS	Yb ppm FUS-MS	Lu ppm FUS-MS	Hf ppm FUS-MS	Ta ppm FUS-MS	W ppm FUS-MS	Tl ppm FUS-MS	Pb ppm FUS-MS	Bi ppm FUS-MS	Th ppm FUS-MS	U ppm FUS-MS
51CM-06-13	83.7	Massive Peridotite Zone	0.46	1.08	0.16	0.86	0.28	0.06	0.39	0.08	0.51	0.10	0.31	0.05	0.32	0.05	0.10	---	---	---	---	---	---	0.03
51CM-06-14	81.7		0.24	0.64	0.10	0.58	0.21	0.15	0.28	0.06	0.40	0.08	0.24	0.04	0.28	0.05	---	---	---	---	---	---	---	0.02
51CM-06-15	79.7		0.33	0.77	0.11	0.65	0.22	0.23	0.31	0.06	0.39	0.08	0.26	0.04	0.26	0.05	---	---	---	---	---	---	---	0.03
51CM-06-16	77.7	Layered Peridotite Zone	0.34	0.83	0.12	0.70	0.24	0.25	0.35	0.07	0.46	0.10	0.30	0.05	0.31	0.05	---	---	---	---	---	0.10	---	0.02
51CM-06-17	75.7		0.45	1.07	0.15	0.86	0.30	0.24	0.47	0.09	0.60	0.13	0.38	0.06	0.37	0.06	---	---	---	---	---	---	---	0.02
51CM-06-18	73.7		0.41	0.93	0.14	0.79	0.28	0.26	0.41	0.08	0.56	0.12	0.35	0.05	0.35	0.06	0.10	---	---	---	---	0.10	---	0.02
51CM-06-19	71.7		0.48	1.07	0.15	0.87	0.30	0.26	0.43	0.09	0.57	0.12	0.35	0.05	0.34	0.06	0.10	---	---	---	---	0.10	---	0.02
51CM-06-20	69.7		0.38	0.92	0.14	0.74	0.25	0.26	0.41	0.08	0.51	0.10	0.31	0.05	0.31	0.05	0.10	---	---	---	---	0.10	---	0.02
51CM-06-23	63.7		0.33	0.80	0.11	0.62	0.21	0.15	0.29	0.06	0.42	0.09	0.27	0.04	0.27	0.04	---	---	0.60	---	---	---	---	0.03
51CM-06-24	61.7		0.40	0.96	0.14	0.76	0.26	0.13	0.37	0.06	0.42	0.09	0.29	0.05	0.31	0.05	0.10	---	---	---	---	0.10	---	0.04
51-84-BRS-140	60.6	Mega-Dendritic Peridotite Zone	0.43	0.96	0.13	0.72	0.24	0.11	0.32	---	0.40	---	0.26	---	0.26	---	---	---	---	---	---	---	---	0.12
51-84-BRS-144	58.5		0.34	0.80	0.12	0.71	0.25	0.10	0.31	---	0.41	---	0.27	---	0.28	0.04	---	---	---	---	---	---	---	---
51-84-BRS-148	56.5		0.35	0.79	0.11	0.64	0.23	0.11	0.31	---	0.41	---	0.27	---	0.29	0.04	---	---	---	---	---	---	---	---
51-84-BRS-152	54.5		0.29	0.60	0.09	0.48	0.16	0.08	0.23	---	0.27	---	0.18	---	0.20	---	---	---	---	---	---	---	---	---
51-84-BRS-156	52.5		0.29	0.72	0.09	0.49	0.17	0.08	0.23	---	0.29	---	0.19	---	0.19	---	---	---	---	---	5.52	---	---	---
51-84-BRS-160	50.5		0.25	0.60	0.08	0.45	0.15	0.07	0.21	---	0.24	---	0.16	---	0.19	---	---	---	1.17	---	---	---	---	---
51-84-BRS-164	48.5		0.31	0.75	0.10	0.51	0.17	0.09	0.23	---	0.28	---	0.18	---	0.18	---	---	---	---	---	---	---	---	---
51-84-BRS-168	46.5		0.29	0.72	0.10	0.51	0.16	0.07	0.24	---	0.29	---	0.19	---	0.22	---	---	---	---	---	---	---	---	---
51-84-BRS-172	44.5		0.33	0.80	0.12	0.64	0.21	0.09	0.28	---	0.34	---	0.21	---	0.25	---	---	---	1.14	---	---	---	---	---
51-84-BRS-176	42.5		0.27	0.66	0.09	0.51	0.17	0.06	0.22	---	0.28	---	0.18	---	0.20	---	---	---	1.20	---	5.91	---	---	---
51-84-BRS-180	40.5		0.37	0.95	0.13	0.72	0.24	0.07	0.30	---	0.39	---	0.25	---	0.24	---	---	---	---	---	---	0.51	---	---
51-84-BRS-184	38.5		0.27	0.68	0.09	0.52	0.20	0.08	0.23	---	0.32	---	0.22	---	0.25	---	---	---	---	---	---	---	---	---
51-84-BRS-188	36.5		0.33	0.85	0.12	0.66	0.23	0.09	0.30	---	0.37	---	0.24	---	0.25	0.04	---	---	---	---	5.45	---	---	---
51-84-BRS-192	34.5		0.33	0.96	0.14	0.86	0.32	0.09	0.42	---	0.57	0.13	0.40	0.06	0.37	0.05	0.31	---	---	---	---	---	---	---
51-84-BRS-196	32.5		0.39	0.96	0.14	0.77	0.24	0.12	0.34	---	0.42	---	0.26	---	0.29	0.04	---	---	---	---	---	---	---	---
51-84-BRS-200	30.5		0.29	0.86	0.14	0.87	0.32	0.10	0.47	---	0.57	0.13	0.38	0.06	0.38	0.06	0.44	---	---	---	---	---	---	---
51-84-BRS-203	29.0		0.22	0.58	0.09	0.50	0.17	0.08	0.25	---	0.34	---	0.23	---	0.22	---	---	---	---	---	---	---	---	---
51-84-BRS-204	28.5		0.20	0.46	0.08	0.47	0.16	0.07	0.24	---	0.29	---	0.19	---	0.20	---	---	---	---	---	---	---	---	---
51-84-BRS-208	26.5		0.21	0.55	0.08	0.44	0.16	0.07	0.22	---	0.28	---	0.19	---	0.21	---	---	---	1.97	---	---	---	---	---
51-84-BRS-212	24.5		0.25	0.56	0.08	0.41	0.13	0.08	0.19	---	0.27	---	0.17	---	0.19	---	---	---	1.70	---	5.80	0.51	---	---
51-84-BRS-216	22.5		0.32	0.80	0.10	0.51	0.16	---	0.23	---	0.35	---	0.26	---	0.31	0.05	0.47	---	---	---	---	---	---	---
51-84-BRS-220	20.5		0.24	0.62	0.08	0.44	0.15	0.08	0.20	---	0.28	---	0.16	---	0.20	---	---	---	---	---	---	---	---	---
51-84-BRS-224	18.5		0.47	1.27	0.18	0.98	0.32	0.10	0.44	---	0.56	0.12	0.38	0.06	0.36	0.05	0.20	---	1.40	---	---	---	---	---

--- below detection limit

LITHOGEOCHEMISTRY: CHROME BODY, BIRD RIVER SILL

Sample ID:	Au	Pt	Pd	Cu	Ni	Co	S	SiO2	Al2O3	Fe2O3(T)	MnO	MgO	CaO	Na2O	K2O	TiO2	P2O5	LOI	Total	Sc	Be
	ppb	ppb	ppb	ppm	ppm	ppm	%	%	%	%	%	%	%	%	%	%	%	%	%	ppm	ppm
	FA-MS	FA-MS	FA-MS	ICP-OES	ICP-OES	ICP-OES	IR	FUS-ICP	FUS-ICP	FUS-ICP	FUS-ICP	FUS-ICP	FUS-ICP	FUS-ICP	FUS-ICP	FUS-ICP	FUS-ICP	FUS-ICP	FUS-ICP	FUS-ICP	FUS-ICP
CM-05-005-2	25.4	170	661	409	150	39.6															
CM-05-006-1	2.84	4.03	1.32	151	64.3	---															
CM-05-010-1	---	0.21	1.59	---	---	---															
CM-05-011-1	---	---	0.85	---	---	28.2															
CM-05-028-1	---	3.78	1.80	---	32.8	---															
CM-05-031-1	33.2	122	216	968	244	29.1															
CM-05-034-1	---	31.0	43.9	32.6	88.2	29.2															
CM-05-040-1	1.18	4.00	4.48	58.6	183	30.5															
CM-05-043-1	7.19	23.0	72.1	310	1881	123															
CM-05-046-1	19.9	157	681	384	4392	190															
CM-05-055-1	16.3	62.4	189	607	1532	133															
CM-05-063-1	6.32	6.50	11.9	16.2	36.0	12.5															
CM-05-083-2	2.41	6.97	13.3	19.0	134	---															
CM-05-092-1	47.6	87.7	229	1210	1030	76.6															
CM-05-099-2	6.84	10.8	30.7	42.4	1376	94.1															
CM-05-124-1	3.74	18.8	20.6	138	126	31.5															
CM-05-134-5	---	5.70	10.7	---	230	70.0	---	34.3	15.1	16.6	0.28	21.0	3.78	0.05	0.02	0.99	0.07	7.87	100	51.0	---
CM-05-135-3	4.00	28.8	177	---	510	80.0	---	33.9	14.9	17.4	0.33	20.8	3.53	0.04	0.03	1.10	0.02	8.00	100	54.0	---
CM-06-122-1	2.00	25.2	73.0	---	320	90.0	---	29.7	17.9	19.2	0.4	20.0	2.08	---	0.02	1.16	0.06	9.28	99.8	55.0	---

--- below detection limit

LITHOGEOC LITHOGEOCHEMISTRY: CHROME BODY, BIRD RIVER SILL (continued)

Sample ID:	V	Co	Ni	Cu	Cr	Zn	Ga	Ge	As	Rb	Sr	Y	Zr	Nb	Mo	Ag	In	Sn	Sb	Cs	Ba
	ppm	ppm	ppm	ppm	ppm	ppm	ppm	ppm	ppm	ppm	ppm	ppm	ppm	ppm	ppm	ppm	ppm	ppm	ppm	ppm	ppm
	FUS-ICP	FUS-MS	FUS-MS	FUS-MS	FUS-MS	FUS-MS	FUS-MS	FUS-MS	FUS-MS	FUS-MS	FUS-ICP	FUS-MS	FUS-ICP	FUS-MS	FUS-MS	FUS-MS	FUS-MS	FUS-MS	FUS-MS	FUS-MS	FUS-ICP
CM-05-134-5	330	65.0	230	---	240	110	14.0	0.70	75.0	2.00	---	17.8	20.0	1.20	---	---	---	---	---	0.10	35.0
CM-05-135-3	278	84.0	550	---	260	190	13.0	0.90	---	---	---	13.3	9.00	0.90	---	---	---	---	---	---	18.0
CM-06-122-1	358	82.0	320	---	320	210	14.0	0.60	---	---	---	17.9	29.0	1.30	---	---	---	2.00	---	0.10	11.0

--- below detection limit

LITHOGEOCHEMISTRY: CHROME BODY, BIRD RIVER SILL (continued)

Sample ID:	La	Ce	Pr	Nd	Sm	Eu	Gd	Tb	Dy	Ho	Er	Tm	Yb	Lu	Hf	Ta	W	Tl	Pb	Bi	Th	U
	ppm	ppm	ppm	ppm	ppm	ppm	ppm	ppm	ppm	ppm	ppm	ppm	ppm	ppm	ppm	ppm	ppm	ppm	ppm	ppm	ppm	ppm
	FUS-MS	FUS-MS	FUS-MS	FUS-MS	FUS-MS	FUS-MS	FUS-MS	FUS-MS	FUS-MS	FUS-MS	FUS-MS	FUS-MS	FUS-MS	FUS-MS	FUS-MS	FUS-MS	FUS-MS	FUS-MS	FUS-MS	FUS-MS	FUS-MS	FUS-MS
CM-05-134-5	1.98	5.55	0.84	4.67	1.46	0.63	2.14	0.43	2.93	0.63	1.91	0.30	2.01	0.32	0.90	0.09	---	---	---	---	0.08	0.12
CM-05-135-3	1.09	3.29	0.49	2.82	1.04	0.53	1.55	0.32	2.19	0.47	1.44	0.22	1.49	0.24	0.60	0.04	---	---	---	---	0.10	0.15
CM-06-122-1	0.75	2.77	0.49	3.11	1.35	0.93	2.20	0.46	3.08	0.63	1.91	0.28	1.90	0.31	1.10	0.09	---	---	---	---	0.10	0.06

--- below detection limit

LITHOGEOCHEMISTRY: PAGE BODY, BIRD RIVER SILL

Sample ID:	Au	Pt	Pd	Cu	Ni	Co	S	SiO2	Al2O3	Fe2O3(T)	MnO	MgO	CaO	Na2O	K2O	TiO2	P2O5	LOI	Total	Sc	Be
	ppb	ppb	ppb	ppm	ppm	ppm	%	%	%	%	%	%	%	%	%	%	%	%	%	ppm	ppm
	FA-MS	FA-MS	FA-MS	ICP-OES	ICP-OES	ICP-OES	IR	FUS-ICP	FUS-ICP	FUS-ICP	FUS-ICP	FUS-ICP	FUS-ICP	FUS-ICP	FUS-ICP	FUS-ICP	FUS-ICP	FUS-ICP	FUS-ICP	FUS-ICP	FUS-ICP
CM-06-003-1								40.9	5.53	13.9	0.12	27.4	4.69	0.04	---	0.35	0.03	7.27	100	24.0	---
CM-06-015-1								37.3	4.36	8.85	0.19	32.5	4.33	---	---	0.11	0.02	11.7	99.3	11.0	---
CM-06-023-2								38.0	4.08	12.6	0.18	31.5	2.75	---	0.01	0.15	0.01	10.8	100	15.0	---
CM-06-030-1	24.0	3.40	4.90	740	40.0	---	0.12	49.9	20.0	8.05	0.10	4.93	12.8	2.03	0.31	0.66	0.07	1.26	100	26.0	---
CM-06-032-1	2.00	2.70	3.70	160	200	---	0.17	48.4	18.6	9.64	0.14	7.05	11.4	2.25	0.40	0.46	0.04	1.48	99.8	40.0	---
CM-06-033-1								39.1	18.3	11.6	0.22	13.7	11.1	0.95	0.18	0.53	0.13	4.25	100	23.0	---
CM-06-035-1	6.00	21.9	71.1	220	2090	120	0.12	34.8	3.21	11.2	0.15	34.3	2.82	---	0.06	0.09	0.02	13.6	100	11.0	---
CM-06-037-1	1.00	6.30	4.90	70.0	120	---	0.03	46.5	27.0	5.17	0.09	3.82	14.1	2.01	0.28	0.14	0.02	1.16	100	14.0	---
BR-06-010-1	5.00	45.4	150	570	2040	140		35.8	5.51	12.7	0.13	32.0	3.03	0.06	0.03	0.10	0.01	10.7	100	10.0	---
BR-06-010-3	91.0	47.2	104	6770	1130	110															
BR-06-010-4	9.00	51.3	155	740	2120	120															
BR-06-010-6	33.0	107	381	2340	4890	210															
BR-06-010-7	16.0	60.0	258	900	3820	190		35.7	4.86	12.1	0.12	35.8	0.28	0.08	0.03	0.18	0.01	11.2	100	15.0	---
BR-06-010-8	10.0	26.4	115	450	2860	170															
BR-06-010-10	7.00	22.2	105	400	1880	110															
BR-06-010-12	9.00	33.0	148	520	2470	130		35.0	3.77	13.8	0.14	34.4	1.41	0.06	0.03	0.10	---	11.6	100	9.0	---
BR-06-010-37	---	1340	4.40	90.0	110	40.0	0.10	48.7	13.9	15.5	0.36	6.28	9.65	3.04	0.39	1.67	0.14	0.76	100	46.0	2.00
BR-06-010-42	---	10.7	7.80	230	90.0	50.0															
BR-06-016-45	3.00	23.4	80.0	130	1900	120															
BR-06-016-46	4.00	33.2	116	270	2160	140															
BR-06-016-47	7.00	118	393	1770	4510	220															

--- below detection limit

LITHOGEOCHEMISTRY: PAGE BODY, BIRD RIVER SILL (continued)

Sample ID:	V	Co	Ni	Cu	Cr	Zn	Ga	Ge	As	Rb	Sr	Y	Zr	Nb	Mo	Ag	In	Sn	Sb	Cs	Ba
	ppm	ppm	ppm	ppm	ppm	ppm	ppm	ppm	ppm	ppm	ppm	ppm	ppm	ppm	ppm	ppm	ppm	ppm	ppm	ppm	ppm
	FUS-ICP	FUS-MS	FUS-MS	FUS-MS	FUS-MS	FUS-MS	FUS-MS	FUS-MS	FUS-MS	FUS-MS	FUS-ICP	FUS-MS	FUS-ICP	FUS-MS	FUS-MS	FUS-MS	FUS-MS	FUS-MS	FUS-MS	FUS-MS	FUS-ICP
CM-06-003-1	139	109	850	30.0	1960	50.0	6.00	1.30	35.0	---	3.00	6.70	16.0	0.70	---	0.70	---	---	---	---	9.00
CM-06-015-1	40.0	122	2210	450	2640	80.0	6.00	1.10	34.0	---	8.00	7.00	4.00	1.10	---	---	---	---	0.30	---	4.00
CM-06-023-2	63.0	119	1130	100	3260	50.0	5.00	1.10	28.0	---	4.00	2.50	9.00	0.30	---	---	---	---	---	---	13.0
CM-06-030-1	204	32.0	90.0	580	60.0	60.0	19.0	1.60	---	3.00	108	16.6	32.0	1.50	---	1.00	---	---	---	0.60	30.0
CM-06-032-1	198	35.0	90.0	100	180	70.0	15.0	1.20	---	7.00	112	11.6	17.0	0.90	---	---	---	---	---	1.40	25.0
CM-06-033-1	149	55.0	130	---	50.0	30.0	21.0	1.20	---	1.00	134	13.8	111	4.00	---	---	---	---	---	---	21.0
CM-06-035-1	43.0	113	1910	210	1680	60.0	3.00	1.10	27.0	---	15.0	2.30	5.00	---	---	0.60	---	---	---	0.40	5.00
CM-06-037-1	66.0	26.0	120	70.0	40.0	40.0	16.0	0.90	---	7.00	154	3.90	7.00	0.40	---	---	---	---	---	0.20	35.0
BR-06-010-1	45.0	151	2030	610	1180	50.0	4.00	1.00	30.0	---	10.0	2.20	9.00	0.20	---	---	---	---	1.00	0.30	3.0
BR-06-010-3																					
BR-06-010-4																					
BR-06-010-6																					
BR-06-010-7	43.0	187	3390	910	2370	80.0	4.00	1.10	64.0	---	4.00	2.90	10.0	0.40	---	---	---	---	1.70	0.40	---
BR-06-010-8																					
BR-06-010-10																					
BR-06-010-12	52.0	125	2210	550	2010	70.0	4.00	1.10	47.0	---	7.00	3.10	---	---	---	---	---	---	2.40	0.30	---
BR-06-010-37	438	60.0	170	100	130	480	19.0	1.40	---	3.00	113	31.1	95.0	4.50	---	---	---	2.00	---	1.30	90.0
BR-06-010-42																					
BR-06-016-45																					
BR-06-016-46																					
BR-06-016-47																					

--- below detection limit

LITHOGEOCHEMISTRY: PAGE BODY, BIRD RIVER SILL (continued)

Sample ID:	La ppm FUS-MS	Ce ppm FUS-MS	Pr ppm FUS-MS	Nd ppm FUS-MS	Sm ppm FUS-MS	Eu ppm FUS-MS	Gd ppm FUS-MS	Tb ppm FUS-MS	Dy ppm FUS-MS	Ho ppm FUS-MS	Er ppm FUS-MS	Tm ppm FUS-MS	Yb ppm FUS-MS	Lu ppm FUS-MS	Hf ppm FUS-MS	Ta ppm FUS-MS	W ppm FUS-MS	Tl ppm FUS-MS	Pb ppm FUS-MS	Bi ppm FUS-MS	Th ppm FUS-MS	U ppm FUS-MS
CM-06-003-1	0.84	2.24	0.32	1.78	0.60	0.19	0.82	0.17	1.17	0.25	0.71	0.11	0.70	0.11	0.60	0.09	---	---	---	0.10	0.12	0.08
CM-06-015-1	1.22	2.89	0.39	1.93	0.57	0.26	0.76	0.15	1.01	0.22	0.69	0.11	0.73	0.11	0.20	0.01	---	---	---	0.30	0.05	0.06
CM-06-023-2	0.29	0.78	0.12	0.60	0.19	0.09	0.28	0.06	0.38	0.08	0.27	0.04	0.31	0.05	0.20	0.03	---	---	---	---	---	0.05
CM-06-030-1	2.27	5.57	0.81	4.46	1.41	0.68	2.09	0.41	2.68	0.57	1.72	0.26	1.77	0.28	1.10	0.15	3.20	---	---	0.60	0.26	0.10
CM-06-032-1	1.31	3.73	0.55	2.96	0.92	0.47	1.39	0.27	1.81	0.40	1.24	0.19	1.28	0.20	0.60	0.04	---	0.07	5.00	0.50	0.13	0.09
CM-06-033-1	17.9	36.9	4.09	15.5	2.67	1.78	2.34	0.41	2.39	0.48	1.40	0.21	1.42	0.22	2.90	0.42	0.70	---	---	---	4.08	1.75
CM-06-035-1	0.36	1.02	0.14	0.78	0.25	0.12	0.32	0.06	0.39	0.08	0.24	0.04	0.23	0.04	0.10	---	---	---	---	1.20	---	0.03
CM-06-037-1	0.58	1.58	0.23	1.19	0.36	0.27	0.48	0.09	0.63	0.13	0.40	0.06	0.40	0.06	0.20	0.01	---	---	---	0.10	0.09	0.19
BR-06-010-1	0.79	1.63	0.21	1.00	0.28	0.09	0.32	0.06	0.38	0.08	0.24	0.04	0.26	0.04	0.20	0.01	---	---	---	0.40	---	0.02
BR-06-010-3																						
BR-06-010-4																						
BR-06-010-6																						
BR-06-010-7	0.50	1.16	0.17	0.87	0.27	0.13	0.37	0.07	0.48	0.10	0.31	0.05	0.32	0.05	0.30	0.02	---	0.06	---	1.20	0.05	0.02
BR-06-010-8																						
BR-06-010-10																						
BR-06-010-12	0.65	1.58	0.23	1.12	0.34	0.15	0.4	0.08	0.53	0.10	0.31	0.05	0.29	0.05	0.10	0.01	---	---	---	0.30	---	0.02
BR-06-010-37	4.72	13.7	1.96	9.99	2.89	0.87	3.99	0.81	5.10	1.08	3.25	0.49	3.35	0.53	2.70	0.37	0.80	---	18.0	0.30	0.49	0.53
BR-06-010-42																						
BR-06-016-45																						
BR-06-016-46																						
BR-06-016-47																						

--- below detection limit

LITHOGEOCHEMISTRY: PETERSON BLOCK AND NATIONAL-LEDIN BODIES, BIRD RIVER SILL AND SURROUNDING BIRD RIVER GREENSTONE BELT FORMATIONS

Sample ID:	Au ppb FA-MS	Pt ppb FA-MS	Pd ppb FA-MS	Cu ppm ICP-OES	Ni ppm ICP-OES	Co ppm ICP-OES	S % IR	SiO2 % FUS-ICP	Al2O3 % FUS-ICP	Fe2O3(T) % FUS-ICP	MnO % FUS-ICP	MgO % FUS-ICP	CaO % FUS-ICP	Na2O % FUS-ICP	K2O % FUS-ICP	TiO2 % FUS-ICP	P2O5 % FUS-ICP	LOI % FUS-ICP	Total % FUS-ICP	Sc ppm FUS-ICP	Be ppm FUS-ICP
Peterson Block body, Bird River sill																					
CM-06-069-2	---	56.7	164	20.0	640	30.0	---	46.4	7.16	11.6	0.21	20.9	8.19	0.16	0.07	0.28	0.03	4.58	99.6	24.0	---
National-Ledin body, Bird River sill																					
CM-06-113-1	1.00	10.6	133	---	50.0	---	0.14	56.7	13.0	10.3	0.05	4.60	9.00	2.87	0.24	1.24	0.21	2.01	100	31.0	1.00
Lamprey Falls Formation																					
CM-06-040-1	---	10.0	10.8	30.0	90.0	---		49.5	15.6	11.7	0.22	8.28	10.1	2.36	0.08	0.91	0.08	1.32	100	48.0	1.00
CM-06-048-1	3.00	7.80	29.1	230	70.0	40.0															
CM-06-052-1	82.0	12.4	13.5	4920	440	190															
CM-06-054-1	---	---	---	20.0	---	---															
CM-06-065-1	---	---	---	50.0	80.0	---															
CM-06-086-1	2.00	7.80	11.0	240	140	60.0															
CM-06-112-1	2.00	9.30	12.0	80.0	90.0	---	0.02	48.3	15.2	13.3	0.22	9.07	9.70	2.03	0.21	0.89	0.07	1.35	100	45.0	---
CM-06-123-1	3.00	4.70	2.60	40.0	50.0	---	0.01	49.6	15.2	13.2	0.21	7.31	10.4	1.51	0.22	1.12	0.10	1.25	100	40.0	1.00
Lamprey Falls Formation (data from Gilbert (2005))																					
32-05-0209-1								48.5	14.6	13.9	0.19	7.58	10.8	2.73	0.34	0.84	0.07	0.29	99.8	40.0	---
32-06-0245-1								49.0	15.0	13.3	0.23	6.88	10.7	3.22	0.24	1.01	0.09	0.82	100	42.0	---
32-05-0205-3								49.6	14.3	13.5	0.15	7.51	11.3	2.02	0.17	0.86	0.06	0.36	99.8	41.0	---
32-05-0207-1								49.6	14.5	12.2	0.15	7.95	12.0	2.11	0.30	0.84	0.07	0.36	100	40.0	---
32-06-0246-1								51.2	15.9	12.2	0.25	5.61	8.62	4.45	0.41	1.07	0.06	0.68	100	47.0	1.00
Peterson Creek Formation (data from Duguet (2006))																					
2102A								47.1	18.8	15.4	0.28	4.00	6.40	3.31	1.92	2.10	0.34	0.63	100	28.0	2.00
2250A								65.0	15.7	4.30	0.06	1.38	4.86	3.36	2.00	0.58	0.19	1.12	98.5	15.0	1.00
2252								62.7	14.3	10.2	0.49	2.75	4.16	1.78	2.38	0.70	0.14	0.57	100	12.0	2.00
2323								65.4	12.9	7.51	0.38	0.75	5.55	3.45	0.85	1.14	0.56	1.00	99.4	17.0	1.00

--- below detection limit

LITHOGEOCHEMISTRY: PETERSON BLOCK AND NATIONAL-LEDIN BODIES, BIRD RIVER SILL AND SURROUNDING BIRD RIVER GREENSTONE BELT FORMATIONS (continued)

Sample ID:	V ppm FUS-ICP	Co ppm FUS-MS	Ni ppm FUS-MS	Cu ppm FUS-MS	Cr ppm FUS-MS	Zn ppm FUS-MS	Ga ppm FUS-MS	Ge ppm FUS-MS	As ppm FUS-MS	Rb ppm FUS-MS	Sr ppm FUS-ICP	Y ppm FUS-MS	Zr ppm FUS-ICP	Nb ppm FUS-MS	Mo ppm FUS-MS	Ag ppm FUS-MS	In ppm FUS-MS	Sn ppm FUS-MS	Sb ppm FUS-MS	Cs ppm FUS-MS	Ba ppm FUS-ICP
Peterson Block body, Bird River sill																					
CM-06-069-2	123	62.0	1020	30.0	1480	100	9.00	1.50	---	---	5.00	9.60	11.0	1.00	---	---	---	---	---	---	5.00
National-Ledin body, Bird River sill																					
CM-06-113-1	206	16.0	90.0	20.0	---	---	18.0	1.10	---	5.00	86.0	32.3	117	6.90	---	---	---	---	---	3.60	39.0
Lamprey Falls Formation																					
CM-06-040-1	322	43.0	120	60.0	260	100	14.0	1.10	---	---	121	18.4	47.0	1.80	---	---	---	---	---	---	24.0
CM-06-048-1																					
CM-06-052-1																					
CM-06-054-1																					
CM-06-065-1																					
CM-06-086-1																					
CM-06-112-1	302	48.0	150	100	330	100	14.0	1.50	---	4.00	84.0	20.1	43.0	1.70	---	---	---	---	---	0.40	49.0
CM-06-123-1	349	46.0	110	50.0	180	80.0	18.0	1.70	---	4.00	172	26.2	65.0	2.70	---	---	---	---	---	0.30	34.0
Lamprey Falls Formation (data from Gilbert (2005))																					
32-05-0209-1	268	51.0	123	60.0	203	71.0	16	2.00	---	3.00	93.0	17.0	44.0	2.00					0.80	---	60.0
32-06-0245-1	319	46.0	110	50.0	230	60.0	18	1.60	---	2.00	117	24.8	56.0	3.00	---	---	--	---	0.40	0.70	33.0
32-05-0205-3	278	37.0	109	47.0	220	90.0	16	2.00	---	---	96.0	19.0	39.0	3.00					1.00	---	28.0
32-05-0207-1	267	51.0	131	74.0	216	66.0	17	2.00	---	2.00	81.0	20.0	47.0	2.00					1.00	---	31.0
32-06-0246-1	337	55.0	200	60.0	200	90.0	14	1.20	---	15.0	122	21.1	44.0	2.40	---	---	--	---	0.30	0.90	100
Peterson Creek Formation (data from Duguet (2006))																					
2102A	285	33.0	---	30.0	---	160	27.0	2.00	---	55.0	432	43.0	244	13.0	---	---	---	---	---	6.90	296
2250A	110	11.0	---	20.0	60	60.0	18.0	1.00	---	74.0	202	21.0	133	8.00	---	---	---	---	---	2.30	254
2252	115	15.0	---	40.0	---	160	16.0	1.00	---	107	124	15.0	113	5.00	---	---	---	---	---	4.70	160
2323	8.00	9.00	---	20.0	---	70.0	19.0	1.00	---	21.0	296	41.0	211	14.0	---	---	---	---	---	1.70	395

--- below detection limit

LITHOGEOCHEMISTRY: PETERSON BLOCK AND NATIONAL-LEDIN BODIES, BIRD RIVER SILL AND SURROUNDING BIRD RIVER GREENSTONE BELT FORMATIONS (continued)

Sample ID:	La ppm FUS-MS	Ce ppm FUS-MS	Pr ppm FUS-MS	Nd ppm FUS-MS	Sm ppm FUS-MS	Eu ppm FUS-MS	Gd ppm FUS-MS	Tb ppm FUS-MS	Dy ppm FUS-MS	Ho ppm FUS-MS	Er ppm FUS-MS	Tm ppm FUS-MS	Yb ppm FUS-MS	Lu ppm FUS-MS	Hf ppm FUS-MS	Ta ppm FUS-MS	W ppm FUS-MS	Tl ppm FUS-MS	Pb ppm FUS-MS	Bi ppm FUS-MS	Th ppm FUS-MS	U ppm FUS-MS
Peterson Block body, Bird River sill																						
CM-06-069-2	0.57	1.92	0.33	2.13	0.83	0.29	1.18	0.24	1.61	0.34	0.95	0.14	0.93	0.15	0.50	0.04	---	---	---	0.30	0.11	0.09
National-Ledin body, Bird River sill																						
CM-06-113-1	16.1	42.5	5.06	20.5	4.15	1.06	4.62	0.87	5.33	1.08	3.21	0.47	3.01	0.45	3.20	0.38	1.70	0.06	---	---	4.25	0.57
Lamprey Falls Formation																						
CM-06-040-1	2.34	6.63	1.01	5.44	1.75	0.84	2.61	0.49	3.18	0.66	1.98	0.30	1.99	0.32	1.40	0.11	---	---	---	---	0.24	0.20
CM-06-048-1																						
CM-06-052-1																						
CM-06-054-1																						
CM-06-065-1																						
CM-06-086-1																						
CM-06-112-1	2.10	6.10	0.92	5.03	1.71	0.67	2.53	0.49	3.25	0.71	2.14	0.32	2.14	0.34	1.30	0.12	---	---	---	---	0.24	0.09
CM-06-123-1	3.93	11.0	1.56	8.11	2.5	0.92	3.46	0.66	4.25	0.90	2.65	0.41	2.72	0.41	1.90	0.20	---	---	---	0.30	0.46	0.14
Lamprey Falls Formation (data from Gilbert (2005))																						
32-05-0209-1	2.80	6.70	0.96	5.30	1.80	0.82	2.60	0.50	3.30	0.70	2.10	0.32	2.10	0.32	1.30	0.10	---	---	---	---	0.30	---
32-06-0245-1	3.45	9.91	1.63	8.23	2.41	0.85	3.17	0.61	4.09	0.87	2.66	0.40	2.58	0.39	1.60	0.21	--	--	---	--	0.54	---
32-05-0205-3	2.50	6.70	1.00	5.50	1.80	0.68	2.50	0.50	3.10	0.70	2.00	0.30	2.00	0.30	1.40	0.10	---	---	---	---	0.30	---
32-05-0207-1	1.50	6.00	1.15	6.80	2.20	0.94	2.90	0.50	3.40	0.70	2.20	0.34	2.20	0.34	1.40	0.10	---	---	---	---	0.30	---
32-06-0246-1	2.77	6.86	1.05	5.45	1.77	0.87	2.49	0.52	3.58	0.75	2.29	0.37	2.43	0.36	1.40	0.17	--	--	---	--	0.60	---
Peterson Creek Formation (data from Duguet (2006))																						
2102A	43.0	84.8	10.4	38.2	8.30	2.40	8.80	1.50	8.10	1.60	4.70	0.71	4.50	0.66	6.30	1.00	---	0.20	13.0	---	6.60	1.40
2250A	22.8	44.5	5.36	19.5	4.20	0.79	3.90	0.60	3.60	0.70	2.10	0.34	2.20	0.32	3.80	1.00	2.00	0.20	12.0	---	8.10	2.60
2252	16.7	31.8	3.80	13.3	3.00	0.77	3.00	0.50	2.60	0.50	1.50	0.22	1.40	0.19	3.00	0.40	---	0.60	8.00	---	2.80	1.10
2323	35.4	75.5	10.2	39.9	8.90	2.49	9.20	1.40	7.90	1.60	4.40	0.66	4.20	0.61	5.60	1.00	---	---	9.00	---	4.50	1.00

--- below detection limit

LITHOGEOCHEMISTRY: PAGE BODY, BIRD RIVER SILL (drillcore assays provided by Gossan Resources Ltd.)

Sample ID:	Pt ppb	Pd ppb	Cu %	Ni %	Co ppm	S %
8503	244	459	0.32	1.33	570	5.00
8505	326	1099	1.33	1.42	610	25.0
8506	336	824	0.81	1.48	640	25.0
8508	73.0	246	0.14	0.36	180	2.00
8509	92.0	417	0.29	0.55	320	3.00
8510	150	555	0.67	0.74	350	3.00
8511	243	737	0.67	1.07	490	5.00
8512	286	779	0.89	1.17	560	5.00
8513	97.0	205	0.28	0.43	210	2.00
8514	140	238	0.16	0.39	200	2.00
8515	67.0	176	0.11	0.31	160	1.00
8517	8.00	94.0	0.18	0.29	170	2.00
8518	18.0	382	0.55	0.40	230	1.00
8522	101	294	0.16	0.25	120	2.00
8523	116	198	0.33	0.33	170	2.00
8524	147	515	0.39	0.59	270	4.00
8525	181	597	0.43	0.70	330	2.00
8526	188	573	0.25	0.67	240	2.00
8527	349	1078	0.47	1.63	600	5.00
8528	326	968	0.55	1.67	670	5.00
8538	84.0	94	0.07	0.17	120	0.25
8545	33.0	168	0.13	0.19	110	0.50
8546	92.0	304	0.08	0.27	130	1.00
8547	60.0	283	0.06	0.16	90.0	1.25
8548	98.0	286	0.05	0.18	90.0	2.25
8549	55.0	402	0.13	0.30	140	2.50
8553	24.0	102	0.06	0.10	100	1.00
8554	59.0	242	0.07	0.22	160	0.25
8555	59.0	275	0.03	0.17	130	0.50
8557	111	401	0.13	0.34	180	2.25
8559	34.0	128	0.01	0.12	80.0	0.75
8560	26.0	100	0.02	0.07	60.0	0.75
8662	22.0	132	0.05	0.16	90.0	0.25
8663	38.0	207	0.16	0.27	140	0.25
8664	104	244	0.15	0.29	150	1.25
8666	36.0	150	0.07	0.18	120	1.75
8667	56.0	244	0.27	0.30	180	1.25
8669	408	1115	0.09	0.36	160	3.75
8670	140	445	0.32	0.40	190	5.25
8671	220	723	0.26	0.72	330	10.3
8672	131	416	0.24	0.37	190	15.5
8673	116	362	0.27	0.36	180	9.25
8674	100	216	0.18	0.30	170	5.00
8675	98.0	179	0.10	0.22	130	3.50
8676	88.0	197	0.09	0.25	140	3.50
8677	135	314	0.22	0.35	190	2.50
8678	157	310	0.21	0.38	200	5.25
8679	43.0	159	0.07	0.22	130	3.50
8680	85.0	303	0.06	0.27	130	0.75
8681	16.0	157	0.05	0.18	100	0.75
8686	39.0	69.0	0.02	0.10	60.0	1.00

PLATINUM GROUP ELEMENT ANALYSIS RESULTS:

Sample ID:	Os ppb NI-FINA	Ir ppb NI-FINA	Ru ppb NI-FINA	Rh ppb NI-FINA	Pt ppb NI-FINA	Pd ppb NI-FINA	Au ppb NI-FINA	Re ppb NI-FINA	Mass g NI-FINA
Chrome body, Bird River sill									
CM-05-136-11	14.0	8.30	69.0	33.0	102	425	34.7	9.00	5.00
Page body, Bird River sill									
BR-05-002-6	13.0	12.0	39.0	75.0	223	744	34.7	24.0	5.00
Maskwa-Dumbarton body, Bird River sill									
40306	36.0	16.9	10.0	31.0	131	807	40.7	10.0	5.00
Quartz-feldspar porphyry dyke									
BR-06-010-29	---	3.80	8.00	48.0	162	4530	237	12.0	5.00

SULFUR ISOTOPE ANALYSIS RESULTS:

Sample ID:	Description:	Mineral Separates:	$\delta^{34}S$:	Repeat:		Average:
Page body, Bird River sill						
BR-05-02-5		po, pn	-0.12			
BR-05-02-7a		po, pn	-0.17			
BR-05-02-7b	metaperidotite	ccp	0.03			0.07
BR-06-016-48a		po, pn	0.16			
BR-06-016-48b		ccp	0.43			
Chrome body, Bird River sill						
CM-05-136-12	metaperidotite	bulk sulfur	-1.06			-1.26
CM-05-145		bulk sulfur	6.13	-1.46		
Maskwa-Dumbarton body, Bird River sill						
40307	metaanorthosite	bulk sulfur	-0.94			-0.94
Dumbarton iron formation, Lamprey Falls Formation						
38450	sulfide bearing iron formation	po, pn	-5.43	-6.09	-6.11	-5.88
Galaxy Occurrence (north of the Peterson Block body in the Lamprey Falls Formation)						
CM-06-052-1	mineralized fracture in metabasalt	bulk sulfur	1.71	0.84		1.28

Appendix C: Platinum-Group Element Summary and Scanning Electron Microscope-Energy Dispersive X-ray Images and Semi-Quantitative Analytical Results

PLATINUM-GROUP ELEMENT MINERALIZATION SUMMARY:

Sample Location:	Grain #:	Sample Description:	Platinum-Group Element Characteristics:				Occurrence:	Association
			Species	Chemical Constituents or Formula	Form	Size (μm)	**Locked:**bound by sulfides; **Boundary**:along sulfide boundaries; **Free:** outside sufide in silicate gangue	
Chrome body	1	Peridotite-lower sulfide enriched zone (disseminated pyrrhotite and chalcopyrite)	Kotulskite	Pd(Te,Bi)	anhedral	10x5	locked	Pentlandite
	2		Merenskyite	PdTe2	anhedral (round)	6 diameter	locked	Pentlandite
	3		Merenskyite	PdTe2	anhedral	6 long	boundary	Pentlandite
	4		Hollingworthite	RhAsS	euhedral (cubic)	8 diameter	locked	Pentlandite
			Sulfurarsenide	CoAsS-NiAsS with Rh			locked	Pentlandite
	5		Sperrylite	PtAs2	subhedral (branching)	15 long	locked	Pentlandite
			Hollingworthite	RhAsS	anhedral	2 to 4 long	locked	Pentlandite
	6		Merenskyite	PdTe2	anhedral (round)	5 diameter	locked	Pentlandite
	7		Merenskyite	PdTe2	anhedral (round)	6 diameter	locked	Pentlandite
	8		Borovskite	Pd3SbTe4	anhedral	5x8	boundary	Chalcopyrite
	9		Borovskite	Pd3SbTe4	anhedral (round)	0.5 diameter	free	Silicate
	10		Merenskyite	PdTe2	anhedral (wedge shape)	1.5 long	free	Silicate
	11		Merenskyite	PdTe2	subhedral (hexagonal)	8 long	locked	Pentlandite
	12		Merenskyite	PdTe2	anhedral (triangular)	2.5 long	locked	Pentlandite
	13		Merenskyite	PdTe2	anhedral (round)	5 diameter	locked	Pentlandite
	14		Merenskyite	PdTe2	anhedral (round)	6 diameter	boundary	Pentlandite
Page body	15	Peridotite with semi-massive net textured pyrrhotite and chalcopyrite stringer mineralization	Sulfurarsenide	CoAsS-NiAsS with Rh, Pt	euhedral (cubic)	10 diameter	locked	Pyrrhotite
	16		Sulfurarsenide	CoAsS-NiAsS with Rh, Pt	subhedral (hexagonal)	30x15	locked	Pentlandite
	17		Pt	Pt	dissolved in sulphide	--	locked	Pyrrhotite
	18		Kotulskite	Pd(Te,Bi)	anhedral	10x5	boundary	Pyrrhotite
	19		Sulfurarsenide	CoAsS-NiAsS with Pd	anhedral	10x6	boundary	Pyrrhotite
	20		Merenskyite	PdTe2	anhedral (ellipse)	2x1	locked	Pyrrhotite
	21		Sulfurarsenide	CoAsS-NiAsS with Rh, Pt	anhedral	2.5	locked	Pyrrhotite
	22		Sulfurarsenide	CoAsS-NiAsS with Pt	anhedral (round)	2 diameter	locked	Pyrrhotite
	23		Sulfurarsenide	CoAsS-NiAsS with Rh, Pt	euhedral (cubic)	60 diameter	locked	Pyrrhotite
	24		Sulfurarsenide	CoAsS-NiAsS with Rh	subhedral (triangular)	10 long	locked	Pyrrhotite
	25		Stutzite	Ag5-xTe3	anhedral	5x2	locked	Pyrrhotite
	26		Stutzite	Ag5-xTe4	anhedral (ellipse)	5x2.5	locked	Pyrrhotite
	27		Sulfurarsenide	CoAsS-NiAsS with Pt	subhedral (cubic)	40 diameter	locked	Pyrrhotite
	28		Sulfurarsenide	CoAsS-NiAsS with Rh, Pt	subhedral (hexagonal)	30 diameter	locked	Pyrrhotite
	29		Sulfurarsenide	CoAsS-NiAsS with Rh, Pt	euhedral (hexagonal)	20 diameter	locked	Pyrrhotite
	30		Sulfurarsenide	CoAsS-NiAsS with Pt	subhedral (triangular)	15 long	locked	Chalcopyrite
	31		Keithconnite	Pd3Te	anhedral	25 long	boundary	Pentlandite
	32		Kotulskite	Pd(Te,Bi)	anhedral	8 long	boundary	Chalcopyrite
	33		Pt	Pt	dissolved in sulphide	--	boundary	Chalcopyrite
	34		Merenskyite	PdTe2	anhedral (round)	2 diameter	locked	Pyrrhotite
	35		Sulfurarsenide	CoAsS-NiAsS with Rh	euhedral (hexagonal)	10 diameter	locked	Pentlandite
Quartz-feldspar porphyry dyke that cross-cuts the ultramafic series of the Page body	36	Fine grained quartz-feldspar porphyry with fracture bound chalcopyrite	Froodite	PdBi2	anhedral	2 long	free	Silicate
	37		Ag	Ag	anhedral	5 long	free	Silicate
	38		Pt	Pt	dissolved in sulphide	--	free	Silicate
	39		Froodite	PdBi2	anhedral (round)	1 diameter	free	Silicate
	40		Froodite	PdBi2	anhedral (round)	2 diameter	free	Silicate
	41		Froodite	PdBi2	anhedral (round)	2 diameter	free	Silicate
	42		Froodite	PdBi3	anhedral (round)	1 diameter	free	Silicate
	43		Unidentified PGM	Pd, Bi, Sb	anhedral	3 diameter	free	Silicate
	44		Froodite	PdBi2	anhedral	1.5 long	free	Silicate

Note:

PGM species identifications are based on SEM-EDS semi-quantitative analyses and may not be entirely accurate.

SEM-EDS Images and Semi-Quantitative Analyses:
Chrome Body Platinum-Group Element Mineralization

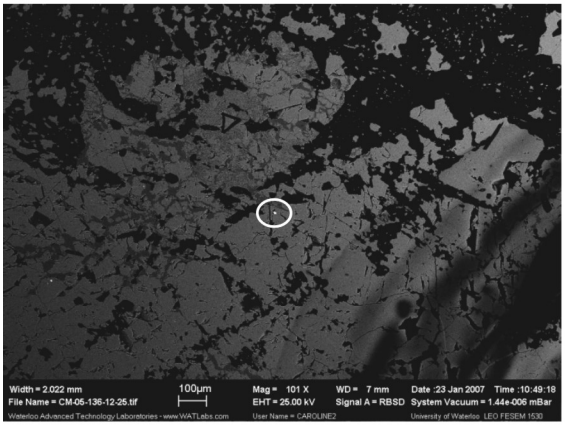

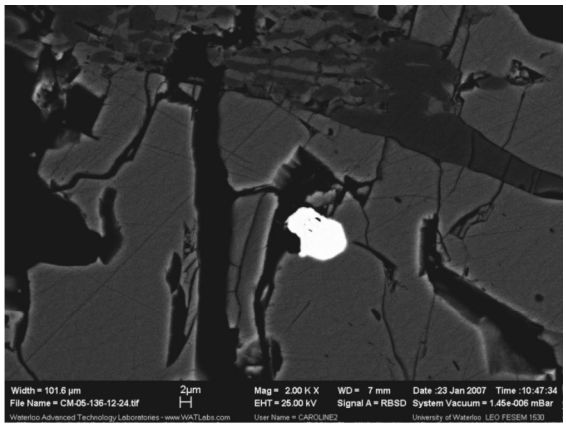

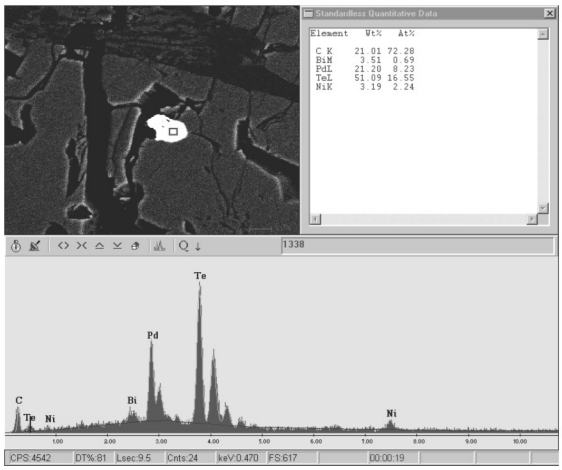

1: PGM - Kotulskite (Pd(Te,Bi)) inclusion in pentlandite.

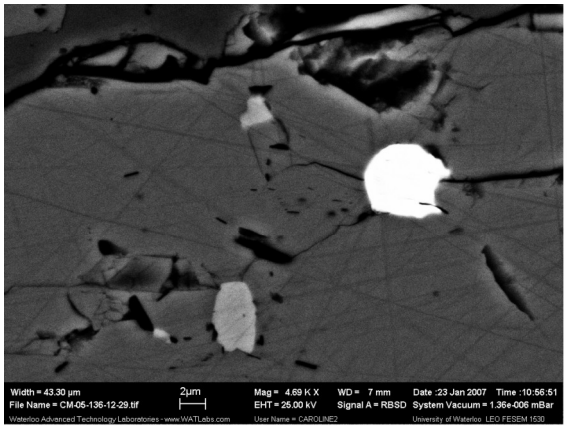

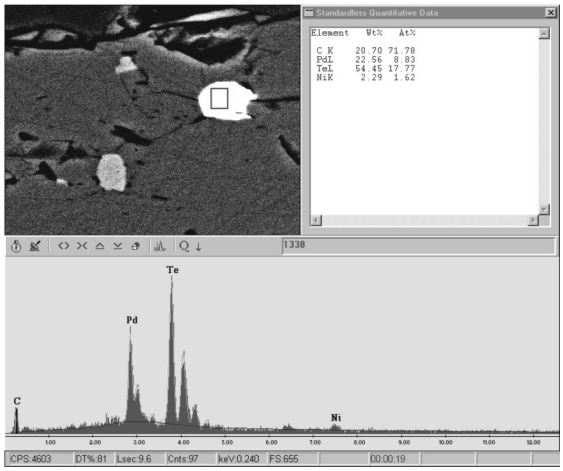

2: PGM - Merenskyite ($PdTe_2$) inclusion in pentlandite.

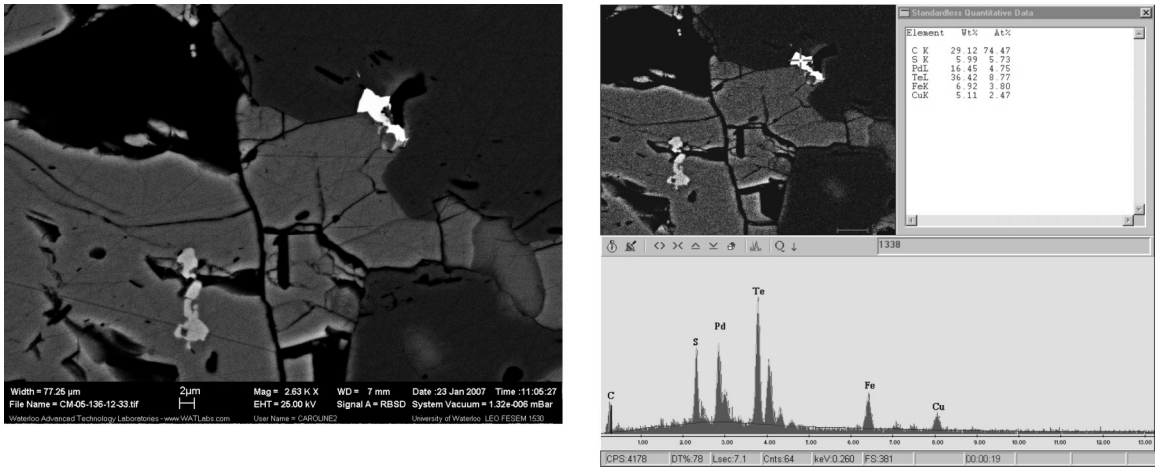

3: PGM - Merenskyite ($PdTe_2$) at the pentlandite and serpentine grain boundary.

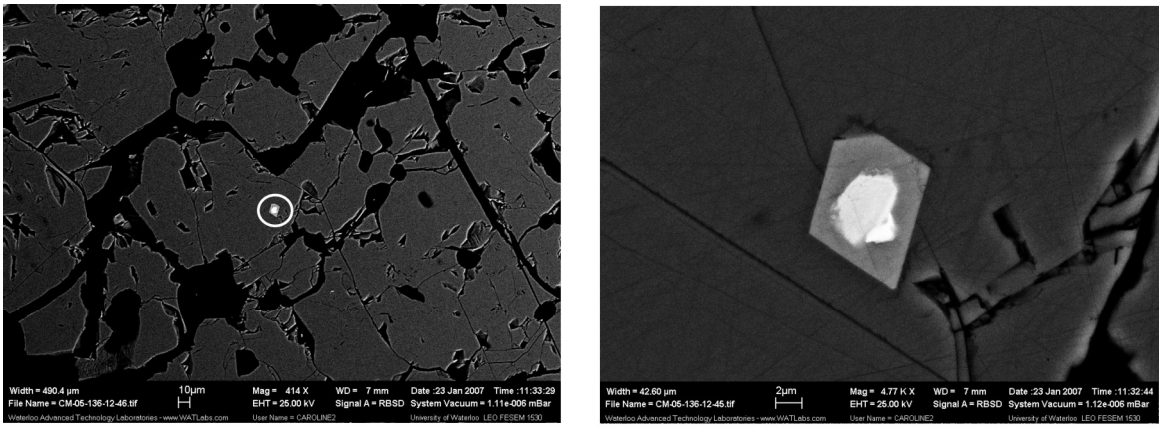

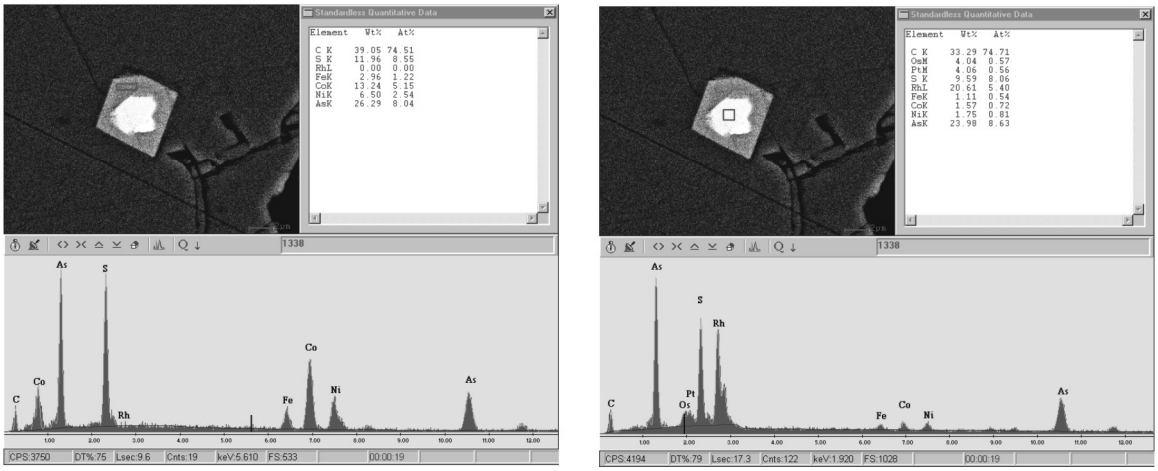

4: PGE – PGE-bearing sulphurarsenide (Co-bearing gersdorffite) inclusion in pentlandite. The sulphurarsenide mineral has a core that has a similar composition to hollingworthite (RhAsS).

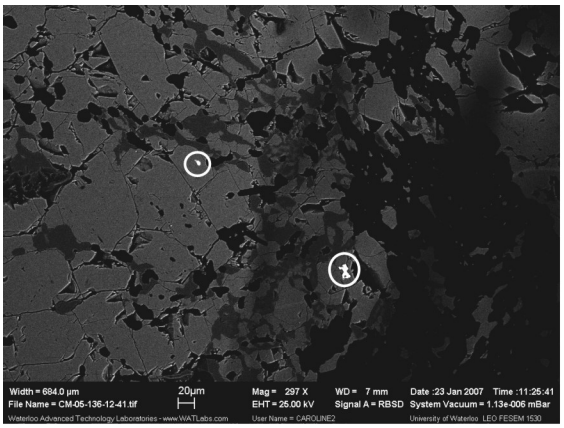

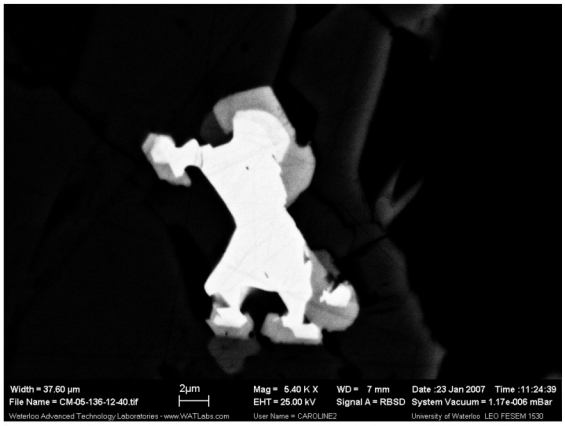

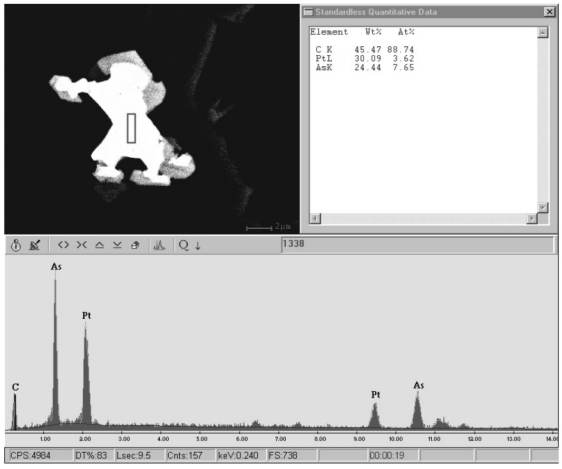

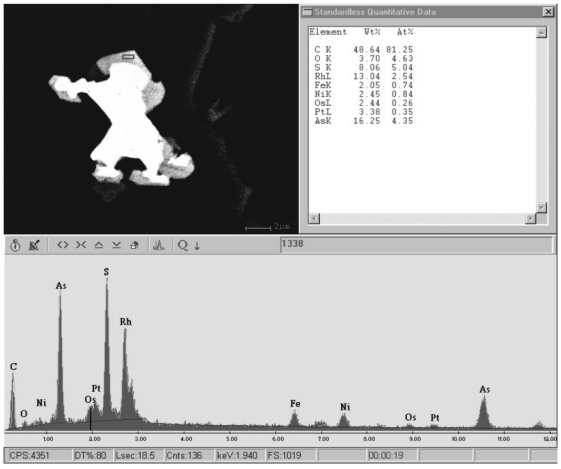

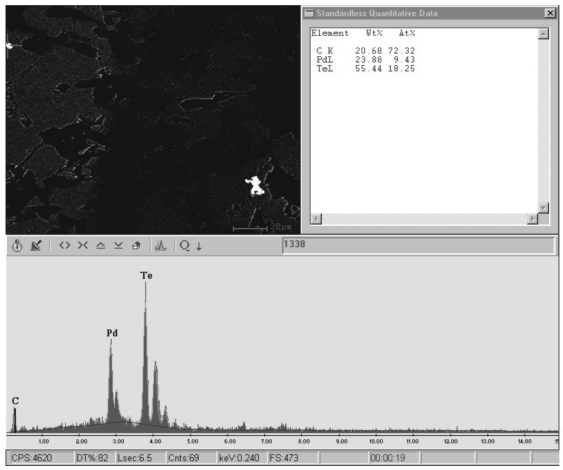

5 and 6: PGM - Sperrylite ($PtAs_2$) and merenskyite ($PdTe_2$) inclusions in pentlandite. The sperrylite inclusion is coated by hollingworthite (RhAsS).

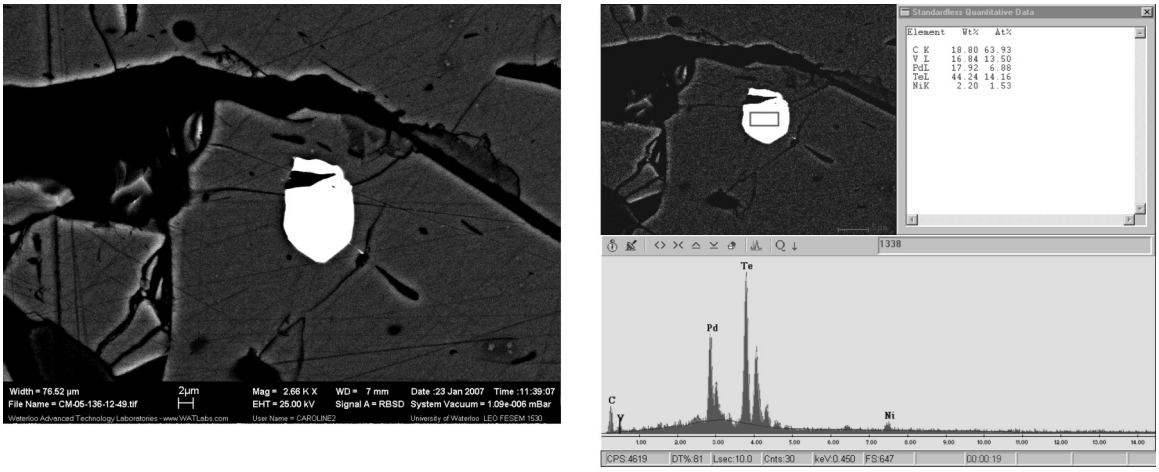

7: PGM - Merenskyite ($PdTe_2$) inclusion in pentlandite.

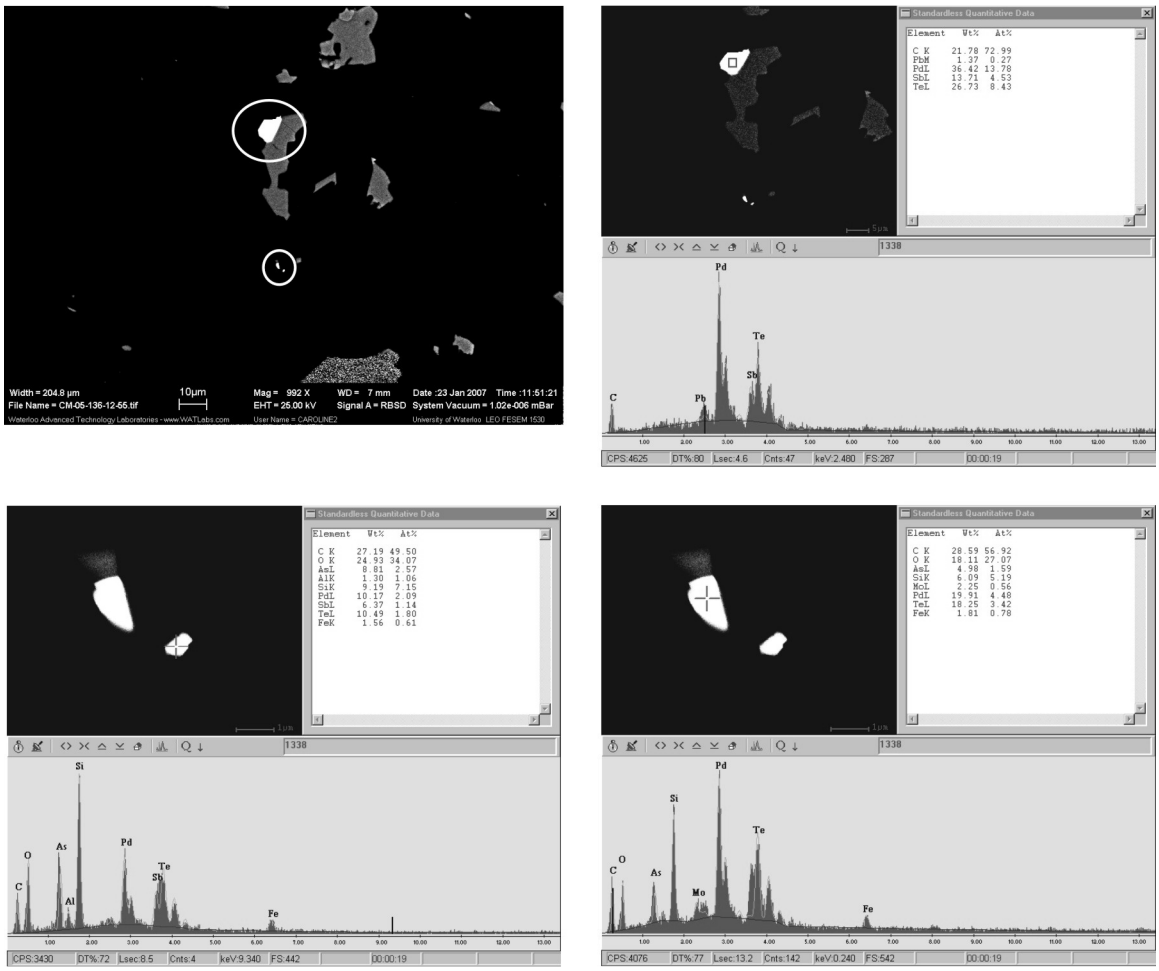

8, 9 and 10: PGM - Borovskite (Pd_3SbTe_4) grain present at the contact between chalcopyrite and silicate groundmass (serpentine). A second borovskite grain and a merenskyite grain ($PdTe_2$) are also present within the serpentine groundmass.

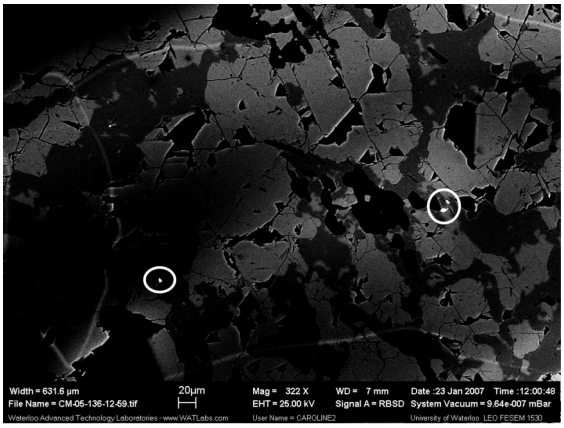

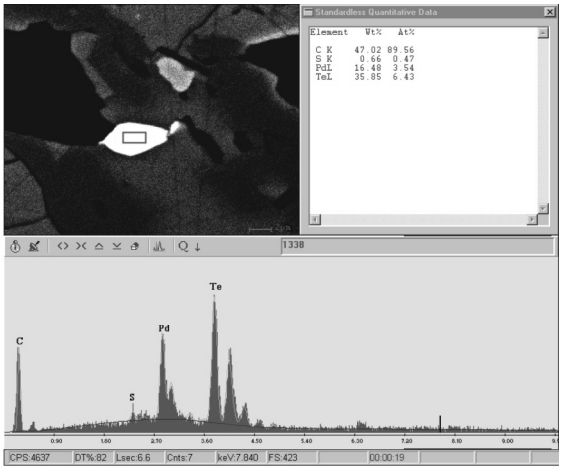

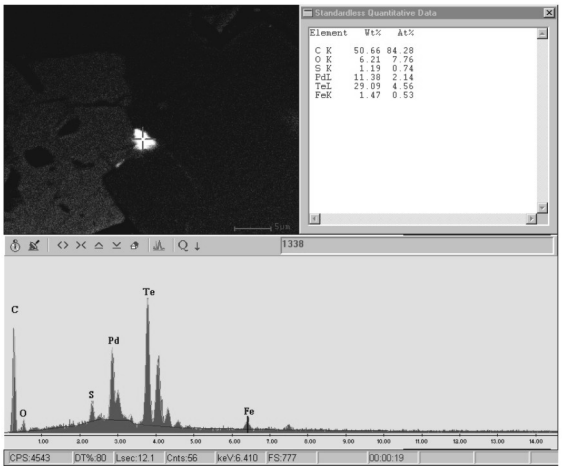

11 and 12: PGM - Two merenskyite grains (PdTe2). One grain is present as an inclusion in pentlandite and the second grain is present along the pentlandite-chlorite grain boundary.

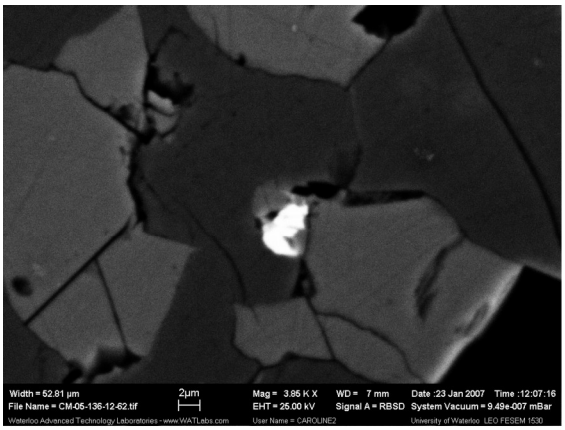

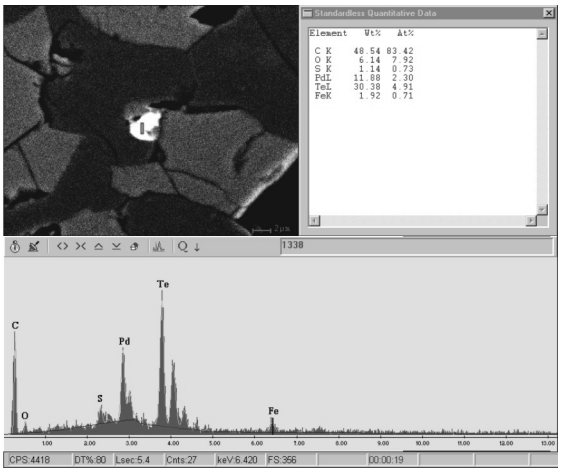

13: PGM - Merenskyite (PdTe2) inclusion in pentlandite.

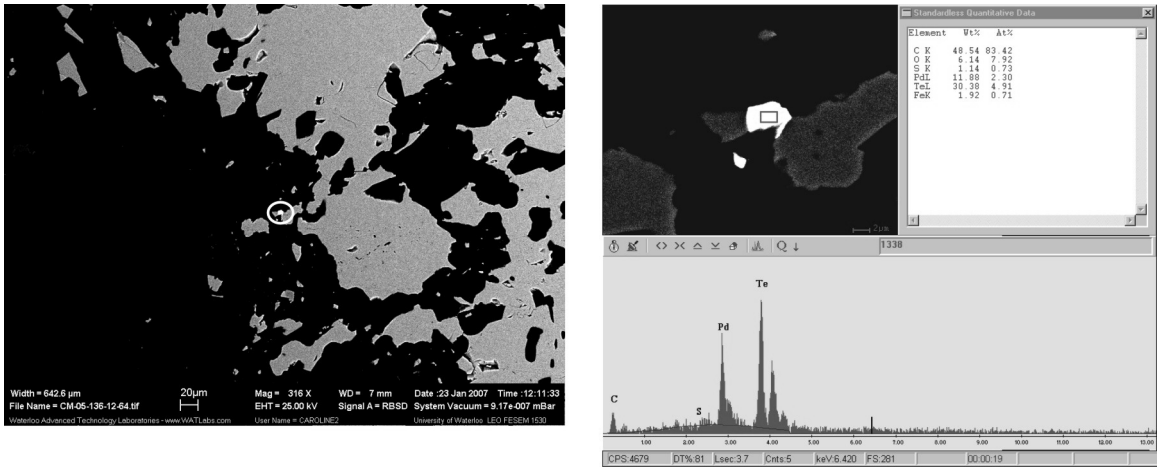

14: PGM - Merenskyite (PdTe2) grain present within pentlandite but is in contact with chlorite groundmass.

Page Body Platinum-Group Element Mineralization

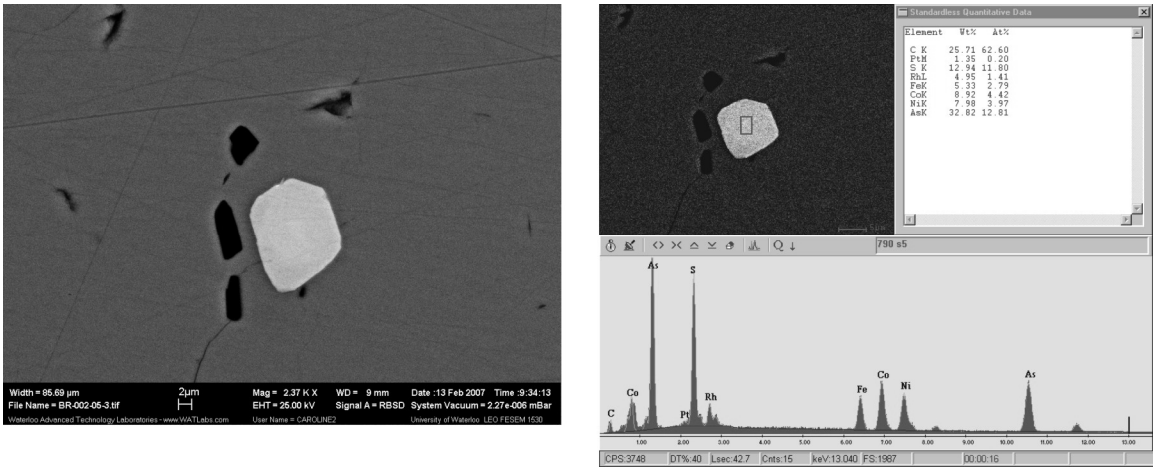

15: PGE - Pt- and Rh-bearing sulphurarsenide inclusion in pyrrhotite.

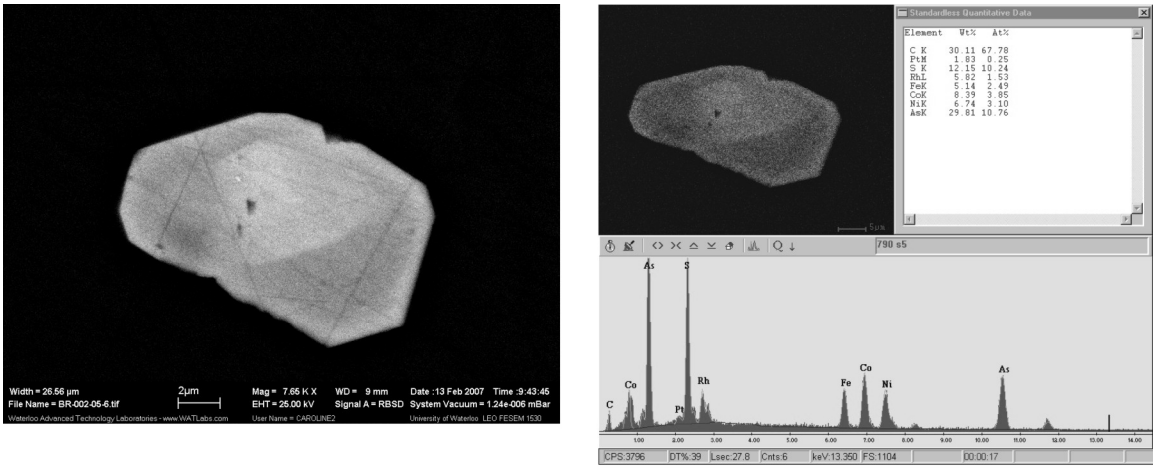

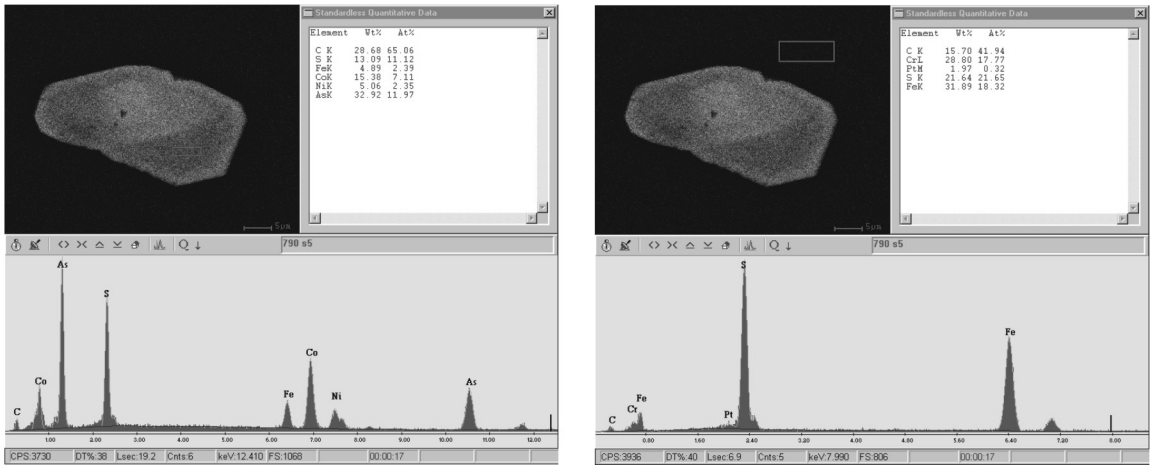

16 and 17: PGE – PGE-bearing sulphurarsenide inclusion in pentlandite. Sulphurarsenide contains a Pt- and Rh-rich core. Pt is also present outside of the sulphurarsenide inclusion within the pentlandite.

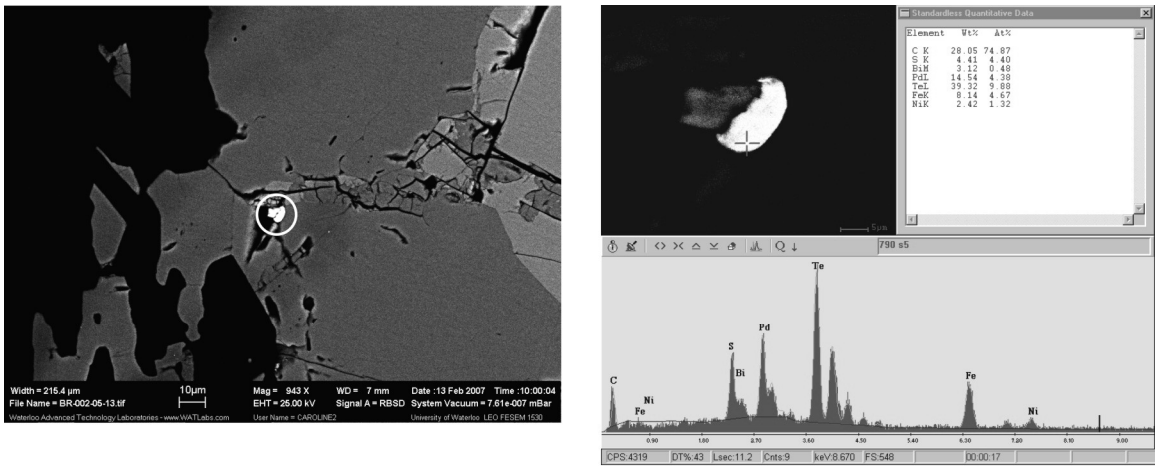

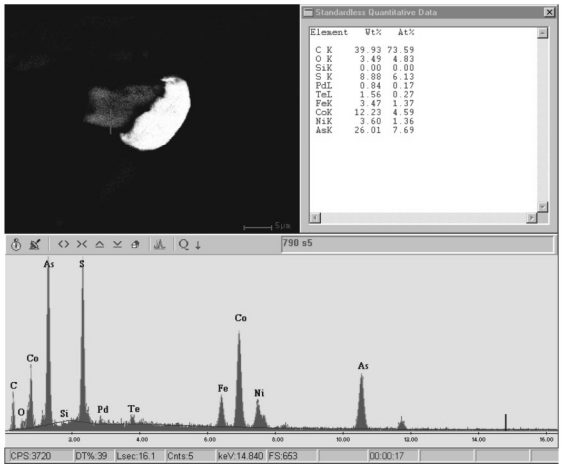

18 and 19: PGM and PGE - Kotulskite (Pd(Te,Bi)) and Pd-rich sulphurarsenide grains present at the contact of pyrrhotite and a silicate inclusion within pyrrhotite.

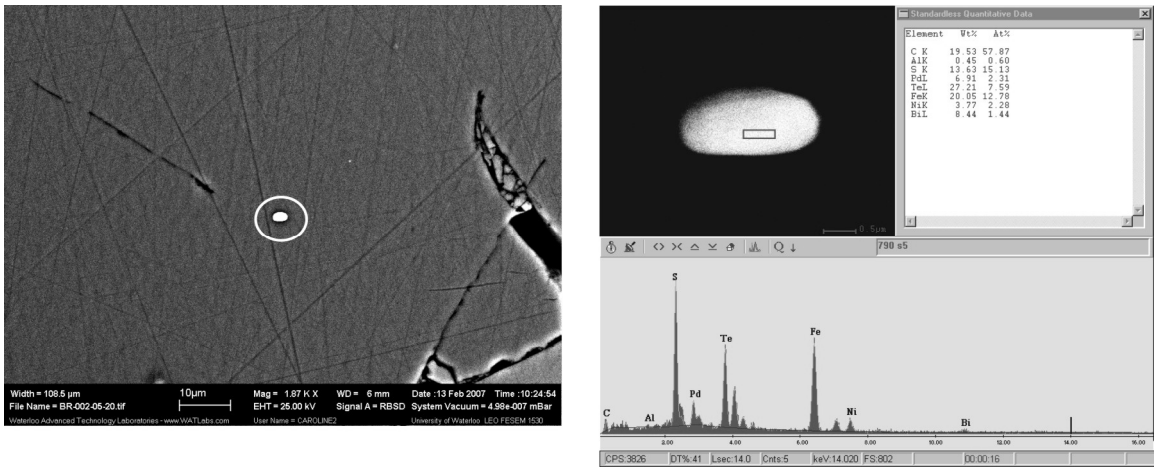

20: PGM - Merenskyite (PdTe2) inclusion in pyrrhotite.

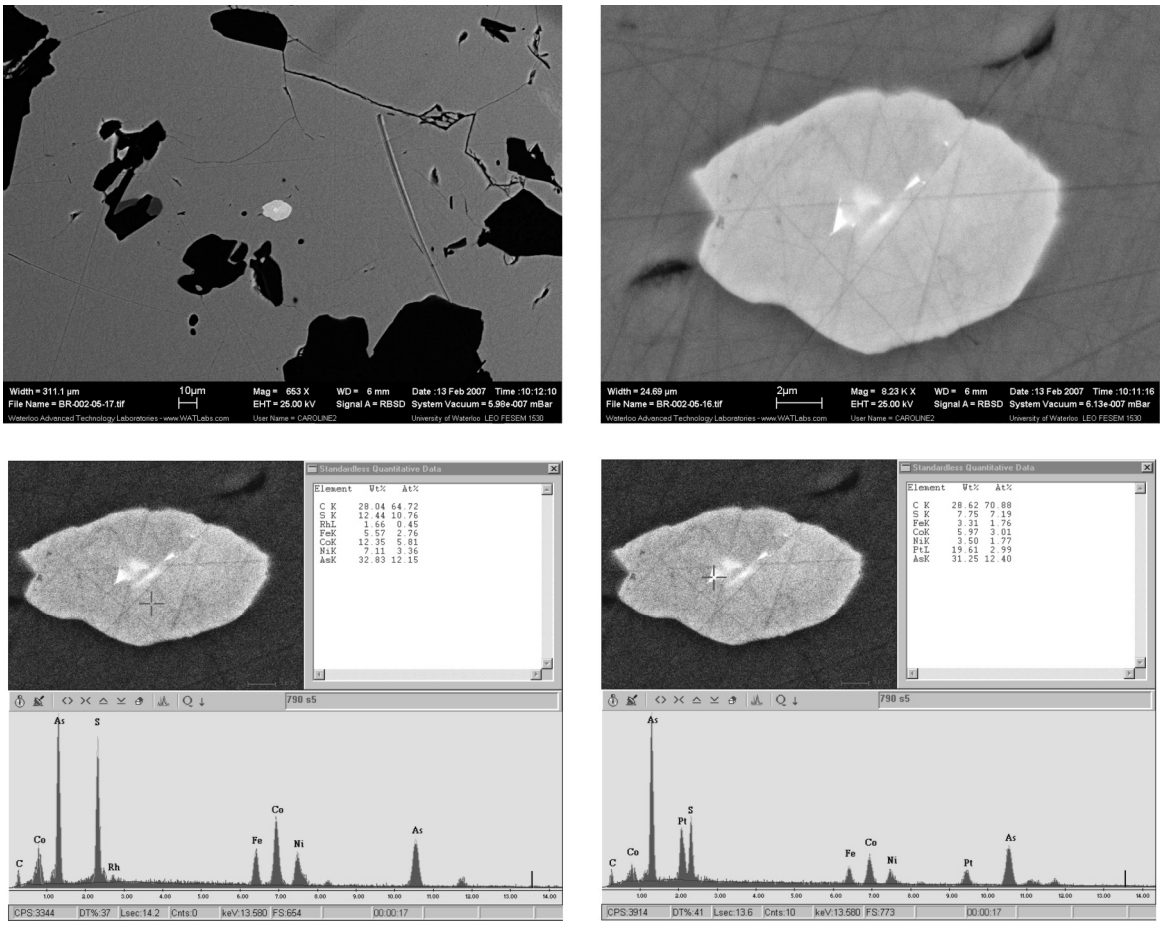

21: PGE - Pt- and Rh-bearing sulphurarsenide inclusion in pyrrhotite.

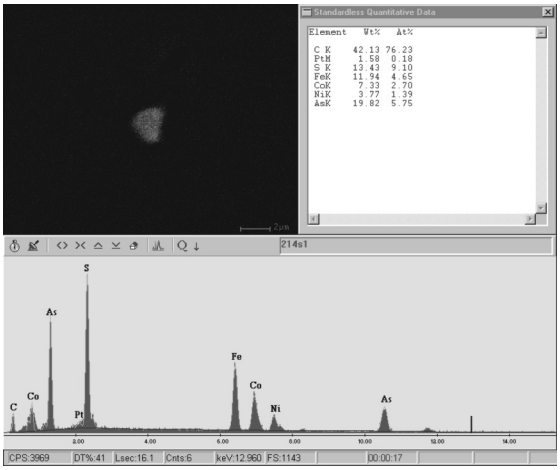

22: PGE - Pt-rich sulphurarsenide inclusion in pyrrhotite.

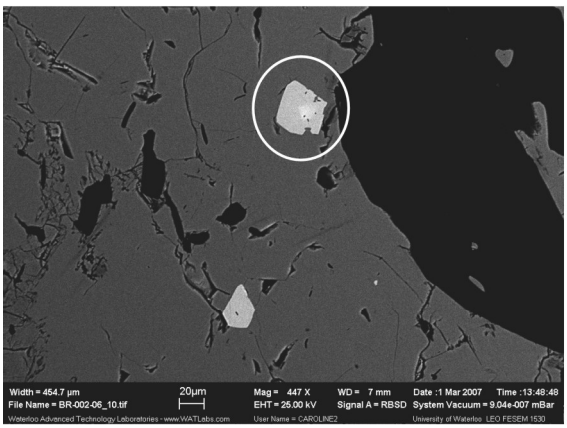

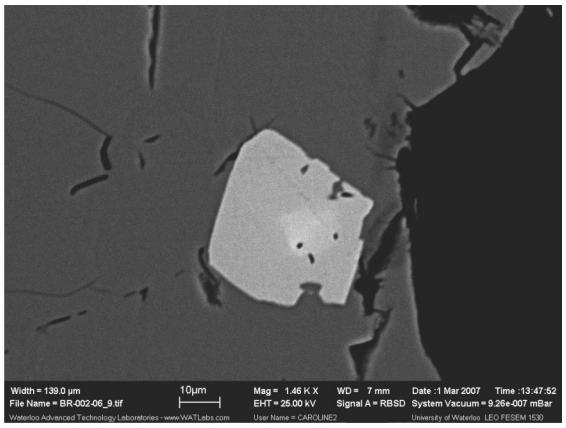

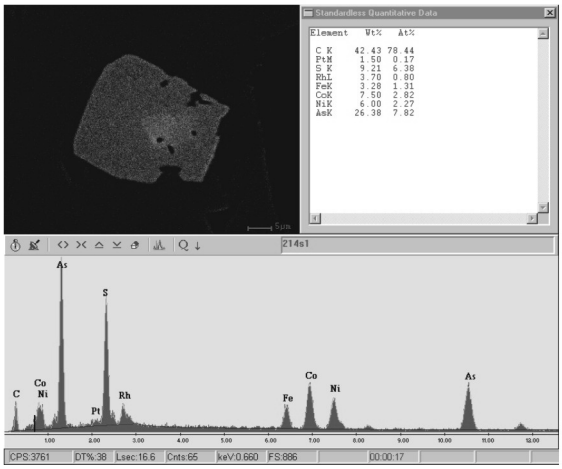

23: PGE - Rh- and Pt-bearimg sulphurarsenide inclusion in pyrrhotite near the pyrhotite-serpentine contact.

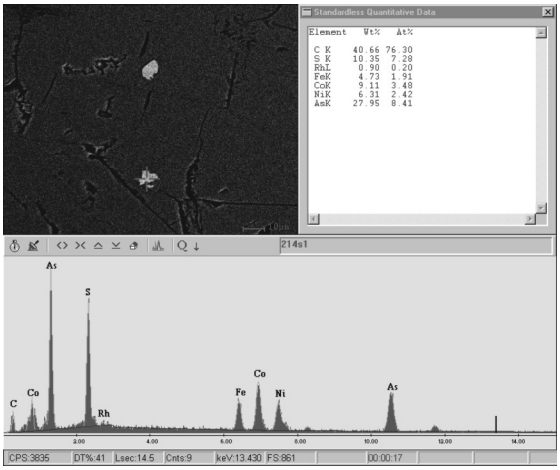

24: PGE - Rh-rich sulphurarsenide inclusion in pyrrhotite.

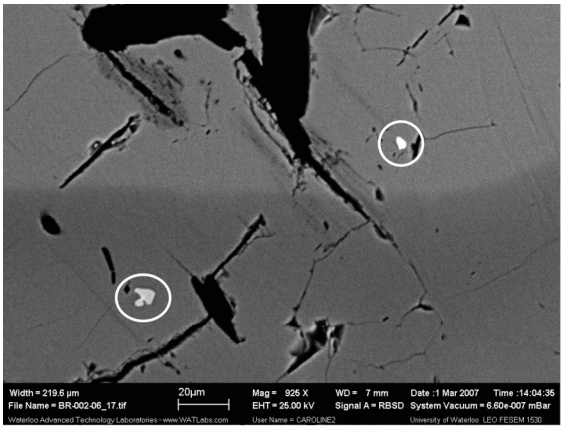

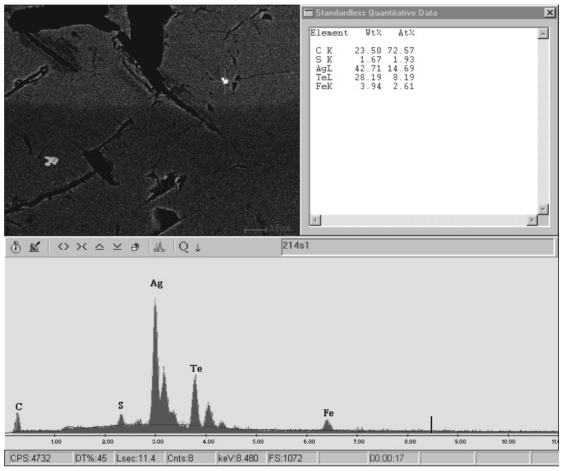

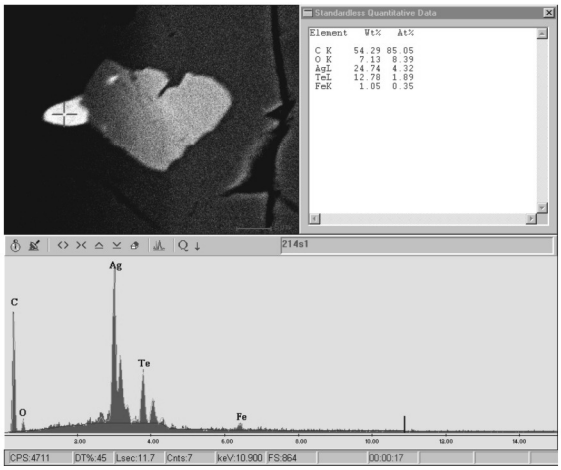

25 and 26: Precious Metals - Two stutzite (Ag5-xTe3) inclusions in pyrrhotite. One stutzite grain is in contact with a sulphurarsenide inclusion.

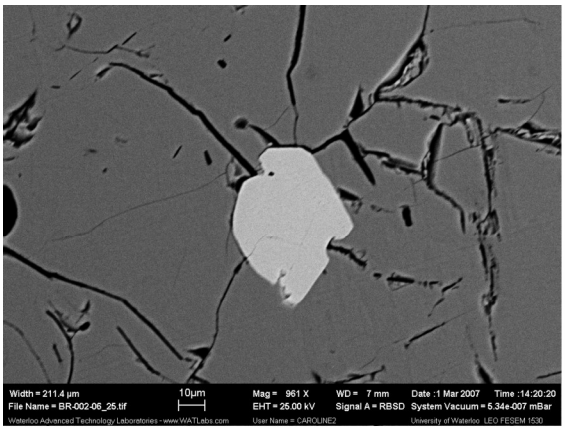

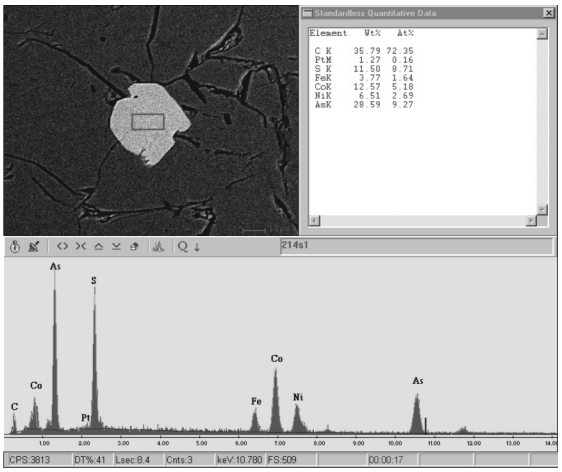

27: PGE - Pt-rich sulphurarsenide inclusion in pyrrhotite.

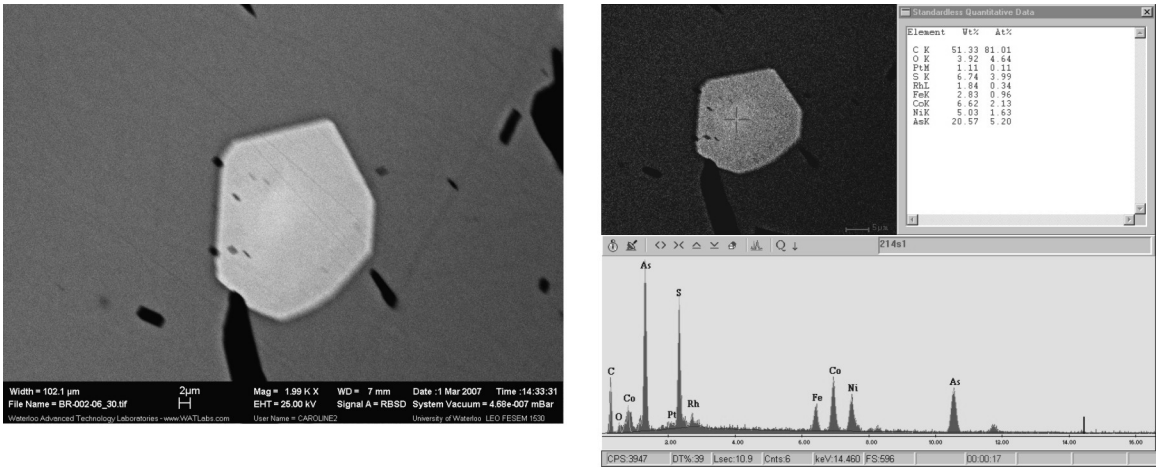

28: PGE - Pt- and Rh-rich sulphurarsenide inclusion in pyrrhotite.

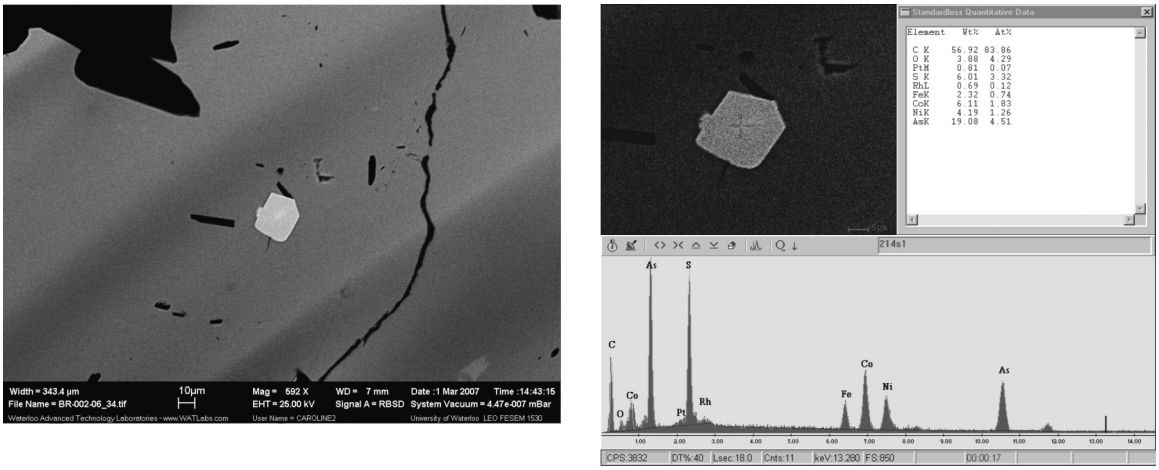

29: PGE - Pt- and Rh-bearing sulphurarsenide inclusion in pyrrhotite.

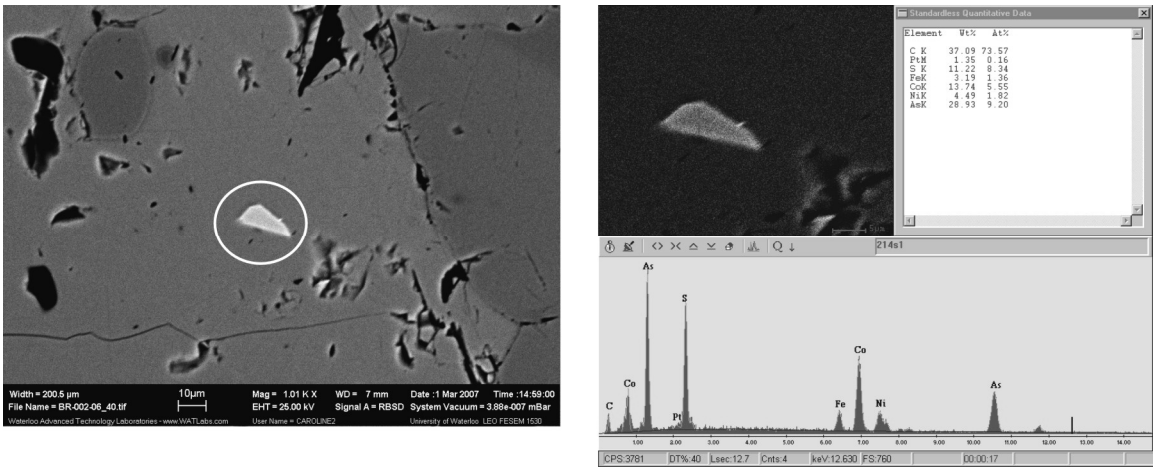

30: PGE - Pt-bearing sulphurarsenide inclusion in chalcopyrite.

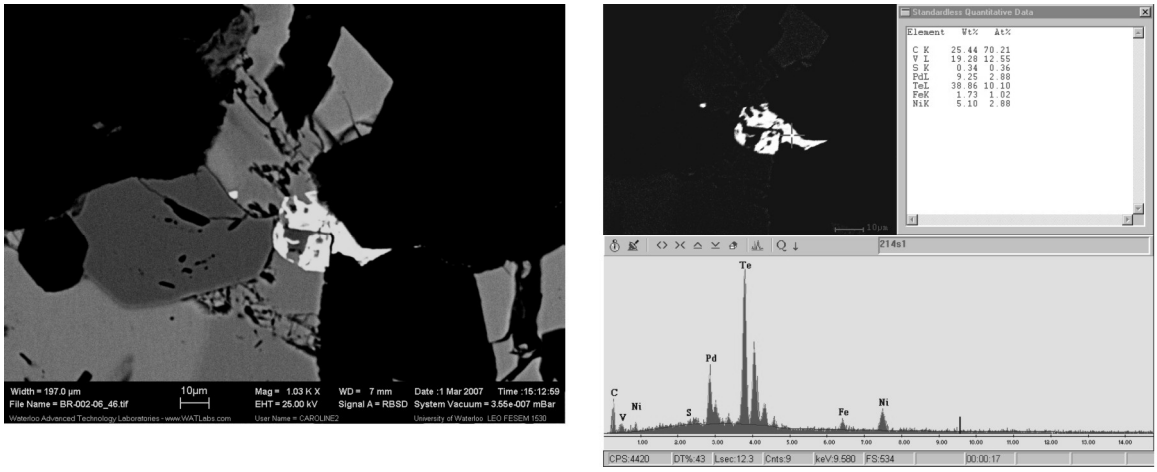

31: PGM - Keithconnite (Pd_3Te) grain present within pentlandite at the pentlandite-chlorite boundary.

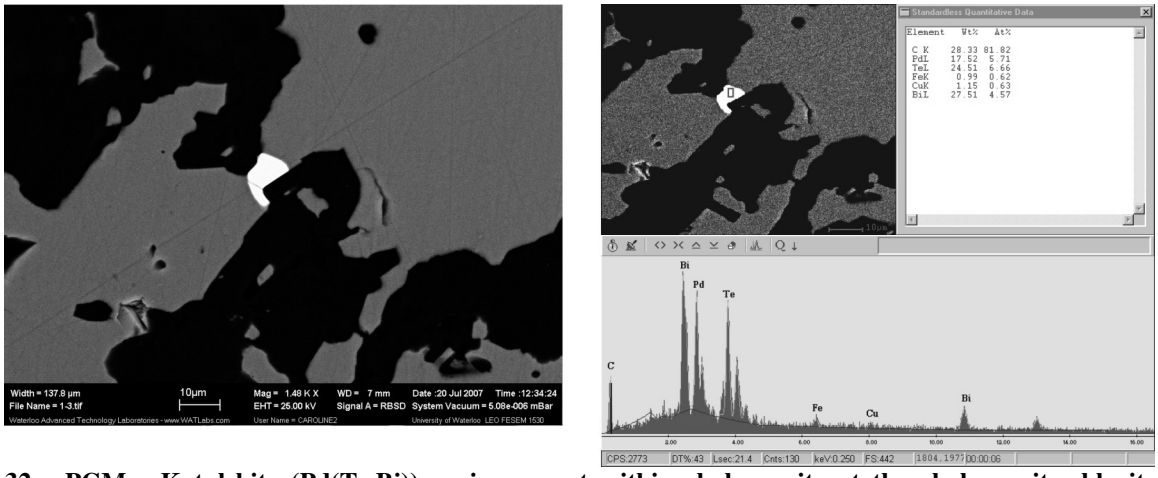

32: PGM - Kotulskite (Pd(Te,Bi)) grain present within chalcopyrite at the chalcopyrite-chlorite grain boundary.

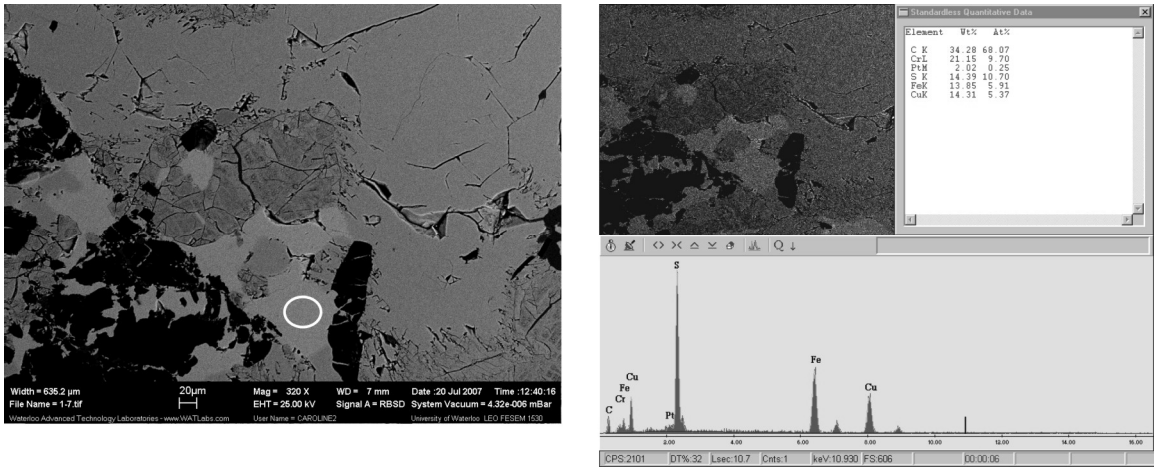

33: PGE - Pt-enriched chalcopyrite.

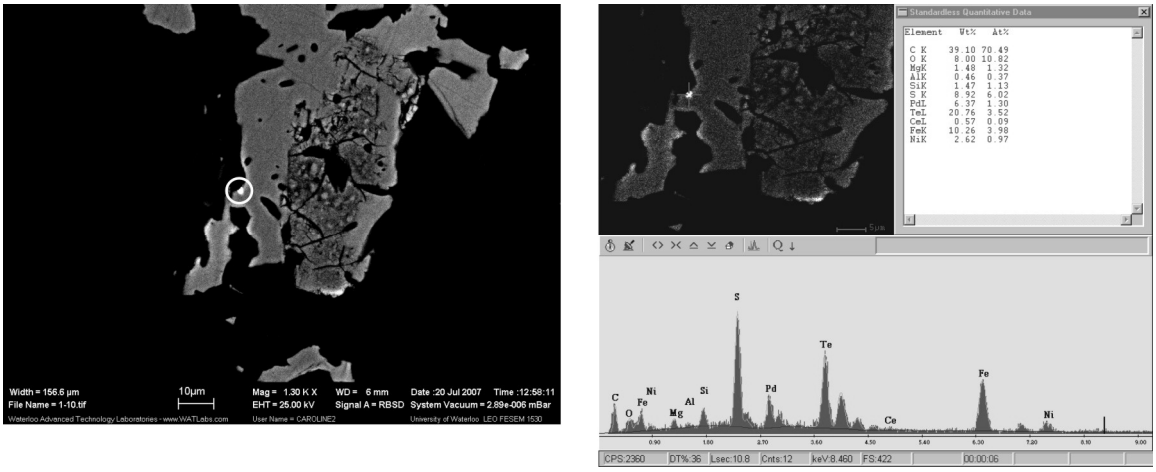

34: PGM - Merenskyite ($PdTe_2$) inclusion in pyrrhotite at the pyrrhotite-chlorite grain boundary.

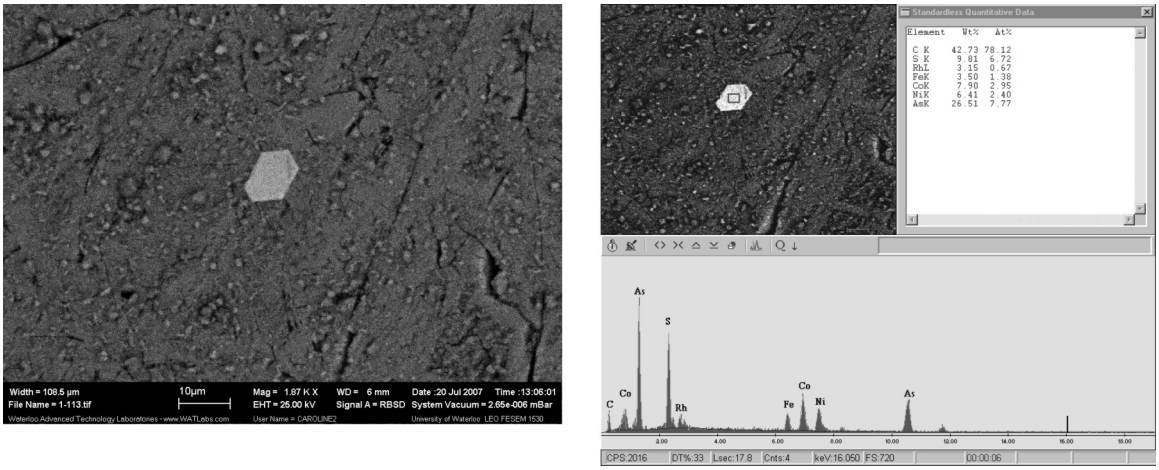

35: PGE - Rh-bearing sulphurarsenide inclusion in pentlandite.

Quartz-Feldspar Porphyry Dyke Platinum-Group Element Mineralization

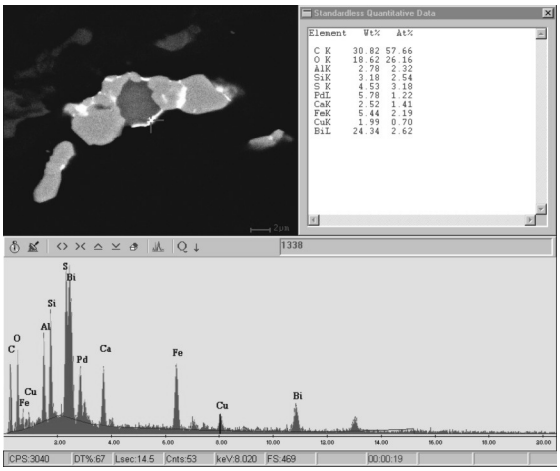

36: PGM - Froodite ($PdBi_2$) intergrown with chalcopyrite and sulphurarsenide minerals within silicate gangue groundmass.

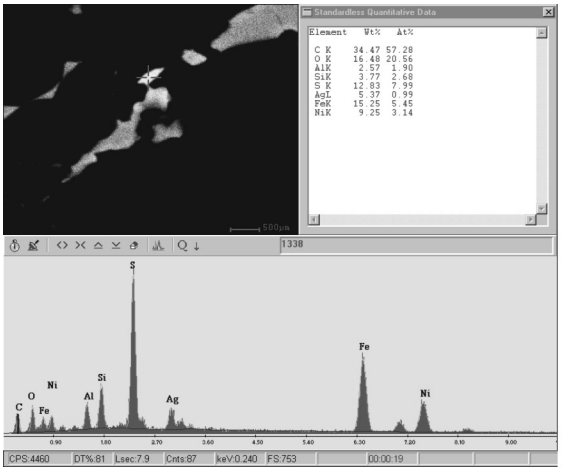

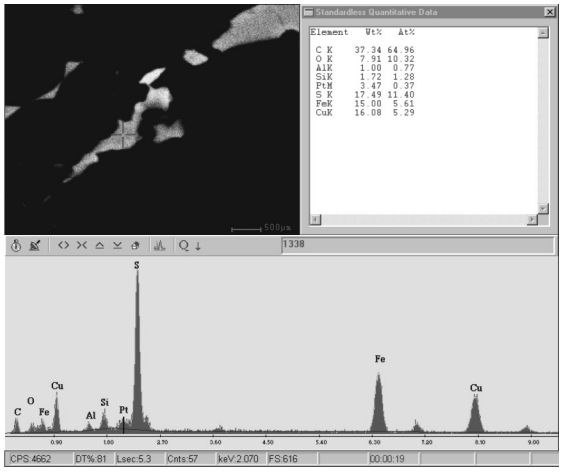

37 and 38: Precious Metals – Ag- and Pt-bearing pentlandite and chalcopyrite, respectively, within a silicate gangue groundmass.

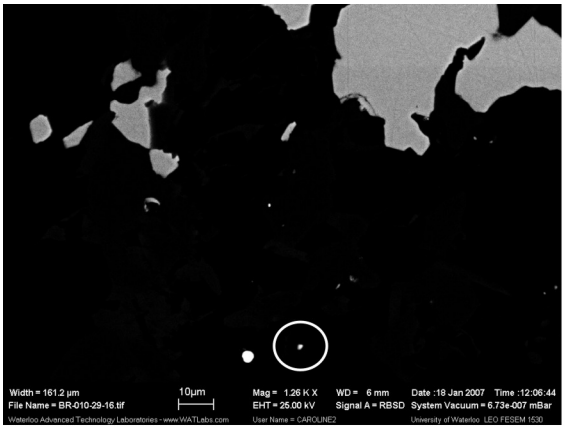

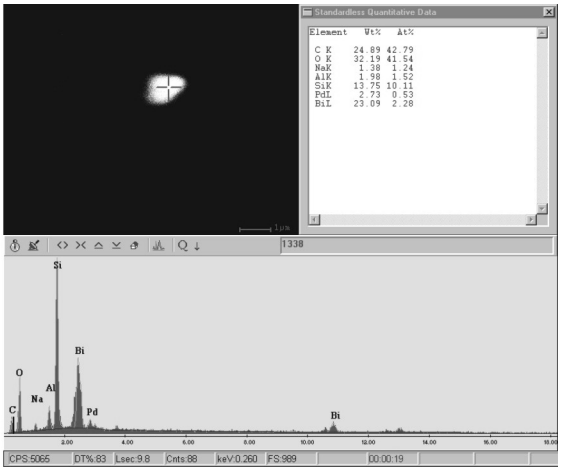

39: PGM – Froodite ($PdBi_2$) grain within silicate gangue groundmass.

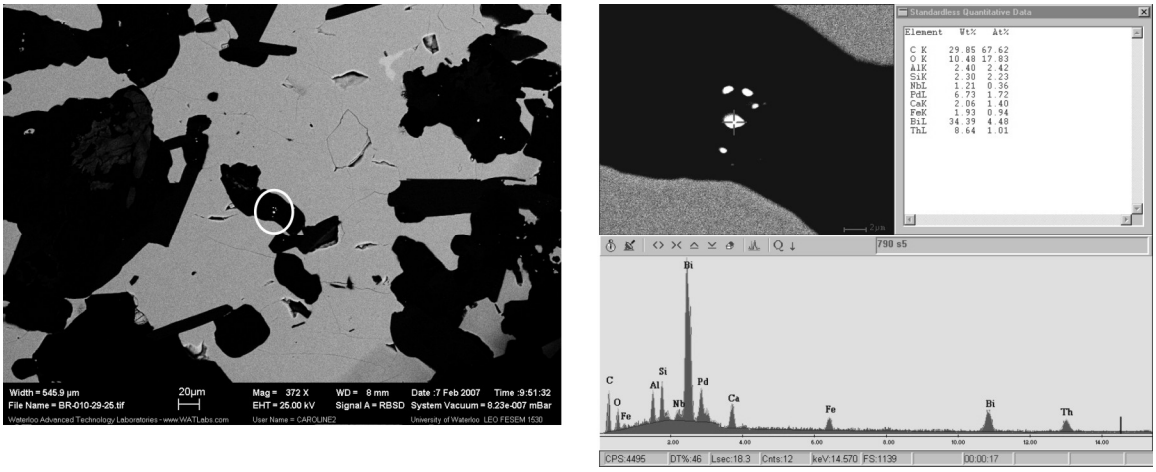

40: PGM – Cluster of froodite grains ($PdBi_2$) within silicate gangue inclusion in semi-massive pyrrhotite.

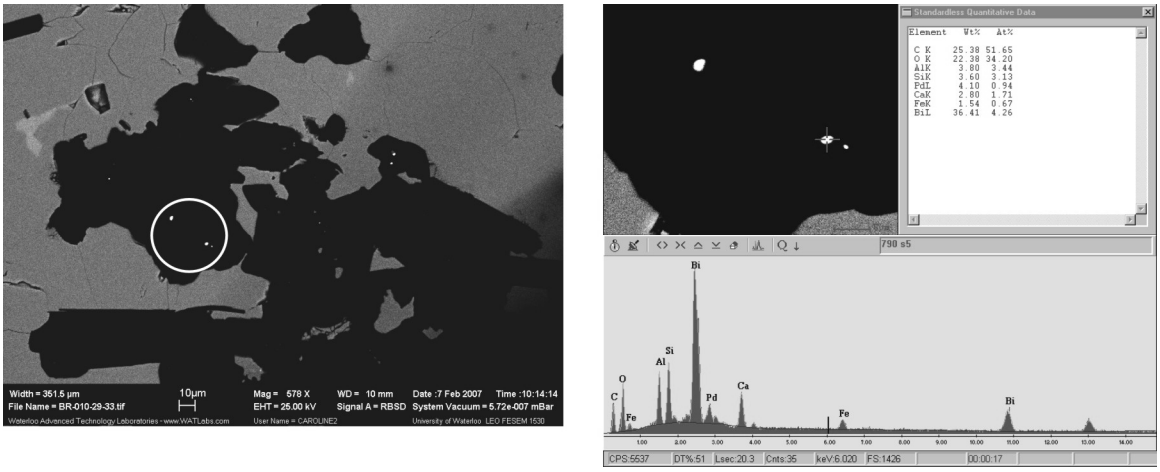

41: PGM – Cluster of froodite grains ($PdBi_2$) within silicate gangue near a contact with semi-massive chalcopyrite.

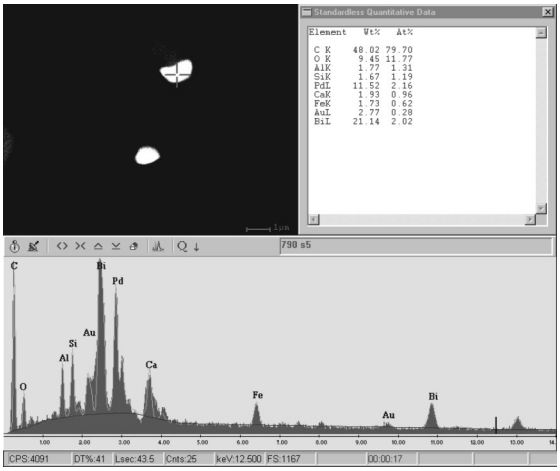

42: PGM – Two froodite grains ($PdBi_2$) within silicate gangue.

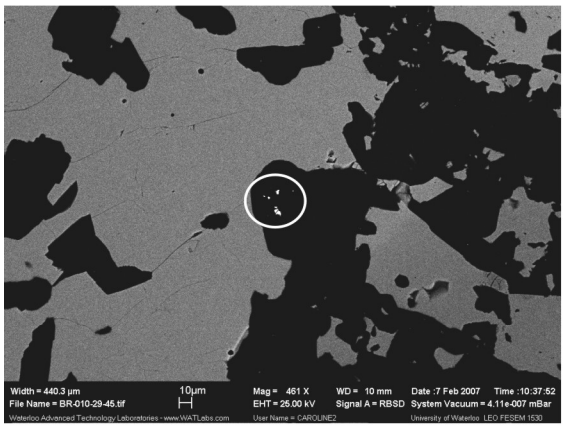

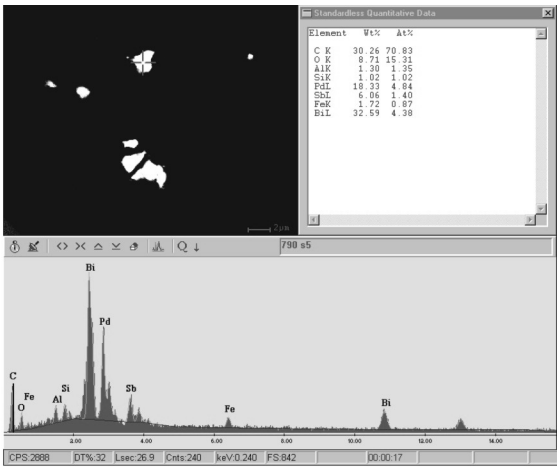

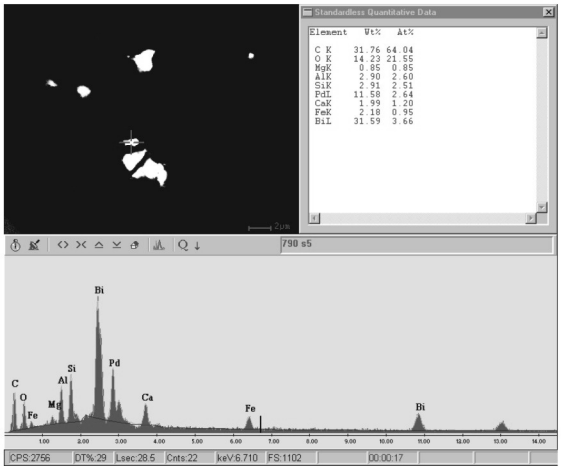

43 and 44: PGM – Cluster of PGM composed predominately of froodite ($PdBi_2$) and one unidentified PGM (Bi,Pd,Sb) species. PGM are present in a silicate gangue groundmass near a contact with chalcopyrite.